Ingenius

Ingenius • Issue 21 • january/june 2019. Semester Journal of Science and Tecnology of the Universidad Politécnica Salesiana of Ecuador. Publication dedicated to studies related to the Sciences of Mechanical Engineering, Electrical Engineering, Electronic Engineering, Mechatronic Engineering, Systems Engineering and Industrial Engineering.

Reviewers board

Federico Dominguez, PhD, Escuela Superior Politécnica del Litoral, Ecuador.

Enrique Carrera, PhD, Universidad de las Fuerzas Armadas, ESPE, Ecuador.

Andrés Tello, MSc, Universidad de Cuenca, Ecuador.

Cristian García Bauza, PhD, Universidad Nacional del Centro de la Provincia de Buenos Aires, Argentina.

Osvaldo Añó, PhD, Universidad Nacional de San Juan, Argentina.

Thalía San Antonio, PhD, Universidad Técnica de Ambato, Ecuador.

Victor Saquicela, PhD, Universidad de Cuenca, Ecuador.

Gonzalo Olmedo, PhD, Universidad de las Fuerzas Armadas, ESPE, Ecuador.

Román Lara, PhD, Universidad de las Fuerzas Armadas, ESPE, Ecuador.

Guillermo Soriano, PhD, Escuela Superior Politécnica del Litoral, Ecuador.

María Fernanda Granda, PhD, Universidad de Cuenca, Ecuador.

Ricardo Cayssials, PhD, Universidad Tecnológica Nacional, Argentina.

Leonardo Solaque Guzman, PhD, Universidad Militar Nueva Granada, Colombia.

José Di Paolo, PhD, Universidad Nacional de Entre Ríos, Argentina.

Astrid Rubiano Fonseca, PhD, Universidad Militar Nueva Granada, Colombia.

Robinson Jiménez, PhD, Universidad Militar Nueva Granada, Colombia.

Alfonso Zozaya, PhD, Universidad de Carabobo, Venezuela.

Mauricio Mauledoux, PhD, Universidad Militar Nueva Granada, Colombia.

Luis Medina, PhD, Universidad Simón Bolivar, Venezuela.

Ernesto Cuadros-Vargas, PhD, Universidad Católica San Pablo, Perú.

Samuel Sepúlveda Cuevas, PhD, Universidad de la Frontera, Chile.

Carlos Cares, PhD, Universidad de la Frontera, Chile.

Rafael Sotelo, PhD, Universidad de Montevideo, Uruguay.

Omar Lopez, PhD, Universidad de Los Andes, Colombia.

Job Flores-Godoy, PhD, Universidad Católica del Uruguay, Uruguay.

Luis Mario Mateus, PhD, Universidad de los Andes, Colombia.

Amadeo Argüelles Cruz, PhD, Instituto Politécnico Nacional, México.

Santiago Bentancourt Parra, PhD, Universidad Pontificia Bolivariana, Colombia.

Germán Zapata, PhD, Universidad Nacional de Colombia, Colombia.

Pedro García, PhD, Universidad Autónoma de Barcelona, España.

Arturo Conde Enríquez, PhD, Universidad Autónoma de Nuevo León, México.

Alberto Cavazos González, PhD, Universidad Autónoma de Nuevo León, México.

Ernesto Vázquez Martínez, PhD, Universidad Autónoma de Nuevo León, México.

Miguel Díaz Rodriguez, PhD, Universidad de Los Andes, Venezuela.

Efraín Alcorta García, PhD, Universidad Autónoma de Nuevo León, México.

Luis Chirinos Garcia, PhD, Pontificia Universidad Católica de Perú, Perú.

Oscar Avilés, PhD, Universidad Militar Nueva Granada, Colombia.

Dora Martínez Delgado, PhD, Universidad Autónoma de Nuevo León, México.

David Ojeda, PhD, Universidad Técnica del Norte, Ecuador.

Irene Beatríz Steinmann, PhD, Universidad Tecnológica Nacional, Argentina.

Mario Serrano, Universidad Nacional de San Juan, Argentina.

Cornelio Posadas Castillo, PhD, Universidad Autónoma Nuevo León, México.

Mario Alberto Rios Mesias, PhD, Universidad de Los Andes, Colombia.

Yudith Cardinale Villarreal, PhD, Universidad Simón Bolivar, Venezuela.

Eduardo Matallanas, PhD, Universidad Politécnica de Madrid, España.

Jose Eduardo Ochoa Luna, PhD, Universidad Católica San Pablo, Perú.

Dante Angel Elias Giordano, PhD, Pontificia Universidad Católica de Perú, Perú.

Manuel Pelaez Samaniego, PhD, Universidad de Cuenca, Ecuador.

Juan Espinoza Abad, PhD, Universidad de Cuenca, Ecuador.

Pietro Codara, PhD, Universidad de Milan, Italia.

Alberto Soria, PhD, Centro de Investigación y de Estudios Avanzados del Instituto Politécnico Nacional, México.

José M. Aller, PhD, Universidad Politécnica Salesiana, Ecuador.

Ferney Amaya F., PhD, Universidad Pontificia Bolivariana, Medellin, Colombia.

Santiago Arango Aramburo, PhD, Universidad Nacional de Colombia, Colombia.

Diego Arcos–Avilés, PhD, Universidad de las Fuerzas Armadas, ESPE, Ecuador.

Pablo Arevalo, PhD, Universidad Politécnica Salesiana, Ecuador.

Roberto Beltran, MSc, Universidad de las Fuerzas Armadas, ESPE, Ecuador.

Leonardo Betancur, PhD, Universidad Pontificia Bolivariana, Medellin, Colombia.

Roberto Gamboa, PhD, Universidad de Lisboa, Portugal.

Paulo Lopes dos Santos, PhD, Universidad do Porto, Portugal.

Pedro André Dias Prates, PhD, Universidad de Coimbra, Portugal.

José Manuel Torres Farinha, PhD, Universidad de Coimbra, Portugal.

Celso de Almeida, PhD, Universidad Estatal de Campinas Unicamp, Brasil.

Ramon Molina Valle, PhD, Universidad Federal de Minas Gerais, Brasil.

Cristina Nader Vasconcelos, PhD, Universidad Federal Fluminense, Brasil.

João M. Ferreira Calado, PhD, Universidad de Lisboa, Portugal.

Guilherme Luz Tortorella, PhD, Universidad Federal de Santa Catarina, Brasil.

Mauro E. Benedet, PhD, Universidad Federal de Santa Catarina, Brasil.

Artemis Marti Ceschin, PhD, Universidade de Brasilia, Brasil.

Gilmar Barreto, PhD, Universidad Estatal de Campinas Unicamp, Brasil.

Ricardo Emilio F. Quevedo Nogueira, PhD, Universidad Federal de Ceará, Brasil.

Weslley Luiz da Silva Assis, PhD, Universidad Federal Fluminense, Brasil.

Ana P. Martinazzo, PhD, Universidad Federal Fluminense, Brasil.

Jorge Bernardino, PhD, Universidad de Coimbra, Portugal.

Luis Geraldo Pedroso Meloni, PhD, Universidad Estatal de Campinas Unicamp, Brasil.

Facundo Almeraya Calderón, PhD, Universidad Autónoma de Nuevo León, México.

Freddy Villao Quezada, PhD, Escuela Superior Politécnica del Litoral, Ecuador.

Jose Manrique Silupu, MSc, Universidad de Piura, Perú.

Germán Ariel Salazar, PhD, Instituto de Investigaciones en Energía no Convencional, Argentina.

José Mahomar Jananías, PhD, Universidad del BIOBIO, Chile.

Arnaldo Jélvez Caamaño, PhD, Universidad del BIOBIO, Chile.

Jorge Andrés Uribe, MSc, Centro de Ingeniería y Desarrollo Industrial, México.

Ricardo Beltran, PhD, Centro de Investigación en Materiales Avanzados, México.

Adi Corrales, MSc, Centro de Ingeniería y Desarrollo Industrial, México.

Jorge Uribe Calderón, PhD, Centro de Investigación Científica de Yucatán, México

Editorial

Editorial Abya Yala (Quito-Ecuador),
Av. 12 de octubre N422 y Wilson,
Bloque A, UPS Quito, Ecuador.
Casilla 17-12-719 Teléfonos: (593-2) 3962800 ext. 2638
email: editorial@abyayala.org

Translator

Adriana Curiel

Tiraje: 800 ejemplares

Typographic system used in the composition of this document LaTeX.

Ingenius

Journal of Science and Technology

Issue 21, january – june 2018

ISSN impreso 1390-650X / ISSN electrónico 1390-860X

The administration of the journal is done through the following parameters:

The journal uses the academic anti-plagiarism system

The articles have an identification code (Digital Object Identifier)

The editorial process is managed through the Open Journal System

The articles of the present edition can be consulted in
http://revistas.ups.edu.ec/index.php/ingenius

Universidad Politécnica Salesiana del Ecuador

INGENIUS Journal, is indexed in the following Databases and scientific information systems:

SELECTIVE DATABASES

REVIEWS EVALUATION PLATFORMS

SELECTIVE DIRECTORIES

SELECTIVE SERIAL LIBRARY

SCIENTIFIC LITERATURE SEARCHERS OPEN ACCESS

OTHER BIBLIOGRAPHICAL DATABASES

CATALOG OF INTERNATIONAL UNIVERSITY LIBRARIES

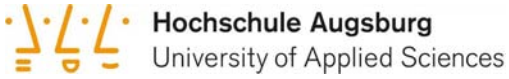

Editorial

Dear readers:

A key aspect to be considered in R+D processes is the interdisciplinary work that contributes to the way challenges are faced for future generations.

Planet Earth is affected by a number of problems such as global warming, climate change, pollution, rising energy demand, deforestation, water scarcity, species under extinction, biodiversity loss, aggressive diseases, inappropriate use of technology and others. These problems cannot be addressed by a group of professionals from the same discipline; integration is needed to address and seek possible solutions in a comprehensive and integral way.

In recent decades, research has been defined more by its topic rather than by the discipline that it addresses; a group of professionals from different areas working together have made advances that were never thought before. This change in the way research is done allows to reflect that the different points of view must be consolidated into a common objective, allowing to eliminate fears, envy and erroneous ideas generated in the different disciplines and that have been favored by an absurd competition to define who is the best, or who gets better incomes without considering the pursuit of the common welfare in society.

From this holistic point of view, it is essential to promote the interaction between different groups of professionals and researchers to achieve better results in investigations in less time and with an efficient use of resources; this requires the help and contribution of actors as well as the governments, institutions of higher education, university authorities, agencies representing the productive sectors and society in general. In the short term, there are many problems to face and experts are called to foster this interdisciplinary interaction that will be consolidated more and more frequently and will support an improved way of researching.

Another point to strengthen the research field is to get science closer to society in order to promote a balanced development, and for future generations to have necessary elements to decide their professional choices adequately; this will lead to greater incorporation of individuals to participate in the exciting world of research, with high research capacity, able to find solutions adapted to their local realities, but from a global perspective. In order to achieve the above, it is necessary to consolidate the teaching systems in science and engineering, which will allow to opt innovative solutions for the future challenges in the medium term.

John Calle Sigüencia, PhD

EDITOR IN CHIEF

Contents

Scientific Paper / Artículo Científico

UNIVERSIDAD POLITÉCNICA SALESIANA ECUADOR
INGENIUS
Revista de Ciencia y Tecnología
https://doi.org/10.17163/ings.n22.2019.01
pISSN: 1390-650X / eISSN: 1390-860X

Technological Innovation of a Comprehensive System to Monitor Electric Consumption

Innovación tecnológica de un sistema integral para monitotear el consumo eléctrico

Pilicita-Garrido, A. E.[1,*], Cevallos-Duque, D. C.[1]

Abstract

The present work focused on the design and implementation of an integral system to monitor, locally and remotely, the electrical consumption in the different areas within a home. In this way, it was considered to create a prototype capable of measuring every minute, the current consumed by the different loads connected to the electrical network of a household. A wireless network based on Zigbee technology was used to transmit the data of electric consumption from the prototype to a server. The data is processed and subsequently stored in a database. Finally, a web page was developed that graphically shows a history of electricity consumption, which the user can access locally or remotely to quickly and practically monitor the electricity consumption within the household. For the development of this integral system, the operation of current sensors, voltage dividers, Xbee modules was analyzed, and the application was developed with the use of Open Source software such as Java, MySQL and PHP. Currently, the user only has the monthly readings, delivered by the electricity service provider, ignoring the reality about critical environments within the household. Through the proposed system, the user can know at any place and at any time the electricity consumption generated in specific areas, and thus take appropriate actions for energy saving.

Keywords: Electricity, Electronic, Software Computer programming.

Resumen

El presente trabajo se enfocó en el diseño e implementación de un sistema integral para monitorear local y remotamente, el consumo eléctrico generado en los diferentes ambientes dentro de un hogar. De esta manera, se consideró la creación de un prototipo capaz de medir la corriente consumida cada minuto, por las diferentes cargas conectadas a la red eléctrica en los ambientes de un hogar. Se utilizó una red inalámbrica basada en la tecnología Zigbee para la transmisión de los datos desde los prototipos hasta un servidor que se encarga de recibir los datos cuando exista un consumo de electricidad en el hogar. Los datos son procesados y posteriormente almacenados en una base de datos. Finalmente, se implementó una página web que muestra gráficamente un historial del consumo eléctrico, a la que el usuario puede acceder local o remotamente y monitorear de forma rápida y práctica el consumo eléctrico en el hogar. Para el desarrollo de este sistema integral se analizó el funcionamiento de sensores de corriente, divisores de voltaje, módulos Xbee, y se desarrolló la aplicación con el uso de *software* Open Source como Java, MySQL y PHP. Actualmente, el usuario cuenta tan solo con las lecturas mensuales, entregadas por el proveedor de servicio de electricidad, desconociendo la realidad sobre los ambientes críticos dentro de su casa. Mediante el sistema propuesto, el usuario podrá conocer en todo lugar y en cualquier momento el consumo eléctrico generado en áreas específicas, y así tomar medidas oportunas de ahorro energético.

Palabras clave: electricidad, electrónica, *software*, programación informática

[1,*]Facultad de Ingeniería Eléctrica y Electrónica, Universidad de las Fuerzas Armadas, Ecuador. Autor para correspondencia ✉: anabelpilicita@gmail.com http://orcid.org/0000-0002-0796-7797
http://orcid.org/0000-0002-7314-5580

Received: 13-01-2019, accepted after review: 30-04-2019

Suggested citation: Pilicita-Garrido, A. E. and Cevallos-Duque, D. C. (2019). «Technological Innovation of a Comprehensive System to Monitor Electric Consumption». Ingenius. N.° 22, (july-december). pp. 9-16. doi: https://doi.org/10.17163/ings.n22.2019.01.

1. Introduction

The electrical distribution networks carry the energy through high-voltage lines to the consumption sites: factories, businesses, hotels, particular households, among others. There is no doubt about the high dependence of actual societies and most human daily activities, both domestic and industrial, on energy sources. Appliances such as lamps, recorders, sound systems, irons, TVs and computers, among others, are used every day. All them require electric energy to operate, thus becoming the main source to drive equipment in general [1].

The energy systems worldwide have been called inefficient, highly contaminant and unsustainable [2]. Due to this, governments of different countries search for system improvement.

It is estimated that due to the future demographic growth, very big cities will be created with more electric appliances required for the development of technology, thus implying a significant energy consumption; simply, the network will not be able to supply the energy demanded [2, 3]. On the other hand, the environmental impact will be greater, the energy distribution needs to evolve and expanding the energy distribution network is very costly; it is sought to generate consciousness about energy saving [4].

Final consumers should be aware of the positive economic and environmental effects of the rational use of electricity. The regional learning curve improves every day, regarding the knowledge about responsible consumption [4]. In order to face this requirement, a tool was created for consumers to know the amount of electricity consumed, when it is being used and which area of the household has the greater consumption. According to the National Institute of Statistics and Census (Instituto Nacional de Estadísticas y Censos, INEC), 62 % of the Ecuadorian population considers as very important to save energy in their households [5].

The project to develop the integral system of electric consumption in four areas of a household, comprises four stages. It is emphasized to use Open Source software for the developing the different codes.

- **Prototype.**A device capable of measuring the electric consumption was designed and implemented. The prototypes were placed in four electric circuits inside the household, to measure the flow of current of the different appliances located in each area.

- **Data transmission.** Xbee devices, which operate under Zigbee technology, were utilized to transmit the data in a wireless manner. A communication network with wye topology was established between the Xbee devices, which were placed in the prototypes located in the different areas. A coordinator established the communication with each of them.

- **Data processing and storage.** The data transmitted by the wireless network are received by the coordinator, which establishes the communication using a program developed in Java, to process the data and store the information in an appropriate database; MySQL was utilized for the project.

- **Remote monitoring.** A web application was designed using PHP language, which enables the user to remotely monitor the electric consumption of the household. A historical is graphically displayed to the user.

2. Design and implementation of the prototype

A device was designed to measure the electric energy consumption. Such device provides an exact measurement of the current consumed by the different loads connected to the electric network. For designing the device, it is assumed that the household consumes only active power, i.e. all the connected load is considered resistive.

The measurements of the magnitudes correspond to peak values; for calculating the power it is necessary to determine that the values are in a same wave, and then transform them to RMS values. The prototype was developed with the components shown in the block diagram of Figure 1.

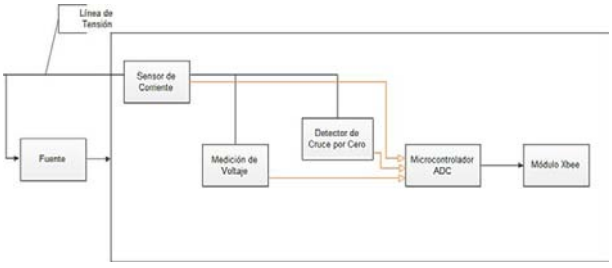

Figure 1. Block Diagram of the prototype.

2.1. Current sensor

The sensor chosen for the design was the Hall effect ACS712, since it is easy to use, has a low price and small error range [6].

The selected current sensor should verify the maximum current that can be consumed in each electrical outlet where the device is connected, such that it can carry out the measurement in an extreme case without being damaged. Since the maximum consumption of electronic appliances is approximately 1100 Watts [7],

the current sensor has to support 10 Amperes maximum. It was found in the technical sheet of this sensor, that the optimal measuring range of this device is 20 Amperes [6]. Therefore, it can be concluded that the sensor will be able to carry out the measurements without being damaged by excessive current. The sensor delivers an output voltage whose magnitude is proportional to the measured current, with a sensitivity of 0.1 [V/A] [6].

2.2. Voltage divisor

Since the voltage of the line is not constant, it should be measured. For this purpose, a voltage divisor with a 100:1 relation is designed to interpret it [8].

This stage constantly measures the value of the voltage. Although the electrical network in Ecuador delivers an AC nominal voltage of 110 Volts [5], this value is not constant due to distribution issues. Therefore, the power cannot be calculated using this nominal value, because it is not necessarily the real value. As a consequence, it is required to measure this voltage.

This is carried out using a voltage divisor, which is fed with the line voltage, to acquire a signal with a magnitude of voltage that does not damage the microcontroller (over voltage). In this case, the implemented equivalence is 100 AC Volts to 1 AC Volt, to proportionally vary the output voltage in response to increases or decreases in the line voltage.

2.3. Zero crossing

In order to have an exact measurement of the consumed current, it is necessary to detect the start of the cycle of the signal [9]. There is a simple method to detect the zero crossing of the alternate current wave, which is useful for measurements at 50 Hz, 60 Hz, and 400 Hz, in systems with voltages of hundreds of Volts. Such method requires a resistance as the unique external component, which makes it more reliable tan other methods that require voluminous condensers or costly transformers. Detecting the zero crossing of the signal was necessary to determine which values of voltage and current should be multiplied in the same cycle. In consists of connecting a resistance of 5M [Ω] in series with the tension line, and input such signal at the interruption of the PIC 12F1840. This is used to know when a cycle ends [10].

2.4. Microcontroller

The microcontroller selected for the prototype was the PIC 12F1840, which has two analog inputs, one for serial output, a 10 bit analog-to-digital converter (ADC), an internal oscillator of 32 MHz and 4 KB of flash memory. These specifications comply with the parameters of the design of the prototype [11].

The program in the microcontroller samples each wave, and determines its peak value with the 10 bits ADC; thus the peak value of each magnitude varies in the range from 0 to 1023. These values are then converted to RMS values and averaged along a one-minute period. At last, it waits until the monitoring system of electric consumption establishes the communication to send the data, controlling the flow using letters of the alphabet (ASCII code) [10]. Figure 2 shows the petitions and responses generated from the prototypes to the code developed in Java.

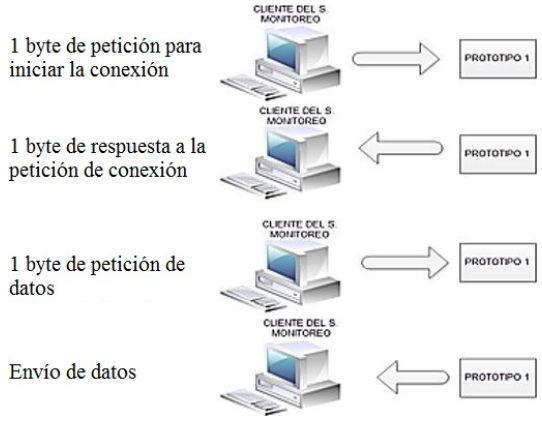

Figure 2. Flow control between the connection of the client of the monitoring system and the prototype measurement system.

2.5. Xbee module

The selected Xbee module belongs to series 1, because the area to be covered is smaller than 30 meters. In addition, the cost is smaller than a series 2 Xbee [12].

Once the microcontroller has captured the information and has sent it through the USATR output pins, the Xbee 1 module is in charge of receiving this information and transmitting it to the coordinating Xbee module [13]. Such coordinator is connected to an Xbee USB explorer which enables the communication with the PC that has the server application that will store and process the obtained data in a database.

2.6. Source

It was designed because it is necessary for feeding the microcontroller, the Xbee module and the current sensor. It consists of a 120 [V] : 12 [V] AC transformer, and this signal is further rectified with a diode and a capacitor; a 3,6 [V] DC limiting diode is connected in parallel with the capacitor [10].

2.7. Calibration of the prototypes

The microcontroller reads the values in a range from 0 to 1023. The following formulas are applied to transform them to RMS values (Table 1) [10]:

Table 1. Values for the formula of the voltage factor

Value of the source	3,6 (V)
Maximum value of ADC levels	1023
Relation of the voltage divisor	100 k [Ω] a 1 k [Ω]
Sensitivity of the Hall sensor	0,072 [V/A]

- Nominal voltage factor

$$\frac{\frac{3,6[V]}{1023} \times \frac{100K\Omega}{1K\Omega}}{\sqrt{2}} = 0,249\ [V] \quad (1)$$

- Nominal current factor

$$\frac{3,6[V]}{1023} \times \frac{1[A]}{0,072[V]} = 0,048\ [A] \quad (2)$$

3. Data transmission

As it was detailed previously, the Zigbee technology was employed. This technology operates under the network standard 802.15.4, required for this short range wireless project (less than 30 meters) [14].

The wireless network is constituted by four Xbee modules, which are known as final devices in a network. There is a necessarily a coordinator Xbee module, which is connected to the computer via an USB port [12], and is in charge of synchronizing all the final devices and receiving the data generated by each prototype. At last, it delivers the data to the code developed in Java. Figure 3 illustrates a block diagram of the data transmission process.

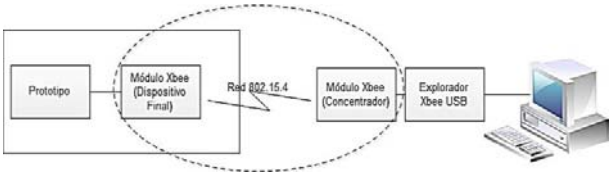

Figure 3. Block diagram of the data transmission process.

3.1. Transmission Mode

The transmission mode of the Xbee modules (coordinator-final device) represents a transparent connection, i.e. basically all that goes through the UART port is sent to the desired module, and what is received by the module is returned through the same UART port [12].

In order to establish the communication, the Xbee modules must belong to the same PAN ID network and to the same channel; according to the IEEE 802.15.4 protocol, 16 channels are available [15].

The configuration of addresses is carried out in the following manner:

- Xbee final device: the address of the Xbee coordinator module is configured in the destination address.
- Xbee coordinador: A «0» is configured in the destination addresses, which corresponds to receiving all the data from any Xbee final device module [16].

4. Data processing and storage

For processing the data delivered by the coordinator Xbee, a program called (*Electric consumption*) was developed in Java. This program establishes a serial communication to obtain the data of electric consumption, then processes them, and finally stores them in the MySQL database manager. Figure 4 illustrates the next stage for data processing.

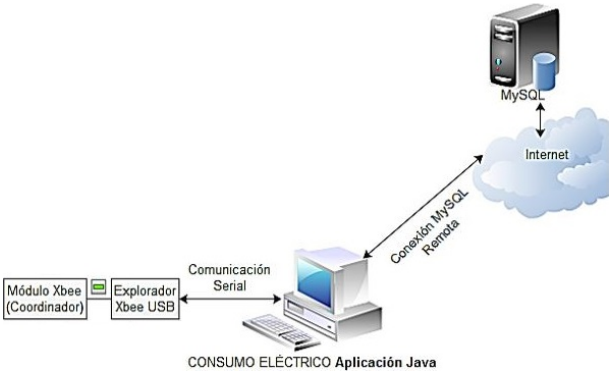

Figure 4. Data processing.

4.1. Processing

The control of flow was established to enable the communication between the computer and the remaining prototypes, determining the beginning and end of a data transmission. Each prototype was identified to receive the voltage and current data that will be used to calculate the electric consumption in the four areas of the household. The control of flow is carried out every minute, taking into account the following steps:

- To initiate the communication and determine which electric consumption prototype is on, a different letter is sent to each device waiting for a response.
- A response is received with the letter that identifies the Xbee final device associated with the measuring prototype, indicating that the petition has been received and, therefore, the electric consumption is being measured.
- Another character is sent to request the voltage and current values.
- The voltage and current values are received.

Then, the power is calculated at every minute using the voltage and current values delivered by the coordinating device. After an hour elapses, the electric consumption of every appliance is calculated as the average of the 60 available samples. The program was developed in Java; Table 2 contains the classes and the function of each of them [10].

Table 2. Structure of the program in Java

Classes	Functions
PuertoSerial .java	– Configure the serial port of the computer. – Send letters of the alphabet in ASCII code to initiate the communication. – Receive the voltage and current data sent by the four prototypes that measure electric consumption. – Close the communication with the serial port.
Conexión .java	– Connect the local program with the MySQL remote database. – Store the data of electric consumption in the remote database using SQL sentences. – Close the communication with the database. – Flow control.
Consumo_Electrico.java Interfaz.java	– Display in a graphical interface the data received from the different final devices. – Process and calculate the electric consumption. – Store the information of the electric consumption in the database.

4.2. Storage

A database that operates with the MariaDB Database Managing System was created to store the data of electric consumption. It was defined using the software Power Designer, working from the conceptual, logical and physical modeling, for the storage of information [17]. Figure 5 shows the structure of the database according to the conceptual model. There is the tabla usuario, which stores the personal information of the final clients, them to register and further access the system and visualize the electric consumption.

There is the tabla dispositivo to store information of the electric consumption generated every hour. At last, there is the tabla prueba which enables the verification of the correct storage of data per minute.

The values of power calculated every minute are averaged to calculate the electric consumption of the appliances after every hour. Then, after 60 samples has been automatically taken, the connection with the remote database is opened, and the data are inserted from the application developed in Java using SQL sentences. The prototype sends the information, the time, date, voltage, current and power [10].

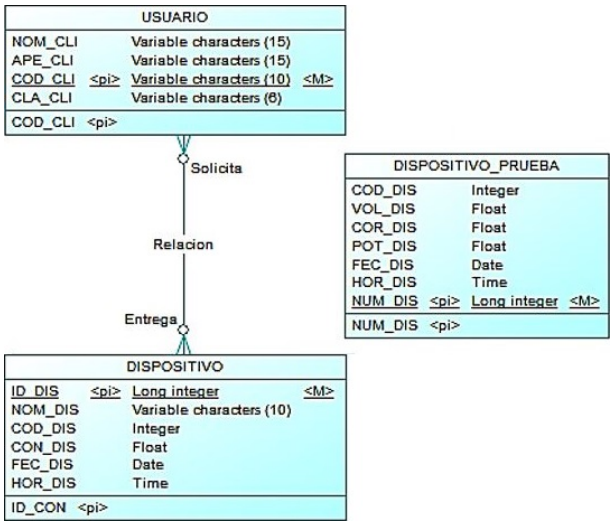

Figure 5. Conceptual model of the DB.

5. Remote monitoring

A web site was developed for the final users or clients to remotely access via Internet and visualize the data generated in their household, as illustrated in Figure 6.

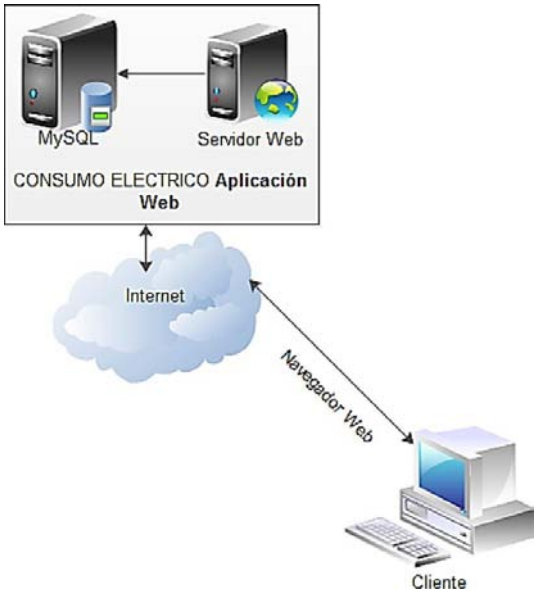

Figure 6. Access to a web site from a client.

The web application enables the communication through the Internet, with the server that houses the web site [18]. The electric consumption can be checked by final device or by entered dates, and it is also

possible to eliminate historic data of the electric consumption.

The web sites were designed in DreamWeaver and developed in the language HTML y PHP. They include information, both text and images, about the energy saving in the household, and visual material, such as dynamic graphs that represent the electric consumption of the appliances in the household, is also available.

The structure of the web site developed can be visualized in Figure 7.

Figure 7. Web map of electric consumption.

6. Tests

Once the integral system for measuring the electric consumption was finalized, tests were carried out to verify a correct delivery of voltage by the source, and also the acquisition and sending of data.

It should be taken into account that for obtaining the value of consumed power of the load connected to a particular prototype, the current consumed by the prototype (38 [mA]) should be subtracted from the magnitude of the current, and the result multiplied by the line voltage [10].

Afterwards, tests with the designed prototype were carried out, as shown in Figure 8.

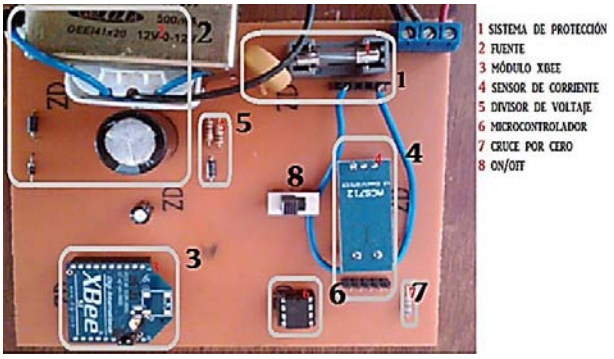

Figure 8. Prototype for measuring the electric consumption.

Each prototype has been distributed in the 4 main areas of a standard household, namely a bedroom, a bathroom, the kitchen and the social section. The distribution of the devices can be observed in Figure 9.

Figure 9. Distribution of measuring devices in a standard household.

Images of the consumption of electric energy detected by prototype 1, are shown in what follows. Figure 10 displays the result obtained using the application generated in Java [10].

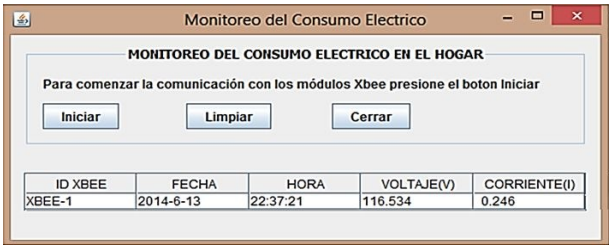

Figure 10. Obtained values of voltage and current consumed by the laptop in the monitoring system.

The multimeter shown in Figure 11 was used to verify these values, and validate the real-time measurements with the values transmitted to the application and further stored.

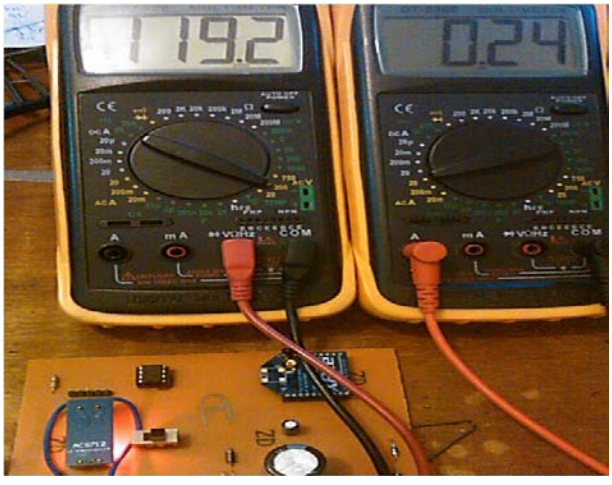

Figure 11. Measured values of voltage and current consumed.

6.1. Measurement tests

Various measurement tests were carried out, with the purpose of calibrating the devices, verifying the data obtained by the systems that measure and monitor the electric consumption and, besides, reducing the measurement errors that may exist [10].

Table 3. Error la potencia medida y la obtenida de los prototipos.

Prototype	Measured power [W/minute]	Obtained power [W/minute]	Error %
1	4,25	4,22	0,07
2	4,2	4,3	2,38
3	4,47	4,46	0,22
4	4,37	4,35	0,45

Table 3 shows the error percentage between the magnitudes measured with the multimeter, and the obtained with the developed integral system of electric consumption. Considering that the system calculates the average of the data collected every minute, while the multimeter registers instantaneous values, the errors are in an acceptable range of operation which indicates accuracy for the system in general.

- Data stored per minute

The data are stored in the database of the system for monitoring the electric consumption. Figure 12 illustrates the collection of data per minute of the four prototypes.

	NUM_DIS	COD_DIS	VOL_DIS	COR_DIS	POT_DIS	FEC_DIS	HOR_DIS
Editar Copiar Borrar	4771	1	116.558	0.25	29.1395	2014-06-14	13:03:58
Editar Copiar Borrar	4772	2	120.139	0.265	31.8368	2014-06-14	13:04:00
Editar Copiar Borrar	4773	4	117.499	2.493	292.925	2014-06-14	13:04:02
Editar Copiar Borrar	4790	3	115.199	0.221	25.459	2014-06-14	13:16:38

Figure 12. Data uploaded in the Table DATOS of the database true_electricidad.

6.2. Test in contrast with the electric meter

In these tests, the data considered included values of the power consumed in the household for a period of 5 hours, calculated by the system for monitoring the electric consumption. The purpose was to compare these values with the registered by the electric meter [10].

The monitoring was initiated at 10:52 and ended at 15:42, after a total of 4 hours and 50 minutes. The electric meter had initial and final consumptions of 32571 [kWh] and 32576 [kWh], respectively, i.e. in such interval 5 [kWh] were approximately consumed. The monitoring system registered a consumption of 5,755 [kWh] during that day, which indicates that the values provided by the system are similar to the values considered by the electric service provider [10].

7. Conclusions

It is important to make optimal use of the electric energy in the household, generating policies, plans and projects that promote the efficient use of electric energy. For this reason, the project informs about the electric consumption in the household, to be aware of the excesses, and start to save energy. For future applications of home automation, the system may be expanded with a module that remotely controls the appliances to maintain electric efficiency in the household.

The percentage between the measured and obtained values of electric consumption in the prototypes, is in an acceptable range of operation, smaller than 2 %, considering that the monitoring system averages the data obtained every minute, while the multimeter measures instantaneous values. However, the error diminishes with higher loads and the obtained data tend to coincide with the values considered by the electric service provider.

The electric meters have to constantly evolve according to the needs of the people. Therefore it is necessary to extend the project, with the purpose of developing a future implementation at a macro level, i.e. monitor the total electric consumption of each household in the country, and provide information of vital interest for the electric service provider.

The project displays a history of the power consumption in the household, which can be used to estimate the daily/monthly consumption capacity. In this way, renewables energies, such as solar panels and eolic turbines among others, may be dimensioned and implemented to fulfill the demand of each household and establish an efficient consumption.

References

[1] ENDESA. (2014) La red eléctrica. Endesa Educa. [Online]. Available: http://bit.ly/2Q1fi7f

[2] C. Vargas, "Sobre la problemática energética," *Comunicación*.

[3] E. Menéndez Pérez, *Las energías renovables: un enfoque político-ecológico*, L. de la catarata, Ed., 1997. [Online]. Available: http://bit.ly/2W11aQP

[4] F. Estenssoro Saavedra, J. M. Zolezzi Cid, M. Tokman Ramos, R. Núñez Muñoz, E. Águila Mancilla, R. Sohr Biss, C. Parker Gumucio, J. Zanelli, A. Cubillos Meza, J. A. Perrotta, J. Griffiths Spielman, I. Witker, and O. Sunkel, *Energía y medio ambiente. Una ecuación difícil para América Latina : los desafíos del crecimiento y desarrollo en el contexto del cambio climático*, IDEA-USACH, Ed. Colección Idea, 2011. [Online]. Available: http://bit.ly/2EjGuJW

[5] INEC, "Módulo de información ambiental en hogares," Instituto Nacional de Estadísticas y Censos, Ecuador., Tech. Rep., 2017. [Online]. Available: http://bit.ly/2VW77zy

[6] M. J. Mnati, A. Van den Bossche, and R. F. Chisab, "A smart voltage and current monitoring system for three phase inverters using an android smartphone application," *Sensors*, vol. 17, no. 4, 2017. [Online]. Available: http://bit.ly/2WSHQCw

[7] NOAO, "Guía para el cálculo de energía," National Optical Astronomy Observatory, Tech. Rep., 2016. [Online]. Available: http://bit.ly/2YEnkWY

[8] W. McAllister. (2019) Divisor de voltaje. Khan Academy. [Online]. Available: http://bit.ly/2LSNyDj

[9] L. Burwell. (2019) ?'qué es un detector de cruce por cero? techlandia.

[10] A. Pilicita and D. Cevallos, *Diseño E Implementación De Un Prototipo Para El Monitoreo Remoto Del Consumo Eléctrico a través de una red Zigbee con médulos Xbee*, S.-E. Universidad de las Fuerzas Armadas-ESPE, Ed. Proyecto de titulación, 2014.

[11] MICROCHIP, "Pic12(l)f1840 data sheet," Microchip Technology Inc., Tech. Rep., 2019. [Online]. Available: http://bit.ly/2QcR9L4

[12] DIGI, "Digi xbee®s2c 802.15.4 rf modules," Digi International Inc., Tech. Rep., 2019. [Online]. Available: http://bit.ly/2wbCtTq

[13] ZOLL, *Manual del usuario de la unidad X Series®*, ZOLL Medical Corporation, 2016. [Online]. Available: http://bit.ly/2M0hAoI

[14] I. Vidri Salgado. (2011) Zigbee y sus aplicaciones. Escuela Técnica Superior de Ingeniería-ICAI. Universidad Pontificia Comillas. [Online]. Available: http://bit.ly/30wH0gV

[15] IEEE, *IEEE 802.15.4-2015 - IEEE Standard for Low-Rate Wireless Networks*, IEEE standards association Std., 2015. [Online]. Available: http://bit.ly/2LXR2V9

[16] Interactivo, *Xbee y arduino*, 2016. [Online]. Available: http://bit.ly/2QfP29b

[17] A. Lozada. Las etapas del diseño de una correcta base de datos relacional. EDteam. [Online]. Available: http://bit.ly/2waK9oN

[18] Hostname. (2014) Servidor web. Servicio Informáticos Hostname Limitada. [Online]. Available: http://bit.ly/2LWDLfz

Scientific Paper / Artículo Científico

UNIVERSIDAD POLITÉCNICA SALESIANA ECUADOR
INGENIUS
Revista de Ciencia y Tecnología
https://doi.org/10.17163/ings.n22.2019.02
pISSN: 1390-650X / eISSN: 1390-860X

Environmental Pollution Analysis Produced by Low-Pressure Cold Plasma in the Sheet Metal Cleaning Process

Análisis de la contaminación ambiental producida por el plasma frío de baja presión en la limpieza de láminas metálicas

Luis M. López[1,*], Janine Villavicencio Ramírez[1],
Kevin Aponte[2], Jorge I. Fajardo[2], Christian P. López[3]

Abstract

The present research addresses an analysis of the level of contamination produced by gases generated from carbon monoxide (CO), carbon dioxide (CO2) and hydrocarbons (HC) in the cleaning of metallic sheets of stainless steel AISI / SAE 304, when applying low pressure cold oxygen plasma for the removal of oils ISO 32, ISO 68 and ISO 220, using different generator control parameters according to the lubricating oil removed from the surface of the stainless steel metallic sheet. The experimentation was carried out in a first phase in which a discharge was applied directly to the surface of the sheet contaminated with a volume of 0.1 ml of oil, and in a second phase in which the sheet with the oil was immersed in an oil degreaser to perform a pre-cleaning prior to the application of low pressure cold plasma on the surface. For analyzing the results in the level of gases generated by each oil, a statistical analysis is applied to determine if there is a significant difference in the level of the gases generated between the two phases.

Keywords: Low pressure cold plasma, contamination.

Resumen

La presente investigación aborda un análisis del nivel de contaminación producido por los gases generados de monóxido de carbono (CO), dióxido de carbono (CO_2) y los hidrocarburos (HC) en la limpieza de láminas metálicas de acero inoxidable AISI/SAE 304 aplicando plasma frío de oxígeno a baja presión para la remoción de los aceites ISO 32, ISO 68 e ISO 220, con diferentes parámetros de control del generador de acuerdo con el aceite lubricante removido de la superficie de la lámina metálica de acero inoxidable. La experimentación se realizó en un primer proceso con una descarga aplicada directamente a la superficie de la lámina impregnada con el aceite colocando con un volumen de 0,1 ml y en un segundo proceso donde la lámina con el aceite impregnado fue sumergida en un desengrasante para aceites y grasas con la finalidad de realizar una limpieza previa a la aplicación del plasma frío a baja presión en la superficie. Para el análisis de los resultados en el nivel de gases generados por cada aceite se aplica un análisis estadístico para determinar si existe una diferencia significativa en el nivel de los gases generados en las dos etapas.

Palabras clave: Plasma frío a baja presión, contaminación.

[1,*]Universidad Nacional Mayor de San Marcos, Perú. Autor para correspondencia ✉:llopez@ups.edu.ec. http://orcid.org/0000-0001-9353-384X, http://orcid.org/0000-0001-8831-2604
[2]Grupo de Investigación GiMaT, Universidad Politécnica Salesiana, Ecuador. http://orcid.org/0000-0003-0359-1750, http://orcid.org/0000-0003-1047-398X
[3]Vaughn College of Aeronautics and Technology, New York, USA. http://orcid.org/0000-0002-0211-4613

Received: 02-04-2019, accepted after review: 06-05-2019

Suggested citation: López, L. M.; Villavicencio Ramírez, J.; Aponte, K.; Fajardo, J. I. and López, C. P. (2019). «Environmental Pollution Analysis Produced by Low-Pressure Cold Plasma in the Sheet Metal Cleaning Process». Ingenius. N.° 22, (july-december). pp. 17-24. doi: https://doi.org/10.17163/ings.n22.2019.02.

1. Introduction

In the production processes it is sought to eliminate or reduce emissions, dumping and wastes with an efficient use of the resources, and technologies that enable to yield the requirements and specifications of a product with the smallest environmental impact [1].

The contamination produced by the pickling baths in the cleaning of metallic sheets with acids and bases, considered toxic, harmful and hazardous for health, infrastructure and environment has considerably increased in recent years. Heavy metals such as zinc, chromium and copper that accumulate in the pickling baths are theoretically considered as suspended substances, and constitute another problematic due to the serious environmental contamination they produce [2–5].

At present, several superficial cleaning processes are carried out to reduce or eliminate the contamination, as new alternatives to traditional processes. They show the same efficiency, considering that the presence of impurities or remains of oils and greases in the different surfaces to be cleaned will decrease adherence in further superficial treatments [6, 7].

According to previous studies, the application of low-pressure cold plasma exhibits satisfactory results in removing oils from metallic sheets using non-pollutant gases, with the purpose of removing both mechanical and organic compounds [8]. The adhesive properties of the material will depend upon the effectiveness of this treatment according to the contact angle, which is directly related to the free superficial energy [9–11].

The superficial cleaning of organic compounds using low-pressure cold plasma, is a method that bombards ions of a particular gas, which is produced by physical effects or chemical reactions, to transform the substances that are on the metallic sheets to the gaseous phase, thus expelling them from the chamber to the atmosphere [12]. Previous research works [6, 13] indicate that the application of cold plasmas in certain industrial processes is more efficient and less expensive, thus reducing the contamination and toxic residues. The cleaning process is more efficient, since it reduces the contact angle when previously immersed in a degreaser [8] (Figure 1).

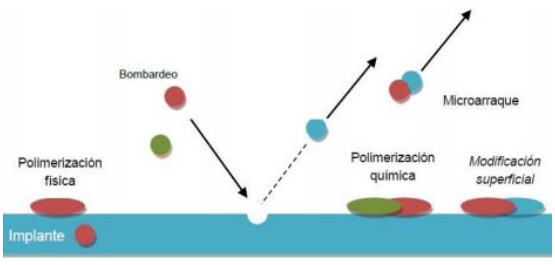

Figure 1. Modifying effects on the surface of the plasma [14].

The angle of contact is a superficial property of the solids, which quantifies its tendency to the hydrophobicity, as an important parameter to analyze the mechanisms of interaction between the solid and liquid phases that appear in many industrial operations. The value of the angle of contact mainly depends on the relation between the adhesive forces of the liquid and the surface, and the internal forces of cohesion of the liquid itself. As the interaction gets smaller, the angle of contact is larger and its value is directly related with the quality of the cleaning, i.e. a smaller angle of contact results in a greater wettability, indicating a smaller presence of contaminant agents in the surface under study; it is considered that values smaller than 30° will show high degree of cleanliness, and that the surface will be ready for further coverings. For rugged surfaces, is it important to determine the apparent angle θ_{ap}, and if the surface has an inclination, the intrinsic angle θ_i [8, 15, 16] (Figure 2).

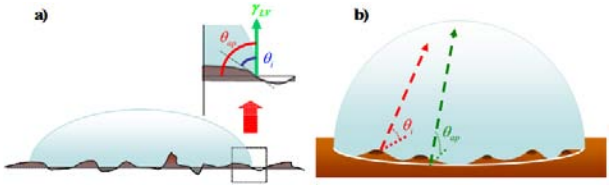

Figure 2. Intrinsic and apparent contact angle on a surface a) Rugged and homogeneous b) Smooth and heterogeneous [16].

2. Materials and methods

2.1. Materials

2.1.1. Stainless steel sheets

Stainless steel sheets AISI/SAE 304 of dimension 7 x 7 cm and thickness of 2 mm were used in the research for laboratory tests, as shown in Figure 3. The sheets were impregnated with 0,1 ml of the lubricant oils ISO 32, ISO 68 and ISO 220, previous to the discharge of the oxygen plasma. The rugosity of the surface of the steel was not considered, since it does not have influence on the effect of the ionized oxygen gas on the controlled volume of oil deposited on the surface.

Figure 3. Stainless steel sheet.

2.1.2. Lubricant oils

The lubricant oils ISO 32, ISO 68 and ISO 220 were utilized as contaminant agents, and placed on the surface of the stainless steel sheets. Such oils were provided by the commercial house Gulf, and have the properties shown in Table 1.

Table 1. Properties of lubricant oils

Oils	Viscosity cSt/40 °C	Density to 15 °C kg/l	Flammability Point °C
ISO 32	32	0,87	202
ISO 68	68	0,88	218
ISO 220	220	0,89	256

2.1.3. Oxygen

High purity oxygen provided by the company AGA, was utilized for generating the ionized gas or plasma. The output pressure of the tank is 1 bar, which was regulated in the plasma generator equipment, according to the stated experimental conditions.

2.1.4. Low-pressure cold plasma generator

The brand of the plasma generator equipment utilized here is Diener, as shown in Figure 4. In this equipment, the neutral particles and the ions arise between 25 and 100 °C, with an electronic temperature between 105 °C and 5000 °C by means of continuous current and pressures below 133 mbar. The equipment is semi-automatic, where three different gases for generating plasma can be used, and pressure, time and power parameters can be controlled [17].

Figure 4. Plasma generator.

The vacuum plasma chamber can be seen in Figure 5, where the stainless steel sheets impregnated with oil are placed. In addition, it comprises a vacuum pump with rotating paddles of two stages, has a residual pressure close to zero and enables the ventilation of the chamber

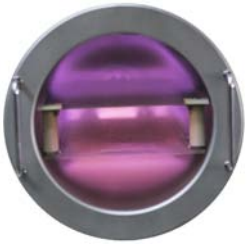

Figure 5. Plasma chamber.

Table 2 contains the parameters established in the oxygen plasma generator equipment that, according to research studies carried out by [8], are suitable for cleaning metallic sheets with low-pressure cold plasma.

Table 2. Parameters of the plasma generator

Processes	Lubricants	Control parameters. Time (min)	Pressure (mbar)	Power (%)
Processes with immersion	ISO 32	10	0,26	90
	ISO 68	10	0,30	90
	ISO 220	15	0,32	90
Processes without immersion	ISO 32	15	0,28	90
	ISO 68	15	0,32	90
	ISO 220	20	0,34	90

2.1.5. Gas analyzer

The level of gases generated in the cleaning of stainless Steel sheets were detected by the QROTECH gas analyzer, model NGA 6000, shown in Figure 6. This analyzer is capable of detecting (i) carbon monoxide, in the measuring range 0.00 to 0.99 %, which is highly toxic and can cause death when present at high levels, (ii) carbon dioxide in the range 0.0 to 20.0 % that affects global warming, (iii) diatomic oxygen in the range 0.00 to 25.00 %, that does not affect the environment, (iv) hydrocarbons in the range 0 to 20000 ppm, combinations of carbon and hydrogen commonly responsible for intoxications, and (v) NOx in the range 0 to 5000 ppm, which are reactive, such as nitric oxide (NO) and nitrogen dioxide (NO_2), and very harmful for health, environment and structures [18,19].

Figure 6. Gas analyzer.

2.1.6. Digital optical goniometer

The KSV CAM100 optical goniometer shown in Figure 7, was utilized to determine the angle of contact of the test liquid on the metallic surface. It incorporates a camera CCD (charged-coupled device) with an optic of 50 mm, and the software CAM 100 for image treatment. A volume of 5 μl of test liquid was utilized for measuring the angle of contact.

Figure 7. Digital goniometer.

2.1.7. Test liquid

Distilled or demineralized water was used as test liquid, with the components of the free superficial energy that are shown in Table 3.

Table 3. Components of the test liquid [20].

Test liquid	Energy of the surface (γ)	Dispersive component (γ^d)	Polar componente (γ^p)
Distilled water	72.80	21.80	51.00

The components of the liquid obtained by means of the angle of contact with distilled water, enable the calculation of the free superficial energy using the theories of Fowkes and Wu.

2.2. Methods

2.2.1. Statistical methods

Five samples of stainless steel sheets impregnated with the oils ISO 32, ISO 68 e ISO 220, were utilized in this research for analysis in the laboratory. The gases were detected in parts per million (ppm) and percentage (%) as measurements of concentration, with no influence of the quantity or volume of oil on the surface. An analysis of variance (Anova) or hypotheses test was applied to determine if there exists a difference in the percentages and part per million of the generated gases in the cleaning with low-pressure cold plasma, to contrast if the mean percentages of carbon monoxide and carbon dioxide and the parts per million of hydrocarbons, are equal with and without immersion in the degreaser; the gas with the greater contamination was further analyzed.

$H_0: \quad \mu_1 = \mu_2$ There is no difference between the levels of gases

$H_1: \quad \mu_1 \neq \mu_2$ There is a difference between the levels of gases

2.2.2. Process

A micropipette was used to place the contaminant oil for impregnating on the surface. As indicated in Figure 8, the tests to determine the contamination level according to the degree on cleanliness, were conducted out with and without immersion in the dissolvent of the test tube, prior to the application of the cold plasma.

Figure 8. Experimental procedure.

A pre-degreasing was carried out with an immersion in a solvent during 3 minutes, according to the quantity of oil to be removed in the lab test. In industrial treatments for cleaning AISI/SAE 304 steel, it is recommended from 30 to 60 minutes to eliminate organic compounds and remove inorganic compounds that may be present on the surface. Table 4 shows the properties of the used degreaser [21].

Table 4. Properties of the dissolvent [8].

Property	Value
Density	0,8 g/cm^3
Fusion temperature	-34 °C
Biling temperature	136 °C
Decomposition temperature	480 °C
Flamability	$<$ 37 °C

3. Results and discussion

Tables 5 and 6 present the levels of gases obtained in the cleaning of the surfaces of the metallic sheets impregnated with oil ISO 32, applying low-pressure cold plasma

Table 5. Values of the angle of contact and levels of gases with ISO 32 without immersion in degreaser

N.	Oil (ml)	Angle of contact	Test liquid (μl)	CO (%)	CO_2 (%)	HC (ppm)
1		16,76°		0,34	0,1	563
2		16,49°		0,38	0,1	576
3	0,1	17,14°	5	0,37	0,1	553
4		16,24°		0,38	0,1	585
5		17,32°		0,41	0,1	601

Table 6. Values of the angle of contact and levels of gases with ISO 32 with immersion in degreaser

N.	Oil (ml)	Angle of contact	Test liquid (μl)	CO (%)	CO_2 (%)	HC (ppm)
1		12,92°		0,34	0,1	1031
2		12,25°		0,33	0,1	1028
3	0,1	12,73°	5	0,34	0,1	1049
4		12,86°		0,34	0,1	995
5		12,27°		0,37	0,1	1026

An analysis of variance was carried out among the group of gases, carbon monoxide and hydrocarbons, to determine if there is a difference between the contamination levels of the obtained gases in the processes with and without immersion in the degreaser. The null hypothesis states that there is no difference between the groups analyzed with a level of significance $\alpha = 0.05$, obtaining the results presented in Tables 7 and 8.

Table 7. Single factor ANOVA. ISO 32 (CO)

Percentage of CO

	Sum of squares	gl	Cuadratic mean	F	Sig.
Inter-grupos	0,003	1	0,003	5,953	0,041
Intra-grupos	0,003	8	0,000		
Total	0,006	9			

Table 8. Single factor ANOVA. ISO 32 (HC)

ppm of HC

	Sum of squares	gl	Cuadratic mean	F	Sig.
Inter-grupos	506700,1	1	506700,10	1387,269	0,000
Intra-grupos	2922,0	8	365,25		
Total	509622,1	9			

As it can be seen in Tables 7 and 8, the p value (Sig.) is smaller than 0.05, which indicates a difference between the percentages of carbon monoxide and hydrocarbons in the processes with and without immersion in the degreaser, determining that there is a greater contamination when the previous immersion takes place. However, it also presents a better cleanliness, as seen in the values of angle of contact in Tables Tablas 5 y 6. The levels of carbon dioxide remained constant in the processes with and without immersion.

Tables 9 and 10 present the levels of gases obtained 563 in cleaning the surface of the stainless steel metallic impregnated with the ISO 68 oil.

Table 9. Values of the angle of contact and levels of gases with ISO 68 without immersion in degreaser.

N.	Oil (ml)	Angle of contact	Test liquid (μl)	CO (%)	CO_2 (%)	HC (ppm)
1		36,93°		0,50	0,2	1177
2		37,55°		0,50	0,2	1151
3	0,1	36,86°	5	0,48	0,2	1098
4		36,91°		0,49	0,2	1133
5		36,05°		0,37	0,2	1088

Table 10. Values of the angle of contact and levels of gases with ISO 68 with immersion in degreaser.

N.	Oil (ml)	Angle of contact	Test liquid (μl)	CO (%)	CO_2 (%)	HC (ppm)
1		16,03°		0,39	0,2	2068
2		16,52°		0,45	0,2	2214
3	0,1	16,35°	5	0,44	0,2	2315
4		16,96°		0,49	0,2	2185
5		16,83°		0,50	0,2	2220

An analysis with a confidence level of 95% was carried out, to determine if there is a difference between the contamination levels of the gases generated in cleaning of surface of the stainless steel sheets impregnated with the ISO 68 oil, in the processes with and without immersion in a degreaser liquid. Tables 11 and 12 present the results obtained.

Table 11. Single factor ANOVA. ISO 68 (CO)

Percentage of CO

	Sum of squares	gl	Cuadratic mean	F	Sig.
Inter-grupos	0,000	1	0,000	0,196	0,670
Intra-grupos	0,020	8	0,003		
Total	0,020	9			

Table 12. Single factor ANOVA. ISO 68 (HC)

ppm of HC

	Sum of squares	gl	Cuadratic mean	F	Sig.
Inter-grupos	286702,5	1	2867602,50	621,460	0,000
Intra-grupos	36914,4	8	4614,30		
Total	2904516,9	9			

The result in Table 11 presented a p value (Sig.) of $0.670 > 0.05$, thus the levels of carbon monoxide are the same in the processes with and without immersion in degreaser. On the other hand, Table 12 showed a p value (Sig.) of $0.000 < 0.05$, which indicates that the levels of hydrocarbons are different, showing an increment when a previous immersion is carried out; the levels of carbon dioxide remained constant, as can be seen in Tables 9 and 10.

Tables 13 and 14 include the levels of gases obtained when using low-pressure cold plasma to clean

the surfaces of the stainless steel sheets impregnated with ISO 220 oil, in processes with and without prior immersion in a degreaser liquid.

Table 13. Values of the angle of contact and levels of gases with ISO 220 without immersion in degreaser

N.	Oil (ml)	Angle of contact	Test liquid (μl)	CO (%)	CO_2 (%)	HC (ppm)
1		71,41°		0,47	0,2	1259
2		71,49°		0,45	0,2	1317
3	0,1	71,16°	5	0,47	0,2	1199
4		71,94°		0,49	0,2	1278
5		71,32°		0,50	0,2	1344

Table 14. Values of the angle of contact and levels of gases with ISO 220 with immersion in degreaser

N.	Oil (ml)	Angle of contact	Test liquid (μl)	CO (%)	CO_2 (%)	HC (ppm)
1		20,50°		0,51	0,4	1885
2		20,69°		0,52	0,3	1902
3	0,1	20,93°	5	0,51	0,4	1925
4		20,80°		0,50	0,4	1975
5		20,00°		0,51	0,4	1932

An ANOVA analysis was carried out to determine if there is a difference between the levels of the gases generated in cleaning of surface of the stainless steel sheets impregnated with the ISO 220 oil, with and without immersion in the degreaser. Tables 15 and 16 present the results obtained.

Table 15. Single factor ANOVA. ISO 220 (CO)

Percentage of CO

	Sum of squares	gl	Cuadratic mean	F	Sig.
Inter-grupos	0,003	1	0,003	13,442	0,006
Intra-grupos	0,002	8	0,000		
Total	0,005	9			

Table 16. Single factor ANOVA. ISO 220 (HC)

ppm of HC

	Sum of squares	gl	Cuadratic mean	F	Sig.
Inter-grupos	1038128,4	1	1038128,40	484,541	0,000
Intra-grupos	17140,0	8	2142,50		
Total	1055268,4	9			

Tables 15 and 16 indicate p values (Sig.) smaller than 0.05, thus it can be stated that there is a difference in the contamination levels when cleaning the surface of the metallic sheet impregnated with the ISO 220 oil, with and without immersion in degreaser before applying the low-pressure cold plasma

Table 17 presents the average of the results obtained in the contamination levels of the generated gases, when applying an oxygen plasma for cleaning the metallic sheets.

Table 17. Summary of the average values of angle of contact and level of generated gases

	ISO 32	ISO 68	ISO 220
WIRH IMMERSIN			
Angle of contact	12,606°	16.538°	20,584°
Percentage of CO	0,344	0,454	0,510
Percentage of CO_2	0,1	0,2	0,38
Parts per million de HC	1025,8	2200,4	1923,8
WITHOUT IMMERSION			
Angle of contact	16,79°	36,46°	71,464°
Percentage of CO	0,376	0,468	0,476
Percentage of CO_2	0,1	0,2	0,2
Parts per million de HC	575,6	1129,4	1279,4

4. Conclusions

The cleaning processes in AISI/SAE 304 stainless steel sheets using low-pressure cold plasma, with and without immersion in a degreaser prior to the application of the ionized gas exhibit differences in the levels of expelled gases. According to the average of the results, when removing ISO 32 oil from the surface with low-pressure cold plasma, the previous immersion in a degreaser aids in reducing the angle of contact 25%, which indicates a better quality cleaning of the surface, but the contamination levels show a variation, especially the hydrocarbons significantly increase 78.21% since the oil is removed from the surface together with the remains of degreaser, the level of carbon monoxide decreases 8.5% and the carbon dioxide remains constant. This indicates that for removing the ISO 32 oil it is not necessary a prior immersion, since without it an optimal angle of contact is obtained (less than 30°), and less contamination is generated.

When removing ISO 68 oil it was observed that with an immersion of the metallic sheets in degreaser before applying the cleaning process with low-pressure cold plasma, the level of hydrocarbons increases 95%, the percentage of carbon monoxide decreases % and the percentage of carbon dioxide remains constant with respect to the values obtained without previous immersion. The angle of contact decreases 54% with a previous immersion in degreaser before discharging the plasma, obtaining optimal values of cleanliness smaller than 30°.

When removing ISO 220 oil from the surface, it was observed an increase in the contamination levels in all generated gases when cleaning the metallic sheets with low-pressure cold plasma, if a prior immersion in degreaser was applied to reduce the angle of contact in 71% with respect to the process without immersion. The parts per million of hydrocarbons increased 50%, the percentage of carbon monoxide raised 7% and the carbon dioxide 90%.

In the cleaning of the surfaces of metallic sheets, the ISO 68 oil showed the greater average contamination in hydrocarbons with 2200.4 ppm at an average angle of contact of 16.53°. The ISO 220 oil showed the greater average contamination of carbon monoxide with 0.51% and of carbon dioxide with 0.38%.

References

[1] C. E. Fúquene Retamoso, *Producción limpia, contaminación y gestión ambiental.* Editorial Pontificia Universidad Javeriana, 2007. [Online]. Available: http://bit.ly/2YNLtud

[2] C. Frías and O. Pérez, "Recuperación de ácidos y metales en baños agotados del decapado de aceros inoxidables," *Revista de Metalurgia*, vol. 34, pp. 427–431, 1998. [Online]. Available: https://doi.org/10.3989/revmetalm.1998.v34.iExtra.786

[3] M. Villalobos, D. Peñalosa, M. Moscona, M. Cram, and F. Heydrich, "Opciones para el tratamiento y la disposición de los licores ácidos agotados provenientes del decapado de hierro," *Revista Internacional de contaminación ambiental*, vol. 6, no. 1, pp. 33–54, 1990. [Online]. Available: http://bit.ly/2WVmXa0

[4] E. Cano Díaz, J. Simancas Peco, L. Narvaéz, and J. M. Bastidas Rull, *Estudio de la corrosión del cobre por vapores de ácido acético al 40 y 80 % de humedad relativa.* Sociedad Española de Cerámica y Vidrio, 2004. [Online]. Available: http://bit.ly/2M48IOX

[5] N. Ipek, N. Lior, and A. Eklund, "Improvement of the electrolytic metal pickling process by inter-electrode insulation," *Ironmaking & Steelmaking. Processes, Products and Applications*, vol. 32, no. 1, pp. 87–96, 2005. [Online]. Available: https://doi.org/10.1179/174328105X23996

[6] R. d'Agostino, P. Favia, C. Oehr, and M. R. Wertheimer, "Low-temperature plasma processing of materials: Past, present, and future," *Plasma Processes and Polymers*, vol. 2, no. 1, pp. 7–15, 2005. [Online]. Available: https://doi.org/10.1002/ppap.200400074

[7] R. Nickerson, "Plasma surface modification for cleaning and adhesion," *AST Products, Inc*, vol. Billerica, MA. 01821, 1998.

[8] P. Sarmiento, L. López, A. Sarmiento, and J. Fajardo, "Efficiency of the low pressure cold plasma in the cleaning of steel for subsequent covering," *VI Andean Region International Conference (ANDESCOM)*, vol. 5, pp. 115–118, 2012. [Online]. Available: https://doi.org/10.1109/Andescon.2012.35

[9] D. Y. Kwok and A. W. Neuman, "Contact angle measurement and contact angle interpretation," *Advances in Colloid and Interface Science*, vol. 81, no. 3, pp. 167–249, 1999. [Online]. Available: https://doi.org/10.1016/S0001-8686(98)00087-6

[10] D. O. Njobuenwu, E. O. Oboho, and R. H. Gumus, "Determination of contact angle from contact area of liquid droplet spreading on solid substrate," *Electronic Journal of Practices and Technologies*, vol. 6, no. 10, pp. 29–38, 2007. [Online]. Available: http://bit.ly/2M34F5K

[11] M. Zenkiewicz, "Methods for the calculation of surface free energy of solids," *Journal of Achievements in Materials and Manufacturing Engineering*, vol. 24, no. 1, pp. 137–145, 2007. [Online]. Available: http://bit.ly/2ErRPYn

[12] J. R. Roth, *Industrial Plasma Engineering.* CRC press. Taylor Francis Group, 2001, vol. 2. [Online]. Available: http://bit.ly/2EoRPZi

[13] F. Gordillo. (2008) Plasmas fríos. Investigación y Ciencia. [Online]. Available: http://bit.ly/2HQqZtV

[14] E. Fuster, "Aplicación de plasma atmosférico en tratamiento superficial de metales para utilización de adhesivos estructurales," Master's thesis, Universidad Politécnica de Valencia, 2016. [Online]. Available: http://bit.ly/2JzOxq5

[15] G. Neira Arenas and L. A. Cañas M, "Procedimiento para medir ángulos de contacto en sólidos particulados finos," *Scientia et Technica*, vol. 1, no. 36, pp. 883–887, 2007. [Online]. Available: http://dx.doi.org/10.22517/23447214.5159

[16] J. M. Ruiz-Cabello, "Efecto de la rugosidad y heterogeneidad superficial en fenómenos de mojado," Ph.D. dissertation, Universidad de Granada, 2009. [Online]. Available: http://bit.ly/2VJYgvu

[17] Diener. (2016) Introducción al plasma. Diener electronic. Plasma-Surface-Technology. [Online]. Available: http://bit.ly/2M1zs2C

[18] D. Galán and R. Fernández, "Implicación de los nox en la química atmosférica," *Revista electrónica de medioambiente UCM*, vol. 2, pp. 90–103, 2006. [Online]. Available: http://bit.ly/2JDI8KC

[19] J. D. Escrig Zaragozá, *El impacto ambiental de las actividades industriales: el cambio necesario.* Universidad Internacional de Andalucía, España, 2008. [Online]. Available: http://bit.ly/2EtFjrv

[20] Z. Navrátil, V. Buršíková, P. St'ahel, M. Šíra, and P. Zvěřina, "On the analysis or surface fre energy of dlc costings deposited in low pressure rf discharge," *Czechoslovak Journal of Physics*, vol. 54, no. 3, pp. 29–38, C877 2004. [Online]. Available: https://doi.org/10.1007/BF03166502

[21] Grupo Böhler, *Libro del decapado. Tratamientos superficiales del acero inoxidable.* Grupo Böhler Soldadura España, 2017. [Online]. Available: http://bit.ly/2EsgJXL

Scientific Paper / Artículo Científic

UNIVERSIDAD POLITÉCNICA SALESIANA ECUADOR
INGENIUS
Revista de Ciencia y Tecnología
https://doi.org/10.17163/ings.n22.2019.03
pISSN: 1390-650X / eISSN: 1390-860X

Evaluation of turbulence models for the air flow in a planar nozzle

Evaluación de modelos de turbulencia para el flujo de aire en una tobera plana

San Luis B. Tolentino Masgo[1,*,2]

Abstract

In gas flows at supersonic speeds, shock waves, flow separation and turbulence are produced due to sudden changes in pressure. The behavior of the compressible flow can be studied by using experimental equipment or by numerical methods with codes of the computational fluid dynamics (CFD). In the present work, the air flow is simulated in a 2D computational domain with the ANSYS-Fluent code version 12.1 for the geometry of a planar nozzle, using the Reynolds averaged Navier-Stokes (RANS) equation, with the objective of evaluating five turbulence models: SST $k-\omega$, $k-e$ standard, $k-\omega$ standard, $k-kl-\omega$ of transition and RSM. Numerical results of static pressure profiles were obtained for the walls of the nozzle and of the shock wave forms in the flow field, for two conditions of pressure ratios $rp = 2.008$ and $rp = 3.413$, which were compared with the experimental data of Hunter's work. It is concluded that the numerical results obtained with the turbulence model SST $k-\omega$ of Menter (1994) are more adjusted to the experimental data of static pressure and shock wave forms.

Keywords: Air flow, turbulence models, Shock wave, Static pressure, Planar nozzle, supersonic speed.

Resumen

En los flujos de gas a velocidades supersónicas se producen ondas de choque, separación del flujo y turbulencia debido a cambios repentinos de la presión. El comportamiento del flujo compresible se puede estudiar mediante equipos experimentales o por métodos numéricos con códigos de la dinámica de fluidos computacional (DFC). En el presente trabajo, el flujo de aire se simula en un dominio computacional 2D con el código ANSYS-Fluent versión 12.1 para la geometría de una tobera plana, utilizando la ecuación de Navier-Stokes de número de Reynolds promedio (NSRP), con el objetivo de evaluar cinco modelos de turbulencia: SST $k-\omega$, $k-e$ estándar, $k-\omega$ estándar, $k-kl-\omega$ de transición y RSM. Se obtuvieron resultados numéricos de perfiles de presión estática para las paredes de la tobera y de formas de ondas de choque en el campo de flujo, para dos condiciones de relaciones de presión $rp = 2,008$ y $rp = 3,413$, los cuales fueron comparados con los datos experimentales del trabajo de Hunter. Se concluye que los resultados numéricos obtenidos con el modelo de turbulencia SST $k-\omega$ de Menter (1994) están más ajustados a los datos experimentales de presión estática y de formas de ondas de choque.

Palabras clave: flujo de aire, modelos de turbulencia, onda de choque, presión estática, tobera plana, velocidad supersónica.

[1,*]Departamento de Ingeniería Mecánica, Universidad Nacional Experimental Politécnica "Antonio José de Sucre" Vice-Rectorado Puerto Ordaz, Bolívar, Venezuela. Autor para correspondencia ✉: sanluist@gmail.com
http://orcid.org/ 0000-0001-6320-6864
[2]Grupo de Modelamiento Matemático y Simulación Numérica, Universidad Nacional de Ingeniería, Lima, Perú.

Received: 24-02-2019, accepted after review: 13-05-2019

Suggested citation: Tolentino Masgo, S. L. B. (2019). «Evaluation of turbulence models for the air flow in a planar nozzle». Ingenius. N.° 22, (july-december). pp. 25-37. doi: https://doi.org/10.17163/ings.n22.2019.03.

1. Introduction

Experimental studies of the behavior of compressible flow at supersonic speeds, are carried out in nozzles with different geometries in the divergent cross section, namely circular, oval, and rectangular among others. When a sudden change in pressure occurs in the divergent section of the nozzle, a shock wave is produced which causes that properties of the fluid such as temperature, velocity, density, among others, vary as a consequence of decompression and compression of the flow. The Mach number is the dominant parameter in the analysis of this type of flow.

Schlieren technique is a manner to obtain the shape of the shock wave, the turbulences and the separation of the flow from the nozzle walls. Such technique is recurrently employed in the field of high velocity flow, and was proposed by the German physicist August Topler in 1864 [1], who was the first to visualize the shape of the wave. It uses an optical process to capture images of the variation of the density.

The images and physical parameters of the compressible flow that are obtained in the lab, are of great importance to know its nature when subject to different variations of pressure and temperature. The magnitude of the physical parameters are obtained by direct observation, and the magnitude of other thermodynamic properties are obtained using empirical equations or mathematical models.

In the literature there are works reported about the limit layer of compressible flow [2]; the limit layer with different conditions of pressure gradient [3]; normal and oblique shock waves, Prndtl-Meyer expansive waves [4, 5] and turbulence [6].

The behavior of compressible flow can be reproduced using computational fluid dynamics (CFD) codes [7, 8], which employ mathematical models of governing equations and turbulence models [9] coupled in the equation of momentum.

Among the different geometry of laboratory experimental nozzles, it has been chosen to study the compressible flow for a flat nozzle. Figure 1 shows an image of its geometry (Hunter [10]).

Based on the one-dimensional theory, the flat nozzle shown in the image has a mean angle of 11.01° in the divergent section, which is considered to be out of design with respect to its geometry. This nozzle was designed for a pressure relationship rp=8.78 at the outlet of the divergent section, for a Mach number 2.07 and a pressure of 102.387 kPa (14.85 psi) at the inlet of the convergent section, for a stagnation temperature of 294.444 °K (530 °R) in the throat, for a Reynolds number $3,2 \times 10^6$ [10].

It can be pointed out that the mean angle of design of the divergent section for conic nozzles is typically in the range 12-18° [11], and the same principle applies for flat nozzles.

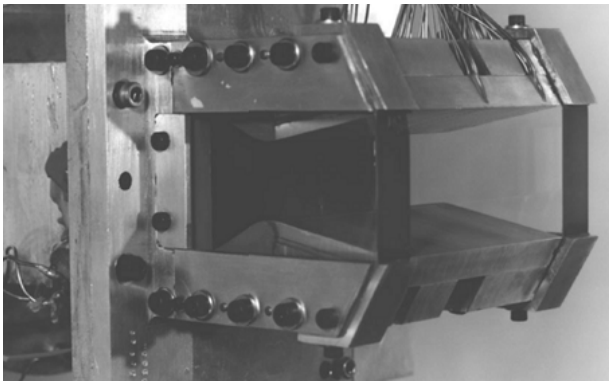

Figure 1. Photograph of a convergent-divergent flat nozzle (Hunter [10]).

Hunter [10] reported experimental results of static pressure measured at the wall of the flat nozzle, for the range of pressure relationship $rp = 1.255 - 9.543$. In addition, the flow of air was simulated for the geometry of the flat nozzle, using three turbulence models, namely Shih-Zhu-Lumley (SZL) [12], Gatski-Speziale (GS) [13] and Girimaji [14], which were compared with the experimental data of pressure for $rp = 3$, and the model SZL showed the best results.

Balabel [15] simulated the flow for the geometry of the flat nozzle [10], with the turbulence models standard $k-e$ [16], extended $k-e$ [17], v^2-f [18], realizable $v^2 - f$ [19], SST $k - \omega$ [20] and RSM [21], and compared the obtained numeric curves with experimental data of static pressure for $rp = 1.255$, $rp = 2.412$ and $rp = 5.423$. In addition, the flow was simulated using the SST turbulence model for low and high Reynolds number, also comparing with experimental data for $rp = 2.412$ and $rp = 5.423$. Based on the results, the SST $k-\omega$ turbulence model best fits the experimental data.

Besides, the geometry of the flat nozzle [10] was also used by Toufique [22], who simulated the flow with the standard $k - \omega$ turbulence model [23], and compared the shapes of the shock waves obtained with experimental data, for $rp = 2.4$ and $rp = 3.0$. Results showed that the width of the Mach disc is slightly smaller than the experimental Mach disc. Kotteda *et al.* [23] also studied the flow for different relationships of pressure and area and simulated the 2D flow with the Sparlat-Allmaras turbulence model, obtaining different configurations of the shape of the shock waves.

Other relevant works for flat nozzles with different dimensions than the flat nozzle studied by Hunter [10], are now mentioned. Forghany *et al.* [24] conducted a 2D computational research of the aerodynamic effects in the vectorization of the thrust by fluid, observing that the free flow reduces the vectorization performance and the thrust efficiency, compared to the static condition without wind.

Shimshi *et al.* [25] used experiments and 2D simulations to study the flow separation for a high Mach

number in the divergent section, and found that the transition to the asymmetric separation resulted in the jet joining the nozzle wall, and the inverse transition is accompanied by a hysteresis effect. Arora *et al.* [26] conducted experiments for the flow in a nozzle with double divergent section, observing that the angle between the two sections influences the structure of the collision.

Sivkovik *et al.* [27] conducted experiments and 2D simulations of the flow under vector control, aiming to establish a methodology of the geometry of the flow. Martelli *et al.* [28] simulated for an asymmetric 3D flow, and reported the instability of the collision and the frequency of the characteristics. Kostic *et al.* [29] simulated the 2D flow for the vector control of the thrust with different positions, obtaining the direction of the thrust force and losses.

Verma *et al.* [30] studied the unstable nature of the structure of the collision, and the results showed that the fluctuations of the pressure on the wall are accompanied of a resonance, and that the tones of such resonance ted to disappear as the pressure relationship increases and the limit layer experiments a transition.

In this work, the behavior of the flow of air in an experimental flat nozzle is simulated in a 2D computational domain [10] for five turbulence models, in order to evaluate and determine which of them produces numeric results closer to the available experimental data of static pressure and shape of the shock waves, reported in the work by Hunter [10] for $rp = 2.008$ and $rp = 3.413$.

In addition, the mathematical fundamentals, simulation results and comparison with experimental data are also presented, as well as the comparison of the numerical and experimental shapes of the shock waves. At last, the conclusions of the analysis conducted are exposed.

2. Materials and methods

2.1. Mathematical fundamentals

The four equations of fluid dynamics that govern stationary flow are the mass conservation equation

$$\nabla \cdot (\rho \vec{u}) = 0 \tag{1}$$

the energy conservation equation

$$\nabla \cdot (\rho u u) = -\nabla P + \nabla \cdot (\bar{\bar{\tau}}) \tag{2}$$

the equation of momentum

$$\nabla \cdot (\vec{u}(\rho E + P)) = \nabla \cdot (k_{eff} \nabla T + (\bar{\bar{\tau}}_{eff} \cdot \vec{u})) \tag{3}$$

and the state equation

$$\frac{\partial \rho}{\partial p} = \frac{1}{RT} \tag{4}$$

Where the tensor of tensions is expressed as $\bar{\bar{\tau}} = \mu \left[(\nabla \vec{u} + \nabla \vec{u}^T) - \frac{2}{3} \nabla \cdot \vec{u} I \right]$, with I the unit tensor, the energy is expressed as $E = h - \frac{P}{\rho} + \frac{u^2}{2}$, ρ is the density, u is the velocity, $\vec{u}$ is the velocity vector, P is the pressure, μ is the viscocity, h us the enthalpy, R is the gas constant and T is the temperature. In addition, k_{eff} is the effective conductivity, which is a function of the turbulent thermal conductivity k_t and the effective tensor of tensions $\bar{\bar{\tau}}_{eff}$.

For compressible flow, the relation of pressures and temperatures as a function of Mach number M are given by

$$\frac{P_0}{P} = \left(1 + \frac{\gamma - 1}{2} M^2 \right)^{\frac{\gamma}{\gamma - 1}} \tag{5}$$

and

$$\frac{T_0}{T} = 1 + \frac{(\gamma - 1)}{2} M^2 \tag{6}$$

respectively, where the parameters are total pressure P_0, total temperature T_0, Mach number$M = \frac{u}{c}$ and speed of sound $c = \sqrt{\gamma RT}$, where R is the gas constant and $\gamma = \frac{C_p}{C_v}$ is the relation of specific heat. Considerations on the Mach number are the following: for incompressible flow $M < 0.3$, subsonic flow $0.3 < M < 0.8$, transonic flow $0.8 < M < 1.2$, supersonic flow $1.2 < M < 3$ and hypersonic flow $M > 3$; and for flow with sonic velocity, $M = 1$ [5].

The variation of the viscosity of gases as a function of temperature can be approximated according to Sutherland law as [5].

$$\frac{\mu}{\mu_0} = \left(\frac{T}{T_0} \right)^{\frac{3}{2}} \frac{T_0 + S}{T + S} \tag{7}$$

where $\mu_0 = 1,716\ kg/(m.s)$, is the reference viscosityia $T_0 = 273,11\ K$, is the reference temperature and $S = 110,56\ K$ is the effective temperature.

There are different turbulence models reported in the literature, with their respective mathematical descriptions. The turbulence models are semi-empirical transport equations that describe the mixing and diffusion that increase due to turbulent eddies, as a function of the viscosity of the fluid and the turbulent viscosity, among other variables. The models of turbulence are coupled in the linear equation of momentum, and the tensor of tensions is a function of viscosity. This mathematical expression is the Average Reynolds number Navier-Stokes equation (RANS). Besides RANS, there is the large eddies simulation model (LES) and the direct numerical simulation model (DNS). Initial research works about turbulence were conducted by Kolmogorov (1941), based on the results obtained by Reynolds (1883).

The five turbulence models used in numerical simulations by means of RANS are SST $k-\omega$ by Menter [20], standard $k-e$ by Launder and Spalding [16], standard

$k-\omega$ by Wilcox [31] and transition $k-kl-\omega$ by Walters and Cokljat [32], which are based in the turbulent viscosity and are supported by Boussinesq hypothesis. The RSM turbulence model by Launder *et al.* [21] for the pressure linear tension [33] and the effects of wall reflection [34] is supported in the tensions models by Reynolds.

2.2. Computational domain, meshing and boundary conditions

The geometry of the flat nozzle [10] studied in this work is shown in Figure 2, and the dimensions of the points of reference can be seen in Table 1.

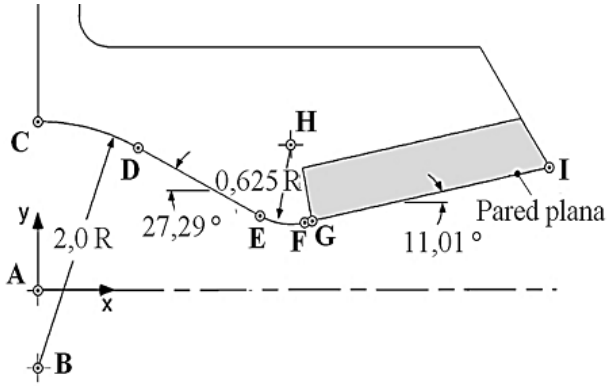

Figure 2. Schematic representation of the flat nozzle projected on the Cartesian xy plane. Adapted from Hunter [10].

Table 1. Dimensions in inches and in millimeters of the points of reference of the flat nozzle. Adapted from Hunter [10]

	Coordinate (in)		Coordinate (mm)	
Points	**x**	**y**	**x**	**y**
A	0,000	0,000	0,000	0,000
B	0,000	-0,614	0,000	-15,595
C	0,000	1,386	0,000	35,204
D	0,917	1,163	23,291	29,540
E	0,988	0,611	25,095	15,519
F	2,394	0,553	60,807	14,046
G	2,430	0,559	61,722	14,198
H	2,275	1,166	57,785	29,616
I	4,550	0,972	115,57	24,688

The geometry of the 2D computational domain can be seen in Figure 3, which is projected in the Cartesian xy plane, considering adiabatic the walls of the domain. The flow for this section was simulated due to the symmetry it possesses. The geometry of the nozzle is constructed with the dimensions in Table 1.

Before the convergent section, there is a straight segment of length $x = -25.4\ mm$; the nozzle starts at $x = 0.0\ mm$, the throat is located at $x = 57.785\ mm$, and the divergent section of the nozzle ends at $x = 115.57\ mm$; the length of the section of the atmosphere ends at $x = 471.17\ mm$.

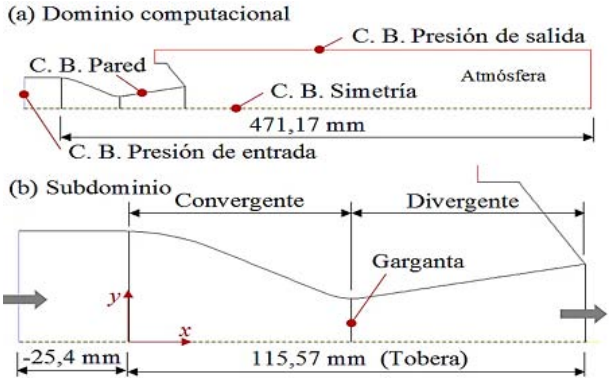

Figure 3. (a) Computational domain. (b) Subdomain: flat nozzle.

Figure 4 shows the meshed domain, which is structured in a total of 20290 quadrilateral cells. The mesh was refined towards the walls of the straight section and of the convergent-divergent section, due to the presence of shear stress in those regions.

The meshing was implemented in the ANSYS-Meshing platform, and the domain was discretized by means of the interaction ICEM-CFD. The dimensioning included: smoothing, medium; center of the expansion angle, fine; curvature of the normal angle, 18°; minimum size, 0.000249 m; maximum size of the surface, 0.0249 m; maximum size, 0.0499 m; growth relationship, 1.2; and minimum length of the boundary, 0.000914 m. For the inflation: transition relationship, 0.272; maximum layers, 2; and grow relationship, 1.2.

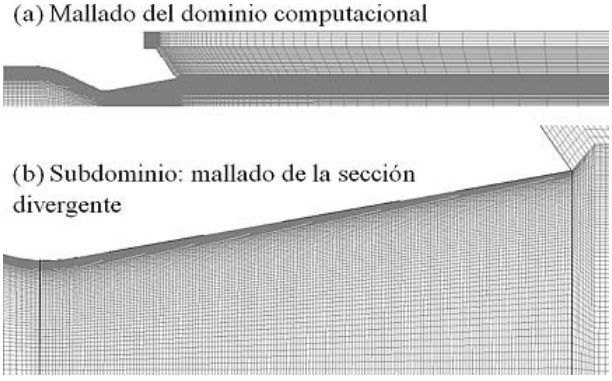

Figure 4. (a) Computational domain meshed with 20 290 quadrilateral cells. (b) Meshed of the divergent section with 11 270 quadrilateral cells.

It is important to mention that, in order to obtain a good quality of the mesh, it should be assured that each cell is not very biased, since this can generate difficulties and inaccuracies in the convergence of the numerical solutions. The most appropriate type of bias for bi-dimensional cells is the equiangular bias with Q_{EAS}, where $0 \leq Q_{EAS} \leq 1$ for any 2D cell, where

an equilateral triangle, and a square or rectangle have zero bias [35]. For the mesh with quadrilateral cells in the domain shown in Figure 4, $Q_{EAS} = 0$ for 98 % of the total cells and $Q_{EAS} = 0.3$ for the remaining 2 % of cells, resulting in a good quality mesh of the computational domain.

As part of a numerical convergence study, the mesh shown in Figure 4 yielded a satisfactory result with a final Mach number 2.0036 at the end of the divergent section in the axial symmetry, at the distance 115.57 mm for $rp = 8.78$, and using a SST $k - \omega$ turbulence model. This is an acceptable value when compared to the design value Mach 2.07 obtained by Hunter [10] at the outlet of the flat nozzle.

The initial and boundary conditions were established as:

- At the atmosphere, the outlet pressure is the total pressure $P_{atm} = 102,387kPa$ (14,85 psi),and the total temperature $T_{atm} = 294,444K$ (530 °R).
- The total inlet pressure of the flow is established for two cases of pressure relationships $rp = 2,008$ y $rp = 3,413$ being the total input pressure $P_0 = rp \cdot P_{atm}$.
- The total inlet temperature $T_0 = 294,444K(530°R)$, is of equal magnitude than the temperature at the atmosphere. Due to the symmetry of the domain in the x axis, in the direction of the y axis the flow velocity is zero.
- The speed of the flow is zero in the adiabatic walls.

where the pressure and temperature data for $rp =$ 2.008 and $rp = 3.413$, have been taken from Hunter [10].

2.3. Method of computational solution and equipment

The code ANSYS-Fluent version 12.1, which applies the finite volume method (FVM), was used for the numerical solutions of the flow of air. Among the different solution alternatives, it was chosen the option of analysis based in the density for a compressible fluid, and 2D symmetry in the Cartesian xy plane.

In each numerical simulation, a unique turbulence model was chosen in the following order: SST $k - \omega$, standard $k - e$, standard $k - \omega$, transition $k - kl\omega$ and RSM, for a total of five models. Sutherland equation was selected for the viscosity of the fluid as a function of temperature. The option Second Order Upwin was selected under the flow conditions, for the turbulence of the kinetic energy and for the type of specific dissipation. For the control solution, a Courant number equal to 2 was determined, keeping the default relaxation factors. A fixed value of 0.00001 was determined for the residual monitor, for continuity, velocity and energy. The final results for the steady-state flow conditions were obtained after 9000-14 000 iterations.

A Síragon Laptop, model M54R, Intel Core 2 Duo, two 1.8 GHz processors and 3 GB of RAM memory, was employed for processing the data obtained in the numerical simulations.

3. Results and discussion

3.1. Comparison of the static pressure profiles with experimental data

In this section, the numerical curves of static pressure obtained for the five turbulence models, namely SST $k - \omega$, standard $k - e$, standard $k - \omega$, transition $k - kl - \omega$ and RSM, were compared with experimental data of static pressure from the work by Hunter [10], for $rp = 2.008$ and $rp = 3.413$, respectively. The profiles of static pressure correspond to the pressures along the nozzle wall, starting at the inlet of the convergent section and ending at the outlet of the divergent section.

Figure 5 shows the static pressure profiles for $rp = 2.008$, where during the drop and after a slight increase in the static pressure, the five numerical curves are close and are superimposed with the experimental data up to an estimated position $x = 70\ mm$. Following these distance the numerical curves become apart with respect to each other, and then become closer in the way to the outlet of the divergent section.

In the extended detail shown in Figure 6, it can be observed how the trajectories of the numerical curves evolve after $x = 70\ mm$, where the static pressure starts to increase, thus starting the separation of the flow from the wall/ The numerical curve corresponding to SST $k - \omega$ is closer to the experimental data. The RSM numerical curve exhibits an oscillatory behavior on the experimental data of pressure. The standard $k - \omega$ numerical curve has a behavior parallel to the SST $k - \omega$ curve in the upper part. At last, the numerical curves standard $k - e$ and transition $k - kl - \omega$ are very far from the experimental data in the lower part, where the minimum pressure drop occurs.

Figure 7 shows the static pressure profiles for $rp = 3.413$, which are close to the experimental data up to $x = 95\ mm$, after which they become separate.

In the extended detail shown in Figure 8, it can be observed how the trajectories evolve after $x = 70\ mm$. Then, after $x = 95\ mm$, the standard $k - \omega$ and the SST $k - \omega$ turbulence models are superimposed, with a slight separation in the vertical direction and close to the experimental data; however, with respect to these two numerical curves, the RSM one is closer to the experimental data with small oscillations in the upper part, the standard k-e is closer in the lower part,

and the transition $k - kl - \omega$ numerical curve is the farthest from the experimental data.

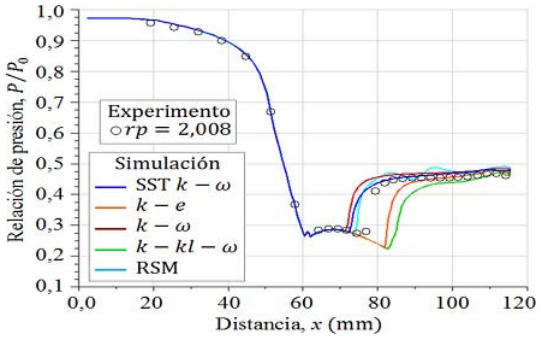

Figure 5. Profiles of static pressure at the wall, for rp=2,008.

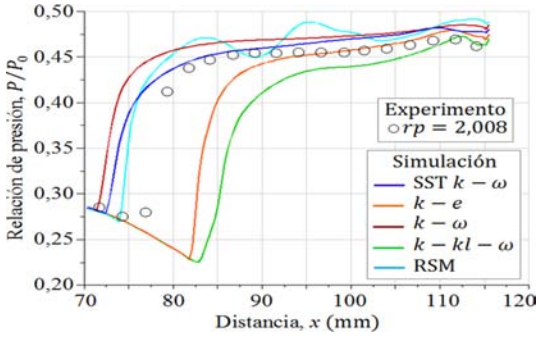

Figure 6. Extended detail of a section of Figure 5.

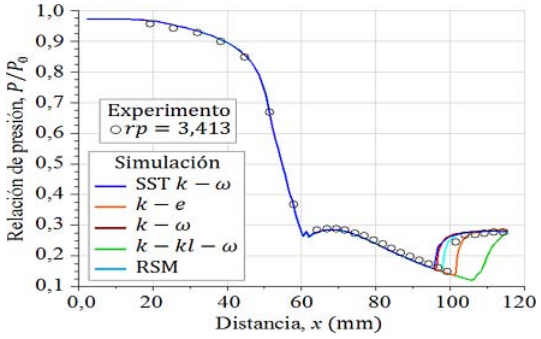

Figure 7. Profiles of static pressure at the wall, for $rp = 3,413$.

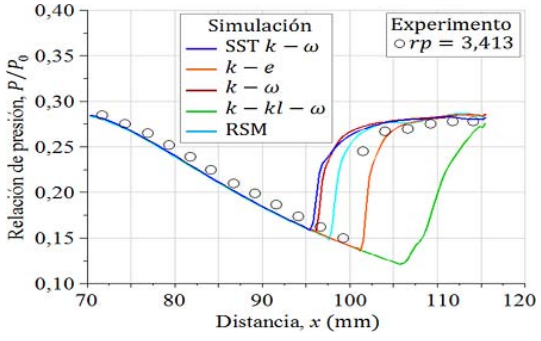

Figure 8. Extended detail of a section of Figure 7.

From the comparison of the numerical curves in Figures 5 and 7, with respect to the experimental data of static pressure of the flat nozzle from the work by Hunter [10], the turbulence model SST $k - \omega$ by Menter [20] better approximates such experimental data.

3.2. Comparison of the numerical and experimental shapes of the shock waves

The numerical simulations of the flow field with presence of shock waves in the flat nozzle, obtained for the five turbulence models are shown in Figures 9 and 10 for $rp = 2.008$, and in Figures 11 and 12 for $rp = 3.413$.

The flow of air with $rp = 2.008$ in the divergent section is over expanded, thus the shock wave is present and it can be seen which regions show the Mach disc, the oblique collision, the reflected oblique collision and the beginning of the flow separation, identifying regions in which the flow is supersonic, transonic and subsonic. The over expanded flow is characteristic when the flow decelerates in the divergent section due to an abrupt increase in the pressure, passing from a supersonic to a subsonic velocity when the collision occurs.

As the pressure of the flow increases at the inlet of the nozzle, the shock wave moves to the outlet of the nozzle. Similarly, the flow of air with $rp = 3.413$ is shown, and the over expanded flow in the divergent section also presents the Mach disc and the reflected oblique collision outside the nozzle; the divergent section is in the range of $x/x_t = 1.0 - 2.0$, where x_t is the variable distance from the position of the throat to the outlet of the nozzle, in the range 57.785-115.57 mm.

For each case, from the beginning of the flow separation downstream for the flow adjacent to the nozzle wall, a recirculation of flow is produced due to the pressure drop. As a consequence, an amount of air mass from the atmosphere is forced to enter grazing the nozzle wall.

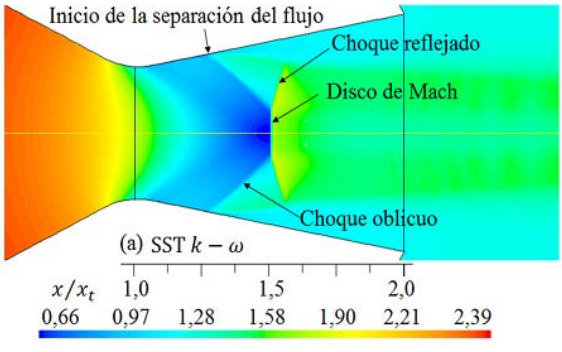

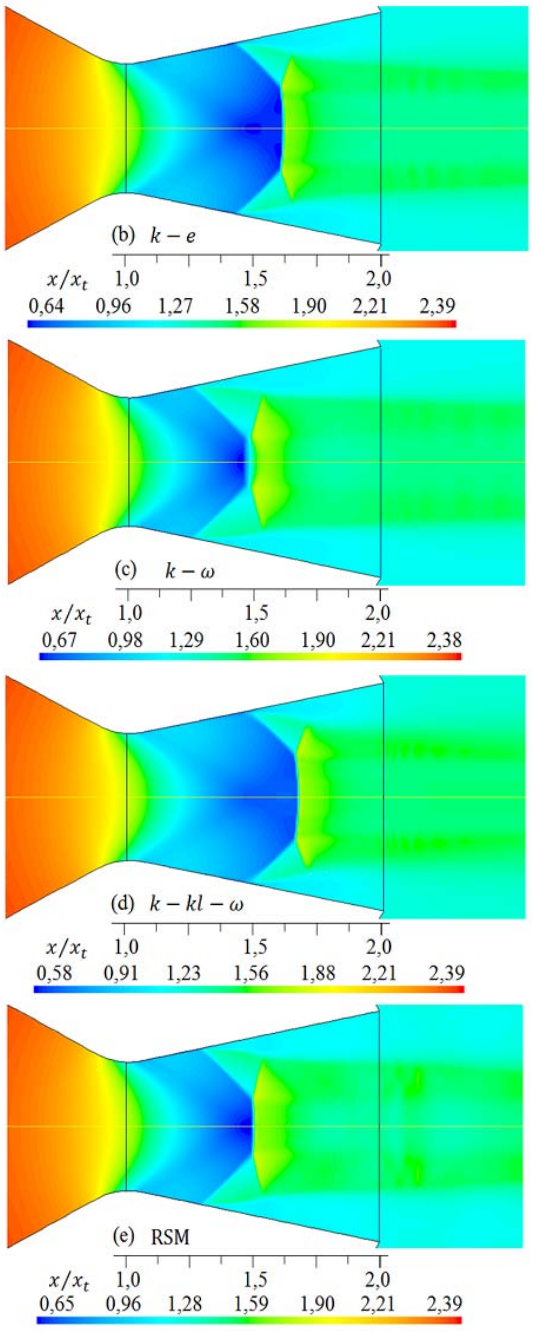

Figure 9. Shapes of the shock waves for different turbulence models. Density (kg/m^3) of the flow for $rp = 3,413$.

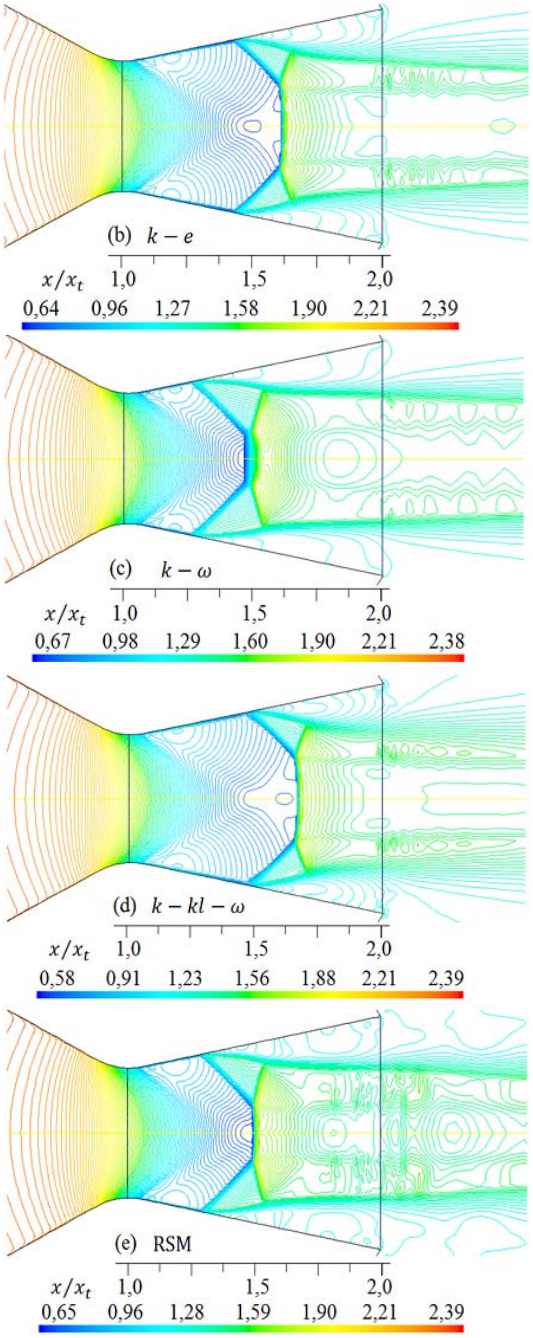

Figure 10. Shapes of the shock waves for different turbulence models. Contour lines of density (kg/m^3) for $rp = 3,413$.

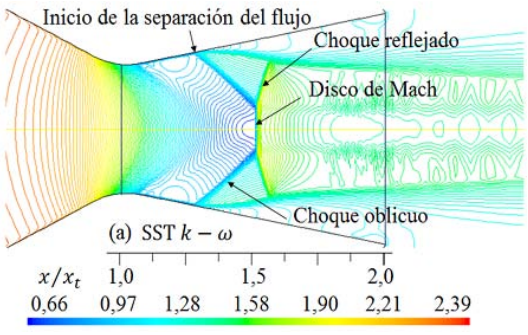

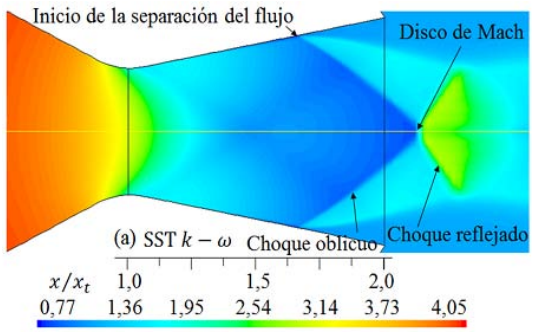

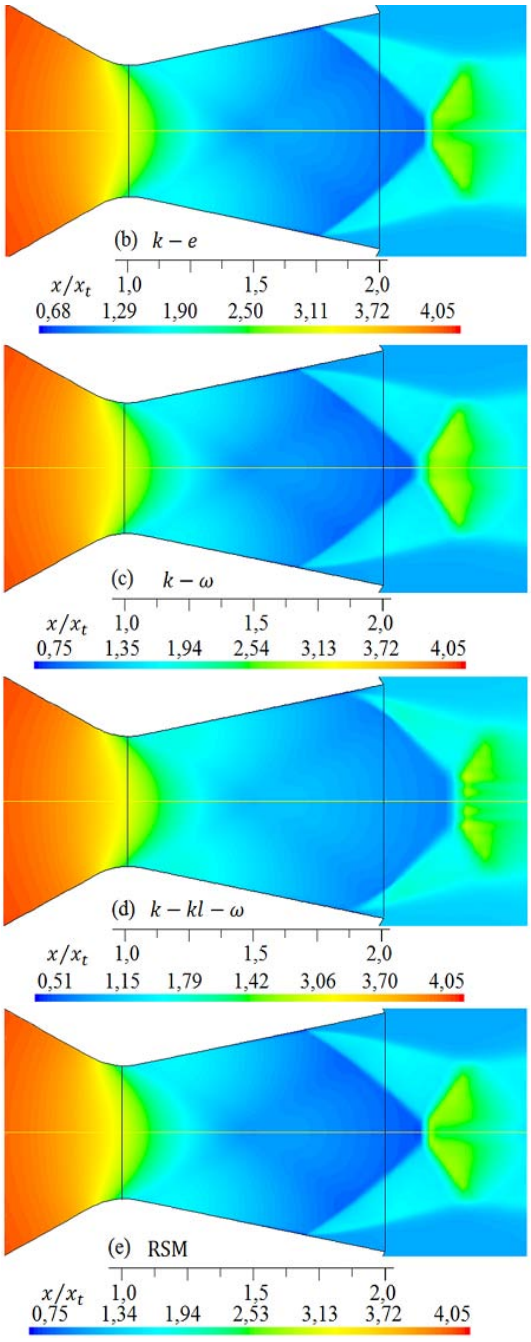

Figure 11. . Shapes of the shock waves for different turbulence models. Density (kg/m^3) of the flow for $rp = 3,413$.

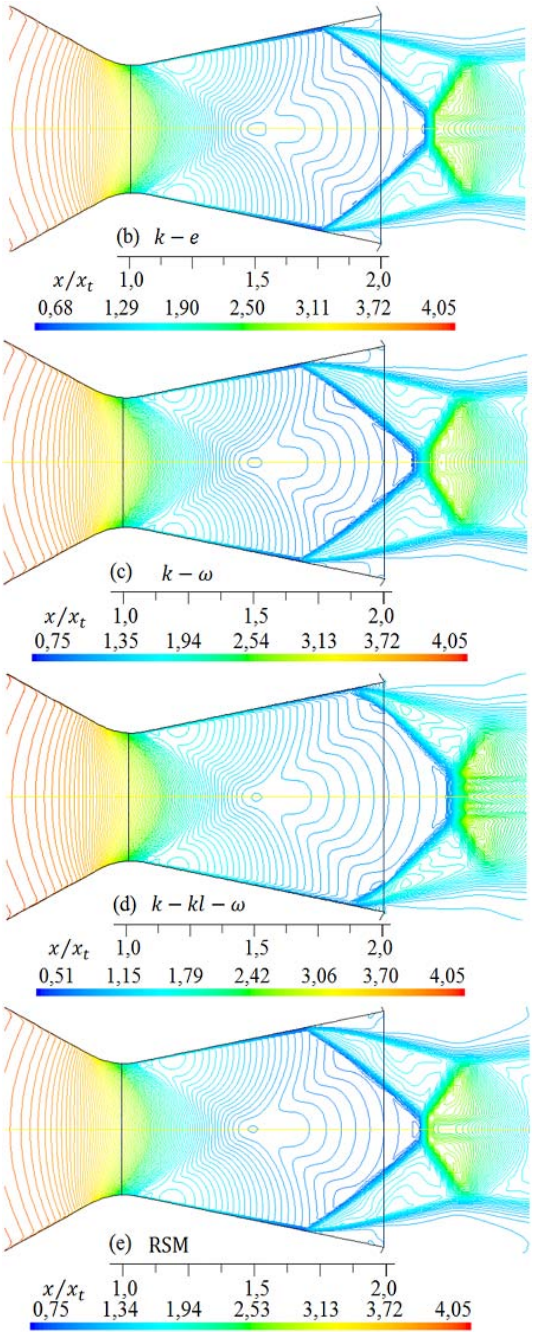

Figure 12. Shapes of the shock waves for different turbulence models. Contour lines of density (kg/m^3) for $rp = 3,413$.

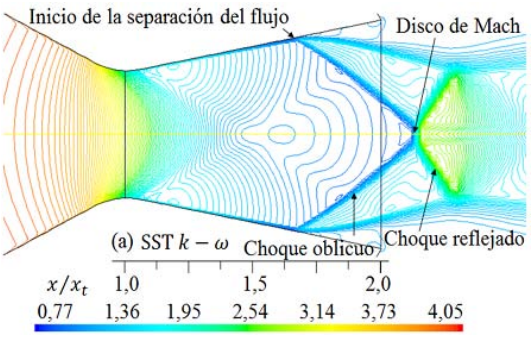

The profiles of the densities of flow obtained along of the symmetry in the direction of the x axis for the five models of turbulence, are shown in Figure 13 for $rp = 2.008$, and in Figure 14 for $rp = 3.413$. For each case, it is seen the behavior of the trajectories of the numerical curves, the decrease and increase in the density where the shock wave is present.

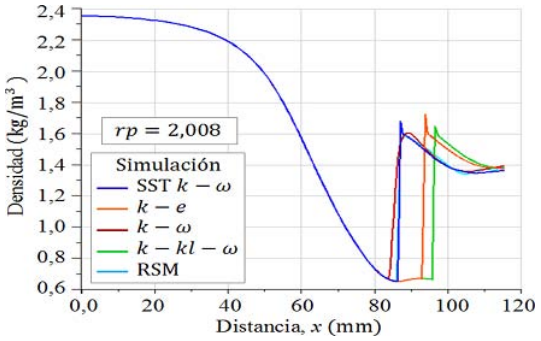

Figure 13. Density profiles evaluated at the symmetry of the x axis, for $rp = 2,008$.

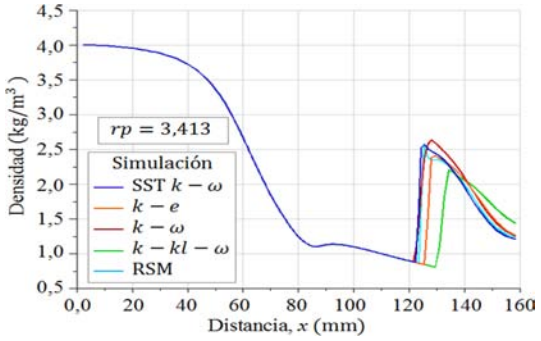

Figure 14. Density profiles evaluated at the symmetry of the x axis, for $rp = 3,413$.

After comparing the numerical results of the shapes of the shock waves in Figures 9 y 10 for $rp = 2.008$, with the shape of the experimental shock wave captured with Schlieren technique that can be observed in Figure 15 (from the work by Hunter [10]), it is seen that for the SST $k - \omega$ turbulence model, the Mach disc at the position $x/x_t = 1.5$, the oblique collision, the reflected collision and the beginning of flow separation, are similar to the experimental results. With respect to the other numerical results of the shapes of the shock waves, some are displaced to the left and some to the right, thus the Mach disc moves to the position $x/x_t = 1.5$. It can be pointed out that the Mach discs, which correspond to a normal wavefront, vary their width for each model of turbulence.

Similarly, comparing the shapes of the shock waves shown in Figures 11 and 12 for $rp = 3.413$, with the shape of the experimental shock wave in Figure 16, it can be seen that the SST $k-\omega$ turbulence model better fits the experimental result, although the Mach disc outside the nozzle is of smaller length with respect to the shape of the experimental shock wave. The other shapes of the numerical shock waves are displaced, some to the left and others to the right, thus the same will occur with the Mach disc.

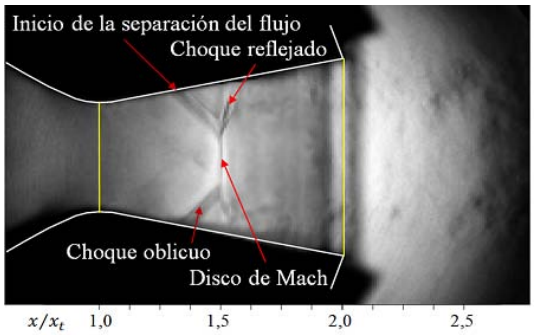

Figure 15. Shape of the shock wave for $rp = 2.008$. Adapted from the work by Hunter [10].

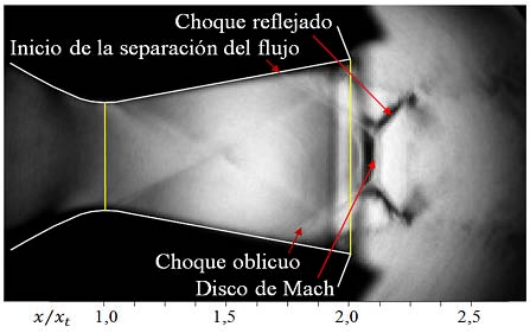

Figure 16. Shape of the shock wave for $rp = 3.413$. Adapted from the work by Hunter [10].

As shown in Figures 9 to 12, the shock waves vary their shape according to the turbulence model employed in the simulations, and the beginning of the flow separation is not kept at a fixed position.

The experimental Mach disc for $rp = 2.008$ is at $x/x_t = 1.5$, with location $x = 86.677\ mm$, where $x_t = 57.785\ mm$. Due to difference in density, which can be appreciated by the gray scale, it can be seen that there is a thickness of the shock wave, since the flow suddenly goes from a low to a high pressure, thus the velocity of the flow suddenly decelerates in a time instant. The same occurs for the shock wave present outside of the nozzle for $rp = 3.413$ at $x/x_t = 2.11$, with location $x = 122.06\ mm$.

The numerical simulations have given for each Mach disc, the thicknesses of the wavefront in the x axis symmetry of the compressible flow domain, the position and the percentage of displacement, which are shown in Table 2 for $rp = 2.008$ and in Table 3 for $rp = 3.413$.

The simulated flow for $rp = 2.008$ shows that the position of the Mach disc coincide for SST $k - \omega$ and standard $k - \omega$, and are separated 0.0068% by the left extreme of the position of the experimental Mach disc; this displacement to the left is indicated by the negative sign in Table 2. On the other hand, by the right extreme are separated 7.86% the standard k-e, 10.96% the transition $k - kl - \omega$ and 0.61% the RSM.

The standard $k-\omega$ has the greater thickness of the Mach disc, while the transition $k-kl-\omega$ has the smallest. The Mach discs for the SST $k-\omega$, standard $k-\omega$ and RSM turbulence models have less than 1% displacement with respect to the position of the experimental Mach disc, which is acceptable in engineering; nevertheless, according to the numerical results, the SST $k-\omega$ is the turbulence model that better fits the experiment.

It should be pointed that the thickness of the Mach disc was obtained from the density profiles, in the x axis symmetry, from the initial position where the density of the flow starts to increase to the final position where the maximum compression is reached. Figure 13 shows the density increase, for the estimated range 85-90 mm, which is the region where the collision front is present for the numerical simulations.

For $rp = 3,413$, the positions of all Mach discs are displaced to the right with respect to the experimental Mach disc, as shown in Table 3. The With 1.27%, the SST $k-\omega$ has the smallest percentage of displacement, while the transition $k-kl-\omega$ has the largest percentage of displacement with 8.14%. For this case, the thicknesses of all Mach discs are greater with respect to the simulated flow for $rp = 2.008$. Similar to the previous case, the result of the SST $k-\omega$ turbulence model exhibits the best fit to the experiment.

Table 2. Thickness, position and percentage of displacement of each Mach disc with respect to the experimental Mach disc at $x = 86.677\ mm$, for $rp = 2.008$

Turbulence model	Espesor (mm)	Position x (mm)	Percentage of displacement
SST $k-\omega$	1,017	86,671	-0,007
$k-e$	1,017	93,492	7,862
$k-\omega$	5,384	86,671	-0,006
$k-kl-\omega$	0,718	96,184	10,968
RSM	2,153	87,21	0,614

Table 3. Thickness, position and percentage of displacement of each Mach disc with respect to the experimental Mach disc at $x = 122.06\ mm$, for $rp = 3.413$

Turbulence model	Espesor (mm)	Position x (mm)	Percentage of displacement
SST $k-\omega$	3,983	123,619	1,277
$k-e$	3,915	127,568	4,512
$k-\omega$	6,49	124,873	2,034
$k-kl-\omega$	4,941	131,996	8,14
RSM	3,1	124,061	1,639

For both cases $rp = 2.008$ and $rp = 3.413$, in which the flow is over expanded in the divergent section of the flat nozzle, the shapes of the shock waves obtained for the SST $k-\omega$ turbulence model have the best fit to the experimental shock waves shown in Figures 15 and 16.

It should be pointed that a case study for the same geometry of the flat nozzle [10] considered in the present work, but with a porous surface in the flat wall of the divergent section, was conducted by Abdol-Hamid *et al.* [36], who simulated the 3D flow for the three turbulence models standard $k-e$ [16], SZL [12] and RSM [21], comparing with experimental results. The 3D results obtained in the symmetry of the flat wall, did not significantly contribute in an improvement when compared to the 2D results, for the range $1.41 < rp < 2.1$ in the pressure relationship.

For flow in domains that have symmetry, the favorable option is to simulate in 2D due to the save in hours of computational cost, which reduces the time of iteration and yields favorable results in specific regions, without having to use 3D flow simulation to obtain similar results in symmetry. Nevertheless, the 3D simulation provides relevant information away from the symmetry, in the corners of the walls, where the flow regime suddenly changes; for this it should be considered the use of turbulence models which have been already validated, and furthermore, if more precision is required in the numerical results the models LES or DNS should be employed.

The obtained numerical results are related to the mathematical fundamentals of each turbulence model, and the evaluation method applied in the region of the turbulent limit layer, because of the presence of shear stress in that region of flow. Besides, in the limit layer there are two parameters involved, namely the thickness and the friction coefficient, for both laminar and turbulent flow.

The SST $k-\omega$ turbulence model is a model of the Shear Stress Transport (SST) which employs two equations, one for the turbulent kinetic energy k, and the other for the specific dissipation rate ω, where the latter determines the turbulence scale. The mathematical expressions which are part of this structure are: the eddy viscosity, which transports the momentum by means of the turbulent eddies; the generation of turbulent kinetic energy due to gradients of mean velocity and the transverse diffusion, among other variables and constants which are used as parameters for the development of the flow regime.

This model has the ability of forecasting the behavior of the compressible fluid with more precision for opposite pressure gradients, which in the simulations demonstrates where the front of the shock wave is present in the symmetry in the direction of the x axis. The sensitivity to abrupt pressure variations, which produce the separation of flow from the divergent wall, is slightly smaller with respect to the turbulence models $k-e$ and RSM, which are closer to the experimental data.

Nevertheless, the SST $k-\omega$ turbulence model ex-

hibits better numerical results compared to the other turbulence models employed.

4. Conclusions

After evaluating the five turbulence models, namely SST $k-\omega$, standard $k-\omega$, standard k-e, transition $k-kl-\omega$ and RSM, which were employed in numerical simulations of an over expanded flow, it can be concluded that:

Regarding the profiles of static pressure obtained in the simulations along the walls of the flat nozzle, the turbulence model SST $k-\omega$ exhibited the best fit to the experimental data for the pressure relationships $rp = 2.008$ and $rp = 3.413$.

The profiles of density evaluated in the symmetry of the x axis, for $rp = 2.008$ and $rp = 3.413$, exhibit an abrupt increase in magnitude where the shock wave is present, and the SST $k-\omega$ turbulence model has the steepest slope.

The shapes of the shock waves for the field of density, obtained in the simulations with the SST $k-\omega$ turbulence model for the pressure relationships $rp = 2.008$ and $rp = 3.413$, are similar to the shapes of the experimental shock waves captured with the Schlieren technique, where for $rp = 2.008$ the Mach disc is displaced 0.007% to the left, and for $rp = 3.413$ the Mach disc is displaced 1.277% to the right.

For further works it is recommended to simulate the 3D flow and compare with the results of this work, to determine the numerical deviations that could occur with respect to the experimental data of pressure. Besides, simulate the flow with the SST $k-\omega$ turbulence model for the fields of static temperature, Mach number and pressure, to obtain the magnitude of the physical parameters before and after the shock wave.

Acknowledgement

My gratitude to Jehovah, mi Almighty God, my source of wisdom and inspiration. To the Mechanical Engineering Department of the Universidad Nacional Experimental Politécnica "AJS" Vice-Rectorado Puerto Ordaz (UNEXPO), Bolívar, Venezuela. To the Group of Mathematical Modeling and Numerical Simulation of the Universidad Nacional de Ingeniería (UNI), Lima, Perú.

References

[1] P. Krehl and S. Engemann, "August toepler — the first who visualized shock waves," *Shock Waves*, vol. 5, no. 1, pp. 1–18, Jun 1995. [Online]. Available: https://doi.org/10.1007/BF02425031

[2] F. White, *Viscous fluid flow.* McGraw-Hill, 1991. [Online]. Available: http://bit.ly/2Wl4Htw

[3] H. Schlichting, *Boundary-layer theory.* McGraw-Hill classic textbook reissue series, 2016. [Online]. Available: http://bit.ly/2wh45Xk

[4] J. D. Anderson, *Fundamentals of aerodynamics.* McGraw-Hill series in aeronautical and aerospace engineering, 2001. [Online]. Available: http://bit.ly/2YHGyeb

[5] F. White, *Mecánica de Fluidos.* McGraw-Hill Interamericana de España S.L., 2008. [Online]. Available: http://bit.ly/2W4dHEd

[6] T. V. Karman, "The fundamentals of the statistical theory of turbulence," *Journal of the Aeronautical Sciences*, vol. 4, no. 4, pp. 131–138, 1937. [Online]. Available: https://doi.org/10.2514/8.350

[7] J. Blazek, *Computational fluid dynamics: principles and applications.* Butterworth-Heinemann, 2015. [Online]. Available: http://bit.ly/2HRC7GM

[8] B. Andersson, R. Andersson, L. Håkansson, M. Mortensen, R. Sudiyo, B. van Wachem, and L. Hellström, *Computational Fluid Dynamics Engineers.* Cambridge University Press, 2012. [Online]. Available: http://bit.ly/2YLOcUR

[9] D. C. Wilcox, *Turbulence modeling for CFD.* DCW Industries, 2006. [Online]. Available: http://bit.ly/2K0NH5o

[10] C. Hunter, "Experimental, theoretical, and computational investigation of separated nozzle flows," *American Institute of Aeronautics and Astronautics*, 1998. [Online]. Available: https://doi.org/10.2514/6.1998-3107

[11] G. P. Sutton and O. Biblarz, *Rocket propulsion elements.* John Wiley & Sons, 2001. [Online]. Available: http://bit.ly/2WkBGxT

[12] T.-H. Shih, J. Zhu, and J. L. Lumley, "A new reynolds stress algebraic equation model," *Computer Methods in Applied Mechanics and Engineering*, vol. 125, no. 1, pp. 287–302, 1995. [Online]. Available: https://doi.org/10.1016/0045-7825(95)00796-4

[13] T. B. Gatski and C. G. Speziale, "On explicit algebraic stress models for complex turbulent flows," *Journal of Fluid Mechanics*, vol. 254, pp. 59–78, 1993. [Online]. Available: https://doi.org/10.1017/S0022112093002034

[14] S. S. Girimaji, "Fully explicit and self-consistent algebraic reynolds stress model," *Theoretical and Computational Fluid Dynamics*, vol. 8, no. 6, pp. 387–402, Nov 1996. [Online]. Available: https://doi.org/10.1007/BF00455991

[15] A. Balabel, A. Hegab, M. Nasr, and S. M. El-Behery, "Assessment of turbulence modeling for gas flow in two-dimensional convergent–divergent rocket nozzle," *Applied Mathematical Modelling*, vol. 35, no. 7, pp. 3408–3422, 2011. [Online]. Available: https://doi.org/10.1016/j.apm.2011.01.013

[16] B. E. Launder and D. B. Spalding, *Lectures in mathematical models of turbulence*. Academic Press, London, New York, 1972. [Online]. Available: http://bit.ly/2Jz9rWt

[17] Y. S. Chen and S. Kim, "Computation of turbulent flows using extended k-ε turbulence closure model," NASA Contractor report. NASA CR-179204, Tech. Rep., 1987. [Online]. Available: http://bit.ly/2HNf6VA

[18] F.-S. Lien and G. Kalitzin, "Computations of transonic flow with the $v^2 - f$ turbulence model," *International Journal of Heat and Fluid Flow*, vol. 22, no. 1, pp. 53–61, 2001. [Online]. Available: https://doi.org/10.1016/S0142-727X(00)00073-4

[19] P. Durbin, "On the $k - \varepsilon$ stagnation point anomaly," *International Journal of Heat and Fluid Flow*, vol. 17, no. 1, pp. 89–90, 1996. [Online]. Available: http://bit.ly/2EsZSnV

[20] F. R. Menter, "Two equation eddy-viscosity turbulence models for engineering applications," *AIAA Journal*, vol. 32, no. 8, pp. 1598–1605, 1994. [Online]. Available: https://doi.org/10.2514/3.12149

[21] B. E. Launder, G. J. Reece, and W. Rodi, "Progress in the development of a reynolds-stress turbulence closure," *Journal of Fluid Mechanics*, vol. 68, no. 3, pp. 537–566, 1975. [Online]. Available: https://doi.org/10.1017/S0022112075001814

[22] A. Toufique Hasan, "Characteristics of over-expanded nozzle flows in imposed oscillating condition," *International Journal of Heat and Fluid Flow*, vol. 46, pp. 70*–83, 2014. [Online]. Available: https://doi.org/10.1016/j.ijheatfluidflow.2014.01.001

[23] V. M. K. Kotteda and S. Mittal, "Flow in a planar convergent–divergent nozzle," *Shock Waves*, vol. 27, no. 3, pp. 441–455, May 2017. [Online]. Available: https://doi.org/10.1007/s00193-016-0694-4

[24] M. Taeibi-Rahni, F. Forghany, and A. Asadollahi-Ghoheih, "Numerical study of the aerodynamic effects on fluidic thrust vectoring," in *Conference: International Congress Propulsion Engineering, At Kharkov, Ukrain*, no. 8, 2015, pp. 27–34. [Online]. Available: http://bit.ly/2W1p6Ew

[25] E. Shimshi, G. Ben-Dor, A. Levy, and A. Krothapalli, "Asymmetric and unsteady flow separation in high mach number planar nozzle," *International Journal of Aeronautical Science & Aerospace Research (IJASAR)*, vol. 2, no. 6, pp. 65–80, 2015. [Online]. Available: https://doi.org/10.19070/2470-4415-150008

[26] R. Arora and A. Vaidyanathan, "Experimental investigation of flow through planar double divergent nozzles," *Acta Astronautica*, vol. 112, pp. 200 – 216, 2015. [Online]. Available: https://doi.org/10.1016/j.actaastro.2015.03.020

[27] S. Zivkovic, M. Milinovic, N. Gligorijevic, and M. Pavic, "Experimental research and numerical simulations of thrust vector control nozzle flow," *The Aeronautical Journal*, vol. 120, no. 1229, pp. 1153–1174, 2016. [Online]. Available: https://doi.org/10.1017/aer.2016.48

[28] E. Martelli, P. P. Ciottoli, M. Bernardini, F. Nasuti, and M. Valorani, "Delayed detached eddy simulation of separated flows in a planar nozzle," in *7th European Conference for Aeronautics and aerospace Sciences*, 2017. [Online]. Available: https://doi.org/10.13009/EUCASS2017-582

[29] O. Kostic, Z. Stefanovic, and I. Kostic, "Comparative cfd analyses of a 2d supersonic nozzle flow with jet tab and jet vane," *Tehnicki vjesnik*, vol. 24, no. 5, pp. 1335–1344, 2017. [Online]. Available: https://doi.org/10.17559/TV-20160208145336

[30] S. Verma, M. Chidambaranathan, and A. Hadjadj, "Analysis of shock unsteadiness in a supersonic over-expanded planar nozzle," *European Journal of Mechanics - B/Fluids*, vol. 68, pp. 55–65, 2018. [Online]. Available: https://doi.org/10.1016/j.euromechflu.2017.11.005

[31] D. C. Wilcox, "Reassessment of the scale-determining equation for advanced turbulence models," *AIAA Journal*, vol. 26, no. 11, pp. 1299–1310, 1988. [Online]. Available: https://doi.org/10.2514/3.10041

[32] K. Walters and D. Cokljat, "A three-equation eddy-viscosity model for reynolds-averaged navier-stokes simulations of transitional flows," *Journal of Fluids Engineering*, vol. 130, no. 12, p. 121401, 2008. [Online]. Available: https://doi.org/10.1115/1.2979230

[33] M. M. Gibson and B. E. Launder, "Ground effects on pressure fluctuations in the atmospheric boundary layer," *Journal of Fluid Mechanics*, vol. 86, no. 3, pp. 491–511, 1978. [Online]. Available: https://doi.org/10.1017/S0022112078001251

[34] B. E. Launder, "Second-moment closure and its use in modeling turbulent industrial flows," *International Journal for Numerical Methods in Engineering*, vol. 9, pp. 963–985, 1989. [Online]. Available: https://doi.org/10.1002/fld.1650090806

[35] Y. A. Cengel and J. M. Cimbala, *Mecánica de fluidos, fundamentos y aplicaciones*. McGraw-Hill, 2006. [Online]. Available: http://bit.ly/2X7THwU

[36] K. S. Abdol-Hamid, A. Elmiligui, C. A. Hunter, and S. J. Massey, "Three-dimensional computational model for flow in an over expanded nozzle with porous surfaces," in *Eighth International Congress of Fluid Dynamics & Propulsion, Cairo, Egypt*, 2006. [Online]. Available: https://go.nasa.gov/2JY3QZe

Scientific Paper / Artículo Científico

UNIVERSIDAD POLITÉCNICA SALESIANA ECUADOR
INGENIUS
Revista de Ciencia y Tecnología
https://doi.org/10.17163/ings.n22.2019.04
pISSN: 1390-650X / eISSN: 1390-860X

Detection of Faults in Combustion Engines Through Indicators of Temperature and Injection Pressure

Detección de fallas en motores de combustión mediante indicadores de temperatura y presión de inyección

Edilberto Antonio Llanes-Cedeño[1,*], Yans Guardia-Puebla[2], Alain de la Rosa-Andino[2], Santiago Cevallos-Carvajal[3], Juan Carlos Rocha-Hoyos[1]

Resumen

The present work aims at proposing indicators for early detection of faults in the fuel-oil generator sets of internal combustion engines, using the injection pressure and temperature of the combustion chamber. As a case study, the generation groups of the Maintenance Company of Fuel-Oil Generating Sets (EMGEF), in the Cuban province of Granma, were evaluated. A multifactorial design was used for the experiment, using 16 engines as main factors, the 9 cylinders of each engine, and a working time of 3 years. The study demonstrated that pressure and temperature are significant indicators of engine failure, and that the number of detected faults from temperature were more significant than those reported from injection pressure. It is concluded that high temperatures in the cylinders are generally related to a high index of gases, and a poor state of the injectors. The differences between the pressures are related to low hermetism, and the technical state of the elements of the feeding system.

Keywords: failure, pressure, injection, temperature combustion chamber, maintenance, generator sets.

Abstract

El presente trabajo tiene como objetivo proponer indicadores para la detección temprana de fallas en los motores combustión interna de los grupos electrógenos de fueloil a partir de la presión de inyección y temperatura de la cámara de combustión. Como caso de estudio fueron evaluados los grupos de generación de la Empresa de Mantenimiento a los Grupos Electrógenos Fueloil (EMGEF) en la provincia cubana de Granma. Para el experimento se utilizó un diseño multifactorial usando como factores principales los 16 motores, los 9 cilindros de cada motor y un tiempo de trabajo de 3 años. El estudio demostró que la presión y la temperatura son indicadores significativos en las fallas de los motores, además de que el número de fallas detectadas por temperatura fueron más significativas que las reportadas por la presión de inyección. Se concluye que las altas temperaturas en los cilindros generalmente están relacionadas con un alto índice de gases y un deficiente estado de los inyectores. Las diferencias entre las presiones están relacionadas con la baja hermeticidad y el estado técnico de los elementos del sistema de alimentación.

Palabras clave: fallas, presión, inyección, temperatura, cámara de combustión, mantenimiento, grupos electrógenos.

[1,*]Grupo de Investigación de emisiones, Facultad de Arquitectura e Ingeniería, Carrera de Mecánica, Universidad Internacional SEK, Quito-Ecuador. Autor para correspondencia ✉: antonio.llanes@uisek.edu.ec http://orcid.org/0000-0001-6739-7661, http://orcid.org/0000-0003-0660-7199,

[2]Facultad de Ingeniería, Carrera de Mecánica, Universidad de Granma-Cuba. http://orcid.org/0000-0002-1347-0963, http://orcid.org/0000-0001-6593-8583.

[3]Departamento de Energía y Mecánica, Universidad de las Fuerzas Armadas, Ecuador. http://orcid.org/0000-0001-7998-4978.

Received: 17-03-2019, accepted after review: 31-05-2019

Suggested citation: Llanes-Cedeño, E. A.; Guardia-Puebla, Y.; De la Rosa-Andino, A.; Cevallos-Carvajal, S. and Rocha-Hoyos, J. C. (2019). «Detection of Faults in Combustion Engines Through Indicators of Temperature and Injection Pressure». Ingenius. N.° 22, (july-december). pp. 38-46. doi: https://doi.org/10.17163/ings.n22.2019.04.

1. Introduction

Electricity generation is a priority for governments, because the quality of life of the people largely depends on it. An alternative to guarantee such objective are the generating groups (GG), which are employed either in an intensive manner or as support. They are continuously improved to guarantee their efficiency and effectiveness [1].

As all equipment for distributed generation, the GG have various advantages and disadvantages in their operation, due to the parameters of the manufacturer and of the generators that constitute them. Their main advantages are that they help with environmental conservation, and that they constitute an important alternative to increase electric generation at peak hours of demand, contributing to decongest energy transmission systems. The main disadvantage of this system, is that they can produce voltage fluctuations that may affect nearby generating groups. Besides, it requires a data acquisition system which is more complex, compared to any other equipment, due to technology used in these cases [2, 3].

Several research works have been carried out, to propose techniques for early detection and diagnose of failures in internal combustion engines. According to Mendonça [4], incipient malfunctions in the components of generators driven by internal combustion engines, may be detected measuring the voltage and current in the stator of the generator; such malfunctions may include failures in the inlet valve, and in the compression due to wear in the piston rings. The study carried out by Xi, Li, Tian and Duan [5] showed that it is possible to detect failures in marine combustion engines, from the analysis of the frequency of the vibrations.

On the other hand, the study by Lee, Cha, Ko, Park and Jung [6] deals with fault detection applications and diagnose algorithms based on the Kalman filter and the fault factor method, which are utilized on an open-cycle liquid propellant rocket engine at steady state, enabling to determine the fault location, either in a sensor or in an internal component. In the study carried out by Czech, Wojnar, Burdzik, Konieczny and Warczek [7], vibration signals and artificial neural networks were used to detect damage on the engine mechanical elements (exhaust valves, injectors, cylinder head gasket). The results confirmed the possibility of diagnosing the technical state of the automobile engine components, while the motor is in operation.

Flett and Bone [8] developed a system based in the vibration, for detection and diagnosis of failures in the valve train of the internal combustion engine. On the other hand, Trujillo *et al.* [9] proposed a methodology that combines numerical and experimental procedures by means of finite element simulations, use of thermocouples and infrared thermography, to estimate the mean temperature in the internal surface of the cylinder of an air-cooled direct injection diesel four strokes engine, improving data acquisition and preventing to take actions from the inside of the combustion chamber, thus reducing the complexity of the experiments during diagnosis.

During normal operation, the GG are subject to different requests that cause their deterioration, and consequently reduces their electric generation capacity. This deterioration comprises all forms of wear and tear produced by phenomena such as: fatigue, corrosion, abrasion, erosion and degradation. These failures may be possibly caused by the effect of the injection pressure and temperature accumulated inside each engine cylinder. Therefore, the objective of this research is to propose indicators that use injection pressure and temperature in the combustion chamber, for early detection of faults of fuel-oil generating groups in internal combustion engines.

2. Materials and methods

The Corporate Base Unit of 110 kV, which belongs to the Granma Cuban Electrical Company, is taken as a case study. Such unit is constituted by sixteen generating groups that operate with fuel-oil.

2.1. Extent of the research

The research lasted a period of 36 months (from January 2015 to December 2017). Data and valuable information was obtained from the following documents: i) letter of technological regime for HHI 1.7 MW PPS (Code: UJ-IG-0304); ii) control of availability GDECU (Code: UJ-IG 0105); iii) book of defect control (Code: UJ-MP 0200.A5); iv) book of operational incidences (Code: UJ-MG 0200.A8); v) operating control of faults. Direct queries were carried out to operators and specialists in charge of the GG exploitation, to extract distinctive features of the operation of such equipment.

2.2. Generating groups (GG) main title

The GGs of the station comprise 16 1.7 MW Hyundai engines. Table 1 summarizes the characteristics of such engines. These machines use fuel-oil, which is a fraction of the oil obtained as residue after distillation. Is the heaviest fuel than can be distilled at atmospheric pressure. It is used as fuel in electric generation plants, boilers and furnaces.

Table 1. Characteristics of the 1.7 MW HYUNDAI engines

Type of engine	HYUNDAY 1,7 MW
Number of cylinders	9
Rotational speed (min^{-1})	1000
Diameter of the cylinders (mm)	210
Power per cylinders (kW)	200
Piston travel (mm)	320

2.3. Control, analysis and failure criteria

This sub-section specifies the considerations assumed during the experimentation.

2.3.1. Control

All the information regarding failures was collected from the operational record of failures. The following was taken into account in such register: i) identification of repetitive damages and failures, classification by type of equipment or system; ii) identification of the causes of the failures; iii) collection of other information such as: repairing cost, mean time between failures (MTBF), mean time per failure (MTPF); iv) identification of previously utilized corrective actions.

2.3.2. Failure criterion

The gravity indicators referred by Aguilar-Otero, Torres-Arcique, Magaña-Jiménez [10], Moubray [11] and Scarpatti [12], were taken into account with the purpose of defining the gravity of the failure. These indicators mainly gather the specialized experience obtained in the analysis, treatment and consequences of the failures that typically affect the control and protection schemes.

2.3.3. Experimental design

The analysis and graphics results were obtained using the statistical package STATGRAPHICS Centurion XV (Trial version 15, StatPoint Inc., USA). A factorial design of experiments was used to study the effects of the quantitative factors in the design mathematical model defined as.

$$y_{ijk} = \mu + \tau_i + \beta_j + \gamma_k + (\tau\beta)_{ij} + (\beta\gamma)_{jk} + \\ +(\tau\beta\gamma)_{ijk} + \epsilon_{ijk} \begin{cases} i = 1, 2, \ldots, a \\ j = 1, 2, \ldots, b \\ k = 1, 2, \ldots, c \end{cases} \quad (1)$$

where the variables τ, β, γ represent the factors *engine*, *cylinder* and *working time*, and their interactions. A variance analysis methodology (Anova) was utilized for analyzing the levels of the factors, where an F value was calculated, for a probability of 0.05, and compared with a value in a table, in order to determine significant differences between the levels of the factors [13–15]. These were defined as follows: factor engine was set equal to 15, each *engine* with 9 *cylinders*, and the *working time* was considered as 3 years (2015-2017)

2.3.4. Measuring instruments

A *Digital Pressure Indicator* Leutert, model DPI-2, was utilized for measuring the injection pressure and combustion chamber temperature which was accumulated in each cylinder. This instrument enables determining the pressure and temperature when entering. The DPI system includes a sensor, to measure the injection pressure in diesel engines. The data obtained was processed and evaluated with the device software, version 3.24 for Windows®.

3. Results and discussion

In this section, the results obtained during the experimentation are presented and discussed.

3.1. Temperature analysis in the combustion chamber (cc) of the engines

Table 2 shows the measurements of combustion chamber temperature, of the 15 engines under study. The main *factors*, *engines*, *working time* and their *combination*, were highly significant with a probability of 95%, since the Anova p-values were smaller than the 0.05 limit.

These results indicate that there is a high variability in the energy delivery of the site, because the work done by the engines is not efficient; this has an influence on the capacity of delivering energy to the national network. Another factor that has significant influence is the working time of some engines, since this depends on the electrical demand. The working order and the amount of energy required, according to the demand, are obtained from the generation plant.

The working order refers to the number of engines and the operating percentage required to supply such demand. This situation also generates a variability in the working time of the set of engines, and thus an inefficient management of the technology. Another important aspect that has influence, is operating the engines under what is considered as optimal (below 70% of the efficient generation capacity).

The Anova (Table 2) also indicated significant differences in the interaction of the factors *engines* and *working time*. Figure 1 shows the interaction *working time* and *engines* as a function of the temperature in the combustion chambers. There is no defined trend

showing an increase in the temperature of the individual engines during summer months (May to October), or a temperature decrease in the winter months (November to April).

This fluctuation in the temperature values is due to the maintenance carried out in each engine, and the variation in the physical properties of the fuel, according to the origin batch and the supplier [16]. This last aspect is very important, since it changes physicochemical parameters of the fuel, such as: viscosity, density, calorific value, coal percentage, asphaltenes and sediments, among others [17].

Table 3 shows a comparison of the mean values of temperature in the combustion chambers and homogeneous groups, between the levels of the factors engine and working time.

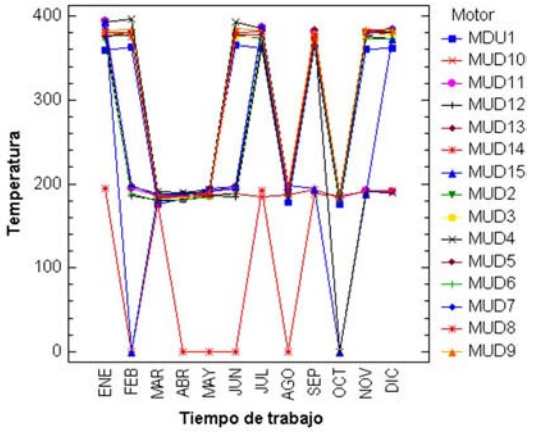

Figure 1. Interaction working time and engines as a function of temperature

Table 2. Anova Table for temperature of the combustion chambers

Source	SS[a]	GL[b]	CM[c]	F-Ratio[d]	p-value
ICE	$7{,}44.10^6$	14	$5{,}3.\ 10^5$	24,66	0,0000[e]
Cylinder	$3{,}92.\ 10^4$	8	4906,88	0,23	0,9860
Working time	$2{,}03.10^7$	11	$1{,}85.10^6$	85,68	0,0000[e]
ICE*Cylinder	$2{,}41.\ 10^5$	112	2157,18	0,10	1,0000
ICE*Working time	$1{,}06.10^7$	154	$6{,}9.\ 10^4$	3,18	0,0000[e]
Cylinder*Working time	$2{,}1.\ 10^4$	88	238,64	0,01	1,0000
RESIDUES	$6{,}18.10^7$	2865	$2{,}15.\ 10^4$		
TOTAL (CORRECTED)	$1{,}0.10^8$	3252			

Note: [a]SS. Sum of squares, [b]DF. Degree of freedom, [c]MS. Mean squares, [d]F-ratio: F-value for a probability 95 %, [e]Significant for a probability 95 %

It can be seen that there is no uniform distribution in the temperature observed in the 15 internal combustion engines (ICE) of the generation facility, indicating a wide range of average temperature which oscillates between 109 and 302 °C. This range of values is below the optimal value of 320 °C. On the other hand, it was observed a trend of the average global temperature of the ICEs to decrease in the months between November and March, which correspond to the coldest months; these results match the ones referred by [1, 10].

3.2. Analysis of the injection pressure in the engines

Table 4 shows the analysis of variance for the injection pressure as a function of the factors previously mentioned. The main factors ICE and *working time* remained significant, indicating that there are differences in the injection pressure among the 15 engines. This variability is mainly due to stops in the operation, which can be related with maintenance, technical revision, damages; or simply because there is no increase in demand, and some engines in the electrical plant are put out of service. The factor *working time* is also closely related to the variability of the injection pressure, since as the working time of the engine increases so does the wear of its components, and the feeding system aggravates due to the variation in the quality of the fuel [18].

No significant differences were detected among the cylinders of the engines, indicating that the fuel injection pressure within the combustion chamber is constant.

It can be observed in Figure 2, that the average values of global injection pressure of the generation facility were almost constant in most of the months. According to the *working time*, only a deviation was observed in the months of April and May. Similarly, the engines ICE1, ICE2 and ICE9 showed pressure increases compared to the rest of the engines. These increments may be caused by lack of relationship between the angle of the toothed bar, and the amount of fuel entering and clogs in the nozzles or in the fuel filters.

Table 3. Comparison of mean values of temperature in the combustion chamber and between the levels of the factors *engine* and *working time*

Engine	Mean (°C)	Homogeneous gropus	Working time	Mean (°C)	Homogeneous groups
ICE1	286,6±9,8	XXXX	ENE	172,9±8,9	X
ICE2	297,9±9,9	XXX	FEB	176,5±8,9	X
ICE3	296,8±9,9	XXX	MAR	177,1±8,9	X
ICE4	258,0±9,9	XX	ABR	369,0±8,9	X
ICE5	298,0±9,9	XXX	MAY	337,9±8,9	XX
ICE6	261,7±9,9	XXX	JUN	353,0±8,9	XX
ICE7	271,4±9,9	XXX	JUL	266,6±8,9	X
ICE8	299,4±9,9	XX	AGO	266,8±8,9	X
ICE9	302,6±9,9	X	SEP	340,8±8,9	XX
ICE10	250,2±9,9	XX	OCT	327,4±8,9	X
ICE11	239,6±9,9	X	NOV	159,8±8,9	X
ICE12	262,2±9,9	XXX	DIC	183,8±8,9	X
ICE13	271,9±9,9	XXXX			
ICE14	109,9±9,9	X			
ICE15	208,4±9,9	X			

Table 4. Analysis of variance for injection pressure

Source	SS[a]	GL[b]	CM[c]	F-Ratio[d]	p-value
Engine	32558,6	14	2325,6	2,19	0,0065[e]
Cylinder	5755,2	8	719,4	0,68	0,7119
Working time	28061,5	11	2551,1	2,4	0,0058[e]
RESIDUES	2,06E+06	1943	1062		
TOTAL (CORRECTED)	2,13E+06	1976			

[a]SS. Sum of squares, [b]DF. Degrees of freedom, [c]MS. Mean squares, [d]F-ratio: F-value for a probability 95 %, [e]Significant for a probability 95 %.

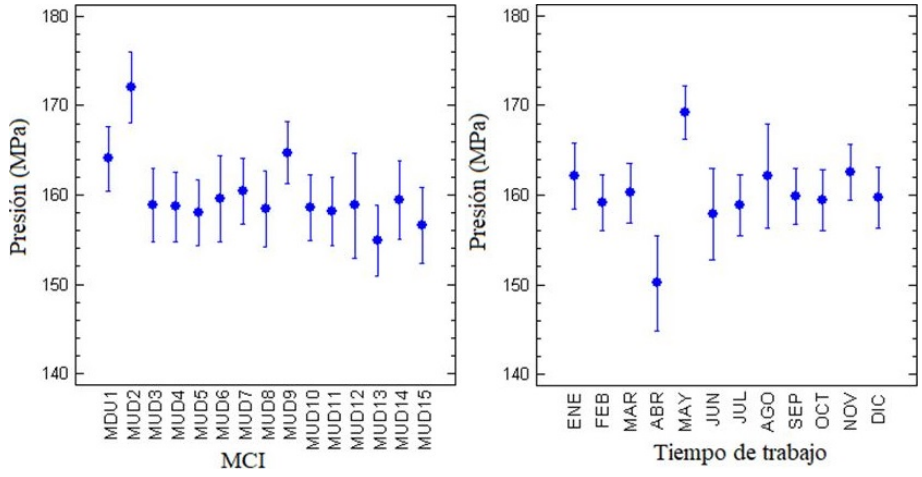

Figure 2. Representation of the ranges of mean pressure per engine and working time.

3.3. Analysis of failures by injection pressure and temperature in the combustion chamber

As observed in Figure 3a, the failures in 2015 were influenced by the high temperatures reached by the ICE of the generation facility. The ICEs 15, 9, 11 and 8, in that order, were the affected by the high temperatures.

This situation was due to various factors, which affected the electric generation capacity of the facility; among these factors, the *working time* and the *fuel quality* should be highlighted. A similar behavior was observed in 2016 (Figure 3b), where the failures due to temperature were greater than the failures due to injection pressure.

Nevertheless, a reduction in the number of failures can be seen in 2017 (Figure 3c); only the ICE8 had more failures, the remaining ICEs of the facility showed smaller values.

Compared with the previous years, this was the years of lowest incidence, demonstrating an improvement in the operation and efficiency of the facility, due to better knowledge and experience acquire by the operators, as well as an enhancement in the maintenance of the equipment.

It can be seen in Figure 4 that the number of failures was reduced in 2018, due to the effects of injection pressure and temperature in the combustion chamber in some ICEs of the facility. This is due to the better management of technology during this period.

Therefore, there were no anomalies in the operation of the facility and energy delivery to the national electrical network. However, failures were reported in some ICEs, such as ICE2, ICE4, ICE8, ICE11, ICE13 and ICE15, with ICE2 and ICE13 having higher incidence with 6 failures in this period. These results indicate a better working efficiency of the generation group.

However, although the number of failures was reduced, it should be sought to optimize the generation of the facility, focusing in improving the efficiency of the operating methods and the decisions of the Board of Directors [19].

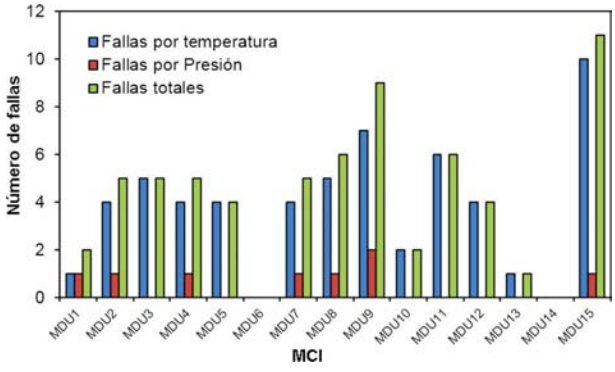

a)

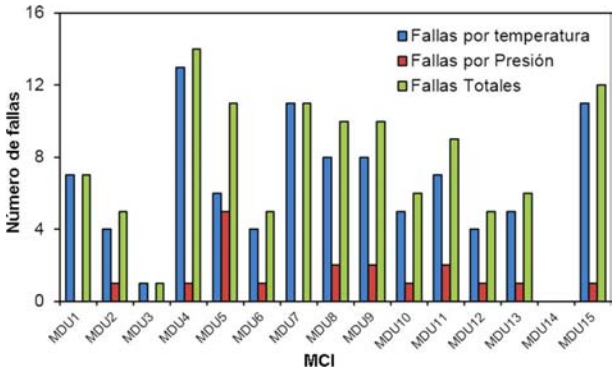

b)

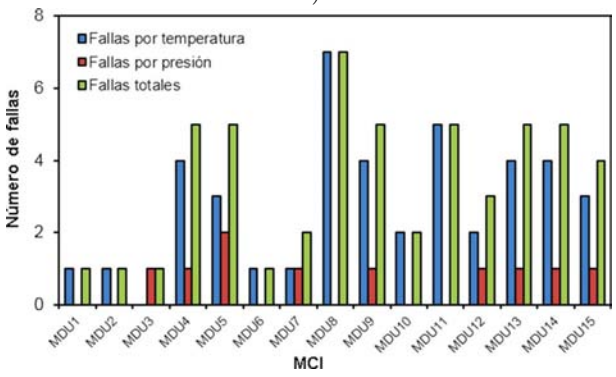

c)

Figure 3. Summary of failures due to pressure and temperature a) 2015; b) 2016; c) 2017.

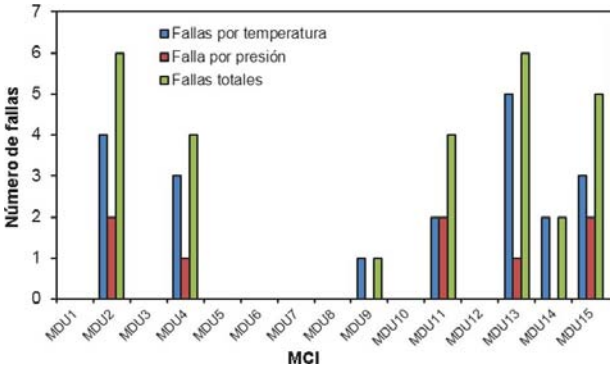

Figure 4. Summary of failures due to pressure and temperature in 2018.

Figure 5 shows the total failures caused by injection pressure and temperature in the combustion chamber, in the period 2015-2017.

During 2015 (Figure 5a), the greatest number of failures was due to high temperature (82 failures), which is directly related with the governor index (55 failures). The «governor» gives the opening angle of the toothed bar, i.e, the accelerator. A high index indicates an increase in the acceleration of the engine, which during a long working period causes high temperatures and pressure in the cylinders [20–22]. A high governor index in conjunction with an inadequate operation of the injector, may cause high temperatures in the

cylinders because it enables the control of the index of the toothed bar and the fuel input [23]. When injectors operator inefficiently, the fuel input to the cylinder increases, and thus the temperature increases due to excess of fuel in the combustion chamber [2]. This phenomenon also generates black residual gases [24].

The third most detected failure were the fuel outlets (23 failures). This phenomenon is directly related with a deficient sealing in the feeding system, due to an inadequate maintenance and revision of the ICE. However, in 2016 various failures observed in 2015 were corrected (Figure 5b). No failures due to sealing were detected in the feeding system, the number of failures in the governor index was reduced 72%, but the number of failures due high temperatures remained large (88 failures); the other indicators reported a range of failures between 5 and 20. In 2017 (Figure 5c) the number of failures due to high temperatures in the cylinders was reduced (64 failures), but there was an increase in the number of failures in the governor index (44 failures) and low hermetism (7 failures).

Figure 6 shows the behavior of the ICEs in 2018. The failures due to high temperatures exhibited the highest incidence (21 failures), even though it was observed a decreasing trend with respect to previous years.

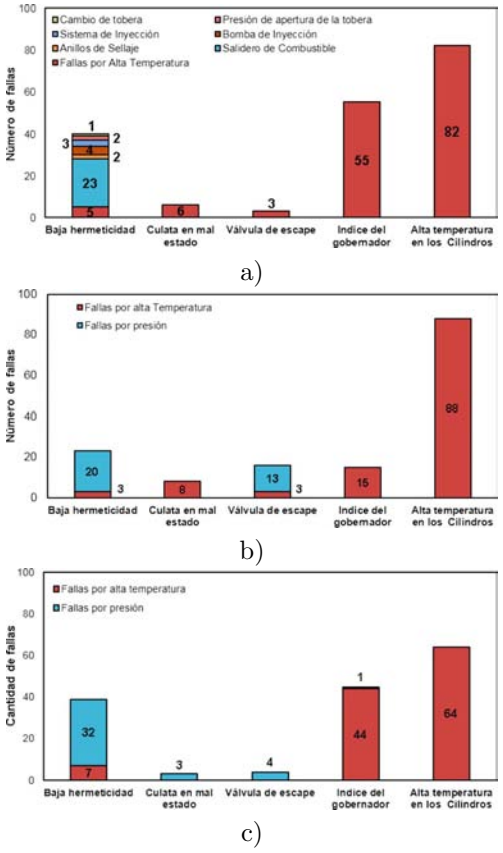

Figure 5. Most significant failures caused by pressure and temperature, and their effects on the ICEs 9H21/32: a) 2015; b) 2016; c) 2017.

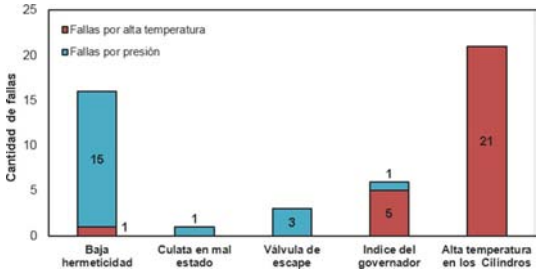

Figure 6. Most significant failures caused by injection pressure and temperature in the combustion chamber in 2018.

4. Conclusions

The analysis demonstrated that the injection pressure and the temperature in the combustion chambers are indicators that influence the occurrence of failures in the 1.7 MW Hyundai ICEs.

The number of detected failures due to temperature in the combustion chamber are significantly higher, compared to the failures reported due to injection pressure.

In general, such high temperatures are related with a high governor index and a deficient operation of the injectors.

The interaction of the factors ICE*working time was statistically significant in the analysis of the temperature in the combustion chamber, producing an inefficient operation of the ICEs and the energy delivered by the facility.

References

[1] M. C. Fernandez, M. F. Fernández, R. D. Fuentes, and A. C. Montiel, "Calidad de la energía y generación distribuida en Cuba," *Revista Cubana de Ingeniería*, vol. 1, no. 3, pp. 41–50, 2010. [Online]. Available: https://doi.org/10.1234/rci.v1i3.28

[2] J. G. Boza, "Estudio de estabilidad en un sistema eléctrico con grupos electrógenos," *Revista de Ingeniería Energética*, vol. 28, no. 2, pp. 26–28, 2007. [Online]. Available: http://bit.ly/2F1S6BD

[3] J. F. Quintana Tamayo, F. Martínez Pérez, Y. G. Vázquez Jorge, and J. Ramírez Arzuaga, "Estudio de factibilidad para optimizar frecuencia de reemplazo del lubricante, en Grupos Electrógenos," *Revista Ciencias Técnicas Agropecuarias*, vol. 3, no. 23, pp. 60–68, 09 2014. [Online]. Available: http://bit.ly/31iGFz3

[4] P. Mendonça, E. Bonaldi, L. de Oliveira, G. Lambert-Torres, J. B. da Silva, L. B. da Silva, C. Salomon, W. Santana, and

A. Shinohara, "Detection and modelling of incipient failures in internal combustion engine driven generators using electrical signature analysis," *Electric Power Systems Research*, vol. 149, pp. 30–45, 2017. [Online]. Available: https://doi.org/10.1016/j.epsr.2017.04.007

[5] W. Xi, Z. Li, Z. Tian, and Z. Duan, "A feature extraction and visualization method for fault detection of marine diesel engines," *Measurement*, vol. 116, pp. 429–437, 2018. [Online]. Available: https://doi.org/10.1016/j.measurement.2017.11.035

[6] K. Lee, J. Cha, S. Ko, S.-Y. Park, and E. Jung, "Fault detection and diagnosis algorithms for an open-cycle liquid propellant rocket engine using the kalman filter and fault factor methods," *Acta Astronautica*, vol. 150, pp. 15–27, 2018. [Online]. Available: https://doi.org/10.1016/j.actaastro.2018.03.001

[7] P. Czech, G. Wojnar, R. Burdzik, L. Konieczny, and J. Warczek, "Application of the discrete wavelet transform and probabilistic neural networks in ic engine fault diagnostics," *Journal of Vibroengineering*, vol. 16, pp. 1619–1639, 2014. [Online]. Available: http://bit.ly/2XBwbIF

[8] J. Flett and G. M. Bone, "Fault detection and diagnosis of diesel engine valve trains," *Mechanical Systems and Signal Processing*, vol. 72-73, pp. 316–327, 2016. [Online]. Available: https://doi.org/10.1016/j.ymssp.2015.10.024

[9] E. Carvajal Trujillo, F. J. Jiménez-Espadafor, J. A. Becerra Villanueva, and M. Torres García, "Methodology for the estimation of cylinder inner surface temperature in an air-cooled engine," *Applied Thermal Engineering*, vol. 31, no. 8, pp. 1474–1481, 2011. [Online]. Available: https://doi.org/10.1016/j.applthermaleng.2011.01.025

[10] J. R. Aguilar-Otero, R. Torres-Arcique, , and D. Magaña Jiménez, "Análisis de modos de falla, efectos y criticidad (AMFEC) para la planeación del mantenimiento empleando criterios de riesgo y confiabilidad," *Tecnología, Ciencia, Educación*, vol. 25, pp. 15–26, 2010. [Online]. Available: http://bit.ly/2I8mAnx

[11] J. Moubray, *Mantenimiento Centrado en la Confiabilidad*. Industrial Press Inc., 2004. [Online]. Available: http://bit.ly/2Izu4yC

[12] F. Scarpatti, "Análisis de modos de fallas y sus efectos," Scarpatti y Asociados. Consultores en Gestión Organizacional, Tech. Rep., 2001. [Online]. Available: http://bit.ly/2F2mprX

[13] D. C. Montgomery, *Design and Analysis of Experiment*. John Wiley & Sons, 2008. [Online]. Available: http://bit.ly/2WyxprV

[14] J. C. Rocha-Hoyos, E. A. Llanes-Cedeño, S. Celi-Ortega, and D. Peralta-Zurita, *Efecto de la Mezcla de Biodiesel en el Rendimiento y la Opacidad del Motor Diesel*. Información Tecnológica., 2019.

[15] Y. Guardia-Puebla, J. Márquez-Delgado, V. Saánchez-Girón, E. A. Llanes-Cedeño, J. C. Rocha-Hoyos, and D. B. Peralta-Zurita, "Mejoras a la asignatura diseõ estadístico de experimentos para estudiantes de la carrera de ingeniería mecánica," *Revista Espacios*, vol. 39, no. 30, pp. 10–25, 2018. [Online]. Available: http://bit.ly/2KJbs2e

[16] F. Martínez Pérez and A. Barroso Moreno, "Aplicación de la tribología y el análisis de la causa raíz (rca) en motores de combustión interna," *Ingeniería Mecánica*, vol. 3, pp. 53–56, 2008. [Online]. Available: http://bit.ly/2IA0ppd

[17] D. Fernández-Fernández and F. Mourdoch-Misa, "Aplicación de técnicas de lubricación predictivas en grupos electrógenos," *Ingeniería Mecánica*, vol. 12, no. 2, pp. 1–8, 2009. [Online]. Available: http://bit.ly/2F3vbpw

[18] K. Riplová, "Tool of risk management: failure mode and effects analysis and failure modes, effects and criticality analysis," *Journal of Information, Control and Management Systems*, vol. 5, no. 1, pp. 111–120, 2007. [Online]. Available: http://bit.ly/2KbKm4i

[19] O. Martínez Rodríguez and S. A. Dorrbercker Drake, "Determinación de las prioridades de mantenimiento en turbogeneradores "Elektrosila ТВФ-100-3600-T3" a partir del comportamiento de sus fallos," *Ingeniería Energética*, vol. 33, no. 3, pp. 250–262, 2012. [Online]. Available: http://bit.ly/2Rak4zR

[20] S. Wu and D. Clements-Croome, "Ratio of operating and maintenance costs to initial costs of building services systems," *Cost Engineering*, vol. 49, no. 12, pp. 30–33, 2007. [Online]. Available: http://bit.ly/2Ialckl

[21] S. You-Cheng, X. Min, G. Yong, C. Yi, S. Lei, and D. Kang-yao, "Effects of injection pressure, exhaust gas recirculation and intake pressure on the cycle-to-cycle variations of hcci combustion," *Journal of the Energy Institute*, vol. 89, no. 2, pp. 293–301, 2016. [Online]. Available: https://doi.org/10.1016/j.joei.2015.01.017

[22] A. K. Agarwal, D. K. Srivastava, A. Dhar, R. K. Maurya, P. C. Shukla, and A. P. Singh, "Effect of fuel injection timing and pressure on combustion, emissions and performance characteristics of a single cylinder diesel engine," *Fuel*, vol. 111, pp. 374–383, 2013. [Online]. Available: https://doi.org/10.1016/j.fuel.2013.03.016

[23] S. Gowthaman and A. Sathiyagnanam, "Effects of charge temperature and fuel injection pressure on hcci engine," *Alexandria Engineering Journal*, vol. 55, no. 1, pp. 119–125, 2016. [Online]. Available: https://doi.org/10.1016/j.aej.2015.12.025

[24] E. A. Llanes-Cedeño, J. C. Rocha-Hoyos, Y. Guardia-Puebla, L. Tipanluisa, and G. Velastegui, "Análisis comparativo de los gases residuales de la combustión y fallas en motores hyundai modelo 9h21/32, en estación de generación eléctrica distribuida," *INNOVA Research Journal*, vol. 2, no. 3, pp. 27–41, 2017. [Online]. Available: http://bit.ly/2R5PE1P

Scientific Paper / Artículo Científico

UNIVERSIDAD POLITÉCNICA SALESIANA ECUADOR
INGENIUS
Revista de Ciencia y Tecnología
https://doi.org/10.17163/ings.n22.2019.05
pISSN: 1390-650X / eISSN: 1390-860X

Performance of Columnar Database

Rendimiento de bases de datos columnares

Jhonatan W. Durán-Cazar[1], Eduardo J. Tandazo-Gaona[1],
Mario R. Morales-Morales[1,*], Santiago Morales Cardoso[1]

Abstract

Companies' capacity to efficiently process a great amount of data from a great variety of sources anywhere and anytime is essential for them to succeed. Data analysis becomes a key strategy for most large organizations to get a competitive advantage. Hence, new issues should be considered when massive amounts of date are to be stored, because traditional relational database are not capable to lodge them. Such questions include aspects that range from the capacity to distribute and escalate the physical storage, to the possibility of using schemes or non-usual types of data. The main objective of this research is to evaluate the performance of the columnar databases in data analysis., comparing them with relational databases, to determine their efficiency using measurements in different test scenarios. The present study seeks to provide (scientific evidence) professionals interested in data analysis with a basic instrument for their knowledge, to include comparative tables with quantitative data that can support the conclusions of this research. A methodology of applied type and quantitative-comparative descriptive design is used, as it is the one of the most appropriate to study database efficiency characteristics. In the measurement, the method of averages is used for a number n of records, and it is supported in the Aqua Data Studio tool that guarantees a high reliability, as a specialized software for the administration of databases. Finally, it has been determined that the columnar databases have a better performance in data analysis environments.

Keywords: data analytics, columnar database, in memory, NoSQL, performance.

Resumen

En la actualidad para el éxito de las empresas es decisiva la capacidad de procesar de manera eficiente una considerable cantidad de datos de una amplia gama de fuentes en cualquier lugar y momento. El análisis de datos se convierte en una estrategia clave para la mayoría de las grandes organizaciones para lograr una ventaja competitiva. Por tanto, surgen nuevas cuestiones a ser tomadas en cuenta a la hora de almacenar y consultar cantidades masivas de datos que, en general, las bases de datos relacionales tradicionales no pueden abarcar. Estas cuestiones incluyen desde la capacidad de distribuir y escalar el procesamiento o el almacenamiento físico, hasta la posibilidad de utilizar esquemas o tipos de datos no usuales. El objetivo principal de la investigación es evaluar el rendimiento de las bases de datos columnares en analítica de datos. Efectuar una comparación con bases de datos de tipo relacional, para determinar su eficiencia, realizando mediciones en distintos escenarios de pruebas. El presente estudio pretende proporcionar (evidencia científica) un instrumento que facilite a los profesionales interesados en la analítica de datos una base para sus conocimientos, al incluir cuadros y tablas comparativos con datos cuantitativos con los que se pueda sustentar las conclusiones de esta investigación. Se usa una metodología aplicada y de diseño descriptivo cuantitativo-comparativo al ser el que mejor se ajusta al estudio de características de eficiencia de bases de datos. En la medición se usa el método de promedios para n número de tomas y se soporta en la herramienta Aqua Data Studio que garantiza una alta confiabilidad al ser un programa especializado para la administración de bases de datos. Finalmente, se ha logrado determinar que las bases columnares tienen un mejor rendimiento en ambientes de análisis de datos.

Palabras clave: análisis de datos, base de datos columnar, en memoria, NoSQL, rendimiento

[1,*]Facultad de Ciencias Físicas y Matemáticas, Universidad Central del Ecuador, Ecuador. Autor para correspondencia ✉: mmoralesm@uce.edu.ec. http://orcid.org/0000-0002-8574-1435, http://orcid.org/0000-0002-2209-3952, http://orcid.org/0000-0002-7493-8072, http://orcid.org/0000-0002-3833-9654,

Received: 11-04-2019, accepted after review: 03-06-2019

Suggested citation: Durán-Cazar, J.; Tandazo-Gaona, E.; Morales-Morales, M. R. and Morales Cardoso, S. (2019). «Performance of Columnar Database». Ingenius. N.°22, (july-december). pp. 47-58. doi: https://doi.org/10.17163/ings.n22.2019.05.

1. Introduction

Among the different data models, the relational one has been dominating from the 80s, with database implementations such as Oracle, MySQL and SQL Microsoft Servers, also known as Relational Database Management Systems (RDBMS) [1].

As a consequence of the significant growth of Internet in the last years and the appearance of the big data phenomenon, new issues should be considered when storing and accessing massive amounts of data that, in general, traditional relational databases are not able to cover. These issues include from the capacity to distribute and scale the processing or the physical storage, up to the possibility of employing non usual schemes or types of data [2].

The capacity of efficiently processing a great amount of data from a wide variety of sources, at any place and moment, is decisive for the success of a company. Data analysis becomes a key strategy for most organizations, to obtain a competitive advantage. Therefore, during the last decade, the worldwide focus on the management business has changed profoundly [3].

In a scenario where the data tend to be more different, the rigid structure of relational systems makes significantly difficult to model them. The performance is limited by the vertical scaling, which does not allow the distribution of the system load among multiple machines, together with the great number of concurrent read and write requests and the own complexity of the logic behind the operation of relational databases; all these factors may lead to a efficiency loss regarding the growth of the data.

As a consequence, it is difficult to respond with low latency in the case of applications that simultaneously serve a large number of requests. Therefore, redundant and easy to scale systems are necessary to provide a service with high scalability and availability, to manage large volumes of data and guarantee their availability [4].

Prior to defining how the research will be carried out, it is necessary to review some key concepts that will be used in the present work.

SQL Database.- The concept of database systems is not new in the society, their predecessors were the file systems. As time has gone by, the database was developed due to the requirement of storing a large amount of information.

The relational model was defined in 1970, from which the first relational databases were originated organized as tables (constituted by rows and columns) and with their own query language [5]. These systems provide necessary characteristics in a transactional environment, following the ACID model. The main commercial success of the relational databases was the SQL (Structured Query Language) language, designed and installed at IBM Research, because it became its standard language [6].

Big data.- The digital world is growing very fast, and becomes more complex in terms of volume (terabyte to petabyte), variety (structured, non-structured and hybrid), speed (growing high speed) and nature. This is known as the big data global phenomenon.

This is normally considered as a data collection that has grown up to a point that it cannot be managed nor exploited in an effective manner using traditional data managing tools: for instance, relational database managing systems (RDBMS) or traditional search engines. To handle this problem, traditional RDBMS are complemented by a collection of specially designed alternative database managing systems (DBMS), such as NoSQL [1].

1.1. Technological Platform

The corporate analytics, and related concepts, that describe the analysis of commercial data for decision making, have received wide attention both by the academic and corporate community. The appearance of database systems in memory, has been promoted even more by means of improved data managing procedures and multicore hardware architectures that recently have become available [7].

1.1.1. Architecture

In recent years, some of the most important developments in computing technology are the multicore CPU and the increase in memory capacity based on a 64-bit architecture, which easily supports directly addressable space in terabytes. The multicore architecture enables the parallel massive processing of the database operations, and since all relevant data are permanently stored in the memory, the processing is carried out at the greatest possible speed.

The read operations are completely independent of any access to devices of slower disk storage. On the other hand, the write operations also take place in the memory, but should also be registered in a non-volatile storage to guarantee persistence of the data [8].

1.1.2. In-memory technology

Has been promoted by the need of processing large volumes of data in a very fast manner, and fundamentally by the progress in the processors and the increment in memory capacity based on the 64-bit architecture. This has enabled the parallel massive processing of the database operations, lodging all relevant data in memory [9].

The performance requirement in the Information Technology (IT) domain combined with the advantages of in-memory computing, are important factors

that have influenced the appearence of in-memory databases (IMDB) [10].

1.2. In-memory database

The IMDB constitute a database management system designed for a high performance, with the condition that the existent memory is enough to lodge the necessary data. They possess a technique of columnar storage, which enables the access to the data at high speeds and with real-time analytical capabilities. In comparison with Cloud Computing, the advantage for the user is immediately understandable, since it comes from a rapid analysis of big data volumes [3].

1.3. NoSQL databases

The development community desires a flexible database that easily adapts to the new types of data, and is not interrupted by changes in the structure of the content. Unfortunately, the rigid approach defined and based on the scheme utilized by relational databases, makes impossible to rapidly incorporate new types of data. NoSQL provides a data model that better adapts to these needs, since it does not require any type of scheme with fixed tables, as opposed to the traditional model.

In general NoSQL scales horizontally, and prevents the main joining operations in the data. The NoSQL database covers a swarm of multiple databases, each with a different model of data storage [11]. Its popularity has increased due to the need of fast processing in large volumes of data, taking advantage of its highly scalable architecture, flexible data structure (free of schemes), reduced latency and high performance [12]. They can be divided in four categories according to different optimizations:

1.3.1. Key-value database

A key-value storage consists of a set of pairs where one part represents the key, and the other the values, such as text chains or lists, and more complex sets. The data queries are made using keys, not values [13]

1.3.2. Documentary or document-based databases

They are designed to store data from documents that use different formats such as JSON; MongoDB and CouchDB can be mentioned among these databases [14].

1.3.3. Graphic or graph-based databases

These databases store the information as nodes of a graph, and the relations as the edges. They are extensively utilized in recommendation systems and content management, among others. Among these, Neo4J, GraphBase and Infinite Graph are employed most frequently [14].

1.4. Column oriented databases

In the columnar format, all the values of an attribute of the table are stored as a vector using multiple memory blocks, and all the vectors of attributes of a table are stored sequentially. Organizing the values as a vector of attributes enables an easier understanding of the data, and also a high scanning and filtering speed. This results in significant sequential processing, where the columnar format has an enormous advantage compared with the traditional row-oriented disk database. In conjunction with the option of parallel processing, a very high speed can be reached for filtering or any type of aggregation (which constitutes some of main loads in analytical processing). In fact, the speed is so high, that the idea of pre-aggregation of the transactional data, which was the foundation of information systems in previous decades, can be set aside. Besides, additional indices for faster access to the data are not required [8]. A scheme of row and column operations can be observed in Figure 1. Some of the most remarkable functional characteristics include: high compression, implementation, direct operation on compressed data, iteration per block and efficiency of Join operators, among others.

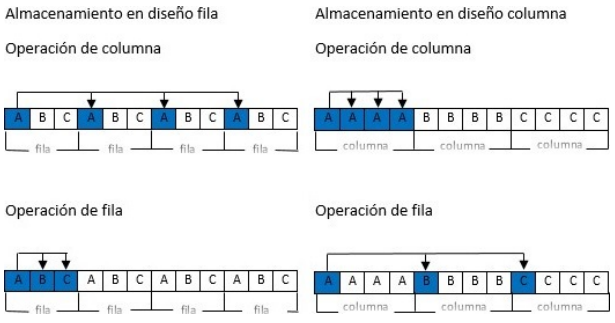

Figura 1. Row and column operations on a data design with rows and columns [8].

1.5. Brewer's Theorem

Since the size of the data grew significantly, it was necessary to find more scalable solutions tan the ACID (Atomicity, Consistency, Isolation and Durability) databases existent so far. As a result, new principles were developed, summarized in the BASE (Basic Availability, Soft-state, Eventual Consistency) paradigm [15].

The ACID properties are centered in the consistency, and are a traditional approach of the databases. Brewer and his team created BASE at the end of the 1990s, to capture the emergent design approaches for

high availability. Modern systems, including the Cloud, use a combination of both approaches, traditional and emergent [16].

The objective of Brewer's theorem was to justify the need to explore a broader design space; hence its formulation. The designers and researchers have utilized Brewer's theorem, as a reason to explore a broad variety on novel distributed systems. It has also been applied by the NoSQL movement, as an argument against traditional databases. In a sense, in the NoSQL movement it is about creating options that first focus in availability and then in consistency; the databases that adhere to the ACID properties do the opposite [16].

According to this theorem, it is impossible to simultaneously guarantee the three characteristics when working with distributed systems. Only two of the three features are possible, it is necessary to resign or even partially sacrifice one feature to obtain the others [17].

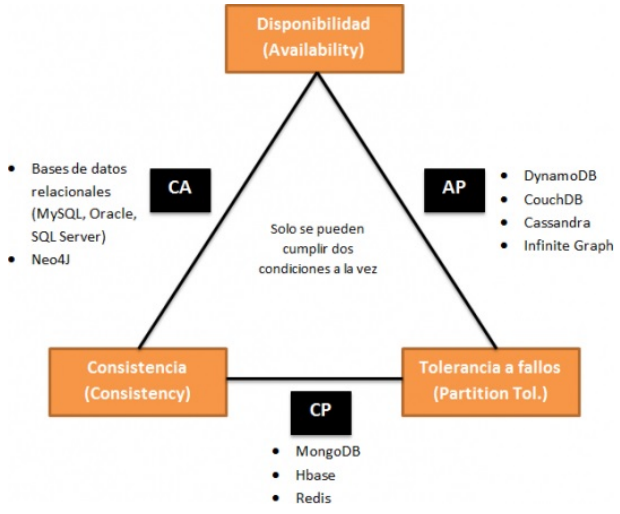

Figura 2. Brewer's theorem [18].

- Consistency (C) is equivalent to have a unique updated copy of the data.
- High availability (A) of these data (for updated).
- Tolerance to partitions of the network (P).

A popular way to characterize NoSQL has been to examine its approach to meet Brewer's theorem of coherence, availability and tolerance to partitions (CAP). Most of the NoSQL systems has been designed to sacrifice consistency in exchange of a high availability in a partitioned environment [19]. Figure 2 presents a view of the theorem, in relation to some example databases.

The option of resigning to the tolerance to partition is not feasible in real environments, since there are always partitions in the network. Therefore, in can be deducted that the decision is between availability and consistency, which can be represented as ACID (consistency) and BASE (availability). Nevertheless, Brewer acknowledged that the decision is not binary. All the intermediate spectrum is useful; in general, mixing different levels of availability and consistency yields a better result [15]. The current objective of the theorem should be maximizing combinations of consistency and availability that make sense for a specific application [16].

2. Materials and methods

This work conducts an applied research, with the objective that the final results are utilized in solving corporate problems. The design is descriptive quantitative-comparative, since it aims at specifying what types of databases have a better performance, by measuring and studying their characteristics. The instruments used in the study include standardized tests to compare two groups of databases: columnar and relational.

The procedure that will be utilized comprises the following steps: i) determine the sample, in which the database engines under study are chosen, through a non-probabilistic sampling by criterion, ii) selection/creation of the data set, iii) design of the test scenario, to establish how tests are carried out, which queries will be executed, the number of measurements that will be conducted, among others; the hardware and software infrastructure that will be used is also specified, iv) data loading, where all the databases determined in the sample are loaded, v) measurement, which are carried out using the method of averages and with a specialized tool; similarly, results are registered in all defined scenarios, vi) analysis of results, where the results are interpreted by means of graphs and tables.

2.1. Determining the sample

Before choosing the sample, it was established that the population is constituted by all columnar and relational databases existing up to the present research work. A non-probabilistic sampling by criterion was used for the selection, which is the best type of non-probabilistic sampling. The inclusion and exclusion criteria for delimiting the population are:

- Open source databases (without license).
- Experience of the researchers.

The SQL databases evaluated in this paper are PostgreSQL and MySQL. In comparison with similar databases, they are included in the quadrant among the best open source relational databases [20].

Under the same criteria, the NoSQL databases evaluated are: MongoDB, Cassandra, MonetDB. These

alternatives were chosen for being open source and of massive utilization; as can be observed in the Ranking of columnar databases [21], they are pioneers among their peers due to characteristics such as scalability, fault tolerance and columnar storage in conjunction with memory storage.

Another factor that was taken into account is that they can interpret the SQL syntax, which reduces the impact of switching to a NoSQL environment. Although it is not a columnar database, MongoDB is a type of NoSQL database specifically documentary. It was chosen to compare columnar databases, not only with SQL databases, but also with other types of NoSQL databases, documentary in this case. Additionally, MongoDB also employs in-memory technology.

Therefore, the final sample will contain the databases in Table 1, which also shows the family of databases that it belongs to, and the version that will be used in this research.

Tabla 1. Details of databases

Name de datos	Type	Version
MySQL	Relacional – SQL	8.1.0
PostgreSQL	Relacional – SQL	9.6.2
Cassandra	Columnar – NoSQL	3.1.0
MonetDB	Columnar – NoSQL	11.29.3
MongoDB	Documental – NoSQL	3.6.5

2.2. Selection / creation of the data set

An existing set of databases obtained from a public source [22], was chosen to evaluate and compare the performance of the databases. This corresponds to the sales of a large commercial corporation, considering the invoices in the period 2015-2016. The file has a total number of 125,000,000 (125 million) records. The data is stored in CSV files for an easy and uniform access. Table 2 includes a description of the fields contained in the file.

Tabla 2. Description of the fields

Field	Type	Description
Id	INT	Unique identifier
Date	DATE	Product registration date
Store_nbr	INT	Store identifier
Item_nbr	INT	Product identifier
Unit_sales	DECIMAL	Number of units sold, it is an integer number, a negative value represents a return
Onpromotion	BOOLEAN	Indicates if the item was on a promotion for a specific date and store

2.3. Design of the test scenario

The tests with incremental loading of the data will be executed first, i.e., the main data file that contains 125 million records will be divided in the following way: one million, ten million, twenty-five million and fifty million records. The resulting four files will constitute for different scenarios; these four files contain the same number of columns and types of data. The queries to all databases will be executed in these four scenarios. In this way, the performance of the relational databases is tested against the columnar databases in similar scenarios. The specification of the test scenarios are detailed in Table 3.

2.4. Design of queries

Three types of query will be executed in the four scenarios already defined.

i. First query (key-value): this type of query returns a single register of all data set, which will be searched for in the database by means of a key (id). Example:

```
SELECT id, item_nbr, store_nbr, date

FROM train

WHERE id = 500023352;
```

ii. Second query (clause where – data set): the following is considered for its design: the resulting set of data should return at least one third or more of the total of data in each scenario. As can be seen in Table 4, the date changes in each query to return approximately 30% of the total of data.

iii. Third query (aggregation function): it will use the aggregation function SUM() to calculate the total sales of a particular store.

```
SELECT SUM (unit_sales)

FROM train

WHERE store_nbr = '12'
```

Tabla 3. Specifications of the scenarios

Specification	Scenario 1	Scenario 2	Scenario 3	Scenario 4
Data size	1 000 000	10 000 000	25 000 000	50 000 000
Variable	Execution time (ms)			
Description	Three types of queries will be executed: · Key – value · Data set · Agregation function			
Query policies	Queries to a table for relational and columnar databases databases			

Tabla 4. Query (set of data) for the four scenarios

Scenarios	Consult	Returned data
1.st scenario (1 million)	SELECT id, item_nbr, store_nbr, date FROM train1m WHERE date >= '2015-07-05';	388 964
2.nd scenario (10 millions)	SELECT id, item_nbr, store_nbr, date FROM train10m WHERE date >= '2015-09-15';	3 392 156
3.rd scenario (25 millions)	SELECT id, item_nbr, store_nbr, date FROM train25m WHERE date >= '2015-12-31';	8 637 780
4.th scenario (40 millions)	SELECT id, item_nbr, store_nbr, date FROM train50m WHERE date >= '2016-06-25';	16 907 734

2.5. Test environment

The tests were carried out in a single machine with the characteristics described in Table 5.

Tabla 5. Characteristics of the test environment

Software / Hardware	Description
Operating sistema	Ubuntu 14.04 (64-bits)
RAM Memory	16 GB
Processor	AMD Radeon R7, 12 compute Cores 4C + 8G – 3,70 GHz
Hard disk	1 Terabyte

2.6. Measurement

The respective queries were executed in each scenario, to register the response times of each database. Aqua Data Studio, a graphical tool for tasks of administration, design and query in different databases, was used here with the objective that measurements are more reliable and human errors are avoided.

Measurement in the first scenario – 1 million of records (Tables 6, 7, 8).

Tabla 6. First query (key-value)

	Time in (ms) Type of data base	M1	M2	M3	M4	M5	Average
MySQL	SQL	2	1	2	3	2	2
POSTGRESQL	SQL	10	10	8	9	8	9
MONGODB	NoSQL	2	3	3	2	4	2,8
MONETDB	NoSQL	5	3	3	4	5	4
CASSANDRA	NoSQL	4	3	3	4	3	3,4

Tabla 7. Second query (data set)

	Time in (ms) Type of data base	M1	M2	M3	M4	M5	Average
MySQL	SQL	515	594	547	484	516	531,2
POSTGRESQL	SQL	462	468	460	497	453	468
MONGODB	NoSQL	130	124	114	110	189	133,4
MONETDB	NoSQL	191	184	190	189	211	193
CASSANDRA	NoSQL	3	12	11	8	13	9,4

Tabla 8. Third query (aggregation)

	Time in (ms) Type of data base	M1	M2	M3	M4	M5	Average
MySQL	SQL	359	344	360	343	359	353
POSTGRESQL	SQL	155	156	158	155	153	155,4
MONGODB	NoSQL	72	64	70	88	68	72,4
MONETDB	NoSQL	83	96	81	84	84	85,6
CASSANDRA	NoSQL	69	72	61	49	62	62,6

Measurement in the second scenario – 10 million of records (Tables 9, 10, 11).

Tabla 9. First query (key-value)

	Time in (ms) Type of data base	M1	M2	M3	M4	M5	Average
MySQL	SQL	4	1	2	2	3	2,4
POSTGRESQL	SQL	9	10	11	10	11	10,2
MONGODB	NoSQL	4	2	2	3	4	3
MONETDB	NoSQL	5	4	4	5	5	4,6
CASSANDRA	NoSQL	5	5	4	6	5	5

Tabla 10. Second query (data set)

	Time in (ms) Type of data base	M1	M2	M3	M4	M5	Average
MySQL	SQL	6375	6141	6469	6672	6453	6422
POSTGRESQL	SQL	4960	5739	4720	4119	5420	4991,6
MONGODB	NoSQL	249	255	246	262	245	251,4
MONETDB	NoSQL	267	287	248	235	305	268,4
CASSANDRA	NoSQL	15	35	16	14	22	20,4

Tabla 11. Third query (aggregation function)

	Time in (ms) Type of data base	M1	M2	M3	M4	M5	Average
MySQL	SQL	4984	3437	3547	3469	3485	3784,4
POSTGRESQL	SQL	1447	1411	1551	1489	1527	1485
MONGODB	NoSQL	632	588	590	596	628	606,8
MONETDB	NoSQL	716	724	704	705	694	708,6
CASSANDRA	NoSQL	523	538	525	521	518	525

Medición del tercer escenario – 25 millones de registros (Tablas 12, 13, 14).

Tabla 12. First query (key-value)

	Time in (ms) Type of data base	M1	M2	M3	M4	M5	Average
MySQL	SQL	3	2	3	4	2	2,8
POSTGRESQL	SQL	11	14	12	12	14	12,6
MONGODB	NoSQL	2	3	2	4	3	2,8
MONETDB	NoSQL	6	6	5	4	4	5
CASSANDRA	NoSQL	6	4	6	4	4	4,8

Tabla 13. Second query (data set)

	Time in (ms) Type of data base	M1	M2	M3	M4	M5	Average
MySQL	SQL	14500	14750	14593	14641	16125	14921,8
POSTGRESQL	SQL	12604	12870	12121	11930	11883	12281,6
MONGODB	NoSQL	147	130	153	131	124	137
MONETDB	NoSQL	406	404	419	397	413	407,8
CASSANDRA	NoSQL	17	8	13	13	22	14,6

Tabla 14. Third query (aggregation function)

	Time in (ms) Type of data base	M1	M2	M3	M4	M5	Average
MySQL	SQL	10781	10937	10579	9204	9078	10115,8
POSTGRESQL	SQL	4660	3778	4846	4109	3709	4220,4
MONGODB	NoSQL	1488	1765	1776	1487	1454	1594
MONETDB	NoSQL	1818	2513	1823	1799	1788	1948,2
CASSANDRA	NoSQL	1855	1715	1936	1962	2017	1897

Medición del cuarto escenario – 50 millones de registros (Tablas 15, 16, 17).

Tabla 15. First query (key-value)

	Time in (ms) Type of data base	M1	M2	M3	M4	M5	Average
MySQL	SQL	3	3	5	2	3	3,2
POSTGRESQL	SQL	12	13	15	12	13	13
MONGODB	NoSQL	4	3	2	2	3	2,8
MONETDB	NoSQL	5	4	4	4	4	4,2
CASSANDRA	NoSQL	7	4	11	6	9	7,4

Tabla 16. Second query (data set)

	Time in (ms) Type of data base	M1	M2	M3	M4	M5	Average
MySQL	SQL	28625	28829	29891	29828	29953	29425,2
POSTGRESQL	SQL	24369	24709	26570	25182	26190	25404
MONGODB	NoSQL	295	298	292	293	296	294,8
MONETDB	NoSQL	779	718	654	656	767	714,8
CASSANDRA	NoSQL	19	8	11	25	14	15,4

Tabla 17. Third query (aggregation function)

	Time in (ms) Type of data base	M1	M2	M3	M4	M5	Average
MySQL	SQL	21172	21266	21125	20641	20562	20953,2
POSTGRESQL	SQL	7930	8110	9876	8504	8179	8519,8
MONGODB	NoSQL	3196	3337	3446	2978	3667	3324,8
MONETDB	NoSQL	3791	4058	3745	3629	4424	3929,4
CASSANDRA	NoSQL	2989	3212	3015	3172	2905	3058,6

3. Results and discussion

The measurement results are analyzed in two sections, by scenario and by query.

3.1. Results by scenario

The average times, in milliseconds, resulting from the execution of the three queries in the four scenarios (with 1, 10, 25 and 50 million records) are presented and analyzed.

3.1.1. First scenario – 1 million records

Table 18 shows the results obtained, in milliseconds, during the execution of the three queries with a total of 1 million records.

Tabla 18. Results 1 million records

First scenario Time in (ms)			
	C1 key-value	**C2 data set**	**C3 agregation**
MySQL	2	531,2	353
PostgreSQL	9	468	155,4
MongoDB	2,8	133,4	72,4
MonetDB	4	193	85,6
Cassandra	3,4	9,4	62,6

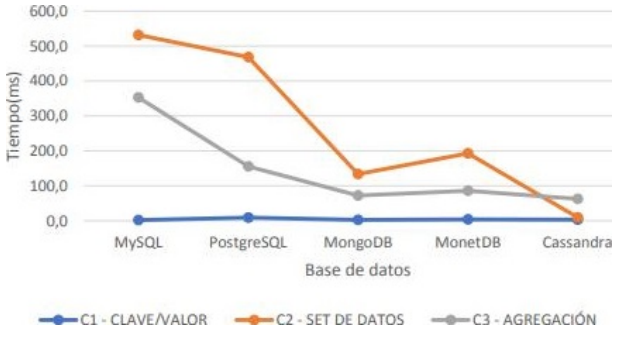

Figura 3. Results 1 million records

Figure 3 shows that for the first query of type key-value, no changes are observed in the execution times among the compared databases. In the second query, in which a where clause that returns a data set is used, variations can be seen between the performance of the databases, with MySQL exhibiting the worst time of response with 531.2 milliseconds, followed by PostgreSQL, compared with the columnar database Cassandra that has a time of response of 9.4 milliseconds, which is 56.51 times more efficient than MySQL. When employing the SUM aggregation function in the third query, it is observed that the best times of responses are obtained with Cassandra, MonetDB and MongoDB; Cassandra is the most efficient with 62.6 milliseconds, which is 5.64 times more efficient than MySQL, that has a time of 353 milliseconds.

3.1.2. Second scenario – 10 million of records

Table 19 shows the results obtained, in milliseconds, during the execution of the three queries with a total of 10 million records.

Tabla 19. Results 10 million records

Second scenario Time in (ms)			
	C1 key-value	**C2 data set**	**C3 agregation**
MySQL	2,4	6422	3784,4
PostgreSQL	10,2	4991,6	1485
MongoDB	3	251,4	606,8
MonetDB	4,6	268,4	708,6
Cassandra	5	20,4	525

Figure 4 shows a significant difference in the times of response corresponding to the second and third queries, of the columnar databases compared to the relational databases; however, for the first query the times of response in the two types of database keep being regular, without variations. The databases MongoDB, MonetDB and Cassandra had similar times. In the second query, MySQL exhibited the lowest performance with 6422 milliseconds, almost similar to Postgres, compared to Cassandra with a time of 20.4 milliseconds, 314.8 times more efficient than MySQL. In the third query, MySQL again showed the highest time with 3784 milliseconds, compared to the 525 milliseconds obtained with Cassandra; hence, the columnar database was 7.21 times more efficient.

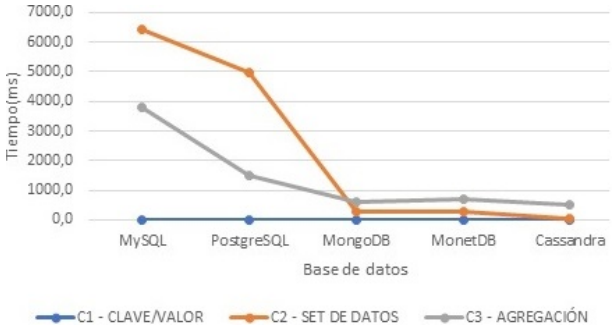

Figura 4. Results 10 million records

3.1.3. Third scenario – 25 million records

Table 20 shows the results obtained, in milliseconds, during the execution of the three queries with a total of 25 million records.

In the results corresponding to the third scenario, which are shown in Figure 5, the times of response for the first query remain similar in all databases. For queries 2 and 3, a good performance is attained for databases MongoDB, MonetDB and Cassandra. Among the column oriented type databases, Cassandra exhibited a time of response similar to MonetDB in queries 2 and 3. In the second query, MySQL exhibited the worst performance with 14921.8 milliseconds, which is 1000 times greater compared to the columnar database Cassandra, which had 14.6 milliseconds. Similarly, in the third query MySQL showed a time of

10115.8 milliseconds, which is 5.38 times slower than the 1879 milliseconds corresponding to Cassandra.

Tabla 20. Results 25 million records

Third scenario Time in (ms)			
	C1 key-value	**C2 data set**	**C3 agregation**
MySQL	2,8	14921,8	10115,8
PostgreSQL	12,6	12281,6	4220,4
MongoDB	2,8	137	1594
MonetDB	5	407,8	1948,2
Cassandra	4,8	14,6	1897

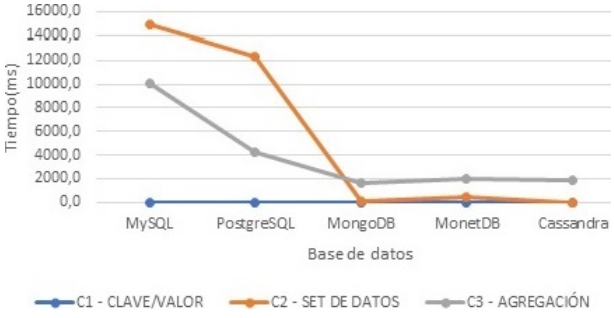

Figura 5. Results 25 million records

3.1.4. Fourth scenario – 50 million records.

Table 21 shows the results obtained, in milliseconds, during the execution of the three queries with a total of 50 million records.

Tabla 21. Results 50 million records

Fourth scenario Time in (ms)			
	C1 key-value	**C2 data set**	**C3 agregation**
MySQL	3,2	29425,2	20953,2
PostgreSQL	13	25404	8519,8
MongoDB	2,8	294,8	3324,8
MonetDB	4,2	714,8	3929,4
Cassandra	7,4	15,4	3058,6

Figure 6 of the fourth scenario shows that the first query remains without variations, in the time of response in all databases. For queries 2 and 3 it can be observed that the databases with the worst performance are MySQL followed by PostgreSQL. MySQL is 46.1 times slower than MonetDB, while the PostgreSQL responded slightly better in the third query being only 2.7 times slower than Cassandra. The latter is the leader in efficiency, being 46 times faster than its counterpart MonetDB in the second query.

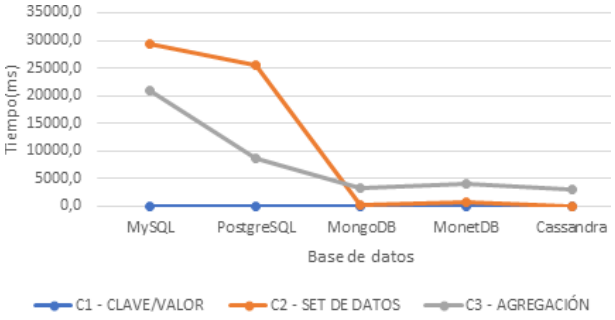

Figura 6. Results 50 million records

3.2. Results by query

The resulting average times, in milliseconds, grouped by query in all scenarios are presented and analyzed.

3.2.1. First query – key-value

Table 22 shows the results obtained, in milliseconds, during the execution of the first query (key-value) in all scenarios.

Tabla 22. Results first query

First query – key-value # records				
Database	**1 MM**	**10 MM**	**25 MM**	**50 MM**
MySQL	2	2,4	2,8	3,2
PostgreSQL	9	10,2	12,6	13
MongoDB	2,8	3	2,8	2,8
MonetDB	4	4,6	5	4,2
Cassandra	3,4	5	4,8	7,4

It can be observed in Figure 7, that the times of response for the first query are very similar and efficient for all databases. For both MySQL and PostgreSQL, the times of response do not vary significantly as the volume of data grows; the same occurs with the times of response of Cassandra, MongoDB and MonetDB, which remain without notable changes. None of these databases delays more than one second in carrying out this query.

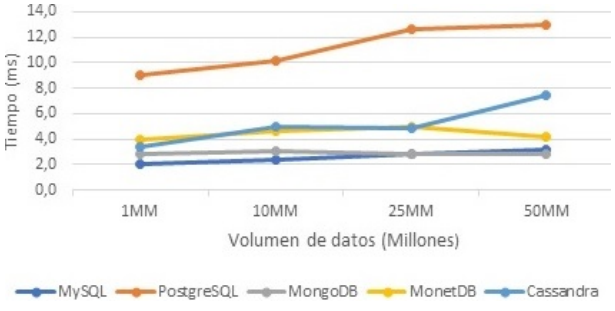

Figura 7. Results first query

3.2.2. Second query – data set

Table 23 shows the results obtained, in milliseconds, during the execution of the second query (data set) in all scenarios.

Tabla 23. Results second query

Second query – data set # records				
Database	**1 MM**	**10 MM**	**25 MM**	**50 MM**
PostgreSQL	468	4991,6	12281,6	25404
MySQL	531,2	6422	14921,8	29425,2
MongoDB	133,4	251,4	137	294,8
MonetDB	193	268,4	407,8	714,8
Cassandra	9,4	20,4	14,6	15,4

When the second query is executed, a clause where is utilized that returns 30% of all the data. A clear difference in the times of response can be observed in Figure 8 as the number of records increase, between the relational and columnar databases. With 1 MM data, the time of response of MySQL was 531 milliseconds, but with 50 MM data its time of response significantly increased to 29425 milliseconds; the case of PostgreSQL was similar. On the other hand, columnar databases maintain an average time which is independent of the volume of data. For instance, with 1 MM records Cassandra had an execution time of 9.4 milliseconds, while for 50 MM records such time was 15.4 milliseconds.

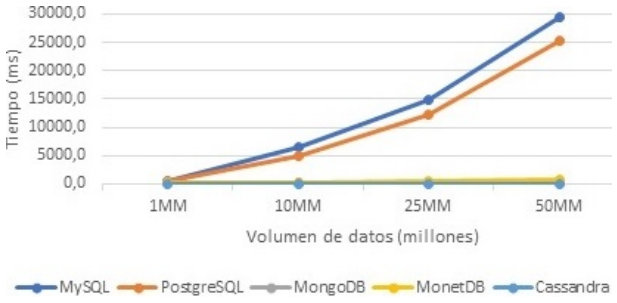

Figura 8. Results second query

3.3. Third query – aggregation function sum ()

Table 24 shows the results obtained, in milliseconds, during the execution of the third query (aggregation function) in all scenarios

Tabla 24. Results third query

Third query – aggregation function (SUM) # records				
Database	**1 MM**	**10 MM**	**25 MM**	**50 MM**
MySQL	353	3784,4	10115,8	20953,2
PostgreSQL	155,4	1485	4220,4	8519,8
MongoDB	72,4	606,8	1594	3324,8
MonetDB	85,6	708,6	1948,2	3929,4
Cassandra	62,6	525	1897	3058,6

Analyzing Figure 9for 1 and 10 million records, the variations on the times of response in all databases do not exhibit a significant difference, as opposed to the cases when the volume of data increases to 25 and 50 million, for which there is a considerable variation in the time of response between the relational and columnar databases; when the query is executed with 50 million records, the time of response for PostgreSQL is 20953 milliseconds and for MongoDB 3324 milliseconds. As the number of records increases, the difference in performance between MongoDB and PostgreSQL becomes evident. The times of response of Cassandra, MonetDB and MongoDB is slightly affected as the volume of data increases.

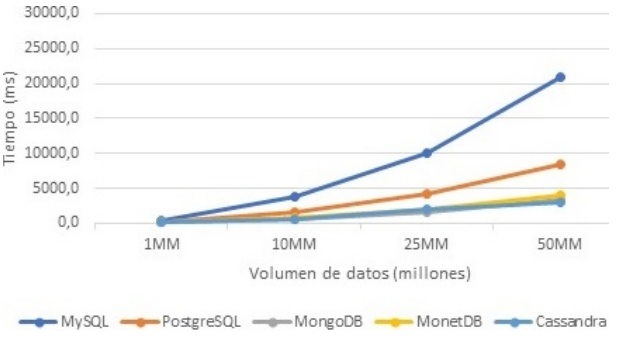

Figura 9. Results third query

Based on the results obtained and the specific characteristics of each database, it was found that for the relational databases MySQL and Postgres there is a directly proportional relationship between volume of data and time, i.e. as the volume of data increases, the time of query increases in a larger proportion. In contrast, for the columnar databases Cassandra and MonetDB, an increase in the volume of data has a smaller impact in the times of response.

The columnar databases exhibit a better performance since they incorporate the in-memory technology (in the RAM memory) for data storage and recovery, which enables a smaller execution time of the queries, as opposed to the relational databases where the performance is affected by the fact that the records should be read from disc, which is much slower compared to the RAM memory.

4. Conclusions

At the end of the present research the stated objectives have been attained, and thus it is concluded that the performance of a columnar database is optimal in data analysis environments.

For the MySQL and Postgres databases, the relationship between volume of data and time is direct and incrementally proportional; on the contrary, in the databases Cassandra and MonetDB that belong to the

columnar family, the times of execution do not show notable variations as the volume of data increases.

All the databases compared had the same efficiency in the execution of the first query of type key-value; due to the presence of the primary key, all databases exhibited similar execution times, thus for this query both types of databases have an optimal performance. On the contrary, for the second (data set) and third (aggregation function) queries the difference in the times of execution is rather evident. The superior performance of the columnar databases, which improved the efficiency up to 7.21 and 1900 times in the second and third queries, respectively, is because they highly occupy the volatile memory for data storage and recovery, which enables a smaller execution time of the queries, as opposed to the relational databases for which the performance is not the best, due to the fact that registers should be read from disc, which is much slower than the volatile memory.

The type of columnar databases and, in general, the NoSQL paradigm is adequate for tackling the current big data problem, which refers to the management of large amounts of data. It is therefore recommended to first analyze the business logic, use case and infrastructure, to verify what type of database is the most appropriate for solving problems of interest; regarding this, other existing types of NoSQL databases may be evaluated.

Data analysis requires databases capable of effectively storing and processing large amounts of data, and demands high performance when reading and writing; hence, traditional relational databases are not the most adequate solution. Columnar databases arise as a solution that fulfill performance expectations in this field.

The SQL and NoSQL databases provide different features, and one cannot replace the other. If the system is not flexible in terms of consistency, the relational database administration system is the correct option. If the system can resign to consistency up to a certain point, the NoSQL databases may be the best option to provide more availability, scalability and high performance.

Therefore, depending on the stated objective, a hybrid model, which combines both the SQL and NoSQL technologies, may be the choice in mind; if it is necessary to maintain greater consistency, a relational way of storage may be implemented, while for immediate or recurrent queries, columnar databases would be used.

A future work may consider carrying out the same study, but in a distributed and parallel environment, to contrast and verify the results obtained in this research. There is also the possibility of continuing this study in more depth regarding issues such as configuration and carrying out queries, to take better advantage of these tools. Another future research line would focus in a detailed analysis of writing in columnar databases, with respect to relational databases.

This work summarizes the most important elements and considerations that were totally developed in thesis [23].

Referencias

[1] A. B. M. Moniruzzaman and S. A. Hossain, "Nosql database: New era of databases for big data analytics - classification, characteristics and comparison," *International Journal of Database Theory and Application*, vol. 6, no. 4, pp. 1–5, 2013. [Online]. Available: http://bit.ly/2XaKoPK

[2] M. F. Pollo Cattaneo, M. López Nocera, and G. Daián Rottoli, "Rendimiento de tecnologías nosql sobre cantidades masivas de datos," *Cuaderno Activa*, no. 6, pp. 11–17, 2014. [Online]. Available: http://bit.ly/2Rb8zrO

[3] I. Mihaela-Laura, "Characteristics of in-memory business intelligence," *Informatica Economică*, vol. 18, no. 3, pp. 17–25, 2014. [Online]. Available: http://doi.org/10.12948/issn14531305/18.3.2014.02

[4] D. Robles, M. Sánchez, R. Serrano, B. Adárraga, and D. Heredia, "?'qué características tienen los esquemas nosql?" *Investigación y desarrollo en TIC*, vol. 6, no. 1, pp. 40–44, 2015. [Online]. Available: http://bit.ly/2MJ1wZa

[5] M. Marqués, *Bases de datos.* Universitat Jaume, 2011. [Online]. Available: http://bit.ly/2RcPtS9

[6] E. Ramez and S. B. N., *Fundamentals of Database Systems.* Pearson Education., 2015. [Online]. Available: http://bit.ly/2IG3pAk

[7] G. Hahn and J. Packowski, "A perspective on applications of in-memory analytics in supply chain management," *Decision Support Systems*, vol. 76, pp. 45–52, 2015. [Online]. Available: https://doi.org/10.1016/j.dss.2015.01.003

[8] H. Plattner and B. Leukert, *The In-Memory Revolution. Springer.* Springer, 2015. [Online]. Available: http://bit.ly/2F3ezhO

[9] M. R. Morales Morales and S. L. Morales Cardoso, "Inteligencia de negocios basada en bases de datos in-memory," *Revista Publicando*, vol. 11, no. 2, pp. 201–217, 2017. [Online]. Available: http://bit.ly/2WB3vmC

[10] R. Babeanu and M. Ciobanu, "In-memory databases and innovations in Business Intelligence," *Database Systems Journal*, vol. 6, no. 1, pp. 59–67, July 2015. [Online]. Available: http://bit.ly/2wZLFL7

[11] V. D. Shetty and S. J. Chidimar, "Comparative study of sql and nosql databases to evaluate their suitability for big data application," *International Journal of Computer Science and Information Technology Research*, vol. 4, no. 2, pp. 314–318, 2016. [Online]. Available: http://bit.ly/2KlNZor

[12] A. T. Kabakus and R. Kara, "A performance evaluation of in-memory databases," *Journal of King Saud University - Computer and Information Sciences*, vol. 29, no. 4, pp. 520–525, 2017. [Online]. Available: https://doi.org/10.1016/j.jksuci.2016.06.007

[13] M. T. González-Aparicio, M. Younas, J. Tuya, and R. Casado, "Testing of transactional services in nosql key-value databases," *Future Generation Computer Systems*, vol. 80, pp. 384–399, 2018. [Online]. Available: https://doi.org/10.1016/j.future.2017.07.004

[14] A. Nayak, A. Poriya, and D. Poojary, "Type of nosql databases and its comparison with relational databases," *International Journal of Applied Information Systems (IJAIS)*, vol. 5, no. 4, pp. 16–19, 2013. [Online]. Available: http://bit.ly/2X2fIQQ

[15] S. Simon, "Report to brewer's original presentation of his cap theorem at the symposium on principles of distributed computing (podc) 2000," University of Basel, HS2012, Tech. Rep., 2018. [Online]. Available: http://bit.ly/2XFBo2l

[16] E. Brewer, "Cap twelve years later: How the "rules" have changed," *Computer*, vol. 45, no. 2, pp. 23–29, Feb 2012. [Online]. Available: https://doi.org/10.1109/MC.2012.37

[17] M. Indrawan-Santiago, "Database research: Are we at a crossroad? reflection on nosql," in *2012 15th International Conference on Network-Based Information Systems*, Sep. 2012, pp. 45–51. [Online]. Available: https://doi.org/10.1109/NBiS.2012.95

[18] GENBETA. (2019) Nosql: clasificación de las bases de datos según el teorema cap. [Online]. Available: http://bit.ly/2WHVvR4

[19] R. D. L. Engle, B. T. Langhals, M. R. Grimaila, and D. D. Hodson, "Evaluation criteria for selecting nosql databases in a single-box environment," *International Journal of Database Management Systems (IJDMS)*, vol. 10, no. 4, pp. 1–12, 2018. [Online]. Available: http://bit.ly/2ZgXEQc

[20] Crowd. Inc. (2019) Best relational databases software. [Online]. Available: http://bit.ly/2RbQPge

[21] DB-Engines. (2019) Db-engines ranking of wide column stores. [Online]. Available: http://bit.ly/2KOBYHs

[22] Kaggle. (2019) Corporación favorita grocery sales forecasting. [Online]. Available: http://bit.ly/2F7QYMS

[23] J. W. Durán Cazar, E. J. Tandazo Gaona, and M. R. Morales Morales, *Estudio del rendimiento de una base de datos columnar en el análisis de datos.* Tesis de Grado. Universidad Central del Ecuador, 2018. [Online]. Available: http://bit.ly/2KhB0nl

Scientific Paper / Artículo Científico

UNIVERSIDAD POLITÉCNICA SALESIANA ECUADOR
INGENIUS
Revista de Ciencia y Tecnología
https://doi.org/10.17163/ings.n22.2019.06
pISSN: 1390-650X / eISSN: 1390-860X

Assessment of the Maintenance Management in Hospitals of the Ecuadorian Institute of Social security of Zona 3 of Ecuador

Evaluación de la gestión del mantenimiento en hospitales del Instituto Ecuatoriano de Seguridad Social de la Zona 3 del Ecuador

Mayra Viscaíno-Cuzco[1,*], Sergio Villacrés-Parra[1],
César Gallegos-Londoño[1] Hernán Negrete-Costales[2]

Abstract

The hospital infrastructure failures have an inestimable impact because they put human lives at stake. Therefore, potential risks contributing to the failure of medical equipment and hospital infrastructure must be identified, reduced or eliminated. The maintenance and its management constitute a tool that ensures the equipment performance. The aim of this work was to obtain quantitative data of the maintenance management at the hospitals of Zone 3 of the Ecuadorian Social Security system. The methodology consists of five phases: selection of assessment criteria, weighting of criteria, development of the assessment instrument, validation of the instrument by applying it to the four hospitals of Zone 3 in Ecuador and, at last, identification of low-performing aspects. Results demonstrate that the maintenance management of the hospitals in Zone 3 reached a quantitative average value of 55.5/100 points.

Resumen

Los fallos en la infraestructura hospitalaria tienen consecuencias inestimables debido a que involucra la vida humana, por lo que los riesgos potenciales que contribuyen al fallo de equipos médicos e infraestructura hospitalaria, tienen que ser identificados, reducidos o eliminados; para ello el mantenimiento y su gestión es una herramienta que se enfoca en asegurar el funcionamiento de un equipo. El propósito de este trabajo fue el obtener una valoración cuantitativa de la gestión del mantenimiento en los hospitales del Instituto Ecuatoriano de Seguridad Social de la Zona 3 del Ecuador. La metodología empleada consta de cinco fases, empezando por la selección de criterios de evaluación, ponderación de criterios, desarrollo del instrumento de evaluación, la validación del instrumento aplicándolo a cuatro hospitales de la Zona 3 del Ecuador; finalmente, la identificación de aspectos con bajo desempeño. Los resultados muestran que la gestión de mantenimiento de los hospitales de la Zona 3, alcanzaron una valoración cuantitativa promedio de 55,5/100 puntos.

[1,*]Grupo de investigación «Gestión del mantenimiento», Escuela Superior Politécnica de Chimborazo, Ecuador, Autor para correspondencia ✉: mayra.viscaino@espoch.edu.ec, mayraviscaino@hotmail.com
http://orcid.org/0000-0003-4987-7797, http://orcid.org/0000-0002-9497-9795.
http://orcid.org/0000-0002-8685-7501.
[2]Facultad de Mecánica. Escuela Superior Politécnica de Chimborazo, Ecuador
http://orcid.org/0000-0002-2678-761X.

Received: 04-05-2019, accepted after review: 18-06-2019

Suggested citation: Viscaíno-Cuzco, M.; Villacrés-Parra, S.; Gallegos-Londoño, C. and Negrete-Costales, H. (2019). «Assessment of the Maintenance Management in Hospitals of the Ecuadorian Institute of Social security of Zona 3 of Ecuador». Ingenius. N.°22, (july-december). pp. 59-71. doi: https://doi.org/10.17163/ings.n22.2019.06.

There are structural deficiencies that compromise the achievement of the maintenance department goals in three hospitals, yet there are viable processes that can be implemented to overcome such deficiencies and increase the level of fulfillment of requirements. It is concluded that the planning, programming and control of maintenance is the criterion with more potential to be improved.

Keywords: hospital maintenance, maintenance management, analytic hierarchy process, maintenance assessment, public health system.

En tres hospitales se evidencian debilidades estructurales que comprometen el logro de los objetivos del departamento de mantenimiento, pero existen procesos viables que pueden ser implantados para superar las deficiencias e incrementar el nivel de cumplimiento de las exigencias. Se concluye que la planificación, programación y control del mantenimiento es el criterio con más potencial para mejorar.

Palabras clave: mantenimiento hospitalario, gestión del mantenimiento, proceso analítico jerárquico, evaluación del mantenimiento, sistema de salud público.

1. Introduction

A high performance of the machines is requested in the industrial area, to avoid economic losses; nevertheless, failures in the infrastructure of hospitals may cause inestimable consequences, because it involves human life. A hospital is a complex structure constituted by medical and industrial equipment, and a multiform infrastructure that supports the provision of health services, which due to its importance requires that medical equipment do not present unexpected failures in their operation, that infrastructure provides a healthful and safe environment as an indispensable resource for doctors to ensure a good attention to patients, that correct diagnostics are generated, and even that the life of such patients is safeguarded.

This indicates that the potential risks that contribute to the failure of medical and industrial equipment and infrastructure, have to be identified and reduced, or as far as possible eliminated [1]. For that matter, the corresponding department has the maintenance and its management as a tool, that essentially focus in assuring the operation of equipment [2], either medical or industrial. According to Gonnelli *et al.* [3], the maintenance is an essential part of the life cycle of a medical equipment; however, the importance of the maintenance for the medical technology is not so known, and is only considered as a support activity [4].

In Ecuador, the health system is mainly constituted by public and private establishments [5]. The public system has more institutions (81.5 %) [6], and the Ecuadorian Institute of Social Security (EISS), that serves its affiliate population from 1970, is one of its constituting institutions. A ruling principle of the Ecuadorian social security system, is that it will work based on sustainability, efficiency, speed and transparence criteria [7]. According to the law of social security, efficiency should be understood as «the best economic utilization of the contributions and the other resources of the obligatory general insurance, to guarantee the timely delivery of enough provisions to its beneficiaries» [8]. Nevertheless, the economic problems faced by this institution for many years become evident in the type of attention provided to its users; the action in health attention is critic and inefficient, according to the president of the Directing Council of the EISS [9]. In addition, there are administrative problems with the hospital infrastructure due to lack of maintenance; in November 2018, the authorities of the EISS hospital in Cotopaxi expressed that the surgeries would be suspended because the sterilization equipment were not available due to lack of maintenance [10].

The availability of specialized medical equipment plays a fundamental role in the provision of health services; improving the maintenance of medical equipment in terms of effectiveness, reliability and availability, ultimately means improving the security of the patient and the user [3]]. According to a research carried out by Mwanza and Mbohwa, the main problems detected in a hospital related to maintenance, are the high unavailability of equipment and the no execution of the equipment maintenance according to the program established [11]. Since the quality of maintenance is key for providing a good medical attention to patients [12], it is necessary to evaluate its performance.

Gonnelli *et al.* [3] and Orozco *et al.* [13] indicated that measuring the performance of maintenance is a multidisciplinary process, and it is considered important for an organization because it is a tool that enables managerial decision making in a timely manner. Its objective tends to be misinterpreted, and the purpose is not judging the responsible people or questioning the results of their work, much less to sanction them, but identifying those aspects susceptible of being optimized [14], justify the investment made in maintenance [15] and avoiding that economic resources are wasted due to a deficient or inefficient maintenance [4]. The systematic evaluation enables assessing the performance of an organization of any area, and proposing the organizational and managerial changes to improve the system. Whether the results of the evaluation are negative or positive, the proposed strategies should aim to continuously improve, for the organization to operate successfully.

From 2014, an international accreditation process known as «Accreditation Canada International» (ACI) is conducted in Ecuador. Forty four public hospitals were evaluated [16], with the purpose of obtaining a certification that endorses the fulfillment of quality standards, and improve the attention in the different health centers. Among the hospitals evaluated according to organizational practices required by ACI, the hospital from Pastaza exhibits the lowest performance [17]. This hospital belongs to the planning zone 3 of Ecuador, constituted by the Cotopaxi, Tungurahua, Chimborazo and Pastaza provinces [18]. It is known that twenty one EISS hospitals have been evaluated by ACI up to 2018 [17], organism that employs an instrument to assess some aspects of hospitals maintenance management [19]. This is considered as positive, because the maintenance and its management constitute a tool that enables reaching the organizational objectives, and provide an essential contribution to the operating security of an element [2, 20], in this case hospital equipment and all infrastructure required for the appropriate functioning of a hospital.

In order to elaborate the evaluation instrument, it is necessary to determine a structure of evaluation criteria that enables to effectively assess the performance. That is a requirement used as a reference to compare the evidence found, while an evidence is the information that enables verifying and endorsing the fulfillment of a criterion [21]. In some cases, it has been found that it is required to breakdown the evaluation

criteria in sub-criteria [22,23]; these constitute rules to assess the fulfillment of the demands [24] established in the evaluation instrument, and contribute to assessing a criterion.

During the evaluation of the maintenance management of a hospital, the functional areas that articulate the maintenance management are determined; such areas include general organization of maintenance, human resources [11, 25], economic control, planning, maintenance programming and control, outsourcing [22], equipment inventory and criticality [26], maintenance documentation and availability of replacement parts in the department [11]. On the other hand, regarding maintenance, the Canadian accreditation system verifies the fulfillment of the existence of an implemented preventive maintenance program for all devices, equipment and medical technology [19], the generation of documented reports of preventive maintenance, the application of a process to evaluate the effectiveness of the preventive maintenance program, the documented tracking of the investigation of incidents and problems involving devices, equipment and medical technology, aiming to identify the causes of the failure.

According to what has been said, the purpose of this work is to design a method that enables the quantitative assessment of the maintenance management of hospitals, through answering the research question: how can the maintenance management be evaluated in hospitals?

Knowing the quantitative assessment of the evaluated criteria and sub-criteria, will enable the on time identification of improvement opportunities in the area of maintenance of hospitals; a methodology that allows attaining this objective is based on [27]: the selection and weighting of evaluation criteria and sub-criteria utilizing the Analytic Hierarchical Process (AHP) tool [20], which is employed to quantitatively prioritize evaluation criteria [23, 26, 27]; then, the development of an evaluation instrument, the validation of the method through the on-site evaluation of health institutions and, at last, the identification of criteria with lowest performance.

2. Materials and methods

A qualitative methodology was utilized to conduct this work. The methodological process is structured in five phases [27]:

1. Selection of criteria and sub-criteria for the evaluation of the maintenance management of hospital facilites.
2. Weighting of the evaluation criteria and sub-criteria.
3. Development of the evaluation instrument.
4. Validation of the method, through the evaluation of the maintenance management in the four hospital establishments of Zone 3.
5. Identification of low performance aspects.

2.1. First phase

Evaluation criteria and sub-criteria were collected from the literature review. Then, hospital maintenance managers of the zone, teachers from the Maintenance Engineering Department of the Chimborazo Superior Polytechnic School (CHSPS) and professionals with graduate studies in maintenance management were consulted, who assessed if the criteria and sub-criteria were adapted to the demands and context of the area under study, and identified and selected seven criteria and 20 sub-criteria. In addition, the objective of each sub-criteria was established in the following manner:

2.1.1. CS: Contraction of maintenance services

CS1 – Contraction policy: evaluate if there exist defined criteria under which the best contractor will be determined, who will be responsible of performing the works of both predictive and corrective maintenance, considering the experience of the contractor in years and in number of executed hospital maintenance service contracts.

CS2 – Supervision of maintenance works: verify if the hospital technical personnel supervises that the contractor fulfills the guidelines and criteria established in the maintenance services contracts.

CS3 – Technical specifications: guarantee that all the contracted maintenance activities are executed using materials and equipment that fulfill the established specifications, that the personnel that takes part has the stipulated expertise, and that the methodology defined in the service offer is followed.

2.1.2. HR: Human resources

HR1 - Training: assess if the training requirements needed by the maintenance personnel of equipment and hospital infrastructure have been defined, for them to complete their activities, and if a training plan has been established that enables the tracking of the percentage of fulfillment of the plan.

HR2: Professional training: determine if the personnel responsible of the department or area of maintenance of medical equipment and hospital infrastructure, has bachelor or master professional training related to the occupied position.

HR3 – Quantity of maintenance personnel: based on the number of delayed maintenance work orders, evaluate if there exist enough number of technicians to

carry out preventive and corrective maintenance activities that ensure the availability of both infrastructure and hospital equipment.

2.1.3. MI: Management of the inventory of the maintenance warehouse

MI1 – Items master: verify that the warehouse of replacement parts and materials for maintenance has an items master and, based on the opinion of the maintenance technicians, evaluate what percentage of such items master has errors in the items description, or if there is duplicate items or if the dispatch units are incorrectly assigned.

MI2 – Valued inventory of items: Confirm that the replacement parts and materials for maintenance are correctly valued, including the ones in the sub-warehouses.

MI3 – Control of stock: Confirm that the stock of replacement parts and materials for maintenance is under control, both in the main warehouse and in the sub-warehouses.

2.1.4. PP: Planning programming and control

PP1 – Maintenance indicators: determine how many indicators of the maintenance management, has been put into operation in the hospital.

PP2 – Maintenance plan: evaluate if there is a preventive maintenance plan, and the level of logistic planning of the maintenance tasks that constitute it.

PP3 – Programming of maintenance activities: establish the level of planning of logistic support in the process of programming the work orders of preventive and corrective maintenance.

PP4 – Risk-based criticality analysis: assess the complexity of the methodology, employed by the hospital to establish the criticality of the hospital equipment and infrastructure.

PP5 – Inventory of goods to be maintained: evaluate the percentage of hospital equipment and infrastructure that is coded and inventoried, and confirm if the code is physically located in the infrastructure and in each equipment that requires maintenance.

PP6 – Maintenance documentation: determine if the hospital possess the minimum maintenance documentation, such as work orders and material requisition. In addition, determine if maintenance indicators can be elaborated based on the information registered in such documents.

2.1.5. OM: Organization of maintenance

OM1 – Maintenance policies: assess if the hospital possesses maintenance policies, if they are updated and if they have been socialized with the hospital personnel.

OM2 – Computing tool for the maintenance management: establish if the hospital possesses a computing tool of type Computer-assisted maintenance management (CAMM), CMMS (computerized maintenance management system) o EAM (enterprise asset management), to administer the maintenance management and its degree of utilization.

2.1.6. EC: Economic control

EC1 – Maintenance budget: determine if the methodology employed to elaborate budgets of preventive and corrective maintenance of hospital equipment and infrastructure is technical and detailed.

EC2 – Percentage of fulfillment of the executed budget: evaluate the percentage of fulfillment of the maintenance budget of the previous year.

2.1.7. MC: Corrective maintenance

CM1 – Documentation and failure analysis, consequences and effects: evaluate if the important information about failures of hospital equipment and infrastructure is registered, and if analysis methodologies are applied to reduce its probability of occurrence.

2.2. Second phase

In order to determine the weightings of evaluation criteria and sub-criteria, the process method AHP developed by Saaty [28] was applied. It is used in research works whose objective is to prioritize alternatives [26, 29, 30], and has been employed in studies related with maintenance [23, 31]. The procedure can be summarized in four steps [28]:

2.2.1. Specification of the multicriteria decision problem

The hierarchical structure comprises three levels (Figure 1):

Level 1: indicates the objective of the application of the AHP technique, which in this case is to weight the evaluation criteria and sub-criteria.

Level 2: comprises the seven criteria that will be considered in the evaluation of the maintenance management.

Level 3: constituted by twenty sub-criteria that contribute to assess the evaluation criteria.

2.2.2. Construction of pair-wise ranking matrices

For the application of the AHP method, specialists related to the area under study were consulted considering three groups of interest related to maintenance and its management. The group of thirty specialists

was constituted by ten maintenance managers of hospitals in the zone, ten maintenance experts with master degree in the area and ten teachers of the Maintenance Engineering Department of the ESPOCH. The average experience in the maintenance area of these specialists is six years, who assessed the alternatives comparing them, according to the scale of the AHP method in Table 1.

With the assessment of the decision makers, pair-wise (by each decision maker) ranking matrices of the evaluation criteria and sub-criteria, respectively, were constructed. A pair-wise ranking matrix is a square matrix Anxn, where n is the number of criteria or sub-criteria, as the case may be, and they were constructed according to equations 1 and 2.

Table 1. Fundamental scale of comparison [32]

Value	Definition	Comments
1	Equal importance	Criterion A is equally important than criterion B
3	Moderate importancea	Importance and judgment slightly favor criterion A over criterion B
5	Big importance	Importance and judgment strongly favor criterion A over criterion B
7	Very big importance	Criterion A is much more important than criterion B
9	Extreme importance	The greater importance of criterion A over criterion B is indubitable
2, 4, 6 y 8	Intermediate values between the previous ones, when they are necessary	
Reciprocal of the previous	If criterion A is of big importance compared to criterion B, the notations would be the following: Criterion A in front of criterion B: 5/1 Criterion B in front of criterion A: 1/5	

$$A_{nxn} = \begin{bmatrix} 1 & a_{12} & \cdots & a_{1n} \\ a_{21} & 1 & \cdots & a_{2n} \\ \vdots & \vdots & \ddots & \vdots \\ a_{n1} & a_{n2} & \cdots & 1 \end{bmatrix} \quad (1)$$

$$A_{nxn} = \begin{bmatrix} 1 & a_{12} & \cdots & a_{1n} \\ 1/a_{21} & 1 & \cdots & a_{2n} \\ \vdots & \vdots & \ddots & \vdots \\ 1/a_{n1} & 1/a_{n2} & \cdots & 1 \end{bmatrix} \quad (2)$$

2.2.3. Calculation of the consistency ratio (CR)

It enables to determine if there are inconsistencies in the assessment of the decision maker. This index results from the quotient between the consistency index (IC) and the random consistency index (RCI), i.e.

$$CR = \frac{IC}{ICA} \quad (3)$$

The values of the random consistency index are established by the AHP method, and are a function of the size of the matrix (Table 2).

Table 2. Random consistency index [32]

Size of the matrix (n)	Random consistency index (RCI)
1	0
2	0
3	0,52
4	0,89
5	1,11
6	1,25
7	1,35
8	1,4
9	1,45
10	1,49

For calculating the consistency index (CI) it is necessary to know the value of $\lambda_{máx}$, and to obtain it matrix A was first normalized by means of the sum, obtaining the normalized pair-wise ranking matrix A_{norm}, applying equation 4, which results in equation 5.

$$\lambda_{norm} = \begin{bmatrix} \frac{a_{11}}{\sum_{n=1}^{n} a_{n1}} + & \frac{a_{12}}{\sum_{n=1}^{n} a_{n2}} + & \cdots + & \frac{a_{1n}}{\sum_{n=1}^{n} a_{nn}} \\ \frac{a_{21}}{\sum_{n=1}^{n} a_{n1}} + & \frac{a_{22}}{\sum_{n=1}^{n} a_{n2}} + & \cdots + & \frac{a_{2n}}{\sum_{n=1}^{n} a_{nn}} \\ \vdots & \vdots & & \vdots \\ \frac{a_{n1}}{\sum_{n=1}^{n} a_{n1}} + & \frac{a_{n2}}{\sum_{n=1}^{n} a_{n2}} + & \cdots + & \frac{a_{2n}}{\sum_{n=1}^{n} a_{nn}} \end{bmatrix} \quad (4)$$

$$A_{norm} = \begin{bmatrix} b_1 \\ 1 \\ b_2 \\ \vdots \\ \vdots \\ b_n \end{bmatrix} \quad (5)$$

From matrix A_{norm}, the vector B of global priorities is obtained as (equation 6).

$$B = \begin{bmatrix} \frac{b_1}{n}, & \frac{b_2}{n}, & \cdots & \frac{b_n}{n}, \end{bmatrix} \quad (6)$$

Then, the total row vector C is calculated as the matrix product A×B (equation 7).

$$A \times B = C = \begin{bmatrix} c_1, & c_2 & \cdots & c_n \end{bmatrix} \quad (7)$$

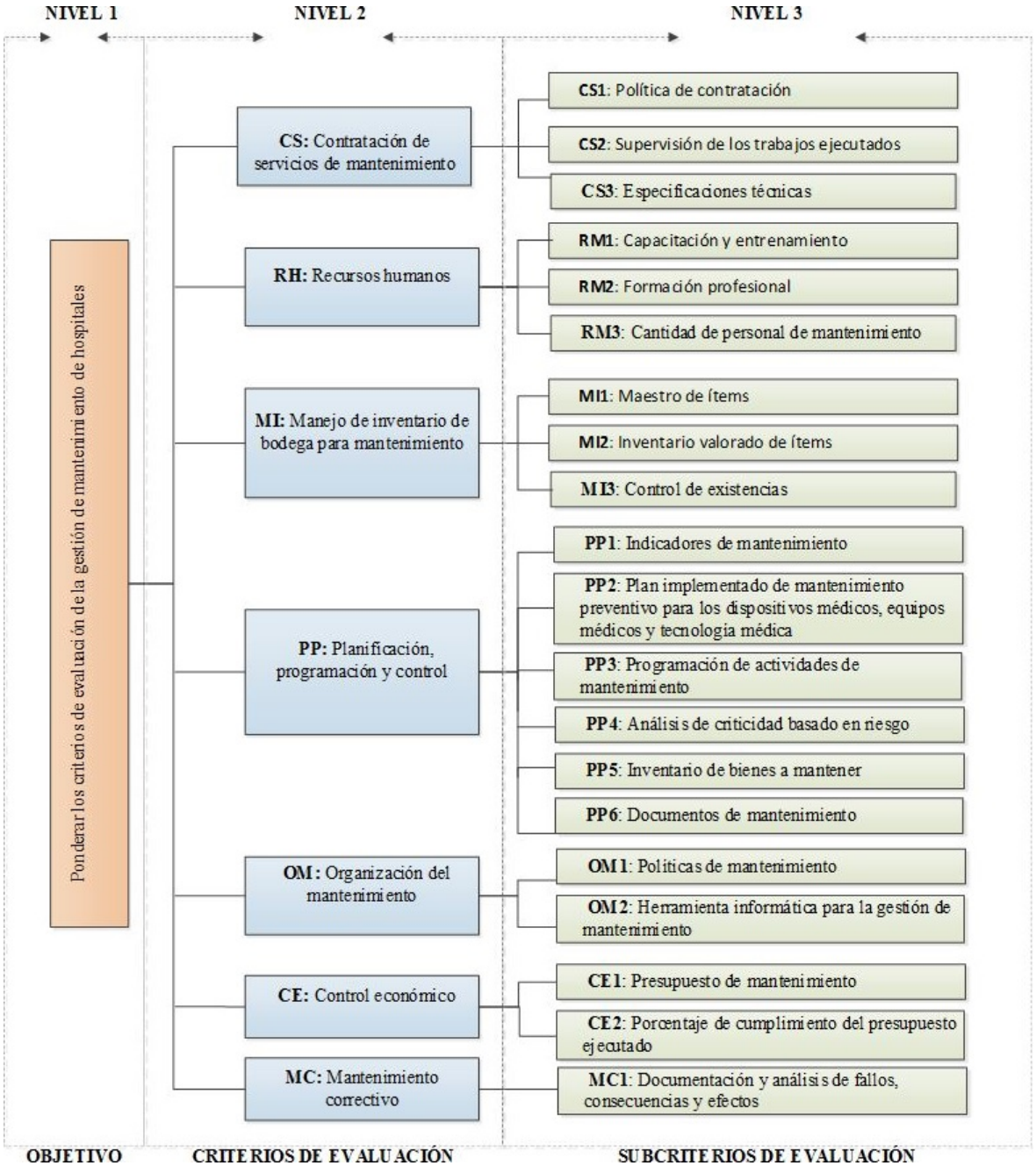

Figure 1. Hierarchical structure of the prioritization problem

Then the quotient between the corresponding elements of matrices C y B is calculated, resulting in the column vector D. The average of the elements of D gives the value of $\lambda_{máx}$, which is used to calculate the consistency index by means of equation 8.

$$IC = \frac{\lambda_{máx-n}}{n-1} \tag{8}$$

After the value of RC has been calculated for each decision maker, it should be verified that this value satisfies what is established by the AHP method; this value is a function of the size of the pair-wise ranking matrix, which for the case of the criteria (n = 7) should not exceed 10 % (Table 3).

Table 3. Maximum values of RC [32]

Size of the pair-wise ranking matrix (n)	Ratio of consistency (RC)
3	5%
4	9%
5 or greater	10%

2.2.4. Determination of the weighting factor of the evaluation criteria and sub-criteria

First, the eigenvectors were calculated employing the power method, determining the square A^2 of the pairwise ranking matrix, and then obtaining a column vector as the sum of the rows of the matrix resulting from the first product; this vector is further normalized by means of the sum and the first eigenvector V_{p1}Vp1 is obtained. The same procedure is followed to calculate the number of necessary eigenvectors, until it is verified that the corresponding elements of vectors V^{pn}, and V^{pn-1} are equal up to four decimal digits.

Since three groups of interest were consulted, the geometric mean [23] was employed to determine the final weighting of criteria and sub-criteria, thus consolidating the individual weightings for each decision maker first, and then by group of interest.

2.3. Third phase

As proposed by Quesada [33], the development of the evaluation instrument considers aspects such as:

- Description of the evaluation criterion
- Evaluation objective of the criterion
- Evaluation method
- Type of evaluation
- Reference levels
- Demands of the criterion
- Grade and assessment

According to the evaluation instrument, four reference levels were determined, which are qualitatively identified as insufficient, good, very good and excellent, with corresponding assessment of 0, 0.35, 0.7 and 1, respectively. The quantitative assessment enabled to define the performance threshold to which the qualitative assessment shown in Table 4 is linked.

2.4. Fourth phase

The validation of the evaluation method was carried out, by means of the application of the instrument developed for four EISS hospitals of the planning zone 3 of Ecuador. The hospitals are located in the province capitals, i.e. in the cities of Latacunga, Ambato, Riobamba and Puyo; the sampling was intentional since one of the hospitals in Zone 3 presented the lowest ACI accreditation performance [17].

Table 4. Scale of development assessment

Assessment		Description
Qualitative	**Quantitative**	
Insufficient	[0 % – 35 %)	Presents structural deficiencies that compromise the achievement of the objectives of the maintenance depart-ment.
Good	[35 % – 70 %)	Presents structural weaknesses that compromise the achievement of the objectives, but there exist viable processes that can be considered to improve.
Very good	[70 % – 100 %)	Presents nonstructural weaknesses that can be overcome through the improvement of the processes put into operation.
Excellent	100%	Fulfills all demands required by this evaluation method.

The hospitals in Riobamba and Ambato are classified as general hospitals, while the ones in Latacunga and Puyo are classified as basic. The average number of beds is 30, and all have a maintenance department. The evaluation was conducted on site based on the physical verification of evidences [21], which enables corroborating the affirmations of the respondent.

2.5. Fifth phase

The aspects of lowest performance were identified employing the technique of the Pareto diagram, which enabled the identification of alternatives to improve the obtained assessment.

3. Results and discussion

3.1. Results

As results of the first and second phase, and prior to the weighting of criteria, it was verified that each value of RC (Table 5) does not exceed the maximum limit (10 %).

Table 5. RC (%) values of decision makers by group of interest

N.°	Teachers of the Maintenance Engineering	Specialists in maintenance	Maintenance administrators
1	8	9,64	7,42
2	9,87	9,23	9,82
3	8,92	7,37	9,95
4	8,62	8,72	8,31
5	9,43	9,85	7,39
6	3,24	9,64	9,66
7	7,16	8,27	5,13
8	9,38	8,95	7,65
9	7,64	9,83	9,36
10	9,69	6,28	9,43

After the consistency in the assessment of the decision makers have been verified, the weightings for the evaluation criteria and sub-criteria shown in Table 6 were obtained.

The assessment instrument constituted by twenty evaluation sub-criteria, was developed in phase three. Table 7 shows an example with the sub-criterion OM2, and the adopted format structure for all sub-criteria, with levels of demand that vary according to each sub-criterion.

Using the evaluation instrument, and having defined the performance threshold, the evaluation of the maintenance departments of the four EISS hospitals – Zone 3 was conducted; the obtained results can be seen in Figure 2.

Table 8 indicates the global quantitative and qualitative assessments attained by the hospitals, while Figure 3 presents the sub-criteria that should be improved in each hospital; the grade that can be attained if such sub-criterion is improved is also indicated for each case.

Once the low performance criteria have been identified, it is necessary to establish an order of priorities to implant a plan of improvement actions, indicating the criteria on which such actions should be first taken to attain 80 % of the points lost in the evaluation (Table 9).

3.2. Discussion

In the phase of weighting the criteria and sub-criteria considered for evaluating the maintenance management, it resulted that the criterion «Contraction of maintenance services» is the most important (25 %) that should be evaluated in the administration, and therefore will have the greatest weight in the quantitative assessment, considering that the maintenance of approximately 90 % of the hospital equipment is carried out by external contractors. Inside this criterion, the sub-criterion to be considered is «Contraction policy», since it establishes the criteria for selecting the best offer that will execute the hospital maintenance activities.

With respect to the results obtained in the quantitative assessment, the EISS hospital of Latacunga exhibited the lowest performance; in the visit conducted for instrument application and on-site verification, it was evident that there was no responsible of the maintenance department designated by the maximum authority of the institution, and that the last responsible of such department did not have training at the bachelor level.

Table 6. Weighting of criteria and sub-criteria to evaluate the maintenance management

Criteria	Weights	Evaluation subcriteria	Weights
CS	0,25	CS1: Contraction policy	0,48
		CS2: Supervision of maintenance works	0,29
		CS3: Technical specifications	0,23
RM	0,18	RM1: Training	0,43
		RM2: Professional training	0,42
		RM3: Quantity of maintenance personnel	0,15
MI	0,17	MI1: Item master	0,46
		MI2: Valued inventory of items	0,28
		MI3: Control of stock	0,26
PP	0,13	PP1: Maintenance indicators	0,38
		PP2: Implemented preventive maintenance plan for medical equipment	0,18
		PP3: Programming of maintenance activities	0,14
		PP4: Risk-based criticality analysis	0,12
		PP5: Inventory of goods to be maintained	0,1
		PP6: Maintenance documentation	0,08
OM	0,11	OM1: Maintenance policies	0,78
		OM2: Computing tool for the maintenance management	0,22
CE	0,1	CE1: Maintenance budget	0,77
		CE2: Percentage of fulfillment of the executed budget	0,23
MC	0,06	MC1: Documentation and failure analysis, consequences and effects	1

This situation considerably affected the performance of the hospital, since the criterion «Human resources» is the second most important one in the as-

sessment, according to this method. On the other hand, the EISS hospital of Latacunga has the greater potential to improve (15.17 %). To quantitatively assess the maintenance management of the EISS hospitals of Zone 3, the average of the quantitative assessments obtained by each hospital was calculated, because when the hospitals were subjected to the certification process, they were evaluated with the same instrument and under the same criteria of the ACI, without considering its category; the instrument proposed here adopted the evaluation criteria of the ACI regarding maintenance. Therefore, the maintenance management in these EISS hospitals has an average of 55.5 points, with a standard deviation of 13 points.

Table 7. Description of the evaluation sub-criterion «Computing tool (software) for the maintenance management»

Evaluation sub-criterion: OM2 - Computing tool (software) for the maintenance management.		
Objective: Establish if the hospital possesses a computing tool of type Computer-assisted maintenance management (CAMM), CMMS (computerized maintenance management system) o EAM (enterprise asset management), to administer the maintenance management and its degree of utilization		
Evaluation method: Physical evidences of the installation and operability of the software are evaluated, for fulfilling the criterion demand		
Levels of reference	**Demands of the criterion**	**Puntuation**
Insufficient	It does not have CMMS/G-MAO (Computer maintenance management system) or has CMMS, but does not use it. Evidence: verify that CMMS is installed.	0
Good	The computing tool for maintenance management is an electronic sheet such as Excel, or a basic database such as Access.	0,35
Very good	It has CMMS and uses it to manage preventive maintenance. Evidence: maintenance plan emitted by the CMMS and preventive work orders emitted in the last 15 days.	0,7
Excellent	It has CMMS and uses it to calculate the indicators of the maintenance management. Evidence: report of costs, availability, mean time between failures and mean time for repairing.	1

Table 8. Global assessment of the performance of the EISS hospitals – Zone 3

EISS Hospital	**Quantitative assessment**	**Qualitative assessment**
General of Riobamba	77,8	Very good
Basic of Puyo	50,9	Good
General of Ambato	50,27	Good
Basic of Latacunga	43,05	Good
Average of the EISS hospitals of Zone 3	55,5	Maintenance management Level: Good

Table 9. Order of the criteria which require action to improve performance

EISS Hospital	**Criteria hierarchy to recover 80 % of the points lost**
General of Riobamba	1. Planning, programming and control 2. Corrective maintenance 3. Human resources
Basic of Puyo	1. Contraction of maintenance services 2. Planning, programming and control 3. Management of warehouse inventories
General of Ambato	1. Human resources 2. Management of warehouse inventories 3. Planning, programming and control
Basic of Latacunga	1. Human resources 2. Contraction of maintenance services 3. Organization of maintenance

One of the limitations of the method is that only the values established for each level of reference, can be assigned at the moment of assessment, i.e. no intermediate assessments can be given in case that one of the demands is partially fulfilled.

It is considered that this developed evaluation instrument can be applied to other hospitals, because all health centers possess an infrastructure that should be maintained to ensure a quality attention. The General Controlling Office of the State has a regulation about maintenance [34] that should be also fulfilled by the hospitals, regardless of their category.

This methodology not only provides a quantitative assessment, but it also indicates the order of the criteria on which action should be first taken to improve. Once the organizational changes have been proposed and put into operation according to the requirements of each sub-criterion, it is recommended to yearly conduct a new evaluation to the maintenance management, applying the same assessment instrument to quantitatively control the progress.

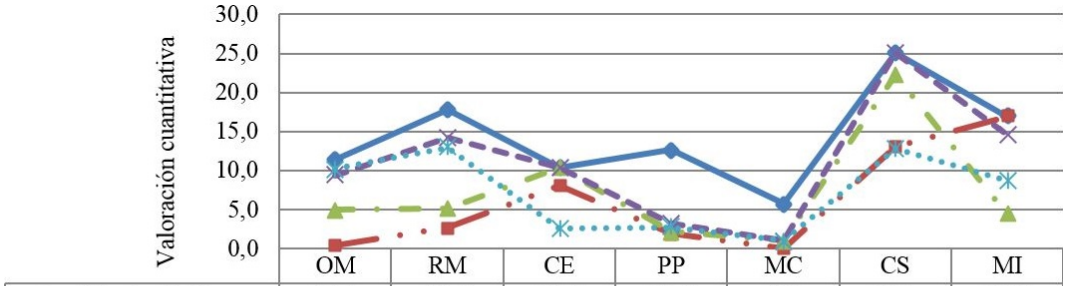

	OM	RM	CE	PP	MC	CS	MI
Nivel exigido	11,4	17,8	10,4	12,6	5,7	25,1	16,9
H. IESS Latacunga	0,4	2,6	8,0	2,0	0,0	13,1	16,9
H. IESS Ambato	5,0	5,1	10,4	2,1	1,0	22,2	4,4
H. IESS Riobamba	9,4	14,2	10,4	3,2	1,0	25,1	14,6
H. IESS Puyo	10,2	12,9	2,6	2,7	1,0	12,8	8,7

Figure 2. Performance of the EISS hospitals – Zone 3, by evaluation criterion.

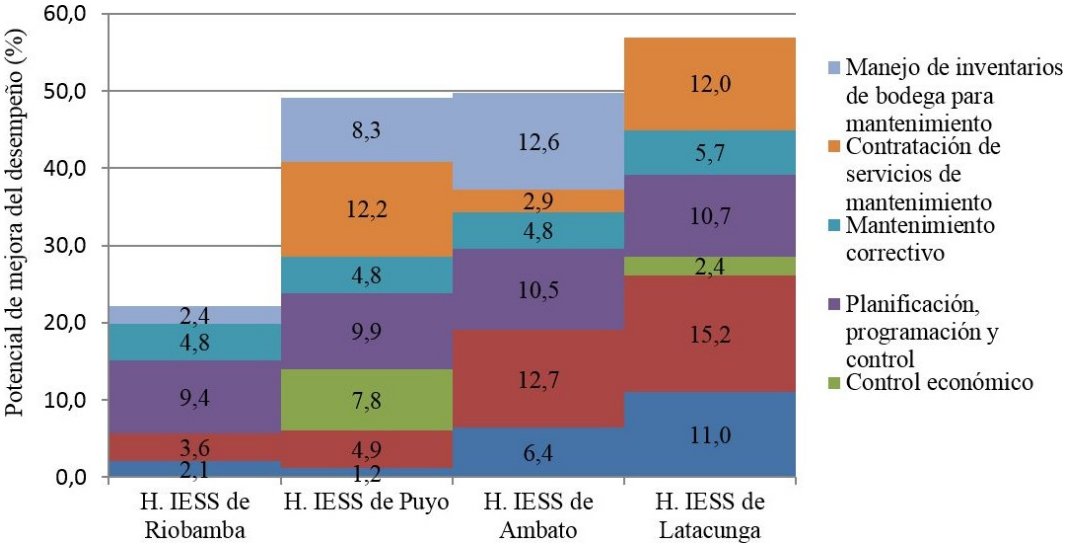

Figure 3. Identification and improvement potential of the criteria with low performance.

4. Conclusions

The survey made to the specialists gave as a result, that the three most important criteria are the contraction of maintenance services (25 %), human resources (18 %) and management of warehouse inventories (17 %); this indicates that these are the evaluation criteria with more weight in the assessment.

It was identified that none of the hospitals has a performance according to the maximum level (desired level) of demand of the proposed method, and three of four hospitals that constitute the Zone 3 have a maintenance management level in the range (35 % – 70 %), which qualitatively represents a good maintenance management. This indicates that there are structural weaknesses that compromise the achievement of the objectives of the maintenance department, but there are viable processes that can be implemented to improve.

There exist four criteria in which the hospitals coincide that they should improve, even though each of them in different measure and sub-criterion. These criteria are: organization of maintenance; human resources; planning, programming and control of the maintenance and corrective maintenance.

References

[1] H. Alzaben, C. McCollin, and L. Eugene, "Maintenance planning in a saudi arabian hospital," *Safety and Reliability*, vol. 34, no. 2, pp. 25–40, 2014. [Online]. Available: https://doi.org/10.1080/09617353.2014.11691004

[2] UNE, *UNE-EN 13306:2018. Mantenimiento. Terminología del mantenimiento*, Normalización

Española Std., 2018. [Online]. Available: http://bit.ly/2RzAv93

[3] V. Gonnelli, F. Satta, F. Frosini, and E. Iadanza, "Evidence-based approach to medical equipment maintenance monitoring," in *EMBEC & NBC 2017*, H. Eskola, O. Väisänen, J. Viik, and J. Hyttinen, Eds. Singapore: Springer Singapore, 2018, pp. 258–261. [Online]. Available: https://doi.org/10.1007/978-981-10-5122-7_65

[4] M. C. Carnero and A. Gómez, "A multicriteria decision making approach applied to improving maintenance policies in healthcare organizations," *BMC Medical Informatics and Decision Making*, vol. 16, no. 1, p. 47, Apr 2016. [Online]. Available: https://doi.org/10.1186/s12911-016-0282-7

[5] R. Lucio, N. Villacrés, and R. Henríquez, "Sistema de salud de Ecuador," *Salud Pública de México*, vol. 53, pp. s177–s187, 01 2011. [Online]. Available: http://bit.ly/2N2sw5O

[6] INEC, *Registro Estadístico de Recursos y Actividades de Salud - RAS 2016*. relax Instituto Nacional de Estadísticas y Censos, Ecuador, 2016. [Online]. Available: http://bit.ly/2WTPIYL

[7] IESS. (2016) Boletín estadístico número 22. Direccion Actuarial, de Investigación y Estadística del Instituto Ecuatoriano de Seguridad Social.

[8] Asamblea Nacional. (2015) Ley de seguridad social. República del Ecuador. [Online]. Available: http://bit.ly/2ZA0y2Q

[9] P. González. (2019) ¿Por qué el IESS se encuentra en crisis? Diario El Comercio. [Online]. Available: http://bit.ly/2WWxB44

[10] F. Maisanche. (2018) El hospital del iess de latacunga suspendió las cirugías programadas por problemas en los esterilizadores. DIario El Comercio. [Online]. Available: http://bit.ly/2WTm0Ox

[11] B. G. Mwanza and C. Mbohwa, "An assessment of the effectiveness of equipment maintenance practices in public hospitals," *Procedia Manufacturing*, vol. 4, pp. 307–314, 2015. [Online]. Available: https://doi.org/10.1016/j.promfg.2015.11.045

[12] A. M. Cruz, G. L. Haugan, and A. M. R. Rincon, "The effects of asset specificity on maintenance financial performance: An empirical application of transaction cost theory to the medical device maintenance field," *European Journal of Operational Research*, vol. 237, no. 3, pp. 1037–1053, 2014. [Online]. Available: https://doi.org/10.1016/j.ejor.2014.02.040

[13] W. Orozco Murillo, J. Narváez Benjumea, W. García Gómez, and A. Quintero Rodas, "Gestión de mantenimiento y producción más limpia en tres instituciones de salud de medellín, colombia," *Revista Ingeniería Biomédica*, vol. 11, no. 21, pp. 21–25, 2017. [Online]. Available: https://doi.org/10.24050/19099762.n21.2017.1168

[14] M. Herrera-Galán and E. Martínez-Delgado, "Management audit applied to the maintenance department in hospital facilities," *Ingeniería Mecánica*, vol. 20, no. 3, pp. 152–159, 2017. [Online]. Available: http://bit.ly/31FcMcp

[15] N. A. A. Rani, M. R. Baharum, A. R. N. Akbar, and A. H. Nawawi, "Perception of maintenance management strategy on healthcare facilities," *Procedia - Social and Behavioral Sciences*, vol. 170, pp. 272–281, 2015. [Online]. Available: https://doi.org/10.1016/j.sbspro.2015.01.037

[16] L. Thompson. (2018) "acreditación es sinónimo de mejora en atención de salud". Diario El Telégrafo. [Online]. Available: http://bit.ly/2X6aswb

[17] O. Espín, "Acreditación internacional de hospitales del iess," in *XI Congreso Internacional de Calidad*, 2017. [Online]. Available: http://bit.ly/2Y2CAgf

[18] SENPLADES, *Plan Estratégico Institucional 2018 - 2021*. Coordinación General de Planificación y Gestión Estratégica, Secretaría Nacional de Planificación y Desarrollo, 2018. [Online]. Available: http://bit.ly/2L38wxh

[19] Acreditation Canada. (2014) Prácticas organizacionales requeridas. Acreditation Canada International, Driving Quality Health Services. [Online]. Available: http://bit.ly/2IufU3j

[20] L. Pecchia and P. Melillo, *Multicriteria and Multiagent Decision Making with Applications to Economics and Social Sciences*, 2013, vol. 305, ch. Analytic Hierarchy Process for Health Technology Assessment: A Case Study for Selecting a Maintenance Service Contract, pp. 275–288. [Online]. Available: http://bit.ly/2IrWM5K

[21] ISO, *ISO 19011: Directrices para la auditoría para sistemas de gestión*, International Standard Organization Std Std., 2016. [Online]. Available: http://bit.ly/2XoX8m4

[22] Acosta-Palmer, H. R, and M. Troncoso-Fleitas, "Auditoria integral de mantenimiento en instalaciones hospitalarias, un análisis objetivo," *Ingeniería Mecánica*, vol. 14, no. 2, pp. 107–118, 2011. [Online]. Available: http://bit.ly/2x1Btld

[23] M. C. Carnero, "Auditing model for the introduction of computerised maintenance management system," *International Journal of Data Science*, vol. 1, no. 1, pp. 14–41, 2015. [Online]. Available: https://doi.org/10.1504/IJDS.2015.069049

[24] E. Martínez, M. Álvarez, A. Arquero, and M. Romero, "Apoyo a la selección de emplazamientos óptimos de edificios. Localización de un edificio universitario mediante el Proceso Analítico Jerárquico (AHP)," *Informes de la construcción*, vol. 62, no. 519, pp. 35–45, 2010. [Online]. Available: http://bit.ly/2Y2G3vh

[25] S. Mullally, T. Bbuku, and G. Musonda, "Medical equipment maintenance personnel and training in zambia," in *World Congress on Medical Physics and Biomedical Engineering May 26-31, 2012, Beijing, China*, M. Long, Ed. Berlin, Heidelberg: Springer Berlin Heidelberg, 2013, pp. 750–753. [Online]. Available: https://doi.org/10.1007/978-3-642-29305-4_197

[26] S. Taghipour, D. Banjevic, and A. K. S. Jardine, "Prioritization of medical equipment for maintenance decisions," *Journal of the Operational Research Society*, vol. 62, no. 9, pp. 1666–1687, 2011. [Online]. Available: https://doi.org/10.1057/jors.2010.106

[27] M. A. Viscaíno Cuzco, J. F. Quesada Molina, and S. R. Villacrés-Parra, "Priorización de criterios para la evaluación de la gestión del mantenimiento en edificios multifamiliares," *Arquitectura y Urbanismo*, vol. 38, no. 3, pp. 60–70, 2017. [Online]. Available: http://bit.ly/2FmNeXI

[28] T. L. Saaty, "Decision making with the analytic hierarchy process," *International Journal Services Sciences*, vol. 1, no. 1, pp. 83–98, 2008. [Online]. Available: http://bit.ly/2IYJEnH

[29] Q. Shen, K.-K. Lo, and Q. Wang, "Priority setting in maintenance management: a modified multiattribute approach using analytic hierarchy process," *Construction Management and Economics*, vol. 16, no. 6, pp. 693–702, 1998. [Online]. Available: https://doi.org/10.1080/014461998371980

[30] G. Middlehurst, R. Yao, L. Jiang, J. Deng, D. Clements-Croome, and G. Adams, "A preliminary study on post-occupancy evaluation of four office buildings in the uk based on the analytic hierarchy process," *Intelligent Buildings International*, vol. 10, no. 4, pp. 234–246, 2018. [Online]. Available: https://doi.org/10.1080/17508975.2018.1495607

[31] M. Fouladgar, A. Yazdani-Chamzini, A. Lashgari, E. Zavadskas, and Z. Turskis, "Maintenance strategy selection using ahp and copras under fuzzy environment," *International Journal of Strategic Property Management*, vol. 16, no. 1, pp. 85–104, 2012. [Online]. Available: https://doi.org/10.3846/1648715X.2012.666657

[32] J. Aznar Bellver and F. Guijarro Martínez, *Nuevos métodos de valoración: modelos multicriterio*. Universitat Politécnica de Valencia, 2012. [Online]. Available: http://bit.ly/2IrDiOO

[33] F. Quesada Molina, "Desarrollo de un método de evaluación de la calidad del ambiente interior para el diseño de viviendas sustentables: Caso de estudio región del bío bío, chile," *Revista Hábitat Sustentable*, vol. 4, no. 1, pp. 56–67, 2014. [Online]. Available: http://bit.ly/2NeG1Qf

[34] Contraloría General del Estado. (2014) Normas de control interno de la contraloría general del estado. Registro Oficial Suplemento 87 de 14-dic.-2009, República del Ecuador. [Online]. Available: http://bit.ly/2x3ZtnP

Scientific Paper / Artículo Científico

UNIVERSIDAD POLITÉCNICA SALESIANA ECUADOR
INGENIUS
Revista de Ciencia y Tecnología
https://doi.org/10.17163/ings.n22.2019.07
pISSN: 1390-650X / eISSN: 1390-860X

Monitoring System for Doors and Windows of a Data Center with IoT

Sistema de monitorización de puertas y ventanas de un centro de datos con IoT

José Ignacio Vega-Luna[1,*], Francisco Javier Sánchez-Rangel[1], José Francisco Cosme-Aceves[1]

Abstract

This paper presents the construction of a prototype of a door and window monitoring system through an IoT platform. The objective was to design a system that reports to a server in the cloud the change of state, open or closed, of three doors and two windows of the equipment room of the data center. The changes of state are registered by the server, and by means of a user interface the status of doors and windows is displayed online. The architecture of the system is based on a wireless sensor network, integrated by a central node and five monitoring nodes. The monitoring nodes consist of a PyBoard card, two digital Hall effect sensors and a WiFi wireless interface. When detecting a change of state in doors and windows, the monitoring nodes notify it to the central node, and this transmits it to the server through a WiFi access point. When a door or window remains open for more than a configurable period of time, an SMS and WhatsApp message is sent to a mobile phone. The reach achieved in the WiFi transmission on the network was 47 meters with line of sight.

Keywords: Data center, Hall effect, monitoring, PyBoard, SMS, WiFi.

Resumen

En este trabajo se presenta la construcción de un prototipo de un sistema de monitorización de puertas y ventanas a través de una plataforma IoT. El objetivo fue diseñar un sistema que reporte a un servidor en la nube el cambio de estado, abierta o cerrada, de tres puertas y dos ventanas de la sala de equipos del centro de datos. Los cambios de estado son registrados por el servidor y por medio de una interfaz de usuario se muestran en línea los estados de las puertas y ventanas. La arquitectura del sistema se basa en una red inalámbrica de sensores integrada por un nodo central y cinco nodos de monitorización. Los nodos de monitorización están compuestos por una tarjeta PyBoard, dos sensores digitales de efecto Hall y una interfaz inalámbrica wifi. Al detectar un cambio de estado en puertas y ventanas, los nodos de monitorización lo notifican al nodo central, y este lo transmite al servidor por medio de un punto de acceso wifi. Cuando una puerta o ventana permanece abierta más de un período de tiempo configurable, se envía un mensaje SMS y de WhatsApp a un teléfono móvil. El alcance logrado en la transmisión wifi en la red fue 47 metros con línea de vista.

Palabras clave: centro de datos, efecto Hall, monitorización, PyBoard, SMS, wifi

[1,*] Área de Sistemas Digitales, Departamento de Electrónica, Universidad Autónoma Metropolitana-Azcapotzalco, Cd. de México, México. Autor para correspondencia ✉: vlji@azc.uam.mx. http://orcid.org/0000-0002-4226-2936, http://orcid.org/0000-0002-4182-5856, http://orcid.org/0000-0002-6875-5683.

Received: 02-05-2019, accepted after review: 19-06-2019

Suggested citation: Vega-Luna, J. I.; Sánchez-Rangel, F. J. and Cosme-Aceves, J. F. (2019). «Monitoring System for Doors and Windows of a Data Center with IoT». Ingenius. N.°22, (july-december). pp. 72-79. doi: https://doi.org/10.17163/ings.n22.2019.07.

1. Introduction

A data center houses equipment for processing and storing information, and telecommunication equipment of companies and organizations. Since the productivity of clients and users depend on such equipment, it is important to keep it safe. The data centers should have highly reliable security systems, which enable the controlled access to the rooms that concentrate the computing equipment. These rooms have a reduced number of doors and windows, and the entrance to authorized administration and maintenance personnel is only allowed, who should keep them locked at all times. When, for any reason, a door or a window remains open for longer than a certain configurable period of time, an audible and luminous signal is activated to warn security personnel [1].

The data centers are periodically and permanently audited by institutions and companies that certify, among other things, the access mechanisms and procedures, to guarantee the quality of the services offered. One of the audited actions is the remote monitoring of the state, either closed or open, of doors and windows [2].

With the current development of technology, it is required that data centers are enabled for remote monitoring of variables, processes and procedures from the Internet, thus allowing people responsible for security and certifying institutions to revise, both online and historically, the operation of the data center [3]. This requirement can be fulfilled with the development of solutions and applications of the Internet of Things (IoT).

1.1. The Internet of Things

The IoT is a concept according to which the information read by electronic sensors used at households, offices, industries, laboratories, mobile phones, automobiles, infrastructure of cities and data centers is transmitted to a central monitoring device. This central device is located in the Internet, thus allowing the connection to it of digital objects of daily used, i.e. it connects the physical and digital worlds by means of computers and web platforms in the cloud, which store and process the information transmitted by sensors [4].

The recent technological advances in electronics, digital systems and communications, as well as the availability of providers of services of information storage and analysis in the cloud, have boosted the development of the IoT. These services enable receiving, storing and processing information from sensors, to perform a remote action on a process. In addition, there are services that can be used to transmit voice, text, video or Whatsapp alert messages to a mobile phone [5], to notify an event.

The present work results from the requirement of a company which owns a data center. The request consisted of developing a system with the purpose of transmitting to a server located in the cloud, the change of state, open or closed, of three doors and two windows in the equipment room of the data center. The changes of state, as well as the date and time, should be stored by the server. The system should have a user interface, accessible from the Internet, which online shows the state of doors and windows and displays a history of the changes of state. In case that a door or window remains open for longer than a configurable period of time, alert SMS and Whatsapp messages should be sent to the mobile phone of the administrator of the system. A Wi-Fi point to access the Internet is installed in the data center, located at a distance of 35 meters from the farthest window.

1.2. Recent research works

An important number of works have been carried out, to remotely monitor environmental variables in data centers. Since IoT is a fast growing area, Wireless Sensor Networks (WSN) have been installed for this purpose in recent years, and almost all of them use Wi-Fi technology [6]. A large number of these applications monitor environmental variables such as temperature and relative humidity [7, 8], other monitor cooling systems [9], air flow in cabinets of computing equipment [10, 11] and electrical supply systems [12]. Some wireless networks use ZigBee [13] and LoRa technologies.

On the other hand, a great variety of applications have been designed using IoT platforms in areas of monitoring vital signs [14–17], health care [18], industrial processes [19], environmental and atmospheric parameters [20], traffic control [21], bridges [22] and flooding prevention systems [23] in intelligent homes and cities, animal feeding systems in farms [24] and infant location at home [25], among others. The majority of these applications use Wi-Fi transceivers, and few utilize LoRa [26, 27] and GPRS [28] technologies.

The system developed in this work is constituted by a network with five monitoring nodes, one for each door and window, and a central node. The monitoring nodes wirelessly transmit the state of the sensors of doors and windows to the central node, which sends them to the server in the cloud through a Wi-Fi access point. The user interface was implanted in the central node using a web server. The two types of nodes were realized based on a PyBoard card. Using the Internet service provider ThinkSpeak, the information transmitted by the monitoring nodes is stored and accessed from the user interface. On the other hand, the Internet service provider Twilio was used to send the SMS and Whatsapp messages. Both the sensors and Wi-Fi transceivers used are of low energy consumption.

1.3. ThingSpeak and Twilio

ThingSpeak is a service platform for information analysis in the cloud, which is used to collect, store, visualize and analyze data from sensors installed in intelligent devices. For applications that transmit to the server up to 3 million messages per year, the ThinkSpeak service has no cost. Twilio is a service platform based on Application Programming Interface (API), which enables the transmission of voice, video and text messages to web, mobile and desktop applications. The free use of Twilio allows sending up to one hundred messages per month.

1.4. Contribution of the work

Taking into account what has been previously stated, no IoT application similar to the one presented here has been developed for a data center. The ones that have been carried out are of greater cost, because they utilize development cards of high price, in which many of its elements are not used, and because they require to install, configure and maintain the server in the cloud. In addition, the maintenance of the system proposed in this work is simpler and faster than others of similar type, since all programming has been done in MycroPython. The contribution of this work it that it solves a real security need, monitoring from the Internet the state of doors and windows, as requested by certifying institutions. Current systems if this type do the monitoring locally.

2. Materials and methods

The methodology that was utilized to develop the system comprised two phases. In the first phase the system was designed, divided in three modules: monitoring nodes, central node and user interface, as indicated in the block diagram in Figure 1. The monitoring nodes and the central node constitute the wireless network of sensors.

Afterwards, the second phase comprised the selection of the appropriate components to perform the function of every module of the system

2.1. The monitoring nodes

Fives monitoring nodes were built, all having the architecture shown in Figure 2.

The monitoring nodes are constituted by a PyBoard card, the cards of the sensors of doors and windows opening, and the wireless interface.

The PyBoard PYBV1.0 card used in this module, is the most commonly used card of its type to execute programs written in MycroPython. It comprises the following hardware resources: STM32F405RG microcontroller with CPU Cortex M4 of 168 MHz and floating point, USB port, flash ROM memory of 1024 KB, RAM memory of 192 KB, slot for Micro SD card, real-time clock, 29 general purpose input/output terminals, 3 analog/digital converters of 12 bits, 2 digital/analog converters of 12 bits, 2 UART ports, 4 USART ports, bootloader program for firmware updating, and is energized with 3.3 V.

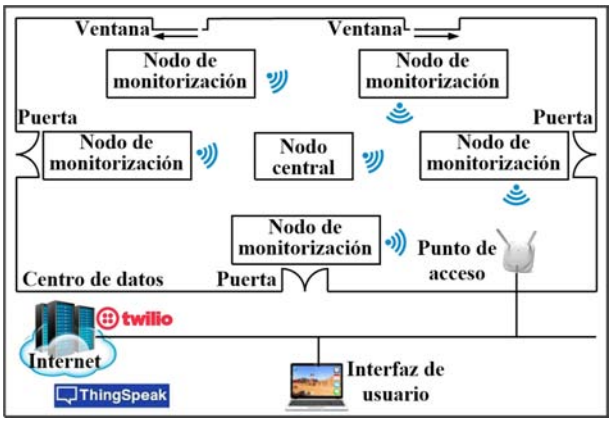

Figure 1. Block diagram of the developed system.

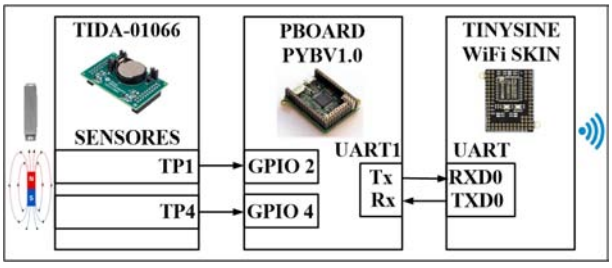

Figure 2. Architecture of the monitoring nodes.

The PyBoard card was used because its microcontroller executes programs written in MycroPython, which simplified the programming by avoiding the use of a complex low level language, and because many functions libraries of free use and open code are available in the cloud, to carry out a variety of tasks.

Two types of devices, namely Reed switches and Hall effect sensors, are commonly used in applications for monitoring the opening of doors and windows. Both devices detect the presence or absence of magnets installed in doors or windows. Reed switches use a physical switch that closes in the presence of a magnetic field, and opens when such field is removed. Due to their mechanical nature, their life time is limited, there is a bouncing effect when closing or opening, and its operation is affected by vibrations. The installation of this type of switches increases the cost of the application, since they should be commonly soldered in the door or window, which may damage the glass encapsulation. When opened, Reed switches consume no current; when closed, a small current flows through the pull-down or pull-up resistance connected in the

output. The magnitude of this current is significant in systems energized by batteries.

In contrast, Hall effect sensors have no moving parts. They detect the presence or absence of a magnetic field in their range, using the voltage difference (V) produced in a conductor when an electrical current (I) flows through it in the presence of such magnetic field (B). They are immune to vibrations and do not bounce. Hall effect sensors have compact size, resistant encapsulating, and consume less current than Reed switches. They activate their output at low level, logical 0, when the magnetic flow density produced by a magnet close to it, exceeds an operating threshold BOP. This output is used as a switch to connect to the input terminal of a controller, which can be in sleep mode or of low energy consumption, and awake when the output of the sensor changes.

Due to the aforementioned reasons, the TIDA-01066 card was used for the implantation of the monitoring nodes. This card includes two Hall effect digital sensors of ultra-low energy consumption, and a CR2032 coin-type battery. These sensors detect the presence of the magnetic field of the magnets installed in the doors and windows. This card also integrates two DRV5032X sensors, to avoid detecting false negatives and to maximize the distance between sensors and magnets. The X indicates the sensitivity of the sensors: high, medium and low. The operating threshold for each sensitivity is 3.1 mT, 7.5 mT and 50 mT, respectively. The sensors are energized by a source of 1.65 to 5.5 V that consume 0.57 μA in average, and operate at a sampling frequency updating the output at 20 Hz or 5 Hz for the low energy consumption. The response of these sensors is omnipolar, which enables them to detect the north or south pole of the magnet, thus simplifying its installation.

In security systems based on sensors wireless networks, one of the main limitations is the electrical supply. It the sensors of the network are energized with batteries, the replacement cost of these batteries becomes a problem. The CR2032 battery of the TIDA-01066 card has a life time of 10 years, which keeps its sensors operating during a prolonged period of time before replacing the battery. This was another reason by which the TIDA-01066 card was used in the monitoring nodes. The CR2032 battery is an ion-lithium small cell that, as opposed to alkaline batteries, keeps the output voltage stable until the end of its life time. It operates in the temperature range between -40 °C and 85 °C, and can be used indoors and outdoors.

The monitoring nodes were installed in the fixed part of the windows and the magnets in the sliding part, separated by a distance of 20 mm. The doors of the data center have two panes, with the monitoring nodes installed in one of them and the magnets in the other, such that when the door or window is closed, the output of the Hall effect sensor shows low level. The outputs of the sensors were connected to the GPIO 2 and GPIO 4 terminals of the PyBoard card. The microcontroller of the PyBoard is in sleep mode, or low energy consumption, most of the time. When a door or window is open or closed, the level change in any of the GPIO 2 and GPIO 4 generates and interruption that awakes the microcontroller. The Interrupt Service Routine (ISR) that serves this interruption, transmits the state of the sensor to the central node.

On the other hand, there is a great amount of magnet types and providers in the market. K&J Magnetics is the provider with the greater variety of magnets, having available Neodymium magnets of N35, N38, N40, N42, N45, N48, N50 and N52 grades, different dimensions, shapes and reach of the magnetic field. The grade indicates level of intensity or strength of the magnetic field of the magnet; N35 is the lowest level. A calculator to determine the appropriate magnet depending on the necessary features, is available in the K&J Magnetics web site. Magnets BZX0X08-N42 with length 101.6 mm, width 25.4 mm, thickness 12.7 mm, magnetic field intensity and reach 3,424 Gauss and 10 mm, respectively, were utilized in this work. The reach of the magnetic field determines the maximum distance for which the intensity of the magnetic field is maintained, before it decreases. The sensors wireless network implanted in this work is a wye network, in which the central node is the coordinator. The central node operates collecting information of the monitoring nodes, and receives messages from them when the associated sensors change of state.

The monitoring nodes use the TinySine Wi-Fi Skin module for PyBoard, as wireless interface to communicate with the central node. This module operates based on the ESP-07S circuit, which belongs to the ESP8266 family. The UART of the ESP-07S was connected to the UART1 port of the PyBoard card, to carry out the serial communication.

The microcontroller program of the monitoring nodes performs the following activities: 1) Configures terminals GPIO 2 and GPIO 4 as inputs, initializes the UART1 and configures the wireless interface, 2) Transmits the message to the central node to join the network and 3) Activates the sleep mode or low energy consumption, from which it exits after receiving an interruption from terminals GPIO 2 or GPIO 4. When the microcontroller awakes and exits this mode, it transmits the message to the central node indicating the value of the output or state of the sensors, and returns to the sleep mode. Figure 3 shows the flow diagram used to create this program.

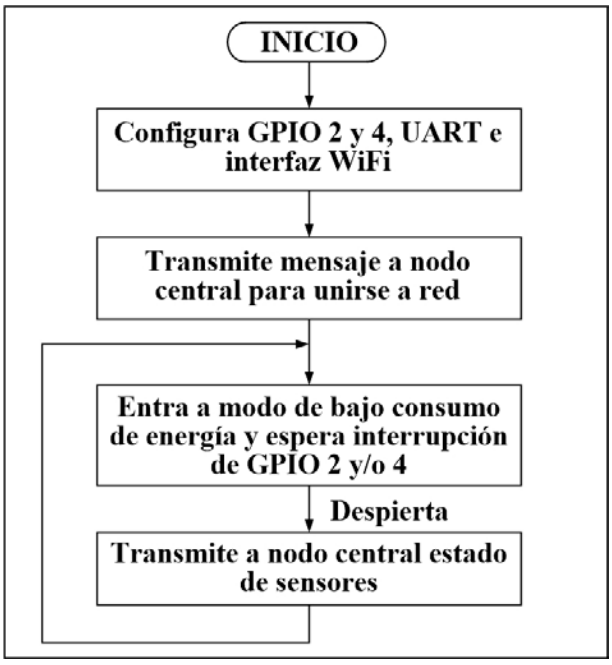

Figure 3. Flow diagram of the monitoring nodes program.

2.2. The central node

The central node is constituted by the PyBoard card and the wireless interface. The central node uses the circuit TinySine Wi-Fi Skin for PyBoard as wireless interface, to communicate with the monitoring nodes and the Internet.

The functions of the central node are the following: 1) Initializes the sensors network, 2) Receives messages with information transmitted by the monitoring nodes, to send it to the server in the cloud and 3) Implants the user interface.

These functions are performed through the program executed by the microcontroller of the PyBoard card, which carries out the following tasks: A) Configures the UART1 and the wireless interface, establishes the value of the timer of open door or window and establishes the mobile phone number of the administrator of the data center and B) Enters in a cycle in which it invokes the function that implants the graphical user interface, and waits for the interruption from the UART1.

The function that serves the interruption from the UART1 is responsible for receiving the information from the nodes of the network, and transmitting it to the server in the cloud. This function uses the write REST API to transmit the message a ThingSpeak. The message contains the identifier of the monitoring module, the state of the associated sensor and the date and time. If the sensor is deactivated, the door or window is open. In this case, the function starts a timer, which interrupts the microcontroller when it expires. The function that serves the interruption of the timer, verifies if the central module received the message that indicates the change of state of the sensor. If this is the case, the door or window has been closed, and the function ends. If this is not the case, it transmits the SMS and Whatsapp alert messages using the Twilio REST API. These messages sent to the mobile telephone of the administrator of the data center, indicate that the door or window has exceeded the allowed opening time.

2.3. The user interface

The user interface is constituted by the web server and the corresponding site. Through the user interface, the state of the sensors of doors and windows can be visualized online, and the historical information collected by the system may be downloaded to a text file. The implantation of the web server was based on the library of open code functions uasyncio. This library was designed to realize web servers with microcontrollers, known as picowebs, using the minimum amount of RAM memory. Figure 4 shows the main screen of the created user interface.

Figure 4. User interface.

3. Results and discussion

Two groups of tests were carried out. The objective of the first group was to determine the type of magnet to be used, considering that the separation between the monitoring node and the magnet is 10 mm. Using the K&J Magnetics calculator of magnetic field, a magnet with block shape with a magnetic field reach of 10 mm was requested. The calculator indicated 7 types of magnets of different grades, dimension, magnetic field intensity and price. To carry out the tests, each of the 7 magnets were placed on a door and on a window, and the distance at which the monitoring node detected its opening was measured. Although the magnetic field reach of the magnets used is of the same magnitude, the results of the tests showed reaches which were slightly different than the nominal value, as can be seen in Table 1.

Table 1. Types of magnets used in the tests

Type of magnet	Dimensions (mm)	Magnetic field (Gauss)	Price (USD)	Reach (mm)
BZ0Z0X0-N52	76.2x76.2x25.4	3798	294.82	14
BZ0Z08-N52	76.2x76.2x12.7	2125	151.36	13
BZ0Z04-N52	76.2x76.2x6.35	1098	79.43	12
BZ0Z02-N52	76.2x76.2x3.17	554	43.34	11
BZX0X0X0-N42	101.6x25.4x25.4	4871	100.15	14
BZX0X08-N42	101.6x25.4x 12.7	3424	43.34	10
BZX0Y04-N42	101.6x50.8x6.35	1152	51.86	12

For this application, it was necessary to use a magnet that activates the sensors at a distance of 10 mm. It was not necessary to use a strong magnet, with a large intensity of magnetic field. For this reason and due to the results obtained in these tests, a BZX0X08 magnet of grade N42 was used, with low price and real reach of 10 mm. No tests were carried out to measure the intensity of the magnetic field, because the function of the magnets is to activate the sensors, and not to attract a metallic element.

Even though there were no communication problems of the network nodes with the Wi-Fi 802.11 n access point, a second group of tests was conducted to determine the reach of the network. To carry out these tests, a monitoring node was located at different points of the data center, including places more distant to the farthest window with respect to the access point. Results showed that the reach of the network is 47 meters with line of sight at a velocity of 230 Mbps, smaller than the 300 Mbps that can be theoretically obtained using the 802.11 n standard. At a distance greater than 47 meters, the power of the received Wi-Fi signal (RSSI- Received Signal Strength Indicator) in the monitoring node decreased in an accelerated manner, and the link was lost when the strength fell to -86 dBm, as shown in the plot of Figure 5.

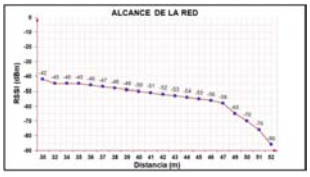

Figure 5. Reach of the sensors network.

The inSSIDer tool installed in a portable computer by the monitoring node, was utilized to measure the RSSI level.

4. Conclusions

The result of this work was a system to monitor doors and windows through the IoT platform, which reports to a server in the cloud the change of state of three doors and two windows in the equipment room of a data center. This system has a user interface that shows online, the state of doors and windows. The installation is non-intrusive, because it uses wireless communication and it does not modify the cabling of the data center. It was programmed using MicroPython and libraries of free use open code functions, which reduced the time and complexity of the implantation. It uses IoT platforms recently created in the cloud, that provide an efficient and reliable service to store information and transmit the alert messages to a mobile telephone, thus implementing an application that fulfills the established requirements. The reach achieved in the Wi-Fi transmission was 47 meters with line of sight.

References

[1] P. A. Lontsikh, V. A. Karaseva, E. P. Kunakov, I. I. Livshitz, and K. A. Nikiforova, "Implementation of information security and data processing center protection standards," in *2016 IEEE Conference on Quality Management, Transport and Information Security, Information Technologies (IT&MQ&IS)*, 2016, pp. 138–143. [Online]. Available: https://doi.org/10.1109/ITMQIS.2016.7751923

[2] Z. Han and L. Yu, "A survey of the bcube data center network topology," in *2018 IEEE 4th International Conference on Big Data Security on Cloud (BigDataSecurity), IEEE International Conference on High Performance and Smart Computing, (HPSC) and IEEE International Conference on Intelligent Data and Security (IDS)*, 2018, pp. 229–231. [Online]. Available: https://doi.org/10.1109/BDS/HPSC/IDS18.2018.00056

[3] D. Achmadi, Y. Suryanto, and K. Ramli, "On developing information security management system (isms) framework for iso 27001-based data center," in *2018 International Workshop on Big Data and Information Security (IWBIS)*, 2018, pp. 149–157. [Online]. Available: https://doi.org/10.1109/IWBIS.2018.8471700

[4] H. Hejazi, H. Rajab, T. Cinkler, and L. Lengyel, "Survey of platforms for massive iot," in *2018 IEEE International Conference on Future IoT Technologies (Future IoT)*, 2018, pp. 1–8. [Online]. Available: https://doi.org/10.1109/FIOT.2018.8325598

[5] P. Datta and B. Sharma, "A survey on iot architectures, protocols, security and smart city based applications," in *2017 8th International Conference on Computing, Communication and Networking Technologies (ICCCNT)*, 2017, pp. 1–5. [Online]. Available: https://doi.org/10.1109/ICCCNT.2017.8203943

[6] E. A. Kadir, S. M. Shamsuddin, S. Hasan, and S. L. Rosa, "Wireless monitoring for big data center server room and equipments," in *2015 International Conference on Science in Information Technology (ICSITech)*, 2015, pp. 187–191. [Online]. Available: https://doi.org/10.1109/ICSITech.2015.7407801

[7] S. Saha and A. Majumdar, "Data centre temperature monitoring with esp8266 based wireless sensor network and cloud based dashboard with real time alert system," in *2017 Devices for Integrated Circuit (DevIC)*, 2017, pp. 307–310. [Online]. Available: https://doi.org/10.1109/DEVIC.2017.8073958

[8] K. Nayak, K. Nanda, T. Dwarakanath, H. Babu, and D. Selvakumar, "Data centre monitoring and alerting system using wsn," in *2014 IEEE International Conference on Electronics, Computing and Communication Technologies (CONECCT)*, 2014, pp. 1–5. [Online]. Available: https://doi.org/10.1109/CONECCT.2014.6740348

[9] M. R. C. Truşcă, Ş. Albert, and M. L. Soran., "The benefits of data center temperature monitoring," in *2015 Conference Grid, Cloud & High Performance Computing in Science (ROLCG)*, 2015, pp. 1–3. [Online]. Available: https://doi.org/10.1109/ROLCG.2015.7367417

[10] R. Lloyd and M. Rebow, "Data driven prediction model (ddpm) for server inlet temperature prediction in raised-floor data centers," in *2018 17th IEEE Intersociety Conference on Thermal and Thermomechanical Phenomena in Electronic Systems (ITherm)*, 2018, pp. 716–725. [Online]. Available: https://doi.org/10.1109/ITHERM.2018.8419650

[11] T. Akiyama, M. Matsuoka, K. Matsuda, Y. Sakemi, and H. Kojima, "Secure and long-lived wireless sensor network for data center monitoring," in *2018 IEEE 42nd Annual Computer Software and Applications Conference (COMPSAC)*, 2018, pp. 559–564. [Online]. Available: https://doi.org/10.1109/COMPSAC.2018.10295

[12] M. Wiboonrat, "Developing diagnostics and prognostics of data center systems implementing with condition-based maintenance," in *IECON 2018 - 44th Annual Conference of the IEEE Industrial Electronics Society*, 2018, pp. 4901–4906. [Online]. Available: https://doi.org/10.1109/IECON.2018.8591203

[13] S. P. Patil and S. C. Patil, "A real time sensor data monitoring system for wireless sensor network," in *015 International Conference on Information Processing (ICIP)*, 2015, pp. 525–528. [Online]. Available: https://doi.org/10.1109/INFOP.2015.7489440

[14] B. Ashish, "Temperature monitored iot based smart incubator," in *2017 International Conference on I-SMAC (IoT in Social, Mobile, Analytics and Cloud) (I-SMAC)*, 2017, pp. 497–501. [Online]. Available: https://doi.org/10.1109/I-SMAC.2017.8058400

[15] S. Mandala, S. N. Anggis, M. S. Mubarok, and Shamila, "Energy efficient iot thermometer based on fuzzy logic for fever monitoring," in *2017 5th International Conference on Information and Communication Technology (ICoIC7)*, 2017, pp. 1–6. [Online]. Available: https://doi.org/10.1109/ICoICT.2017.8074640

[16] K. A. Zilani, R. Yeasmin, K. A. Zubair, M. R. Sammir, and S. Sabrin, "R^{3}hms, an iot based approach for patient health monitoring," in *2018 International Conference on Computer, Communication, Chemical, Material and Electronic Engineering (IC4ME2)*, 2018, pp. 1–4. [Online]. Available: https://doi.org/10.1109/IC4ME2.2018.8465482

[17] Y. Uomoto and A. Kajiwara, "Heartbeat monitoring uwb sensor robust to body movement," in *2018 IEEE 4th World Forum on Internet of Things (WF-IoT)*, 2018, pp. 280–285. [Online]. Available: https://doi.org/10.1109/WF-IoT.2018.8355194

[18] S. Shaikh, D. Waghole, P. Kumbhar, V. Kotkar, and P. Awaghade, "Patient monitoring system using iot," in *2017 International Conference on Big Data, IoT and Data Science (BID)*, 2017, pp. 177–181. [Online]. Available: https://doi.org/10.1109/BID.2017.8336594

[19] E. Kadiyala, S. Meda, R. Basani, and S. Muthulakshmi, "Global industrial process monitoring through iot using raspberry pi," in *2017 International Conference on Nextgen Electronic Technologies: Silicon to Software (ICNETS2)*, 2017, pp. 260–262. [Online]. Available: https://doi.org/10.1109/ICNETS2.2017.8067944

[20] S. H. Kim, J. M. Jeong, M. T. Hwang, and C. S. Kang, "Development of an iot-based atmospheric environment monitoring system," in *2017 International Conference on Information and Communication Technology Convergence (ICTC)*, 2017, pp. 861–863. [Online]. Available: https://doi.org/10.1109/ICTC.2017.8190799

[21] S. Wang, Y. Hou, F. Gao, and X. Ji, "A novel iot access architecture for vehicle monitoring system," in *2016 IEEE 3rd World Forum on Internet of Things (WF-IoT)*, 2016, pp. 639–642. [Online]. Available: https://doi.org/10.1109/WF-IoT.2016.7845396

[22] J.-L. Lee, Y.-Y. Tyan, M.-H. Wen, and Y.-W. Wu, "Development of an iot-based bridge safety monitoring system," in *2017 International Conference on Applied System Innovation (ICASI)*, 2017, pp. 84–86. [Online]. Available: https://doi.org/10.1109/ICASI.2017.7988352

[23] T. Perumal, M. N. Sulaiman, and C. Y. Leong, "Internet of things (iot) enabled water monitoring system," in *2015 IEEE 4th Global Conference on Consumer Electronics (GCCE)*, 2015, pp. 86–87. [Online]. Available: https://doi.org/10.1109/GCCE.2015.7398710

[24] L. Nóbrega, A. Tavares, A. Cardoso, and P. Gonçalves, "Animal monitoring based on iot technologies," in *2018 IoT Vertical and Topical Summit on Agriculture - Tuscany (IOT Tuscany)*, 2018, pp. 1–5. [Online]. Available: https://doi.org/10.1109/IOT-TUSCANY.2018.8373045

[25] R. Kamalraj and M. Sakthivel, "A hybrid model on child security and activities monitoring system using iot," in *2018 International Conference on Inventive Research in Computing Applications (ICIRCA)*, 2018, pp. 996–999. [Online]. Available: https://doi.org/10.1109/ICIRCA.2018.8596771

[26] C.-S. Choi, J.-D. Jeong, I.-W. Lee, and W.-K. Park, "Lora based renewable energy monitoring system with open iot platform," in *2018 International Conference on Electronics, Information, and Communication (ICEIC)*, 2018, pp. 1–2. [Online]. Available: https://doi.org/10.23919/ELINFOCOM.2018.8330550

[27] F. Wu, C. Rudiger, J.-M. Redouté, and M. R. Yuce, "We-safe: A wearable iot sensor node for safety applications via lora," in *2018 IEEE 4th World Forum on Internet of Things (WF-IoT)*, 2018, pp. 144–148. [Online]. Available: https://doi.org/10.1109/WF-IoT.2018.8355234

[28] A. Kekre and S. K. Gawre, "Solar photovoltaic remote monitoring system using iot," in *2017 International Conference on Recent Innovations in Signal processing and Embedded Systems (RISE)*, 2017, pp. 619–623. [Online]. Available: https://doi.org/10.1109/RISE.2017.8378227

Scientific Paper / Artículo Científico

UNIVERSIDAD POLITÉCNICA SALESIANA ECUADOR
INGENIUS
Revista de Ciencia y Tecnología
https://doi.org/10.17163/ings.n22.2019.08
pISSN: 1390-650X / eISSN: 1390-860X

Evaluation Of Mechanical Properties In of Double-Dip Galvanized Coatings on Carbon Steel

Evaluación de propiedades mecánicas en recubrimientos galvanizados por doble inmersión en caliente sobre acero al carbono

Yraima Rico O.[1,*], Edwuin Carrasquero[2], Jaime Minchala [3]

Abstract

Little is known about the operational conditions, the microstructure and properties of the coatings manufactured by hot double-dip. The objective of this work is to evaluate the mechanical properties of Zn / Zn-5%Al coatings applied by the hot double-dip technique, varying the immersion times in liquid baths. For the evaluation, Vickers microhardness profiles and bending tests were made. The microhardness profiles for different immersion times show similarities, exhibiting great heterogeneity due to the microstructural characteristics. It is observed that increasing the immersion time decreases the critical angle, and the immersion time does not significantly influence the density of confined and unconfined cracks. It is concluded that the ductility of the coatings is influenced by their total thickness, and possibly by the thickness of the different areas and residual stresses, with the samples being coated for a 60 s immersion time, which present better behavior in the bending test.

Keywords: Microcrack, double-dip, galvanized coatings.

Resumen

Poco se conoce sobre las condiciones operacionales, la microestructura y propiedades de los recubrimientos fabricados por doble inmersión en caliente. Este trabajo tiene como objetivo evaluar propiedades mecánicas de recubrimientos Zn/Zn-5%Al aplicados por la técnica de doble inmersión en caliente, variando los tiempos de inmersión en los baños líquidos. Para la evaluación se realizaron perfiles de microdureza Vickers y ensayos de doblez. Los perfiles de microdureza para diferentes tiempos de inmersión presentan similitudes, mostrando gran heterogeneidad debido a las características microestructurales. Se observa que al aumentar el tiempo de inmersión disminuye el ángulo crítico y el tiempo de inmersión no influye significativamente en la densidad de grietas confinadas y no confinadas. Se concluye que la ductilidad de los recubrimientos se ve influenciada por el espesor total de los mismos, y posiblemente por el espesor de las diferentes zonas y esfuerzos residuales, siendo las muestras recubiertas con tiempo de inmersión de 60 segundos, las que presentan mejor comportamiento ante el ensayo de doblez.

Palabras clave: microgrietas, doble inmersión, recubrimientos galvanizados.

[1,*] Departamento de Ingeniería Metalúrgica, Universidad Nacional Experimental Politécnica «Antonio José de Sucre», Barquisimeto, Venezuela. Autor para correspondencia ✉: iraricovi@unexpo.edu.ve, iraima.rico@gmail.com. http://orcid.org/0000-0002-6670-7741.

[2]Grupo de Investigación en Caracterización, Procesamiento y Protección de Materiales, Facultad de Ciencias de la Ingeniería, Universidad Estatal de Milagro, Ecuador http://orcid.org/0000-0001-6551-7316.

[3]Facultad de Sistemas y Telecomunicaciones, Universidad Estatal Península de Santa Elena, Ecuador http://orcid.org/0000-0002-9427-738X.

Received: 25-04-2019, accepted after review: 20-06-2019

Suggested citation: Rico O., Y.; Carrasquero, E. and Minchala, J. (2019). «Evaluation Of Mechanical Properties In of Double-Dip Galvanized Coatings on Carbon Steel». Ingenius. N.°22, (july-december). pp. 80-89. doi: https://doi.org/10.17163/ings.n22.2019.08.

1. Introduction

After processes of hot galvanizing, the pieces of coated steel may be subjected to plastic deformations in pressing, stamped and bending processes. These processes cause a great deformation in the structure of steels, which in turn may induce the beginning and propagation of cracks in the coatings. Once the cracks propagate, their openings provide air and humidity passages that lead to adverse oxidation reactions and corrosion, both in the coatings and in the steel substrates. The mechanical behavior of galvanized coatings on steels, may alter the performance of its response to operations that involve plastic deformations.

While the behavior regarding corrosion of galvanized steels has been rigorously investigated, the mechanical behavior of the galvanized coatings is currently limited [1].

In general, the hot galvanized coatings are complex multilayer systems, constituted by phases or layers with different thermomechanical properties. This makes difficult to analyze the mechanical behavior of the system steel/coating; in addition, the lack of information about the thermomechanical properties of the individual phases that constitute the coating should be added to this difficulty, as well as the properties of the interfaces [2].

The failures of hot galvanized coatings have been related with the residual stresses generated in their manufacturing process. The microcracks induced in the solidification process frequently occur on the galvanized coating, due to large mismatch between the thermal expansion coefficients of the zinc coating and the steel substrate. This may significantly influence on the density of cracks that are formed in the zinc layer, and in the further delamination of the coating under load [3].

There is a diversity of mechanical properties that may be evaluated in the coatings. Both the elastic and plastic properties are important for a specific application or demand. The ductility of the coatings depends on factors such as grain size, crystallographic orientation, working temperature, thickness of the coating, chemical composition, morphology and distribution of the phases that constitute the microstructure of the coating [4].

The double-dip process consists of consecutively submersing the steel in two liquid baths with different chemical composition. It is important to mention that most of the galvanizing processes by hot immersion are of simple or unique immersion, where the steel is submersed in a bath with specific chemical composition that provides the coating its mechanical, chemical and physical properties.

Nevertheless, the operational conditions in the manufacturing process, the microstructure and properties of the Zn/Zn-5%Al double-dip galvanized coatings have been scarcely studied. It is known that Galfan®(Zn-5%Al) baths provide greater resistance to corrosion and better ductility than conventional Zn baths. These characteristics may be found in the external zone of the coating, once the second immersion has been carried out, without requiring to change the fluxing systems in the preparation of the steel. Information regarding the possible industrial application of double-dip coatings has been little disseminated, but it is estimated that they can be used in components located in more severe corrosion environments, where traditional Zn coatings exhibit a lower protecting performance.

For that matter, the objective of this research work is to evaluate the mechanical properties of Zn/Zn-5%Al coatings applied using the hot double-dip technique, with varying times of immersion in the liquid baths.

2. Materials and methods

Samples of AISI 1020 steel, of dimensions 100 mm x 38 mm x 3 mm, were employed to conduct this research. The surfaces of the samples were degreased with 17 % NaOH for 5 minutes at 60 °C; for the abrasion they were submersed in a solution of 18% hydrochloric acid for 1.5 minutes at 80 °C and, at last, they were submersed for 5 minutes in a 30 g/600 ml solution of ammonia chloride for fluxing, at a temperature of 70 °C, and then dried with air at ambient temperature. The double-dip hot galvanizing process was carried out experimentally, in a vertical electrical furnace that contains two crucible with each of the liquid baths, namely a type I bath of pure Zn, and a type II bath of Zn with 5 % in weight of Al (Galfan®); the temperature of the baths was 550 °C ± 10 °C.

The working temperature was determined by means of previous tests, where it was found that the fluidity of the dip baths was notably low at smaller temperatures, thus making difficult the immersion and emersion of the steel samples in the liquid baths.

It is important to remark, that the microstructural evaluation of the double-dip coating under the same operational conditions was previously reported [5]; the microstructural characteristics described in [5] will be taken as reference in this work.

The Zn/Zn-5%Al coatings were made with different immersion times: 30 s in each bath (pure Zn and Zn with 5% in weight of Al), for a total immersion time of 60 s; 45 s in each bath for a total immersion time of 90 s and 60 s in each bath for a total immersion time of 120 s; 3 samples were galvanized with each total immersion time. Table 1 shows the operational parameters of the double-dip galvanized process.

The transverse sections of the double-dip galvanized samples were prepared using conventional methods, cut with abrasive disc, roughing with sandpaper,

and mechanical polished with alumina suspension, to determine the thicknesses of the coatings by means of optical microscopy and carry out Vickers microhardness profiles.

Table 1. Parameters of the double-dip galvanized process

Operational parameters	
Chemical composition of the baths	Type I bath: 100 % Zn Type II bath: Zn-5 % weight Al
Time of immersion in each bath	30, 45 y 60 s
Total immersion time	60, 90 y 120 s
Immersion way	Quieto
Temperature of the baths	550 °C ± 10 °C
Cooling after the extraction	Quiet air

The Vickers microhardness tests were conducted taking measurements from the steel/coating interface through the coating up to its surface, with a load of 50 g. Six microhardness profiles were carried out for each total immersion time, making indentations every 50 μm (approximately), and the obtained values were plotted vs. distance, for each total immersion time.

In order to evaluate the relative ductility of the coatings, the samples were deformed up to the critical angle, which is the angle under which the beginning of the macroscopic cracking in the critical deformation zone, can be visually observed at the moment of the test [6]. The B arrangement for semi-guided tests, suggested by the standard ASTM E-290 [7], was utilized for the bending test (see Figure 1).

Afterwards, the transverse sections of the samples, tested by means of optical microscopy, were examined, in order to identify the different types of cracks, and describe qualitative and quantitatively the damage induced by the flexion. For this purpose, it was determined the density of cracks (number of cracks/mm) formed perpendicularly to the steel/coating interface, in the tensioned zone of the samples. These measurements were carried out along a 20 mm long arc, symmetric with respect to the maximum point of flexion (Zone A), as shown in Figure 1 [8].

On the other hand, a statistical analysis of the results was carried out by means of a unidirectional variance analysis (ANOVA), comparing the probability factors obtained with the Fisher F statistic, for a reliability of 95 %. The total immersion times were related with the thickness of the coating, the critical angle and the density of confined and not confined cracks

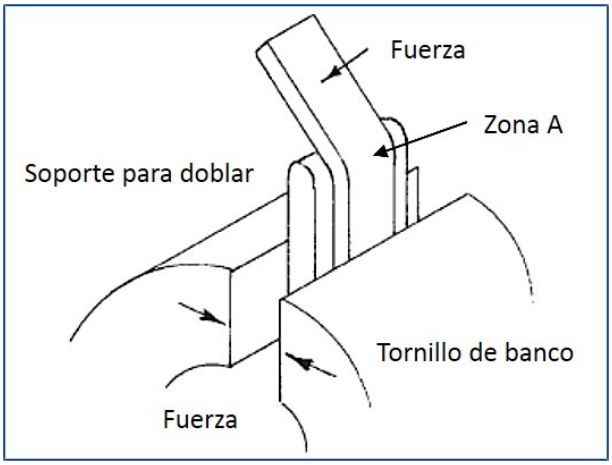

Figure 1. Scheme of the flexion test according to the ASTM E-290 standard. Arrangement B for semi-guided bending test of thin samples with a retained extreme; zone A will be the examined zone [7].

3. Results and discussion

All the coatings obtained using the double-dip method, are according the specifications of the ASTM A-123 standard: «Standard Specification for Zinc (Hot-Dip Galvanized) Coatings on Iron and Steel Products» [9] (see Figure 2).

The coatings presented commercially acceptable superficial characteristics. Regarding the superficial finish, all samples exhibit continuity and do not have zones without coating nor of varying roughness. With respect to the superficial appearance, the double-dip galvanized coatings do not have ampoules nor slag.

The thicknesses of the coatings were sufficiently large, in the range 450-650 μm (see Figure 3), compared to commercial zinc coatings that are in the order of 100 μm. Figure 3 clearly shows that the thicknesses of the coatings vary significantly with the total immersion time: as the total immersion time increases, the total thickness of the coating also increases.

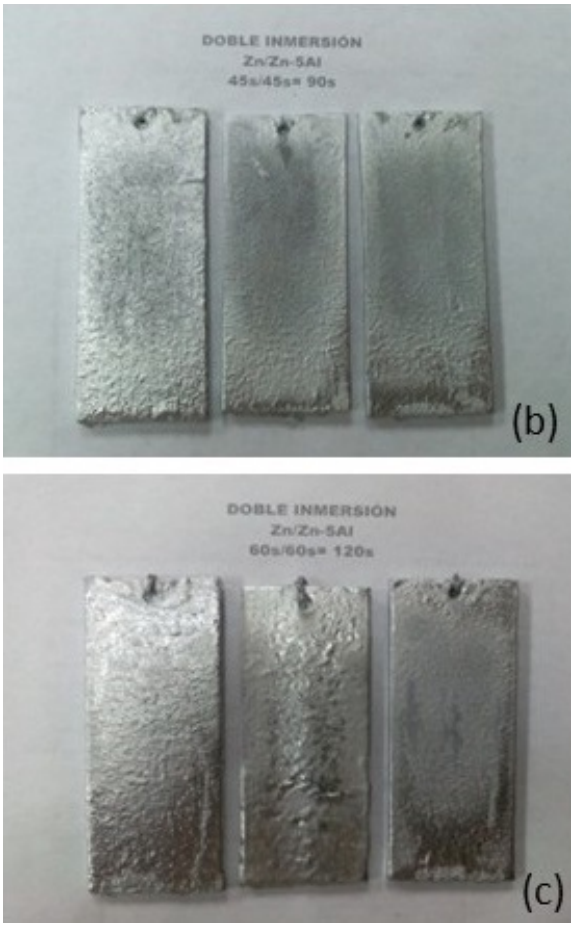

Figure 2. Muestras de acero recubiertas con la técnica de doble inmersión, para diferentes tiempos de inmersión a) 60 s, b) 90 s y c) 120 s.

The ANOVA carried out shows that $F_{experimental} = 171,51$ and $F_{0,05}(2,51) = 3,18$; i.e., $F_{experimental} > F_{0,05}(2,51)$ and $P_{experimental} < 0,05$; therefore, the null hypothesis is rejected and the thickness of the coating varies significantly with the total immersion time.

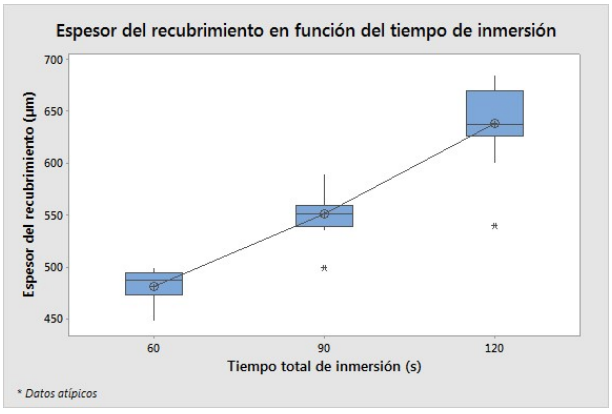

Figure 3. Gráfica de caja del ANOVA para el espesor total de los recubrimientos galvanizados por doble inmersión en función del tiempo total de inmersión.

The large thicknesses obtained, compared to commercial zinc coatings, suggest that the immersion in the second bath (Zn-5%Al) and the reactivity or synergy of both dip baths, determine the increase in the total thickness of the coating.

The reactivity of the chemical species, mainly Zn, Al and Fe and the growth kinetics of the formed phases in the second immersion, may be preponderant in the increase of the thickness of the double-dip galvanized coatings. Another important factor that may increase the velocity of the reactions and the growth kinetics is the working temperature, which was 550 °C; this value is utilized in the called galvanized at «high temperatures».

For the case of the double-dip galvanized coatings, it is difficult to determine which mechanism controls the kinetics of the total growth of the coating. It is estimated that for the first immersion bath (pure Zn), the growth of the coating thickness follows a nonlinear behavior with respect to the immersion time, as indicated by the literature [2, 10, 11]; but when the steel is immersed in the second bath, which contains 5 % of weight of aluminum, it could give place to the fast formation of Fe-Al-Zn compounds, which influences the type of behavior of the growth of the coating [5], thus increasing the velocity of initial growing, as shown by the large thicknesses obtained.

Nevertheless, the type of kinetics of the growth of the double-dip galvanized coating is still nonlinear, which indicates that the total mechanism that controls the growth of the coating is the diffusion of species, despite of the chemical reactions that can be generated in the second dip bath. It is estimated that the velocity at which these reactions occur, may determine the growth of the thickness of the coating in the second dip bath, but does not determine the type of kinetics of this growth.

The general microstructural characteristics independent of the total immersion time, were described in [5]. They defined three zones in the double-dip galvanized coatings: Zone I, constituted by phase δ of faceted morphology in the steel/coating interface, which significantly varies with the total immersion time and phase η; zone II shows high microstructural heterogeneity and is mainly constituted by three phases, namely phase η which appears as a matrix, phase δ and Fe-Al-Zn micro-segregated ternary compounds of rounded morphology; and zone III is constituted by phases η and $Fe_2Al_5Zn_x$ compounds of rounded morphology.

It is evident in Figure 4 that there exists a similar trend in the microhardness values obtained for the three total immersion times. In zone I, specifically in the area adjacent to the steel/coating interface, the microhardnesses are elevated, with a general average of 254 HV, because it corresponds to the value of microhardness of phase δ ($FeZn_{10}Al_x$ - $FeZn_7Al_x$).

After this area, a considerable decrease in the values

of microhardness is observed, with a general average of 19 HV, which corresponds to phase eta, η (pure Zn).

In zone II there exists a slight trend of the microhardness to increase to values in the range 100-200 HV, due to the presence of Fe-Al-Zn precipitated ternaries in a hard phase δ; however, this zone presents a large microstructural heterogeneity and, as a consequence, there is a high variability of the values of microhardness. At last, in zone III the microhardness oscillates around 100 HV, in a microstructure basically constituted by $Fe_2Al_5Zn_x$ precipitated in a matrix η of practically pure Zn.

The values of microhardness for phase δ and η formed in zone I of the coatings, for each total immersion time, are similar to the values of microhardness reported by other authors [4, 10–14]. For zones II and III, it is difficult to find reference values of microhardness, especially for zone II because of the presence of great heterogeneity; the microhardness values of zone III could be compared with the hardness values in Galfan®coatings, but these values may vary depending on the cooling conditions of the coating after it is extracted from the bath, since it may modify its eutectic structure making it thinner for faster cooling. It has been found that for coatings with 4.5 % weight of Al, the microhardnesses are between 75.1 and 76.2 HV [15], slightly smaller than the obtained for zone III in this study, which are close to 100 HV.

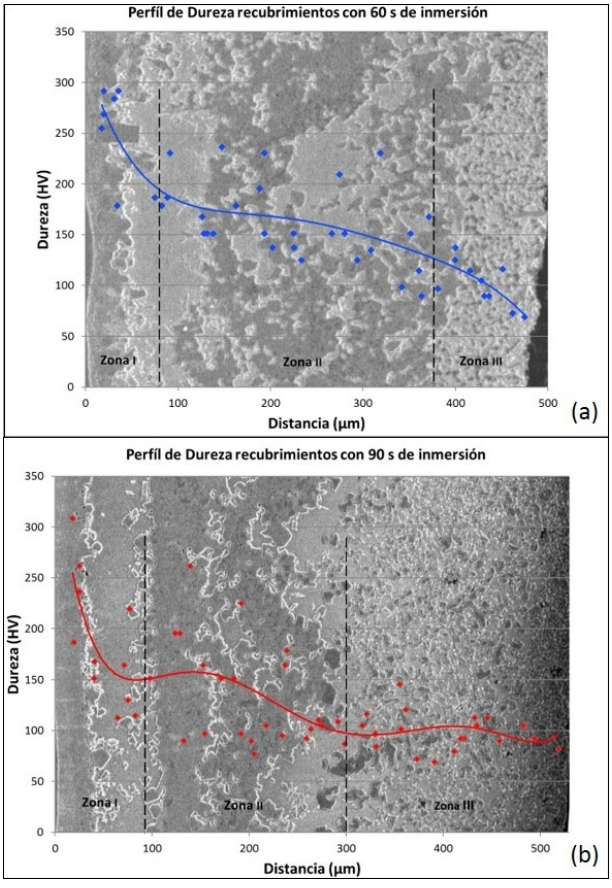

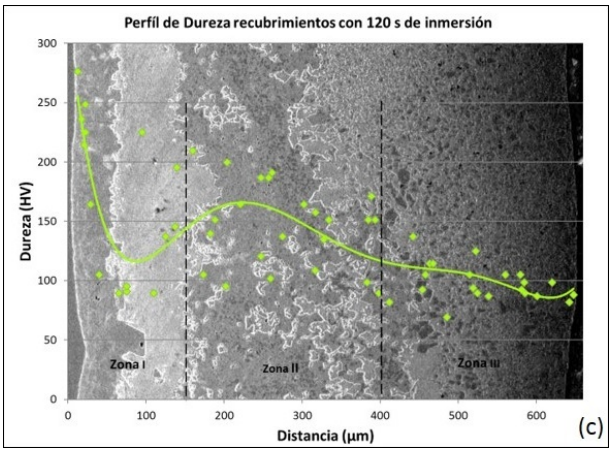

Figure 4. Vickers microhardness profiles for double-dip galvanized coatings, with total immersion time: a) 60 s, b) 90 s y c) 120 s.

The thickness of each zone of the double-dip galvanized coatings, depends on the immersion time in each bath; therefore, the trend of the microhardness values for each zone of the coatings is widened or reduced depending on the length of each zone. For example: the length of zone III in the coatings with an immersion time of 60s is much smaller compared to the length of zone III in the coatings with an immersion time of 120s, so the extension or trend of the microhardness values in this zone is broader in the coatings with 120s immersion time. This condition might influence the mechanical behavior of the coatings, specifically in their ductility.

Figure 5 shows the coated samples tested by bending up to the critical angle, for a total immersion time of 60s.

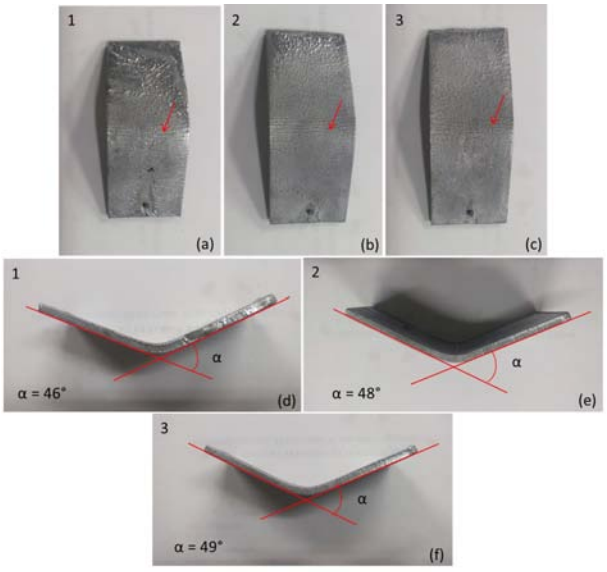

Figure 5. Samples 1, 2 y 3 with double-dip galvanized coatings with a total immersion time of 60s, tested by bending. The critical angle can be observed: superior view (a, b y c), transverse view (d, e y f).

The superior view of the surfaces of maximum bending in the tested coated samples is shown, where it can be seen the beginning of the macroscopic cracking of the coating (indicated by red arrows); the transverse view of the critical angle for each of the samples is also shown.

A unifactorial ANOVA variance analysis was conducted, to determine the influence of the total immersion time on the critical angle. For this experiment, the null hypothesis was that the critical angle does not vary with the total immersion time for the three levels under study, i.e. 60, 90 and 120 seconds.

Figure 6 is a box plot that shows the results of the ANOVA, and the influence of the total immersion time on the critical angle of the double-dip galvanized coatings. Observe the means and the intervals according to the standard deviation of the measured values of critical angle for each total immersion time. Since the mean values are significantly different, the representative boxes of each level of study (60, 90 y 120 s) do not overlap.

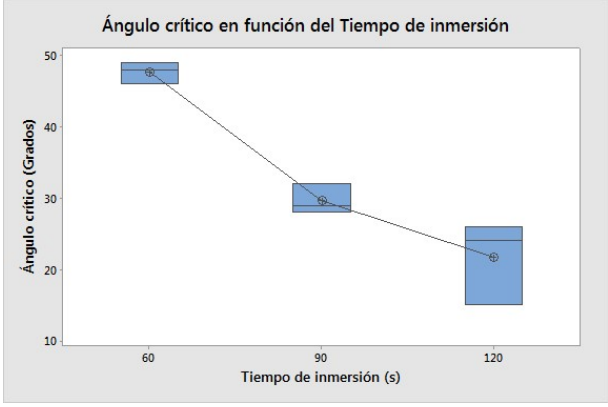

Figure 6. ANOVA box plot of the critical angle as a function of the total immersion time, in double-dip galvanized coatings.

The ANOVA shows that $F_{experimental} = 38,93$ and $F_{0,05}(2,6) = 5,14$; therefore, $F_{experimental} > F_{0,05}(2,6)$ and $P_{experimental} < 0,05$; therefore, the null hypothesis is rejected and the critical angle varies significantly with the total immersion time: as the total immersion time increases, the critical angle decreases.

In thick coatings, as the ones under study, the magnitude of the residual stress depends on the thickness of the coating. This residual stress develops during the formation of the coating and the further cooling; in general, it is produced during the formation of individual layers, due to the differences in the molar volume of each of these layers, as well as during the cooling from the immersion temperature, due to the mismatch of the thermal tensions as a result of the differences in the thermal expansion coefficient of the substrate and the different phases that constitute the coating; these residual stresses significantly increase as the thickness of the coating increases [2, 16].

Due to this, it is expected that the critical angle varies with the total thickness of the coating. For large thicknesses, it is estimated that the residual stress will be greater in the coatings, and therefore pre-existing microcracks in phase δ, new microcracks formed in the same phase during the deformation, and in other zones of the coating subject to tension in the bending state, evolve to macrocracks which are visible at smaller bending angles, when compared with coatings of lesser thicknesses.

In bending tests, the critical angle has been related to the total thickness of the layer $\delta + \zeta$, phases adjacent to the steel/coating interface for traditional galvanized [6], determining that the critical angle decreases as the thicknesses of the intermetallic layers Zn-Fe increase. Nevertheless, for double-dip galvanized coatings, it is estimated that the critical bending angle depends, not only on the thickness of the phase δ but, as it has been already commented, also the total thickness of the coating has a significant influence due to the residual stresses generated in thick coatings. Another important factor that could have influence in the critical bending angle, are the thicknesses and sizes of the different zones of the double-dip galvanized coatings, and thus the mechanism of formation and growth of the microcracks generated in each of them.

The quantified cracks were classified in two types: not confined, which extend along the coating and expose the steel substrate to the atmosphere, and confined, which do not extend along the whole thickness of the coatings. The latter were sub-classified in a qualitative manner in the double-dip galvanized coatings.

Figure 7 is a box plot which shows the results of the ANOVA, and the influence of the total immersion time on the density of confined and not confined cracks of the double-dip galvanized coatings.

Similarly, observe the means and the intervals according to the standard deviation, of the measured values of crack densities for each total immersion time. Since the means are not significantly different, the representative boxes of each level under study (60, 90 y 120 s) overlap, which indicate that changes in the immersion times do not significantly influence the density of both types of crack.

The ANOVA shows that $F_{experimental} = 3,59$ for the density of confined cracks, the $F_{experimental} = 3,73$ for the density of not confined cracks and $F_{0,05}(2,6) = 5,14$; therefore, for both cases $F_{experimental} < F_{0,05}(2,6)$ y $P_{experimental} > 0,05$. Then, the null hypothesis is accepted, and the density of confined and not confined cracks do not vary significantly with the total immersion time, for double-dip galvanized coatings tested up to the critical angle.

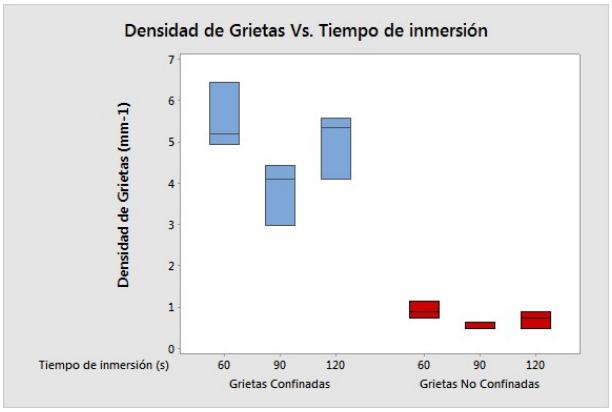

Figure 7. ANOVA box plot of the density of confined and not confined cracks as a function of the total immersion time, in double-dip galvanized coatings

Nevertheless, it is important to remark that the bending test applied to the double-dip coated samples, for the different total immersion times, was conducted up to the critical angle which, as has been statistically demonstrated, varies significantly with the total immersion time. Therefore, the samples were tested at different angles, for the different immersion times, up to the beginning of the macroscopic cracking; this implies that all tested samples present macroscopic cracking in the critical deformation zone (see Figure 5).

This could explain why the density of the cracks do not vary significantly with the total immersion time. All the double-dip coated samples were tested by bending up to the macroscopic cracking and, hence have, in average, the same density of confined and not confined cracks.

In the double-dip galvanized coatings tested by bending up to the critical angle, independently of the total immersion time the following general characteristics and type of perpendicular microcracks to the steel substrate were observed, and studied qualitatively:

i. Confined cracks in phase δ, which could be in turn divided in microcracks pre-existing at the bending test, and microcracks formed in the bending test (Figure 8a); these represent the majority of confined cracks.

ii. Confined cracks that are present along the whole zone II of the coating, formed at the bending test (see Figure 8a).

iii. Confined cracks that extend from phase δ up to the end of zone II of the coatings. It is possible that these cracks result from the advancement of type i cracks in the bending test (see Figure 8a).

iv. Confined cracks that extend from the surface of zone III of the coatings up to zone II, formed during the bending test (see Figure 8b).

v. Not confined cracks that extend along the whole double-dip galvanized coating (see Figure 8b).

The macroscopic cracking of the coatings constitute the step previous to the failure, in general by delamination of the galvanized coatings; however, in the double-dip coated samples tested by bending up to the critical angle, there was no evidence of macroscopic delamination of the coating. The beginning of cracking longitudinal or parallel to the substrate in the steel/coating interface, was determined in the base of some not confined cracks.

It is important to remark that it was not noted longitudinal cracking inside the described zones or between them in any of the double-dip coated samples, which implies an excellent cohesion between the zones formed in each of the dip baths.

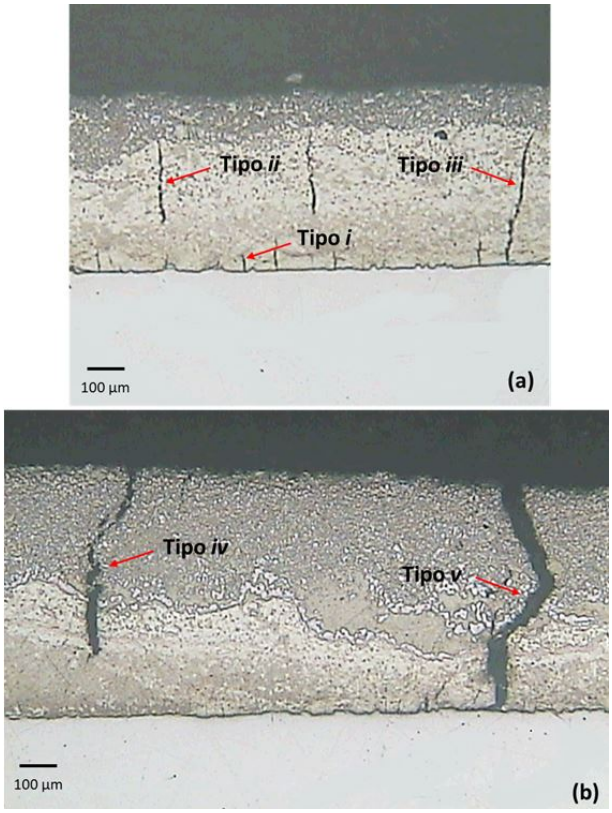

Figure 8. Optical micrography of the types of microcrack found in double-dip galvanized coatings tested up to the critical angle: a) Coating with a total immersion time of 60 s, showing microcracks of type i, ii and iii, b) Coating with a total immersion time of 120 s, showing microcracks of type iv and v.

Even though in the present study no observations were performed about the behavior in the initiation and propagation of cracks for different bending angles, based on what was observed in the double-dip galvanized coatings tested up to the critical angle, the initiation and propagation of cracks can be described in the following manner:

First, once the steel samples have been coated by the double-dip, there is a great quantity of residual stresses in the coating that increase with the total

thickness of the coatings, and cause the formation of confined microcracks in the phase δ of zone I, type i microcracks pre-existing at the bending test, which in general are perpendicular to the steel substrate, for a bending angle of 0°, α_0.

Once the deformation of the double-dip coated samples begins in the bending test, new type i microcracks are generated in the phase δ, and it is possible that microcracks extending along the whole zone II will simultaneously start to generate, type ii microcracks for bending angles $\alpha_0 > \alpha_0$. It is important to remember that phase δ is one of the hardest in double-dip coatings, with an average microhardness of 254 HV. Zone II presents values of microhardness in the range 100-200 HV, with great microstructural heterogeneity; it is constituted by phases δ, η and Fe-Al-Zn ternary precipitates. The latter could act as stress concentrators that facilitate the growth and propagation of cracks, which would imply the presence of critical areas for the formation of new type ii microcracks.

The advancement of pre-existing cracks and the formed in the bending test, in phase δ towards zone II of the double-dip galvanized coating, require that these microcracks cross phase η in zone I. This phase is soft and the microcracks could tend to be blocked in it, without advancing towards zone II of the coatings; in fact, the majority of these cracks seem to stay as type i confined cracks, and represent the majority of the confined microcracks observed in the double-dip coatings; this could explain the difference between the density of confined and not confined cracks (Figure 7). Perhaps, only a small amount of these type i cracks will exceed the necessary critical stress to advance through phase η, and once in zone II (zone with more hardness than phase δ) continue advancing through its end, becoming type iii cracks for bending angles $\alpha_2 > \alpha_1$.

On the other hand, in the opposite direction, from the surface of the coating in zone III, even though this zone presents a microhardness ≈ 100 HV, with a soft matrix of η and $Fe_2Al_5Zn_x$ hard precipitates, microcracks resulting from the tensions generated by the bending test initiate and propagate towards the steel substrate; this zone is subjected to the greatest tension during the test, and type iv cracks are generated; these cracks formed on the surface penetrate towards the steel/coating interface, for bending angles $\alpha_3 > \alpha_2$.

With the increase of the applied tension, and thus of the bending angle up to the critical angle $\alpha_{crit} > \alpha_3$, possibly the type ii and iii cracks and the microcracks generated in the type iv tensioned surface will generate type v cracks, not confined cracks that extend along the whole coating, which become evident macroscopically in the surface of the double-dip galvanized coatings. In general, the space between the transverse cracks decreases at this moment, and the type v cracks extend or grow in the longitudinal direction adjacent to the steel/coating interface, initiating the delamination of the galvanized coating.

As it has been said before, it is estimated an increment of the residual stresses generated in the manufacturing process of double-dip galvanized coatings, with the increase of the total thickness of the coating. For example, it has been observed that for coatings with a total immersion time of 120s, the thickness of the zones is, in general, greater than the thickness of the zones in coatings with total immersion times of 90 s and 60 s; therefore, it is estimated that the possible residual stresses that are generated in each of the zones described in the coatings increase with the thickness of such zones. On the other hand, in the coatings tested by bending, the confined microcracks represent the majority of the cracks observed and described for double-dip galvanized coatings, and these microcracks are the ones that evolve and grow becoming not confined cracks. Even though the density of the confined and not confined microcracks does not vary with the total immersion time in the samples tested up to the critical angle, as has been statistically shown, the thickness of each of the zones of the coatings indeed seem to increase with the immersion time. The thickness of each zone might determine the evolution and growth of the confined cracks, thus determining the critical angle. The microcracks type i, ii and iii might be longer in more tensioned zones for thicker coatings, which would help these to evolve more easily to type v microcracks.

Therefore, it is estimated that, for thicker coatings with possible residual stresses in tension, the confined microcracks evolve and grow until becoming not confined cracks for smaller bending angles, as compared with thinner coatings.

Then, the relative ductility of the double-dip galvanized coatings is significantly influenced by the total thickness of the coatings, and possibly the thickness of the different zones of the coatings and the residual stresses present in each of them have influence on this property, where it is observed a significant decrease of the critical angle as the immersion time increases.

4. Conclusions

The total immersion times utilized in this study are statistically influential in the total thicknesses of the coatings and on the critical angle, but not on the density of the cracks encountered in the samples tested by bending up to the critical angle.

The relative ductility of the double-dip galvanized coatings is influenced by the total thickness of the coatings; possibly the thickness of the different zones of the coatings and the residual stresses present in each of them have influence on this property, where it is observed a significant decrease of 54 % of the

critical angle as the total immersion time increases; the samples coated with a total immersion time of 60 s show the best behavior in the bending test.

References

[1] R. Parisot, S. Forest, A. Pineau, F. Grillon, X. Demonet, and J.-M. Mataigne, "Deformation and damage mechanisms of zinc coatings on hot-dip galvanized steel sheets: Part i. deformation modes," *Metallurgical and Materials Transactions A*, vol. 35, no. 3, pp. 797–811, Mar 2004. [Online]. Available: https://doi.org/10.1007/s11661-004-0007-x

[2] E. Tzimas and G. Papadimitriou, "Cracking mechanisms in high temperature hot-dip galvanized coatings," *Surface and Coatings Technology*, vol. 145, no. 1, pp. 176–185, 2001. [Online]. Available: https://doi.org/10.1016/S0257-8972(01)01323-8

[3] V. Kuklík and J. Kudláček, "2 - hot-dip galvanizing," in *Hot-Dip Galvanizing of Steel Structures*. Boston: Butterworth-Heinemann, 2016, pp. 7–16. [Online]. Available: https://doi.org/10.1016/B978-0-08-100753-2.00002-1

[4] A. Marder, "The metallurgy of zinc-coated steel," *Progress in Materials Science*, vol. 45, no. 3, pp. 191–271, 2000. [Online]. Available: https://doi.org/10.1016/S0079-6425(98)00006-1

[5] Y. Rico and E. J. Carrasquero, "Microstructural evaluation of double-dip galvanized coatings on carbon steel," *MRS Advances*, vol. 2, no. 62, pp. 3917–3923, 2017. [Online]. Available: https://doi.org/10.1557/adv.2017.608

[6] S. Ploypech, P. Jearanaisilawong, and Y. Boonyongmaneerat, "Influence of thickness of intermetallic layers on fracture resistance of galvanized coatings," *Surface and Coatings Technology*, vol. 223, pp. 1–5, 2013. [Online]. Available: https://doi.org/10.1016/j.surfcoat.2013.02.017

[7] ASTM, *ASTM E290 - 14 Standard Test Methods for Bend Testing of Material for Ductility*, ASTM International, West Conshohocken, PAASTM Std., 2014. [Online]. Available: http://bit.ly/2ZHgBvY

[8] Y. Rico O and E. Carrasquero, "Efecto de la composición química en el comportamiento mecánico de recubrimientos galvanizados por inmersión en caliente: una revisión," *INGENIUS*, no. 18, pp. 30–39, 2017. [Online]. Available: https://doi.org/10.17163/ings.n18.2017.04

[9] ASTM, *ASTM A123 / A123M-17, Standard Specification for Zinc (Hot-Dip Galvanized) Coatings on Iron and Steel Products*, ASTM International, West Conshohocken, PA Std., 2017. [Online]. Available: http://bit.ly/2N4adgP

[10] C. E. Jordan and A. R. Marder, "Fe-zn phase formation in interstitial-free steels hot-dip galvanized at 450°c: Part i 0.00 wt% al-zn baths," *Journal of Materials Science*, vol. 32, no. 21, pp. 5593–5602, Nov 1997. [Online]. Available: https://doi.org/10.1023/A:1018680625668

[11] P. Pokorny, J. Kolisko, L. Balik, and P. Novak, "Reaction kinetics of the formation of intermetallic fe - zn during hot - dip galvanizing of steel," *Metallurgy*, vol. 55, no. 1, pp. 111–114, 2016. [Online]. Available: http://bit.ly/2XyXZAU

[12] S. Ploypech, Y. Boonyongmaneerat, and P. Jearanaisilawong, "Crack initiation and propagation of galvanized coatings hot-dipped at 450°c under bending loads," *Surface and Coatings Technology*, vol. 206, no. 18, pp. 3758–3763, 2012. [Online]. Available: https://doi.org/10.1016/j.surfcoat.2012.03.029

[13] M. Dutta, A. K. Halder, and S. B. Singh, "Morphology and properties of hot dip zn–mg and zn–mg–al alloy coatings on steel sheet," *Surface and Coatings Technology*, vol. 205, no. 7, pp. 2578–2584, 2010. [Online]. Available: https://doi.org/10.1016/j.surfcoat.2010.10.006

[14] N. Parvini Ahmadi and E. Rafiezadeh, "Effect of aluminum on microstructure and thickness of galvanized layers on low carbon silicon-free steel," *International Journal of Iron & Steel Society of Iran*, vol. 6, no. 1, pp. 25–29, 2009. [Online]. Available: http://bit.ly/2ZBLLVh

[15] D. R. Raut and S. H. Poratkar, "Study the effect of aluminum variation on hardness & aluminum loss in zn-al alloy," *International Journal of Modern Engineering Research (IJMER)*, vol. 3, no. 2, pp. 884–887, 2013. [Online]. Available: http://bit.ly/2IxBPXc

[16] ASM, "Surface engineering." ASM Interenational., 2002. [Online]. Available: http://bit.ly/2KD2RyT

Scientific Paper / Artículo Científico

UNIVERSIDAD POLITÉCNICA SALESIANA ECUADOR
INGENIUS
Revista de Ciencia y Tecnología
https://doi.org/10.17163/ings.n22.2019.09
pISSN: 1390-650X / eISSN: 1390-860X

Performance and efficiency of different control techniques in an electrical heater

Rendimiento y eficiencia de distintas técnicas de control en un calefón eléctrico

Gabriel V. Moreano[1,*], César D. Arregui[1], Camilo G. Tenesaca[1], Henry J. Pilco[1]

Abstract

Water heating in the Ecuadorian residential sector has become a space for research and development, due to the attempt to mitigate the current spending of people and at the same time contribute actively to the energy efficiency processes that are gaining strength in the country. This paper conducts a comparative analysis between different techniques for controlling the water temperature in a residential system using an electric heater. The response of a direct phase control AC / AC converter was analyzed, which allows to delay the firing angle of the AC wave and the response of the ON / OFF control that activates or deactivates the heater during a pre-established number of half-cycles of alternating current. For the tests, a prototype of electric heater was implemented with a coil of 14 meters based on electrical resistances. Then, with the temperature responses generated from each converter, the transfer function of each system was identified, since both differ in its heat transmission technique and, thus in its mathematical model. Afterwards, a PID controller was tuned for each system, obtaining good results of temperature response in both cases, but only one was efficient regarding energy saving.

Keywords: control, PID, AC / AC converters, temperature, water, efficiency

Resumen

El calentamiento de agua en el sector residencial ecuatoriano se ha convertido en un espacio de investigación y desarrollo, debido al intento de mitigar el gasto corriente de las personas y a la vez contribuir de manera activa a los procesos de eficiencia energética que van tomando fuerza en el país. En el presente documento se muestra un análisis comparativo entre diferentes maneras de controlar la temperatura del agua para un sistema residencial utilizando un calentador eléctrico; se analizó la respuesta de un conversor AC/AC de control de fase directa que permite retrasar el ángulo de disparo de la onda de corriente alterna y la respuesta del control ON/OFF que activa o desactiva el calentador durante un número preestablecido de semiciclos de corriente alterna. Para las pruebas se instaló un prototipo de calentador eléctrico con un serpentín de 14 metros a base de resistencias eléctricas; con las respuestas de temperatura que se generan de cada conversor se procedió a identificar la función de transferencia de cada sistema ya que ambos difieren en su técnica de transmisión de calor y a la vez en su modelo matemático. Posteriormente se procedió a sintonizar un controlador PID para cada sistema, obteniendo buenos resultados de respuesta de temperatura en ambos casos, pero solo uno resultó eficiente en ahorro energético.

Palabras clave: control, PID, conversores AC/AC, temperatura, agua, eficiencia

[1,*]Grupo de Investigación y Mantenimiento (GIMAN), Escuela Superior Politécnica de Chimborazo (ESPOCH), Ecuador, Autor para correspondencia ✉: gabriel.moreano@espoch.edu.ec. http://orcid.org/0000-0002-9331-8223, http://orcid.org/0000-0002-6055-916X, http://orcid.org/0000-0001-8254-7998, http://orcid.org/0000-0002-0391-9755.

Received: 15-05-2019, accepted after review: 21-06-2019

Suggested citation: Moreano, G. V.; Arregui, C. D.; Tenesaca, C. G. ad Pilco, H. J. (2019). «Performance and efficiency of different control techniques in an electrical heater». Ingenius. N.°22, (july-december). pp. 90-99. doi: https://doi.org/10.17163/ings.n22.2019.09.

1. Introducción

The liquid petroleum gas (LPG) is the most commonly used energy source in Ecuador for heating water and cooking food, but starting from the change of the energy matrix, these type of devices are subject to a tax of 100 % over its commercial value, according to article 82 of the tax regime regulation [1], which is the reason why it has been decided to promote the use of other type of heaters as alternative to the significant cost increase of LPG heaters.

Original patents of a gas heater are shown in [2] and [3]; note that these devices have been in the market for a considerable time. The method of operation of these devices is found in [4], while a complete study of control techniques for this type of heater can be observed in [5]. One of the main problems of these devices is their high pollution, as mentioned in [6] based on a study conducted in the city of Loja – Ecuador; this problem generates major drawbacks in the health of persons. A pertinent analysis about these health issues can be found in [7].

On the other hand, the heaters that use GLP have a greater or smaller operating cost depending on the value of the GLP in each region; [8–10] show comparative studies between the use of a GLP heater and other residential water heating alternatives, such as, solar heaters or natural gas heaters. The benefit of one or other system specifically depends on the price of each energy source, taking into account that this will depend on the resources of each nation; there are countries with enormous hydric sources, such as Ecuador, and countries which have easy availability of petroleum derivatives, while in some developed nations, such as Germany, it has been chosen to regulate the self-consumption; more than one million households incorporate solar panels. Recently Spain also adopted this way by eliminating the solar tax [11], action with which the Government expects an increase in the self-consumption to benefit national resources.

A valid alternative for replacing the water heating systems that use GLP, for increased security and reduced generation of contaminant gases, are the electric heaters. According to [12], electric heaters play an important role in heating systems, and convert to heat 99 % of the energy they consume, i.e. the electric power is almost the same as the thermal power. In [13], various authors show the efficiency of an electric heater with a control technique to regulate the temperature.

The authors in [14] make a very complete summary of some types of electric heaters, and explain different techniques for temperature control.

Currently, the most important drawback of electric heaters is their high energy consumption, since a high electric power is required for heating a certain flow of water; in general, this power is generated by a neckline that remains connected to the electrical network at 100 % of its power while a water faucet is open, thus representing an elevated portion of the payment corresponding to the electrical service, moreover if this device stays on various hours per day.

The proposal presented in this work results from the combination of power electronics and the theory of automatic control systems, to develop a prototype that regulates the power dissipated in an electric neckline, thus reducing the energy consumption and also improving the response in the water temperature.

To observe this type of response, regarding both the efficiency and the temperature response, two static AC/AC converters were put into operation, to command the on and off of four electric necklines, a full cycle converter and a direct phase control converter; the direct benefit can be found in [15]: both types of converter can be implemented with the same power electronics circuit (see Figure 1).

The microprocessor utilized to control the system was one of the versions of the Arduino, which provide certain degree of versatility. According to [16], an automatic faucet that enables a high temperature of the fluid (around 40 °C) can be designed using an Arduino Mega 2560 plaque, without problems of electromagnetic noise nor interferences.

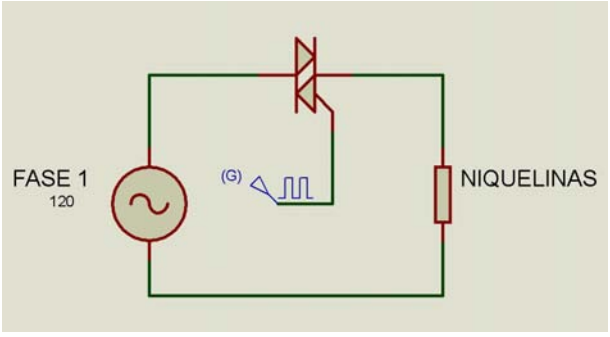

Figure 1. Simulation scheme of the AC/AC converter.

The operational principle of Arduino is analyzed in [17], besides the interest of persons for utilizing this plaque because it employs an easy to use simplified version of C++.

According to [18] Arduino has memory, capacity of autonomous processing, compilers of programming languages such as C, and physical ports to interconnect with devices that provide certain stability and reliability in their utilization.

It is mentioned in [19] that, due to their low cost, Arduino microcontrollers are used in engineering applications that commonly involve instrumentation, machine and structures monitoring, and control of mechanical systems.

For the implementation of the PID control system, it is necessary to measure the physical variables to be controlled. In this case, the controlled variable is the temperature, which is measured using a NTC

thermistor of a vehicle; these types of sensors are reliable, because they are designed to work in contact with water, and have very low cost. In [20], the authors present a simple explanation of the operation of the NTC thermistors, and how they transform the temperature signal into an electric signal.

It is mentioned in [21] that a circuit consisting of a source, a thermistor and a resistor should be installed for conditioning the thermistor; this circuit generates a voltage divisor that is read by the microprocessor. The temperature sensor maintains its characteristic exponential curve; thus it is required to acquire the value with the thermistor equation in the microprocessor.

An analysis of the control circuit by phase angle is included in [22]. The operation of this type of control is based on an angle of delay to turn on the necklines, both in the positive and negative semi-cycles of the commercial electrical sinusoidal wave. Therefore, by varying the firing angle, the power in each neckline is controlled and the temperature transfer is regulated. It is mentioned in [23] that the switch or circuit element that controls the on and off of the necklines may be a TRIAC or a set of 2 SCR in antiparallel connection.

The authors in [24] analyze the operation of the ON/OFF control, namely control by integral cycle. Its operation is based on turning a load on and off various occasions in a period of time, such that the necklines are on for a known number of cycles, which may change according to the requirements of temperature.

A technique for tuning PID controllers is explained in [5]. In this work it was chosen to utilize the Matlab ARMAX model to obtain the transfer function of each system, and subsequently tune two effective controllers by means of the same software. The automatic tuner of Matlab performs an iterative analysis to find the best proportional (Kp), integral (Ki) and derivative (Kd) parameters of the PID regulator. The author in [25] mentions that although much more robust new control techniques have been developed, the proportional-integral-derivative (PID) controller is the control strategy mostly used in industrial applications; it is estimated that more than 90 % of the control loops utilize a PID controller, because it is a simple and effective strategy, and it does not require a great theoretical foundation to be utilized in common processes.

2. Methods

The main objective of this work was to develop a prototype capable of heating water from a daily state in the Ecuadorian mountain range, i.e. from approximately 17 °C to 40 °C, and by means of the prototype, provide evidence of the control technique that has the best performance in maintaining the temperature and in energy efficiency.

The prototype is constituted by a coil with a length of 14 meters, constructed based on 4 electric necklines that are connected and disconnected from the commercial electrical network of 220 VAC, as indicated by the control techniques.

The control by integral cycle varies the number of cycles in which the necklines remain open, with the aid of a PID regulator. A cycle refers to a complete period of the sinusoidal wave of the commercial electrical network.

On the other hand, the control by phase angle varies the firing angle that activates the necklines. If the period of the sinusoidal wave is 16.66 ms, each semi-cycle lasts 8.33 ms, and thus the firing angle may vary between 0 and 8.33 ms to turn on and off the necklines, according to the temperature requirements.

2.1. Power of the necklines

The power is dimensioned considering a flow of 4 liters per minute and a pipe with a 3/8 inches' diameter. The required area of the pipe is given by

$$A = \frac{\pi}{4} \times \theta^2 \tag{1}$$

The velocity of the water for the aforementioned flow is determined as is

$$v = \frac{Q}{A} \tag{2}$$

If the objective is to heat 4 liters of water each minute, it is determined that each liter of water should remain exposed to the heater for 15 seconds, and thus the length of the heating pipe is given as

$$L = v \times t \tag{3}$$

It is concluded from the calculations, that it is required a heating coil of at least 14 m long. Then, the volume of water inside the coil is calculated as

$$V = A \times L \tag{4}$$

The next step is to determine the heat that needs to be transmitted, which is given by

$$Q = m \times c \times \Delta T \tag{5}$$

Where:

Q is the heat, m is the mass of the substance, c is the specific heat of the water, and ΔT is the variation of the temperature.

Then, the mass of water contained in the coil is calculated with the desired variation of the temperature, the volume of water in the coil and density of the water. AT last, the required power for the necklines is obtained as

$$P = \frac{Q}{t} \tag{6}$$

It is concluded that the required minimum power is 6500 watts.

2.2. Configuration of the flow sensor

The flow sensor is configured, determining the number of pulses generated by this element when a liter of water passes through it.

The flow is determined counting the number of pulses generated by the sensor in a second by means of an interruption, as shown in the flow diagram of Figure 2.

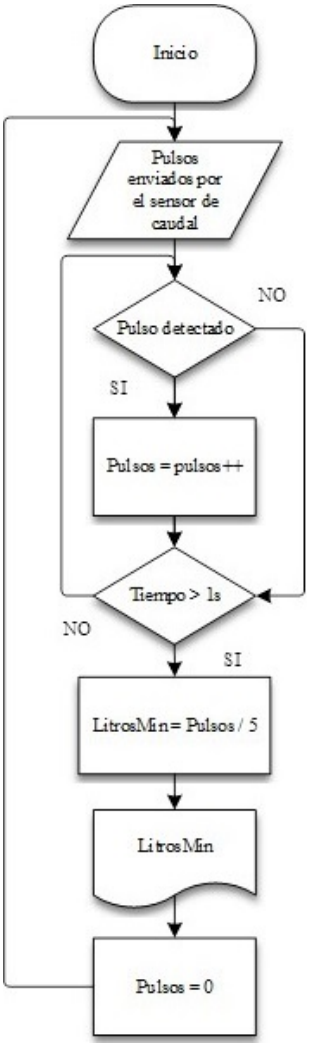

Figure 2. Calibration of the flow sensor.

2.3. Configuration of the temperature sensor

The temperature is determined by means of a thermistor, whose specific characteristic is given by

$$\beta = \frac{ln\left(\frac{RT1}{RT2}\right)}{\frac{1}{T1} - \frac{1}{T2}} \tag{7}$$

where T1 is the temperature given in Kelvin degrees, β is a parameter of the sensor, RT1 is the resistance of the thermistor, RT2 is the reference resistance of the thermistor and T2 is the reference temperature of the thermistor.

To calculate the β parameter, it is necessary to have resistance values at two different temperatures of the thermistor, and those values should be simply substituted in equation (7). A voltage divisor that indicates the variation of temperature is used to acquire the signal of the thermistor, but without linearizing the sensor to keep a more reliable reading.

Further the programming is done, to enable applying the values that determine the real temperature, as can be seen in the flow diagram of Figure 3.

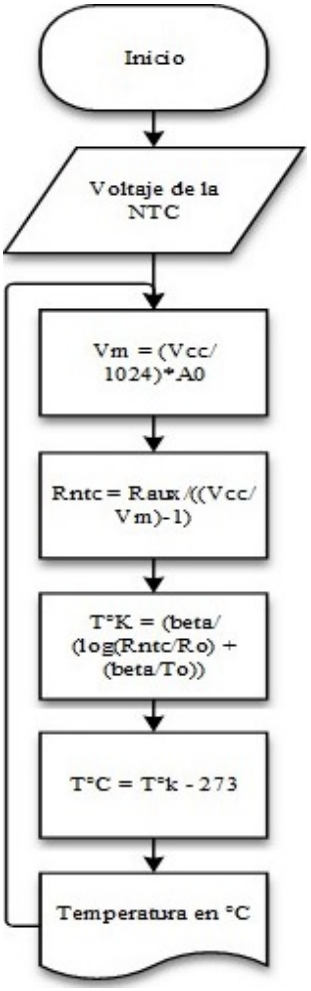

Figure 3. Reading of the temperature sensor.

2.4. Programming of the ON/OFF control

The ON/OFF control is initialized with an interruption, generated by a pulse sent by a circuit that detects the zero crossing of the alternate current wave. This detection initializes a counter, which will be compared with the variable t_{on} that acts as the set-point of the

system, and is controlled by an external device; this variable may take values in the range from 0 to 600 semi-cycles of the AC wave.

Values in this range were used because there are 120 pulses in one second, and the control is designed for a fixed period of 5 seconds. If the counter is smaller than t_{on}, a new comparison is carried out to verify if there is water circulating in the system. If both comparisons are true, the TRIACS are turned on (two per phase), otherwise the TRIACS are deactivated. At last, if the counter is greater than 600 it is reinitialized, thus starting a new cycle.

The information generated, such as the real temperature and the value of set-point, are sent through the serial port to a software designed in Matlab, to obtain information to model the system and to analyze the operation.

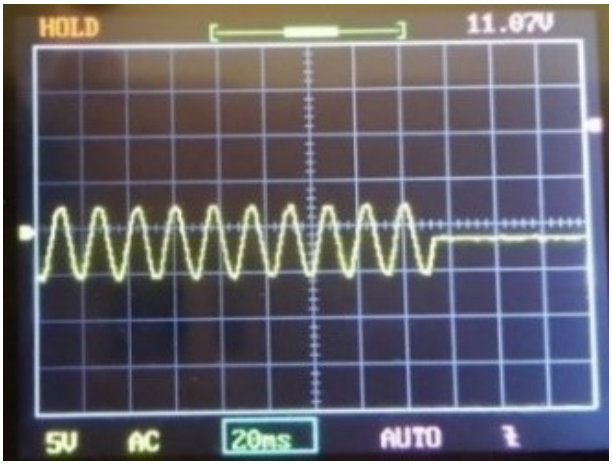

Figure 4. ON/OFF control signal.

2.5. Programming of the direct phase control

In the programming of the direct phase control, a counter is initialized once the pulse generated by the zero cross circuit is detected. This counter will be compared with a variable Set Point, which is similarly controlled by an external device that takes values in the range from 0 to 180. Considering that a semi-cycle of the alternating current wave last 8.33 milliseconds, a Set Point of 0 represents a delay time of 0 ms for the firing, while a Set-Point of 180 represents a delay time of 8.33 ms.

Since the timer of the microprocessor was defined at a frequency of 46.28 microseconds, this should be multiplied by values from 0 to 180 to have the counter of the timer in the range from 0 to 8.33 milliseconds, respectively.

If the counter is greater than the Set Point, a new comparison is carried out to verify if there is circulation of water in the system. If both comparisons are true, the TRIACS are turned on and thus the necklines; otherwise, they are deactivated.

At last, once the TRIACS have been activated, the counter is reinitialized waiting to be activated by a new interruption.

3. Experimental results

3.1. Test of the operation of the ON/OFF control

Once the ON/OFF controller was put into operation, its normal functioning was verified by means of an oscilloscope. Figure 4 shows the waveform of how the necklines are turned on and off, during a certain number of alternating current semi-cycles.

3.1.1. Test of the operation of the direct phase control

After the control by phase angle was programmed, its correct operation was verified observing the form of the voltage wave across the load with the aid of an oscilloscope. It can be seen in Figure 5, that the alternating current wave is varying its firing angle.

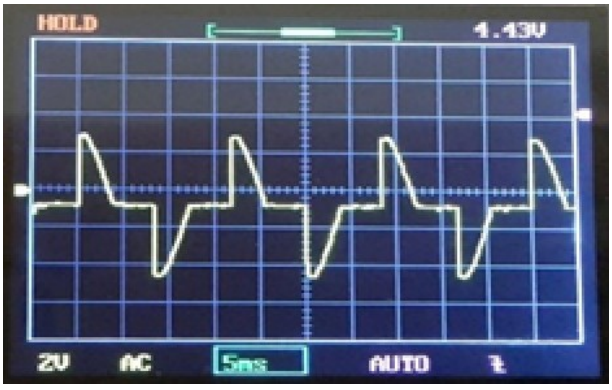

Figure 5. Wave form of the control by phase angle.

3.2. PID and ON/OFF control

3.2.1. Data collection

Once the communication port and the bounds in the Matlab software are configured, data of real temperature of the system and values of set-point are collected during 17 minutes and 33 seconds, thus obtaining a total of 30111 data points.

Once the data sampling is finalized for different values of Set Point, the plot shown in Figure 6 was obtained.

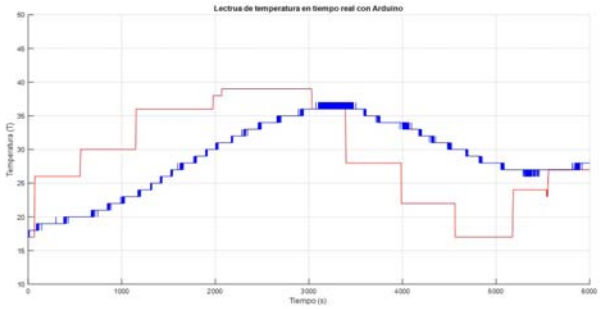

Figure 6. Real-time reading of temperature (ON/OFF).

3.2.2. Tuning of the PID control

With the data collected, the transfer function was obtained, corresponding to the system with ON/OFF control.

$$Ft = \frac{0.0185s + 2.389e^{-8}}{s^2 + 0.0003364s + 2.087e^{-8}} \tag{8}$$

Using the PID Tuner tuning tool provided by Matlab, the response shown in Figure 7 was obtained corresponding to a steady-state with an excessively long stabilization time; this situation was confirmed in the physical prototype.

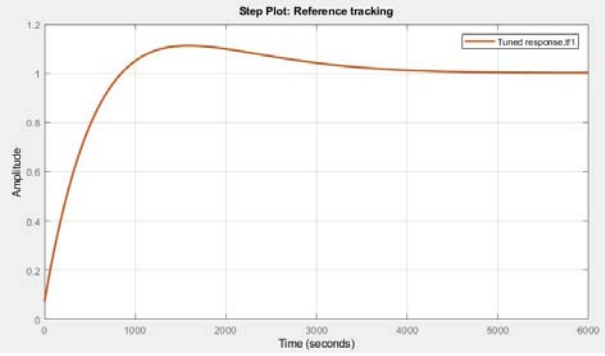

Figure 7. Temperature response for ON/OFF control with PID.

Once the necessary adjustments in the PID controller are carried out, the following PID constant parameters were obtained

$$\begin{aligned} K_p &= 13,534 \\ K_i &= 0,0126 \\ K_d &= 498,9476 \end{aligned} \tag{9}$$

3.3. PID and direct phase control

3.3.1. Data collection

The data were sent in the same manner than the utilized for the ON/OFF control, and the time of data collection was 17 minutes and 47 seconds, for a total of 30523 data obtained.

Once the collection of information was finalized, the plot shown in Figure 8 and the transfer function eres obtained.

$$Ft = \frac{0.00016s + 4.58e^{-7}}{s^2 + 0.002929s + 3.62e^{-7}} \tag{10}$$

The transfer functions corresponding to both control systems are different, due to the method utilized to transmit the temperature of the water.

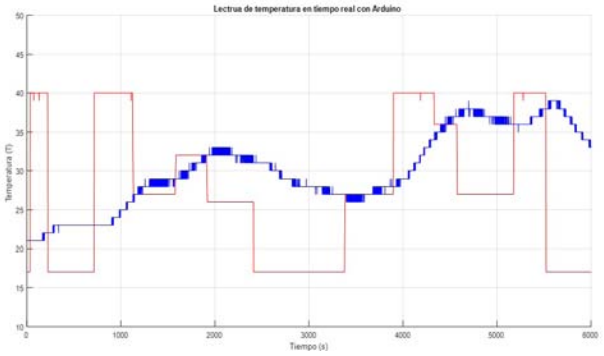

Figure 8. Real-time reading of temperature (direct phase).

3.3.2. Tuning of the PID controller

The tuning of the PID controller is carried out in a manner similar to the one utilized for the ON/OFF control, thus obtaining the plot shown in Figure 9 that represents the behavior of the system when this controller is applied.

After the speed of response and the robustness of the controller have been configured, the parameters of the PID regulator were obtained as

$$\begin{aligned} K_p &= 15,8519 \\ K_i &= 0,0126 \\ K_d &= 498,9476 \end{aligned} \tag{11}$$

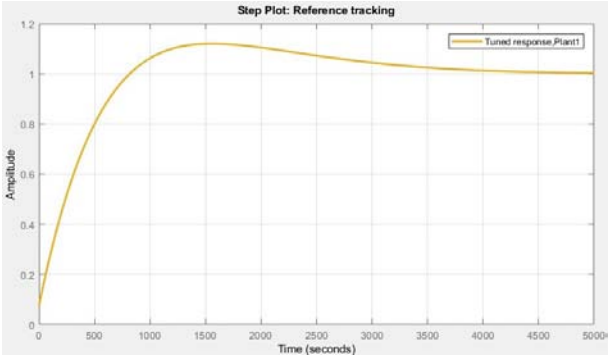

Figure 9. Temperature response for the direct phase control with PID.

3.4. Tests of the operation of the controllers with the implemented PID

3.4.1. Tests of the operation of the ON/OFF control with the implemented PID

Figure 10 shows the temperature response of the system with the implemented PID, where it can be observed that the temperature stabilizes at the set-point (red line) with an error smaller than one degree Centigrade; in addition, it can be seen that the stabilization time is around 500 seconds.

Figure 10. Operation of the ON/OFF control with PID.

3.4.2. Tests of the operation of the control by phase angle with the implemented PID

Figure 11 represents the operation of the control by phase angle, once the PID controller has been implemented. It can be seen that the temperature remains stable after 1000 seconds.

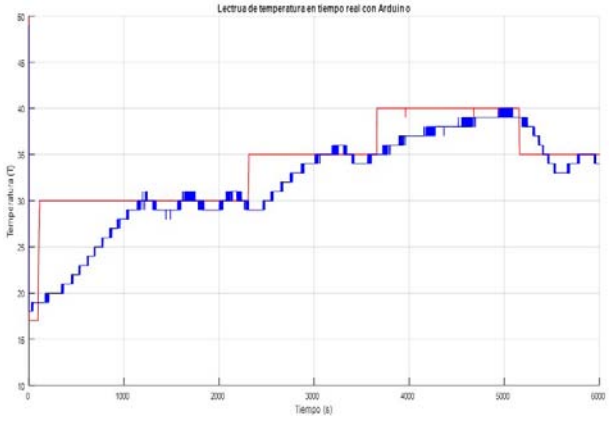

Figure 11. Operation of the direct phase control with PID.

3.5. Comparison of the controllers

3.5.1. Error elimination comparison between the direct phase control and ON/OFF control, after the PID has been implemented

Based on the data obtained after more than 17 minutes of testing for each control system, it is concluded that the ON/OFF control stabilizes the water temperature in almost half of the time than the control by phase angle.

As can be observed in Figures 10 and 11 after the temperature is stabilized, the direct phase control maintains the temperature value in a more effective manner than the ON/OFF control, namely, the direct phase control is more robust than the ON/OFF control.

3.5.2. Stability comparison between the direct phase control and ON/OFF control, after the PID has been implemented

Figure 12 shows the real-time water temperature response signal, using the ON/OFF control. It can be appreciated that the control system takes approximately 1000 seconds to heat the water up to 38 ºC (temperature of the test), and once this value has been reached it remains stable for the time of duration of the test, which was 90 minutes, with the exception of a small variation of 2 degrees Centigrade for the last 500 seconds of the test.

Figure 13 shows the real-time water temperature response signal, using the direct phase control. In this case it is observed that the water reaches the set-point of temperature in approximately 1100 seconds, almost two minutes later than the ON/OFF control, and it is observed that is has a variation of +/-1 degree Centigrade every 10 seconds. This may be due to a bad tuning of the PID regulator or to the slowness of the necklines in heating the water.

From this test it may concluded that, although the temperature responses are very similar regarding stability, robustness and stabilization times, the ON/OFF is more efficient.

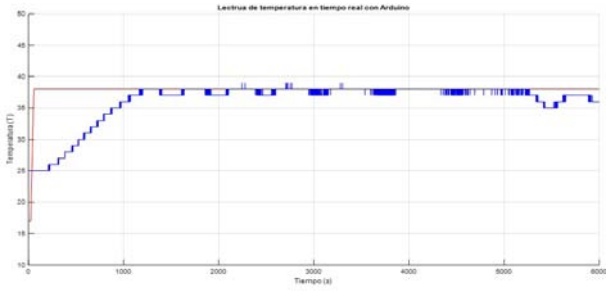

Figure 12. Stability test of temperature for the ON/OFF control with PID.

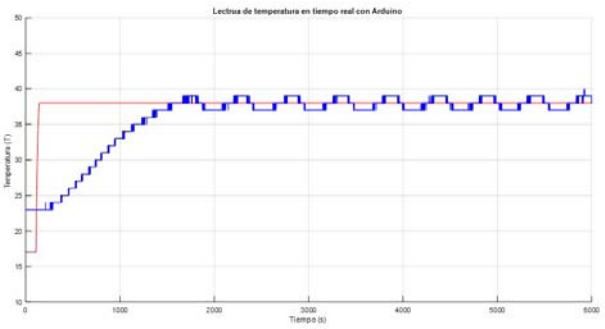

Figure 13. Stability test of temperature for the control by phase angle with PID.

3.6. Utilization cost of the control by phase angle, ON/OFF control, electric shower and gas heater

In the stability tests, each control system was utilized for 90 minutes. The electric consumption of each controller was measured considering such time, and it was observed that the ON/OFF control consumed 5.45 kWh, while the control by phase angle consumed 2.93 kWh. These measurements were directly obtained from an energy meter.

Taking into account that 5 persons consume 195 liters of water daily, and that the prototype has the capacity of heating 240 liters in one hour, the costs were calculated considering the aforementioned consumption for 22 days per month, which was estimated as the average water usage for personal hygiene activities.

With these precedents, an approximate cost of 8.66$ was calculated when utilizing the ON/OFF controller, and 4.97$ for the direct phase control.

The same projection was conducted for evaluating the consumption of the electric shower. A consumption of 8.98$ was determined considering a 4500 watts' shower, while heating the same amount of water with a gas heater will require about two Ecuadorian commercial cylinders, which represents a projected consumption of 4.59$ of GLP.

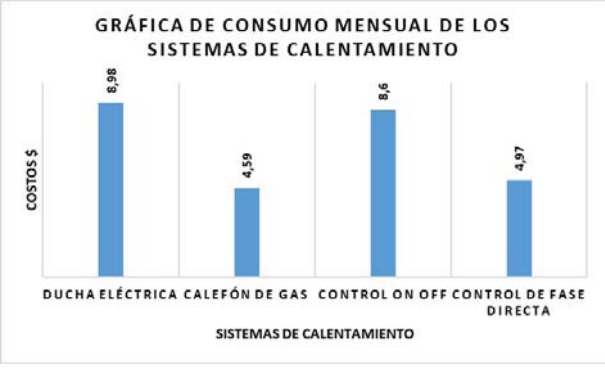

Figure 14. Monthly consumption of the heating systems.

Revising the utilization costs of the electric shower, the gas heater and the ON/OFF control, it is observed that the latter consumes 38 cents less than the electric shower, but 4.01$ more than the gas heater.

On the other hand, the utilization of an electric heater with control by phase angle consumes 4$ less than the electric shower, 3.63$ less than the heater with ON/OFF control and only 38 cents more that the GLP heater.

4. Conclusions

With the implementation of the water heating system, and after conducting tests of operation of such system, it was found that four necklines of 1650 watts each and a 14 meters long coil built with a copper pipe of 3/8 inches' diameter, were capable of increasing the temperature of 4 liters per minute of water from 17 to 40 °C, as was theoretically described in the calculation of the power of the heating resistances.

The prototype operates with a two-phase voltage of 220 VAV, with each phase of 120 VA feeding two necklines in parallel by means of two TRACS. Considering the power of the necklines, it can be said that each power element should withstand a current of at least 14.77 A. Once the tests of operation were carried out, it is concluded that the electric and electronic elements of the prototype efficiently withstand this value of current, and they can operate without any risk.

By means of the tests of operation of the temperature controllers, it could be appreciated that the ON/OFF control has a better response regarding operation than the direct phase controller, namely, the ON/OFF control has a lesser stabilization time and better steady-state performance.

From an analysis of costs, it was found that the direct phase controller has a consumption of 2.93 kWh at maximum temperature, and the ON/OFF controller consumes 5.45 kWh at the same condition. In other words, from the energy viewpoint the direct phase control is more advantageous than the ON/OFF control.

Based on an evaluation of the benefits of each controller, it is concluded that although the ON/OFF controller exhibits a better response in operation, the enormous saving of the direct phase control tilts the balance to its implementation in future works. It is also concluded that it is necessary to test more control techniques, such that the best model regarding response in operation and costs is found. It is also suggested to conduct a comparative analysis, to find the effect of the different control techniques on the electrical distribution network.

References

[1] República del Ecuador. (2015) Ley Orgánica de Régimen Tributario Interno (LORTI). Registro Oficial Suplemento 463 de 17 de noviembre de 2004. [Online]. Available: http://bit.ly/2X40v2B

[2] N. Yamamoto, H. Yamaguchi, T. Nagano, M. Higashiuchi, and T. Nanbu, "Gas water heater," United States Patent US D483,451 S, 2003. [Online]. Available: http://bit.ly/2X0UKNY

[3] O. Tsutsui, S. Murakami, H. Kuwahara, and S. Yasunaga, "Instantaneous gas water heater," United States Patent 4,501,261, 1985. [Online]. Available: http://bit.ly/2FGK8yj

[4] T. W. Clifford, "Gas water heater and method of operation," United States Patent US 6,880,493 B2, 2005. [Online]. Available: http://bit.ly/2Yj5bOk

[5] J. H. Brandt, R. T. Meyer, and B. N. Plank, "Control system for a water heater," U.S. Patent 5,797,358, 1998. [Online]. Available: http://bit.ly/2Fvj192

[6] C. Samaniego-Ojeda, O. H. A. Hernández, and J. M. Correa, "Emisiones provocadas por combustión de GLP a partir de calefones en la ciudad de Loja y su posible relación con enfermedades respiratorias agudas (ERA's)," *CEDAMAZ*, vol. 6, no. 1, pp. 60–67, 2016. [Online]. Available: http://bit.ly/2Ybqvp5

[7] M. Linares, "Contaminación intradomiciliaria," *Medwave*, vol. 9, no. 1, p. e3697, 2009. [Online]. Available: http://doi.org/10.5867/medwave.2009.01.3697

[8] E. N. Correa, A. Herrerías, A. Albornoz, G. Villarroel, and A. P. Arena, "Comparación económico-ambiental del uso de energía solar respecto al gas natural para agua caliente sanitaria en la ciudad de Mendoza," *Avances en Energías Renovables y Medio Ambiente*, vol. 8, no. 1, pp. 01.105–01–110, 2004. [Online]. Available: http://bit.ly/2FreMvq

[9] J. Pesántez, "Reducción de costos en el calentamiento de agua en Ecuador, a través de la sustitución de calefones con uso de glp por sistemas de energía solar térmica," *Revista Científica y Tecnológica UPSE*, vol. 1, no. 1, 2012. [Online]. Available: https://doi.org/10.26423/rctu.v1i1.2

[10] E. A. Meléndez Aguilera and H. Soto Nilo, *Análisis comparativo, energético y ambiental, en calefones de uso doméstico que operan con gas licuado de petróleo y gas natural.* Universidad de Chile, 2007. [Online]. Available: http://bit.ly/2N9UY63

[11] Agencia Estatal Boletín Oficial del Estado. (2019) Real decreto 244/2019, de 5 de abril, por el que se regulan las condiciones administrativas, técnicas y económicas del autoconsumo de energía eléctrica. Ministerio de la Presidencia, Relaciones con las Cortes e Igualdad, España. [Online]. Available: http://bit.ly/31QYG7Q

[12] Y. Valdivia Nodal, Y. A. DÃaz Torres, and M. Lapido RodrÃguez, "Alternativas de producción de agua caliente sanitaria en instalaciones hoteleras con climatización centralizada," *Revista Universidad y Sociedad*, vol. 7, pp. 88–94, 12 2015. [Online]. Available: http://bit.ly/2Y9MRrd

[13] B. Supriyo, Dadi, S. Warjono, A. Wisaksono, S. W. P. Astuti, and K. Utomo, "Pid based air heater controller implemented with matlab/simulink and arduino uno," *2018 5th International Conference on Information Technology, Computer, and Electrical Engineering (ICITACEE)*, pp. 28–32, 2018. [Online]. Available: https://doi.org/10.1109/icitacee.2018.8576955

[14] S. Lanfredi, R. L. Grosso, A. C. Antunes, S. R. M. Antunes, and M. A. L. Nobre, "Comportamento eléctrico a alta temperatura de termistor cerámico alfa-Fe_2O_3 com coeficiente de temperatura negativo," *Cerâmica*, vol. 54, pp. 443–450, 12 2008. [Online]. Available: http://bit.ly/2J82hpx

[15] M. H. Rashid, *Electrónica de potencia: circuitos, dispositivos y aplicaciones.* Pearson Education, 2004. [Online]. Available: http://bit.ly/2Kzz75A

[16] M. D. Khairunnas, E. Ariyanto, and S. Prabowo, "Design and implementation of smart bath water heater using arduino," in *2018 6th International Conference on Information and Communication Technology (ICoICT)*, May 2018, pp. 184–188. [Online]. Available: https://doi.org/10.1109/ICoICT.2018.8528772

[17] Y. A. Badamasi, "The working principle of an arduino," in *2014 11th International Conference on Electronics, Computer and Computation (ICECCO)*, Sep. 2014, pp. 1–4. [Online]. Available: https://doi.org/10.1109/ICECCO.2014.6997578

[18] A. M. Vega E., F. Santamaría P., and E. Rivas T., "Internet de los objetos empleando arduino para la gestión eléctrica domiciliaria," *Revista EAN*, pp. 23–41, 07 2014. [Online]. Available: http://bit.ly/2RB2sxw

[19] A. L. Silva, M. Varanis, A. G. Mereles, C. Oliveira, and J. M. Balthazar, "A study of strain and deformation measurement using the Arduino microcontroller and strain gauges devices," *Revista Brasileira de Ensino de Física*, vol. 41,

no. 3, pp. e20 180 206–1–e20 180 206–7, 00 2019. [Online]. Available: http://dx.doi.org/10.1590/1806-9126-RBEF-2018-0206

[20] A. A. Custodio Ruiz and R. Torres, "Conexión directa de múltiples sensores a microcontroladores sin utilizar convertidor analógico digital," *Universidad, Ciencia y Tecnología*, vol. 10, no. 39, pp. 147–151, 07 2006. [Online]. Available: http://bit.ly/2J2ig8n

[21] P. H. Guadagnini and V. E. Barlette, "Um termômetro eletrónico de leitura direta com termistor," *Revista Brasileira de Ensino de Física*, vol. 27, no. 3, pp. 369–375, 09 2005. [Online]. Available: http://dx.doi.org/10.1590/S1806-11172005000300011

[22] H. B. Prevez, H. M. García, L. V. Seisdedos, F. C. M. n, and L. A. E. García, "Comparación entre rectificador trifásico con conmutación simétrica y convertidor ac/ac para la mejora del factor de potencia en microcentrales hidroeléctricas," *Revista Iberoamericana de Automática e Informática industrial*, vol. 15, no. 1, pp. 101–111, 2017. [Online]. Available: https://doi.org/10.4995/riai.2017.8816

[23] C. Scianna, "Dimming circuit for led lighting device with means for holding triac in conduction," Unioted States Patent WO 2005/115 058 A1, 2005. [Online]. Available: http://bit.ly/2X0f3Lx

[24] A. Dytch, M. Lane, A. Keatley, and W. Wright, "Microprocessor controlled through-flow electric water heater," U.S. Patent 4,638,147, 1987.

[25] L. F. Lozano-Valencia, L. F. Rodríguez-García, and D. Giraldo-Buitrago, "Diseño, Implementación y Validación de un Controlador PID Autosintonizado," *TecnoLógicas*, no. 28, pp. 33–53, 06 2012. [Online]. Available: http://bit.ly/2WXkb3f

Scientific Paper / Artículo Científico

UNIVERSIDAD POLITÉCNICA SALESIANA ECUADOR
INGENIUS
Revista de Ciencia y Tecnología
https://doi.org/10.17163/ings.n22.2019.10
pISSN: 1390-650X / eISSN: 1390-860X

Mechanical Flexural Characterization of Composite Materials with Photopolymer Matrix Reinforced with Abaca and Cabuya Fibers Using 3D Printing

Caracterización mecánica a flexión de materiales compuestos con matriz fotopolimérica reforzados con fibras de abacá y cabuya mediante impresión 3D

Edilberto Antonio Llanes-Cedeño[1,*], Diana Peralta-Zurita[1], Marco Pucha-Tambo[1], Juan Carlos Rocha-Hoyos[1,*]

Abstract

Composite materials and 3D printing currently constitute an alternative for manufacturing automotive parts. The objective of the present research was to characterize a material composed by a photopolymer resin matrix reinforced with natural abaca and cabuya fibers and made by 3D printing, for its application in auto parts manufacturing. The directional grid of the air conditioning duct of an automotive is selected as the subject of study, and its mechanical characteristics are compared by means of experimental analysis and computational simulation. A composite volumetric reinforcement fiber with a fraction of 20% in the two types of fibers, was proposed for manufacturing the test specimens, and the bending test was carried out according to the ASTM 790 standard.

Resumen

Los materiales compuestos y la fabricación por impresión 3D son en la actualidad una alternativa en la fabricación de autopartes. La presente investigación tuvo como objetivo caracterizar el material compuesto con matriz de resina fotopolimérica reforzada con fibras naturales de abacá y cabuya fabricados por impresión 3D, para su aplicación en la fabricación de autopartes. Como objeto de estudio se seleccionó la rejilla direccional del ducto de aire acondicionado de un automotor; mediante análisis experimental y simulación computacional se compararon sus características mecánicas. Para la fabricación de las probetas de ensayos se propuso una fracción volumétrica de fibra refuerzo del composite del 20 % en los dos tipos de fibras, el ensayo a flexión se procedió según la norma ASTM 790.

[1,*]Grupo de Investigación en Innovación en el diseño de procesos y productos en el Ecuador, Facultad de Arquitectura e Ingeniería, Carrera de Mecánica, Universidad Internacional SEK, Quito – Ecuador. Autor para correspondencia ✉: antonio.llanes@uisek.edu.ec, carlos.rocha@uisek.edu.ec.
http://orcid.org/0000-0001-6739-7661, http://orcid.org/0000-0002-9523-0743,
https://orcid.org/0000-0003-2054-370X, http://orcid.org/0000-0003-0660-7199.

Received: 14-05-2019, accepted after review: 25-06-2019

Suggested citation: Llanes-Cedeño, E. A.; Peralta-Zurita, D.; Pucha-Tambo, M. and Rocha-Hoyos, J. C. (2019). «Mechanical Flexural Characterization of Composite Materials with Photopolymer Matrix Reinforced with Abaca and Cabuya Fibers Using 3D Printing». Ingenius. N.°22, (july-december). pp. 100-112. doi: https://doi.org/10.17163/ings.n22.2019.10.

As a result of the mechanical characterization of the manufactured materials, it was obtained that the maximum bending stress of the compounds reinforced with abaca (77.53 MPa) and cabuya (83.26 MPa) decreased with respect to the matrix material (92.77 MPa), while the modulus of elasticity to bending of the compounds reinforced with abaca (2211,33 MPa) and cabuya (1806,03 MPa) increased with respect to the matrix material (1689,64 MPa). This indicates an increase in the rigidity of the characterized materials, making possible the substitution of the matrix material.

Keywords: composite materials, 3D printing, abaca fibers, cabuya fibers, photopolymer matrix.

Como resultado de la caracterización mecánica de los materiales fabricados se obtuvo que el esfuerzo máximo a flexión de los compuestos reforzados con abacá (77,53 MPa) y cabuya (83,26 MPa) disminuyeron con respecto al material matriz (92,77 MPa). El módulo de elasticidad a la flexión que presentaron compuestos reforzados con abacá (2211,33 MPa) y cabuya (1806,03 MPa) aumentaron con respecto al material matriz (1689,64 MPa), lo que se traduce en un aumento de la rigidez de los materiales caracterizados, haciendo posible la sustitución del material matriz.

Palabras clave: materiales compuestos, impresión 3D, fibras de abacá, fibras de cabuya, matriz fotopolimérica.

1. Introduction

Natural fibers are used as reinforcement of polymers in different places worldwide for manufacturing auto parts, due to their features of light weight, low cost, good mechanical properties, easy recycling which reduces waste and, since the vehicle becomes lighter, they enable reducing contaminant emissions and saving fuel, thus contributing to the worldwide environmental policies [1, 2].

Faruk *et al.* [3] state that in recent years the automotive industry has focused in the elaboration and utilization of composite materials, integrating natural fibers as a reinforcement element, for manufacturing external and internal parts of the vehicle, contributing to the environment by adequately utilizing the natural fibers with the best mechanical properties. In 2015 Ahmad *et al.* [4] analyzed the use and application of natural fibers such as jute, bamboo and abaca, as reinforcement for composite materials in the manufacturing of auto parts, from the analysis of its chemical, physical and mechanical properties. In addition, Roshdestwensky *et al.* [5] remark that the use of these new materials is consolidating in the aerospace and naval areas, favoring its application in the manufacturing sector in particular the automotive, employing natural fibers as replacement of synthetic fibers present in the vehicle, reducing the weight and cost of the automobile.

Guo and Leu [6] studied composite polymers reinforced with natural fibers in industrial applications, evaluating the viability of fibers of data palms for the automotive industry, obtaining an improvement in the door panels of a Class E Mercedes-Benz regarding the mechanical properties of the original material; this was achieved utilizing an epoxy resin as matrix material and embedding fibers of linen/sisal, reducing the original weight in 20 %.

Li and Huang [7] researched about the application of the fast prototyping technology in the manufacturing of automotive parts, applying different methods of 3D printing technology, such as stereolithography (SLA), fused deposition modeling (FDM) and selective laser sintering (SLS). The manufacturing times were reduced, even for elements whose development is geometrically complex; this enabled manufacturing companies to reduce production times and costs, obtaining significant economical earnings in series production.

Berchon and Luyt [8] stated that the 3D printing technology brings benefits, such as: decrease of manufacturing times, obtaining geometries of elements of great complexity, reduction of the production chains or stations, saving in the material utilized and decrease of residues of the manufacturing process, compared with conventional production methods.

Bonada, Muguruza and Ramis [9] stated that additive manufacturing may generate 3D parts or elements, adding material layer by layer to manufacture complex geometries without utilizing specific accessories or tools. The PolyJet technology is a 3D printing method that offers a superficial finish of better quality compared to other methods of additive manufacturing, with a great variety of materials for different industries and requested applications [10].

Callister [11] mentioned that the final properties of the composite materials depend on the characteristics of the two main components: matrix, interface and reinforcement, taking into account in the latter the shape, size, distribution and orientation; besides, suggests that one of the main combinations of composite materials are those reinforced with fibers that exhibit excellent mechanical properties: resistance to the traction and elevated specific modulus, from low density base elements both in the matrix and in the fiber. In addition, the orientation, quantity and distribution of the composite material, directly influence the final mechanical properties of the composite [12], as shown in Figure 1.

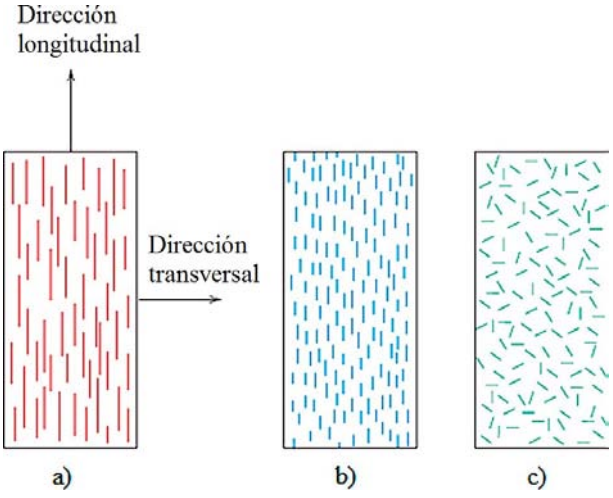

Figura 1. Possible orientations of the reinforcement in a composite material: a) continuous and aligned fibers, discontinuous and aligned fibers, and c) randomly oriented discontinuous fibers; taken from [11].

Thanks to the advantage over traditional manufacturing techniques, the samples manufactured using 3D printing exhibit better mechanical properties than fused models, thanks to the correct matrix-fiber interface adhesion of the printed samples [13].

In current automotive vehicles, manually regulated grilles are employed to direct the flow of air conditioning; due to this, breaks are produced. Replacing them by originals is occasionally not feasible, thus the use of composite materials and manufacturing by 3D printing results an attractive option.

From what has been previously explained, the objective of this study is to characterize the composite material with photopolymer resin matrix reinforced

with abaca and cabuya natural fibers and made using 3d printing, by means of computational simulation and mechanical tests, for its application in manufacturing of auto parts.

2. Materials and methods

The process of obtaining composite materials by means of additive manufacturing technologies, to improve mechanical properties according to the abaca and cabuya reinforcement fibers with a 20 % volumetric proportion, is shown in Figure 2.

The constitutive materials of the composite were two types of natural fibers (abaca and cabuya as reinforcement elements), and a photopolymer element as the matrix for manufacturing the composite.

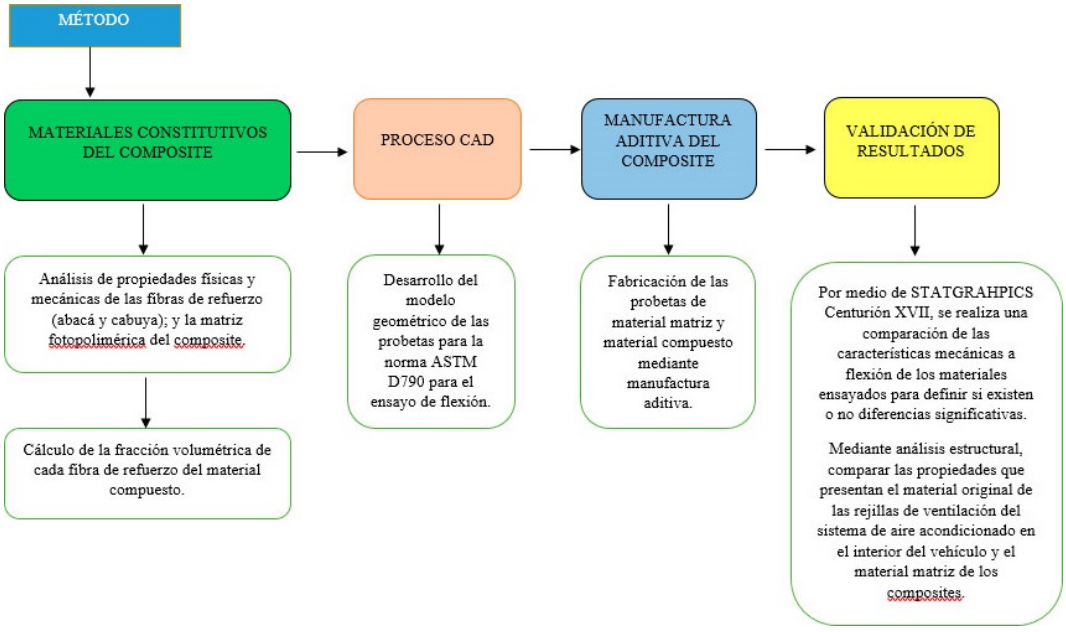

Figura 2. Steps for obtaining and validating the composite material.

2.1. Calculation of the fiber density of the abaca and the cabuya

The procedure proposed by [13] is employed, which determines the density of the pineapple fiber finding the density of the resin by means of the construction of test specimens, and then the construction of test specimens with composite material. The density of the fiber is determined as the difference.

2.2. Photopolymer matrix

The element used as organic/polymer matrix of the composite material, is a photopolymer utilized in additive manufacturing with PolyJet technology VeroClear RGO8 10) whose properties are shown in Table 1.

Tabla 1. Physical and mechanical properties of the matrix material of the composite

Material	Density (g/cm^3)	Resistance to traction (MPa)	Resistance to bending (MPa)	Young Module (GPa)
Photopolymer matrix	1.181	50-65	75-110	2-3

The rule of the mixtures for composites reinforced with fibers, is utilized for calculating the volumetric fraction of the reinforcement fiber (cabuya and abaca, respectively).

2.3. Rule of the mixtures for composites reinforced with fibers

«The rule of the mixtures will always give the density of the composite reinforced with fibers» [14,15], which shows the mathematical expression to obtain the density of the composite material, relating the volumetric fractions and densities of the matrix and reinforcement fiber as observed in Equation 1, where ρ_c = density of the composite material, f_m = volumetric fraction of the matrix, ρ_m = density of the matrix, f_f = volumetric fraction of the fiber and ρ_f = density of the fiber

$$\rho_c = f_m \cdot \rho_m + f_f \cdot \rho_f \tag{1}$$

considering

$$f_m = 1 - f_f \tag{2}$$

For the analysis, it is proposed a 20 % volumetric fraction of the reinforcement fiber in the composite of the two types of fibers, namely abaca and cabuya, from previous studies which reference the best results for a volumetric fraction of fiber between 20 and 23 %.

2.4. Development of the geometrical model of the test specimens

For the geometrical development of the test specimens of the composite material, the ASTM 790 standard for the bending test was applied with dimensions 153.6 × 13 × 4 mm.

2.5. Additive manufacturing of the test specimens

The additive manufacturing of the test specimens was carried out in a 3D printer, injecting photopolymers on a surface, deposited layer by layer with a 0.1 mm resolution. An ultraviolet treatment between layers is further applied hardening the resin; the printing is paused to place a fiber layer with a volumetric fraction of 20 %, and then the printing is resumed, as shown in Figures 3, 4 and 5.

Figura 3. Additive manufacturing of the bending test specimen with base material.

Figura 4. Additive manufacturing of the bending test specimen with the composite material reinforced with abaca fibers.

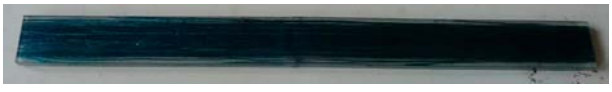

Figura 5. Additive manufacturing of the bending test specimen with the composite material reinforced with cabuya fibers.

2.6. Equipment

1) Universal test machine. The test machine Metrotec, MTE 50 series, with a capacity of 50 kN, was employed to conduct tests for polymeric materials, composite and light metals.
2) 3D Printer. The PolyJet technology, model Objet 30 PRO, which works with various engineering materials and has a net printing capacity of 300 x 200 x 150 mm, was used for additive manufacturing of all test specimens.
3) Stove. Used for drying the fibers. It enables the digital visualization of the temperature.
4) ASPEX Scanning electron microscope. Is employed to obtain micrographs of the transverse sections of the test specimens tested for bending, considering the three configurations carried out in a detection range from 500 nm to 5 mm.

NX 10, which is a powerful engineering simulation tool, was the software employed for the structural simulation of the materials.

The results of the analysis and the graphs were obtained using the statistical software STATGRAPHICS Centurion XV (Trial version 15, StatPoint Inc., USA). A factorial experimental design was utilized, in which the effects of the abaca and cabuya fibers are studied regarding the mechanical properties of the composite materials with photopolymer matrix.

3. Results and discussion

The average density obtained for the abaca fiber was 1.226 g/cm^3 and for the cabuya 0.665 g/cm^3. The results obtained in the characterization of the base material, and of the composite materials reinforced with the two types of fibers, namely abaca and cabuya, are presented in the following.

3.1. Results of the bending test on the matrix material

The additive manufacturing of five test specimens was carried out for the bending test of the matrix material under the ASTM 790 standard, with the purpose of obtaining reference values. Figure 6 shows the test specimens which, as can be seen, were fractured after the test.

Figura 6. Test specimens of the matrix material.

Table 2 shows the values of the bending test carried out on five test specimens of the matrix material of the composite. The average value of the maximum bending stress is 92.77 MPa, with a standard deviation of 9.67 MPa; of the modulus of elasticity secant to bending

is 1689.64 MPa with a standard deviation of 216.59 MPa, and of the deflection is 8.72 mm with a standard deviation of 0.96 mm.

Tabla 2. Results of the bending test on the matrix material

Material	Recount	Average	Standard Deviation
Maximum Force (N)	5	189,33	19,58
Maximum bending stress (MPa)	5	92,77	9,67
Modulus of elasticity secant to bending (MPa)	5	1689,64	216,59
Maximum deformation (%)	5	5,13	0,61
Deflection (mm)	5	8,71	0,96

Note. The bending specimens of the composite matrix material manufactured with 3D printing and PolyJet technology.

3.2. Scanning electron microscopy of the matrix material

Figure 7 shows the micrographs of the transverse section of the photopolymer resin, matrix material of the composite materials.

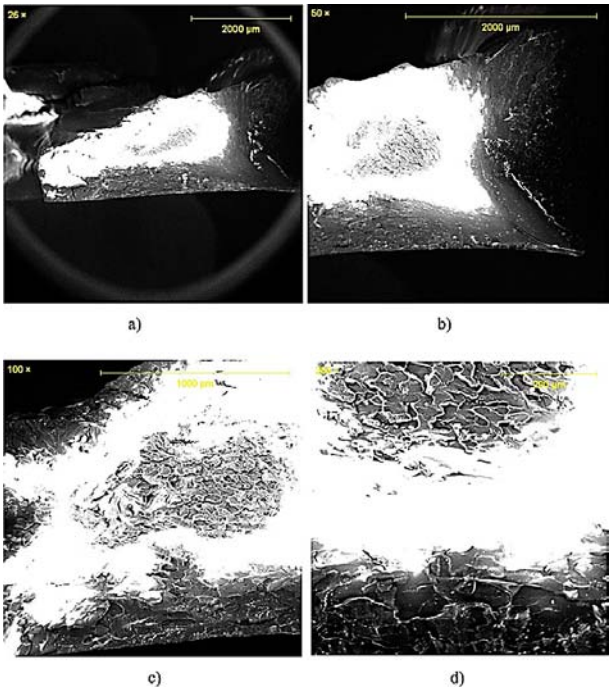

Figura 7. Photopolymer resin of the matrix material of the composite materials: a) 26X, b) 50X, c) 100X and d) 250X.

The micrographs shown were taken at different magnifications to one of the test specimens after the bending test, with the purpose of verifying if the test specimen presents internal cracks between the printed layers. The micrograph taken with a magnification of 250X, enables verifying that the sample tested is homogeneous and does not have internal fissures, thus consolidating the values of mechanical properties of the matrix material obtained after the bending test.

The additive manufacturing of five test specimens of the composite material reinforced with abaca fibers was carried out, for bending tests under the ASTM 790 standard. Figure 8 shows the test specimens after the test, where it can be observed a partial tear of the matrix material in the tested zone.

Figura 8. Test specimens of the composite material reinforced with abaca fibers.

Table 3 shows the results obtained on the bending test, under the ASTM 790 standard, to the composite material reinforced with 20 % of abaca fibers, manufactured by 3D printing and PolyJet technology. The following average values of the material reinforced with abaca fibers were found: maximum bending stress 77.53 MPa, modulus of elasticity secant to bending 2211.33 MPa and deflection 5.60 mm.

Tabla 3. Ensayo de flexión del material compuesto reforzado con fibra de abacá

Material	Recount	Average	Standard deviation
Maximum force (N)	5	153,99	20,73
Maximum bending stress (MPa)	5	77,53	11,88
Modulus of elasticity secant to bending (MPa)	5	2211,33	225,41
Maximum deformation (%)	5	3,25	0,50
Deflection (mm)	5	5,60	0,89

3.3. Scanning electron microscopy of the composite material reinforced with abaca fibers

Figure 9 shows the scanning electron microscopy taken to one of the test specimens tested, in the area of fracture after the bending test.

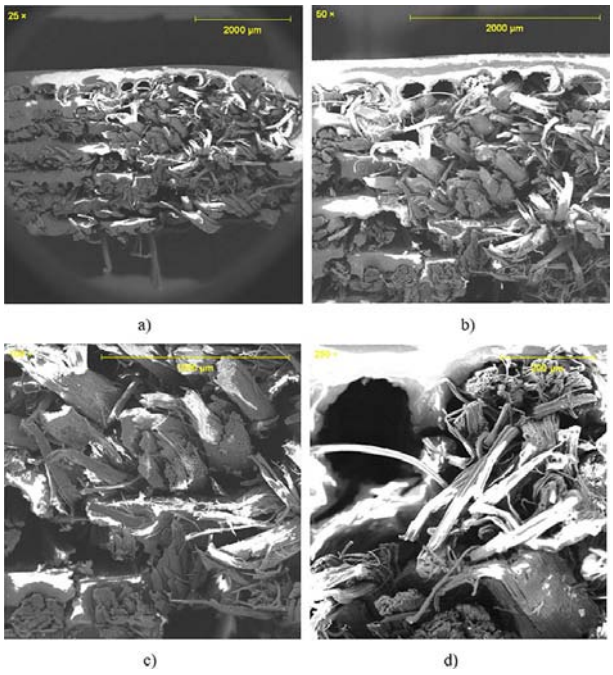

Figura 9. Composite material reinforced with abaca fibers: a) 25X, b) 50X, c) 100X and d) 250X.

The micrographs were taken at different magnifications to one of the test specimens of the composite material after the bending test. The micrograph taken with a magnification of 250X, shows the poor adherence between the reinforcement fibers and the matrix material of photopolymer resin, namely, there is not a good interface in the composite material.

The additive manufacturing of five test specimens of the composite material reinforced with cabuya fibers was carried out, for bending tests under the ASTM 790 standard. Figure 10 shows the test specimens after the test. It can be observed that the test specimens did not present a total tear, only a partial tear of the matrix material in the tested zone.

Table 4 shows the results obtained on the bending test, under the ASTM 790 standard, to the composite material reinforced with 20 % of cabuya fibers. The following average values of the material reinforced with cabuya fibers were obtained: maximum bending stress 83.26 MPa, modulus of elasticity secant to bending 1806.03 MPa and deflection 7.93 mm.

Figura 10. Test specimens of the composite material reinforced with cabuya fibers.

Tabla 4. Bending test of the composite material reinforced with cabuya fibers

Material	Recount	Average	Standard deviation
Maximum force (N)	5	185,86	13,54
Maximum bendign stress (MPa)	5	83,25	6,48
Modulus of elasticity secant to bending (MPa)	5	1806,03	220,52
Maximum deformation (%)	5	4,67	0,74
Deflection (mm)	5	7,93	1,27

Note. The bending test specimens of the composite were manufactured with 3D printing and PolyJet technology.

3.4. Microscopía electrónica de barrido del composite reforzado con fibra de cabuya

En la Figura 11 se muestra una microscopía electrónica de barrido realizada a una de las probetas ensayadas en el área de la fractura posterior al ensayo de flexión.

Figura 11. Composite material reinforced with cabuya fibers. a) 28X, b) 50X, c) 100X and d) 250X.

The micrographs were taken at different magnifications to one of the test specimens of the composite material after the bending test, with the purpose of verifying if there is a good interface between the polymeric matrix and the cabuya natural fiber. The micrograph taken with a magnification of 250X, enables to verify

that there is a poor adherence between the reinforcement fibers and the matrix material of polymeric resin, namely, there is not a good interface in the composite material.

It should be considered that there is no previous study in this field, thus the results given by the scanning electron microscopy that show a deficient adherence between the fibers and the matrix material is a referent for further works.

3.5. Results of the structural simulation of the air conditioning grilles as application

The structural simulation is performed with the aid of the NX 10 software by Siemens, with the purpose of observing the values of nodal displacement and elemental stress presented by both the original material of the air ducts and the matrix material of the composite materials.

1) Polypropylene air conditioning grilles. Figure 12 shows the values of the maximum nodal displacement generated in the air conditioning grilles, with an average value of 0.026 mm.

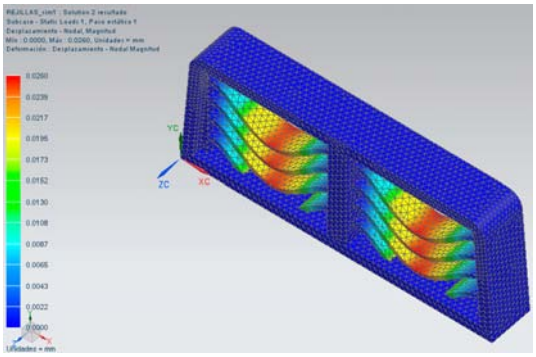

Figura 12. Graph of nodal displacement of the air conditioning grilles.

Figure 13 displays the maximum values of stresses generated on the air conditioning grilles, under the Von Mises failure analysis or criterion, resulting in a maximum stress of 0.204 MPa.

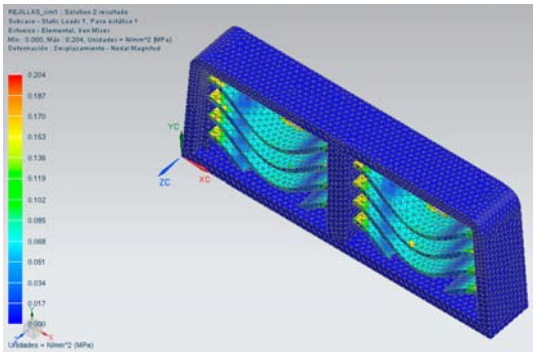

Figura 13. Graph of stresses generated on the air conditioning grilles.

2) Air conditioning grilles of the matrix material of the composites. Figure 14 shows the values corresponding to the maximum nodal displacement generated in the air conditioning grilles, resulting in an average value of 0.048 mm.

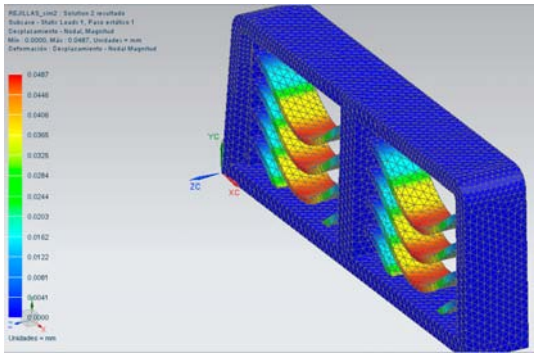

Figura 14. Graph of nodal displacement of the air conditioning grilles.

Figure 15 shows the maximum values of stresses generated on the air conditioning grilles, under the Von Mises failure analysis or criterion, resulting in a maximum stress of 0.21 MPa.

In the two types of structural analysis, an average force of 5 N was applied as load on the element; such value was calculated idealizing a grille as a beam placed on two supports, and placing a mass (0.49 kg) which multiplied by the acceleration of gravity (9,81 m/s2) generates an average value of 5 N.

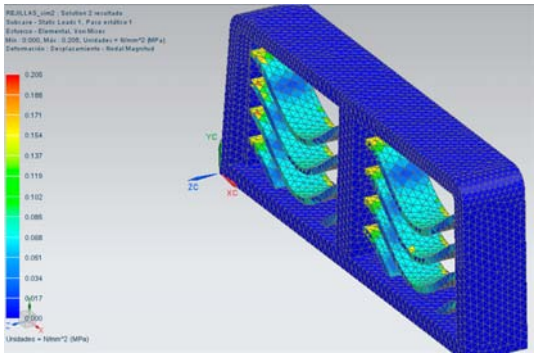

Figura 15. Graph of stresses generated on the air conditioning grilles.

The software Statgraphics Centurion XVII was used for assessing the mechanical properties obtained for the tested composite materials and matrix material. An ANOVA variance analysis and Fisher method of least significant difference (LSD) were applied to discriminate between the means of the studied variables, and perform multiple comparison [16]. Table 5 applies a multiple comparison procedure, to determine which means of maximum bending stress are significantly different than others among the manufactured materials.

Tabla 5. Fisher method of least significant difference (LSD), with 95 % confidence.

Material	Cases	Mean	Homogeneous groups
Matrix material (1)	5	92,77	X
Composite reinforced with cabuya (2)	5	83,25	X
Composite reinforced with abaca (3)	5	77,53	XX

Note. In the analysis each material was identified with a number.

It can be seen that between materials (1) and (2), there are statistically significant differences with a confidence level of 95 %. Material (3) does not possess a significant difference with the other two. This is graphically shown in Figure 16.

Ponton and Guerrero [12] obtained a maximum stress to bending in a composite material with a matrix of polyester reinforced with a 20 % volumetric fraction of longitudinal fiber of abaca, by means of manual stratification, which increased with respect to the matrix material. On the contrary, in this study the obtained value of maximum bending stress, of the composite material reinforced with a 20 % volumetric fraction of longitudinal fiber of abaca manufactured using 3D printing, decreased with respect to the matrix material, even though this decrease was not statistically significant.

In the aforementioned study of the composite material reinforced with fiber of abaca, the fibers were pre-wet with polyester resin diluted with styrene at 10 % v/v and the catalytic system constituted by octoate and cobalt and MEKP in concentrations of 0.5 and 0.75 %, which favored the adhesion of the reinforcement fibers on the matrix of such composite material [12].

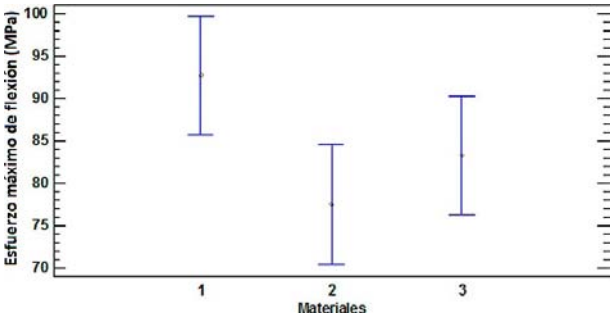

Figura 16. Mean comparison using the LSD test with 95 %.

The study carried out in [15] establishes that the maximum bending stress of a composite material with polyester matrix reinforced with a volumetric fraction of 23 % of longitudinal fiber of cabuya, by means of manual stratification, decreased with respect to the matrix material; this coincides with the results obtained in this study, where the maximum bending stress of the composite material reinforced with a 20 % volumetric fraction of longitudinal fiber of cabuya manufactured using 3D printing, also decreases with respect to the matrix material.

The decrease of this mechanical property of the composite materials with respect to the matrix material, is directly related with a poor interface between the matrix material and the reinforcement fiber, as shown in the scanning electron microscopy.

Table 6 applies a multiple comparison procedure, to determine which means of the modulus of elasticity secant to bending are significantly different among the materials subject of study. It can be seen that materials (1) and (3) show statistically significant differences with a confidence level of 95 %, with respect to material (2).

Figure 17 graphically shows the comparison of the means of the modulus of elasticity secant to bending of the materials subject of study.

Tabla 6. Fisher method of least significant difference (LSD), with 95 % confidence.

Material	Cases	Mean	Homogeneous groups
Matrix materiañ (1)	5	1689,64	X
Composite reinforced with cabuya (3)	5	1806,03	X
Composite reinforced with abaca (2)	5	2211,33	X

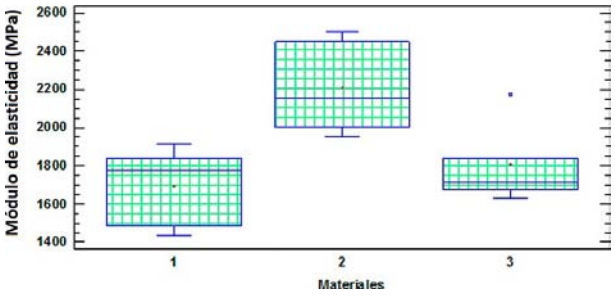

Figura 17. Box and moustache plots for the modulus of elasticity secant to bending.

As it can be seen in Figure 18, the modulus of elasticity secant to bending of the composite materials reinforced with longitudinal fiber of abaca and cabuya, increased with respect to the matrix material of photopolymer resin.

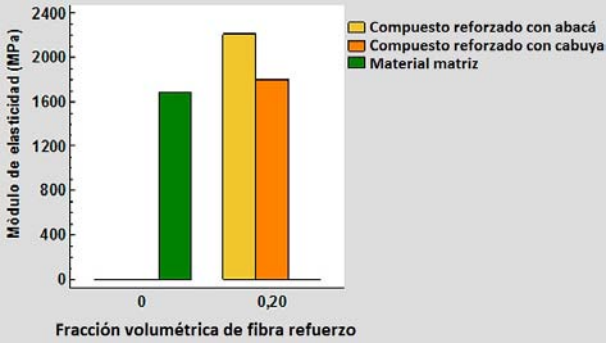

Figura 18. Modulus of elasticity secant to bending of the composite materials depending on the volumetric fraction of reinforcement fiber.

The increase of the modulus of elasticity for the composite material reinforced with longitudinal fiber of abaca was 31 %, while such increase was 7 % for the composite material reinforced with longitudinal fiber of cabuya.

It is important to remark that in the study carried out in [15], the modulus of elasticity of a composite material with biodegradable polymer matrix reinforced with a 20 % volumetric fraction of longitudinal fiber of abaca, by means of molding with manual compression (5570 MPa), increases with respect to the matrix material, which is comparable with the result obtained in this study of the modulus of elasticity of the composite material reinforced with a 20 % volumetric fraction of longitudinal fiber of abaca manufactured using 3D printing (2211.33 MPa), which similarly increased with respect to the matrix material. In addition, in the study carried out in [17] the modulus of elasticity increased with respect to the matrix material analyzed in that study.

Figure 19 shows, in a box and moustache plot, the comparison of the means of the deflection by means of the Fisher method of least significant difference (LSD), with 95 % confidence.

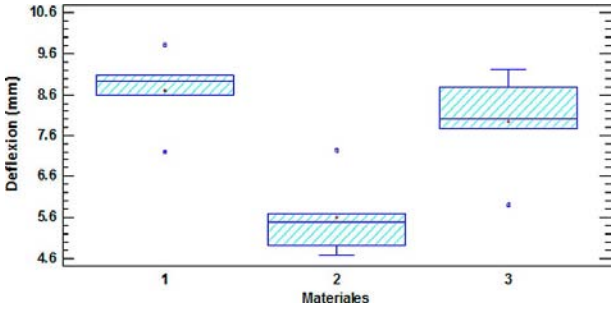

Figura 19. Box and moustache plot for the deflection.

It can be observed that materials (1) and (3) exhibit statistically significant differences with a confidence level of 95 % with respect to material (2).

As it can be seen in Figure 20, the deflection presented by composite materials reinforced with longitudinal fiber of abaca and cabuya, decreased with respect to the matrix material of polymer resin.

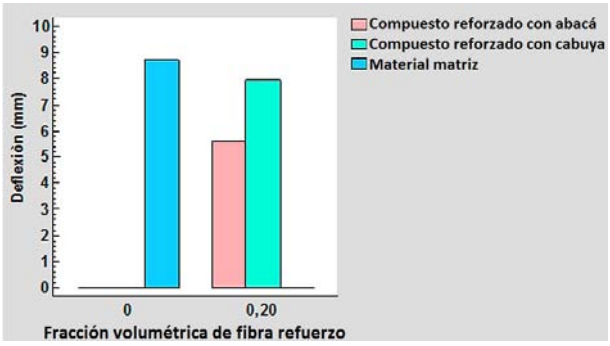

Figura 20. Deflection of the composite materials depending on the volumetric fraction of the reinforcement fiber.

The deflection decrease for the composite material reinforced with the longitudinal fiber of abaca was 36 %, while such decrease was 9 % for the composite material reinforced with longitudinal fiber of cabuya.

3.6. Comparison of the bending mechanical properties of the composite materials manufactured by 3D printing, with other materials

The present section presents a comparison of the mechanical properties to bending, obtained in the characterization of composite materials reinforced with fibers of abaca and cabuya and manufactured by 3D printing, with other composite materials reinforced with different natural fibers and matrices and other manufacturing processes, as well as with plastic materials utilized in the automotive industry. Table 7 shows the values of maximum bending stress, modulus of elasticity, type of process utilized for manufacturing the material, volumetric fraction of the reinforcement fiber, type of matrix and orientation of the reinforcement fiber.

Tabla 7. Mechanical properties to bending of different composite and plastic materials utilized in the automotive sector.

Designation the material	Typo of material	Matrix material	Reinforce ment fiber	Manufacturing process	Volumetric fraction of reinforcement	Orientation of reinforcement fiber	Maximum bending stress (MPa)	Modulus of elasticity of bending (MPa)
MCFI20%AL	*Composite material*	*Photopolymer*	*Abaca*	*3D Printing*	*20%*	*Longitudinal*	*77,534*	*2211,33*
MCFI20%CL	*Composite material*	*Photopolymer*	*Cabuya*	*3D Printing*	*20%*	*Longitudinal*	*83,256*	*1806,03*
MCPE20%AL	Composite material	Polyester	Abacá	Stratification manual	20%	Longitudinal	100	10000
MCPE23%CL	Composite material	Polyester	Cabuya	Stratification manual	23%	Longitudinal	51,39	2355,58
Polyester	-	Polyester	-	-	-	-	56,62	1867,82
MCPB20%AL	Composite material	Biodegradable polymer	Abacá	By compresion	20%	Longitudinal	104,4	5570
PLA	-	Biodegradable polymer	-	-	-	-	69	2755
MCP20%AT	Composite material	Polyester	Abaca	-	20%	Tejido	62,4	3976

Note. A code was assigned to each material depending on the type of material, matrix material, reinforcement fiber, manufacturing process, volumetric fraction of the reinforcement fiber and orientation of the reinforcement fiber.

The data are presented through an X-Y dispersion plot of the different materials, which contains the values corresponding to maximum bending stresses in the Y-axis, and the values corresponding to the modulus of elasticity to bending in the X-axis (see Figure 21).

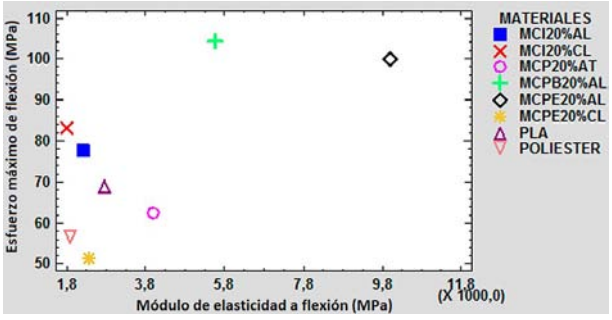

Figura 21. Comparison of the mechanical properties to bending of the different materials.

The composite materials reinforced with fibers of abaca and cabuya, and manufactured using 3D printing, exhibit better bending mechanical characteristics compared to the composite materials of polyester matrix and base materials such as biodegradable polymers and resins.

From the structural analysis using simulation, it is important to mention that the polypropylene air conditioning grilles had a nodal displacement of 0.02 mm, while the air conditioning grille with the matrix material of the composites had a nodal displacement of 0.048 mm. This indicates the existence of a difference between the nodal displacements of these two simulated materials.

The structural analysis performed through simulation in the polypropylene air conditioning grilles, resulted in a maximum stress of 0.204 MPa, while the air conditioning grille with the matrix material of the composites had a maximum stress of 0.206 MPa; therefore, there is no significant difference between these two simulated materials.

Based on what has been previously mentioned where the composite materials reinforced with fibers of abaca and cabuya, the matrix material and the original material of the air conditioning grilles do not exhibit significant differences between them, it is proposed the option of replacing the original material, with composite materials reinforced with fibers of abaca and cabuya, manufactured in Ecuador.

4. Conclusions

The maximum bending stress of the composite materials reinforced with a 20 % volumetric fraction of fibers of abaca and cabuya obtained by means of 3D printing, decreased with respect to the matrix material. This is possibly caused by the lack of previous study in the compatibility of the materials employed.

The reduction in certain mechanical properties of the composite materials obtained by additive manufacturing with respect to the matrix material, were due to the low level of adherence of the reinforcement fibers with the matrix material, which generated a poor interface between those constitutive elements.

The modulus of elasticity of the analyzed reinforced composite materials increased with respect to the matrix material, which results in an increased rigidity of the characterized materials.

The composite materials manufactured by means of 3D printing are an alternative for manufacturing auto parts, since in some cases their mechanical characteristics are better than other materials considered in the automotive industry.

The computational simulation of the air conditioning grilles subject to a load, enables verifying the signif-

icant differences between these two analyzed materials regarding nodal displacement, and besides enabled verifying that there is no significant difference between the simulated materials in the analysis of stresses.

Referencias

[1] A. K. Bledzki, O. Faruk, and V. E. Sperber, "Cars from bio-fibres," *Macromolecular Materials and Engineering*, vol. 291, no. 5, pp. 449–457, 2006. [Online]. Available: https://doi.org/10.1002/mame.200600113

[2] K. Quesada-Solís, P. Alvarado-Aguilar, R. Sibaja-Ballestero, and J. Vega-Baudrit, "Utilización de las fibras del rastrojo de piña (*Ananas comusus*, variedad *champaka*) como material de refuerzo en resinas de poliéster," *Revista Iberoamericana de Polímeros*, vol. 6, no. 2, pp. 157–179, 2005. [Online]. Available: http://bit.ly/2J8ddTT

[3] O. Faruk, A. K. Bledzki, H.-P. Fink, and M. Sain, "Progress report on natural fiber reinforced composites," *Macromolecular Materials and Engineering*, vol. 299, no. 1, pp. 9–26, 2014. [Online]. Available: https://doi.org/10.1002/mame.201300008

[4] F. Ahmad, H. S. Choi, and M. K. Park, "A review: Natural fiber composites selection in view of mechanical, light weight, and economic properties," *Macromolecular Materials and Engineering*, vol. 300, no. 1, pp. 10–24, 2015. [Online]. Available: https://doi.org/10.1002/mame.201400089

[5] K. N. Roshdestwensky, J. L. Mroginski, C. A. Morel, R. B. D'Ambra, and J. M. Podestá, "Modelado numérico del comportamiento de la interface en materiales compuestos," *Asociación Argentina de Mecánica Computacional*, vol. 32, no. 19, pp. 1653–1670, 2013. [Online]. Available: http://bit.ly/2KEWMSr

[6] N. Guo and M. C. Leu, "Additive manufacturing: technology, applications and research needs," *Frontiers of Mechanical Engineering*, vol. 8, no. 3, pp. 215–243, 2013. [Online]. Available: https://doi.org/10.1007/s11465-013-0248-8

[7] P. C. Li and S. C. Huang, "Application of rapid prototyping technology in automobile manufacturing industry," in *Modern Tendencies in Engineering Sciences*, ser. Applied Mechanics and Materials, vol. 533. Trans Tech Publications Ltd, 5 2014, pp. 106–110. [Online]. Available: https://doi.org/10.4028/www.scientific.net/AMM.533.106

[8] M. Berchon and B. Luyt, *La impresión 3D. Guía definitiva para makers, diseñadores, estudiantes, profesionales, artistas y manitas en general.* Editorial Gustavo Gili, 2016. [Online]. Available: http://bit.ly/2YcsNEp

[9] J. Bonada, A. Muguruza, X. Fernández-Francos, and X. Ramis, "Influence of exposure time on mechanical properties and photocuring conversion ratios for photosensitive materials used in additive manufacturing," *Procedia Manufacturing*, vol. 13, pp. 762–769, 2017. [Online]. Available: https://doi.org/10.1016/j.promfg.2017.09.182

[10] Stratasys. (2017) Make it more realistic and accurate with polyjet. Stratasys Ltd. [Online]. Available: http://bit.ly/31VRQhq

[11] W. Callister, *Introducción a la Ciencia e Ingeniería de los Materiales.* Editorial Reverté. S. A., 2007. [Online]. Available: http://bit.ly/2XuZ4JF

[12] P. Pontón and V. H. Guerrero, "Obtención de materiales compuestos de matriz poliéster reforzados con fibra de abacá mediante estratificación manual," *Revista Tecnológica ESPOL*, vol. 23, no. 3, pp. 47–54, 2010. [Online]. Available: http://bit.ly/2ZLLPSw

[13] J. G. Paredes Salinas and A. D. Jácome León, *Estudio de la configuración de fibras del material compuesto de matriz epoxi reforzada con fibra de piña y su incidencia en las propiedades mecánicas en la fabricación de butacas deportivas.* Tesis de Grado, Universdad Técnica de Ambato, 2015. [Online]. Available: http://bit.ly/2X0ZKCf

[14] J. Summerscales, A. S. Virk, and W. Hall, "Enhanced rules-of-mixture for natural fibre reinforced polymer matrix (nfrp) composites (comment on lau et al. in volume 136)," *Composites Part B: Engineering*, vol. 160, pp. 167–169, 2019. [Online]. Available: https://doi.org/10.1016/j.compositesb.2018.10.021

[15] D. S. Ponce and V. Guerrero, "Propiedades mecánicas de compuestos biodegradables elaborados a basa de ácido poliláctico reforzados con fibra de abacá," *Revista Politécnica*, vol. 33, no. 2, 2014. [Online]. Available: http://bit.ly/2X12KhZ

[16] J. C. Rocha-Hoyos, E. A. Llanes-Cedeño, S. F. Celi-Ortega, and D. C. Peralta-Zurita, "Efecto de la Adición de Biodiésel en el Rendimiento y la Opacidad de un Motor Diésel," *Información tecnológica*, vol. 30, pp. 137–146, 06 2019. [Online]. Available: http://bit.ly/2XzptpO

[17] N. A. Tamayo Duque, *Obtención y Caracterización de Materiales Compuestos de Matriz Poliéster Reforzados con Fibra de Cabuya Mediante Estratificación.* Tesis de Grado, Escuela Politécnica Nacional, 2012. [Online]. Available: http://bit.ly/2NnLNPA

Scientific Paper / Artículo Científico

UNIVERSIDAD POLITÉCNICA SALESIANA ECUADOR
INGENIUS
Revista de Ciencia y Tecnología
https://doi.org/10.17163/ings.n22.2019.11
pISSN: 1390-650X / eISSN: 1390-860X

Analysis of storage in Liquefied Petroleum Gas systems: Stationary Tanks vs. Cylinders

Análisis del almacenamiento en sistemas de gas licuado de petróleo: tanques estacionarios *vs.* cilindros

Diego Venegas Vásconez[1,*], César Ayabaca Sarria[2]

Abstract

In Ecuador, liquefied petroleum gas (LPG) is used as an energy source for residential, commercial and industrial equipment. In its natural state this fuel is in gas phase, but for easiness of transportation and storage it is liquefied and stored in containers called cylinders (by spare) or tanks (stationary), where it is re-gasified for consumption. The present work measures the remaining LPG that is returned in cylinders to the marketers, by 20 commercial and industrial users in Ecuador during a month, 8 with 15 kg cylinders and 12 with 45 kg cylinders. The average return was 3.82 kg/cyl. (25.49%) and 9.69 kg/cyl. (21.54%) respectively. Then, 8 safety parameters considered in the current Technical Standard in Ecuador were verified for these 20 facilities, and the results of those users who do not comply with these parameters are presented. Finally, some arguments are given about why there are economic and security advantages in the storage of LPG in stationary tanks over the storage in cylinders.

Keywords: Liquefied petroleum gas, tanks, cylinders, vaporization, remainder, safety.

Resumen

En el Ecuador se utiliza el gas licuado de petróleo (GLP) como fuente de energía para equipos residenciales, comerciales e industriales. En estado natural este combustible se encuentra en fase gaseosa, pero por facilidad de transporte y almacenamiento es licuado y depositado en recipientes denominados cilindros (por recambio) o tanques (estacionarios), donde se vuelve a gasificar para su consumo. El presente trabajo mide el GLP remanente que es devuelto en cilindros a las comercializadoras por veinte usuarios comerciales e industriales en el Ecuador durante un mes, 8 con cilindros de 15 kg y 12 con cilindros de 45 kg. El promedio de devolución fue de 3,82 kg/cil. (25,49 %) y 9,69 kg/cil. (21,54 %) respectivamente. Luego se verificaron ocho parámetros de seguridad contemplados en la norma técnica vigente en el Ecuador para estas veinte instalaciones, y se presentan los resultados de aquellos usuarios que no cumplen con estos parámetros. Finalmente, se entregan algunos argumentos sobre por qué existen ventajas económicas y de seguridad en el almacenamiento de GLP en tanques estacionarios sobre cilindros.

Palabras clave: gas licuado de petróleo, tanques, cilindros, vaporización, remanente, seguridad.

[1,*]Departamento de Ingeniería de Materiales y Procesos Sustentables, Universidad del Bío-Bío, Concepción-Chile. Autor para correspondencia ✉: diego.venegas1801@alumnos.ubiobio.cl. http://orcid.org/0000-0002-7376-6272.
[2]Departamento de Ingeniería Mecánica, Escuela Politécnica Nacional, Quito-Ecuador.
http://orcid.org/0000-0002-3728-7514

Received: 15-05-2019, accepted after review: 25-06-2019

Suggested citation: Venegas Vásconez, D. and Ayabaca Sarria, C. (2019). «Analysis of storage in Liquefied Petroleum Gas systems: Stationary Tanks vs. Cylinders». Ingenius. N.°22, (july-december). pp. 113-122. doi: https://doi.org/10.17163/ings.n22.2019.11.

1. Introduction

The liquefied petroleum gas (LPG) is a fuel which is utilized as energy source in residential [1], commercial [2] and industrial [3] applications. Its use has various advantages, such as

- High calorific power compared to other energy sources [4].
- It satisfies various energy needs as a unique source [5].
- It is easy to transport and store, reducing its temperature and increasing its pressure [6].
- It is not toxic for humans [7].

Despite all these benefits reported about the handling of the GLP, there are various disadvantages regarding its use, such as:

- It generates complacency in the user regarding its manipulation. This has caused accidents with severe physical and human consequences [8].
- Lack of foresight in the design of new buildings on the part of builders, which makes that the recipients (cylinders) should be stored in stacked places, without ventilation and piled one on top of the other (Figure 1), which causes insecurity for the user.

Figura 1. Storage of LPG in cylinders.

1.1. Transportation and storage of LPG

At environmental conditions the LPG is found in gaseous phase [9] obtained from a petroleum refining process, and then is transformed to liquid phase increasing its pressure and reducing its temperature before being stored in big containers, from which it is transported to filling plants or delivered to the final users.

The delivery is made in containers [10] known as cylinders, which are easily manipulable and replaced when the fuel is over, or tanks which are permanently stored and a cistern truck is required for recharging them [11]. Figure 2 shows the main characteristics of the storage, both in cylinders and tanks.

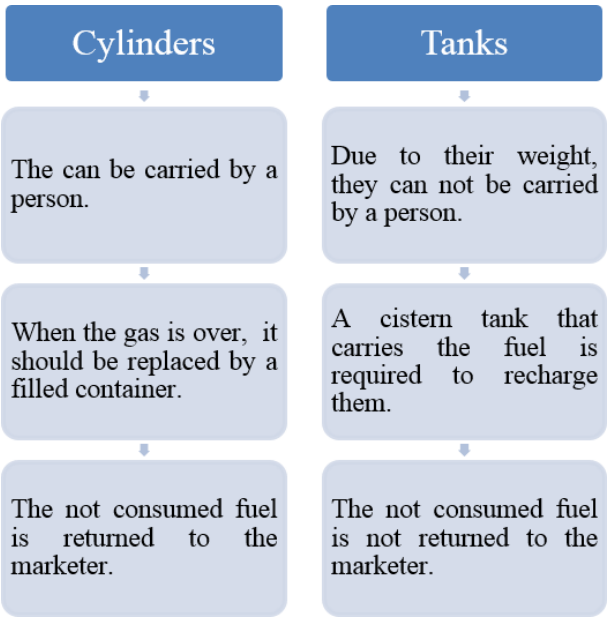

Figura 2. Differences between the storage of LPG in cylinders and tanks [12].

1.2. Consumption of LPG

With the exception of particular cases, the LPG is required in gaseous phase by the consuming equipment. This phase is obtained inside the containers, through a heat transfer process from the fuel to the surrounding environment. The «vaporization capacity» of the containers depends on [13]:

- ***Exterior environmental temperature:*** a greater exterior environmental temperature, will cause a greater variation of the temperature with the fuel, and thus the vaporization capacity of the container will also be greater.
- ***Size of the container:*** For a greater size of the container, there is a greater area of contact with the fuel.
- ***Material of the container:*** It should favor the heat transfer between the fuel and the surrounding environment

When the fuel required by the consuming equipment is greater than the vaporization capacity of a container, the vaporization of the LPG is very fast and the walls of the container cool down, starting the

condensation of water drops which are suspended in the air surrounding the container (humid air). Then, a water film appears in the exterior area, corresponding to the internal zone in which there is fuel. If the request for fuel by the consuming equipment continues, the water in the exterior will start forming ice layers in the same area, as shown in Figure 3a. As a consequence of this excessive cooling, the fuel delivery to the equipment decreases, and they will start to operate inadequately.

In order to counteract this phenomenon, empirical mechanisms have been utilized to enable consuming the fuel remaining in a container whose walls have frozen. One of these practices is to put the containers in hot water (Figure 3b), to increase the temperature difference between the exterior and the fuel in the interior, and vaporize more LPG.

a) b)

Figura 3. a) Ice layers on a cylinder due to the loss of natural vaporization capacity. b) LPG cylinder in a container with hot water to improve the natural vaporization capacity.

1.3. LPG consumption in Ecuador

In Ecuador, the LPG is commercialized with two fares:

- A subsidized fare for residential consumption and nonprofit activities [14, 15].
- An industrial fare for food sale, profit-seeking industrial activities and sumptuous residential uses, such as heating water for pools, jacuzzis and sauna baths. This fare is set by the National Government through the Executive Decree N° 799 [16], is revised monthly, is in accordance with international oil prices, and is published in the web site of the governmental agency [17].

Each local Fire Department and the Hydrocarbon Regulation and Control Agency (HRCA), are the competent authorities with regards to the supervision and inspection of the LPG facilities in Ecuador.

1.4. Problems detected in LPG handling in Ecuador and problem justification

The following problems have been identified related the handling of LPG in Ecuador:

- Due to the difference between the residential and industrial fares, 15 kg cylinders with subsidized LPG (0,10666 USD/kg) are utilized in commercial and industrial facilities, instead of using the fuel without subsidy (0,767229 USD/kg), and because of the high fuel consumption in this type of systems, the saving due to the difference in fare is significant.
- Lack of planning in the design of new buildings for commercial and industrial use, which do not consider safe rooms to locate the gas supply.
- Due to the high flammability of LPG [18], there is high probability for the occurrence of disasters with the presence of fire and explosion, known as «Boiling Liquid Expanding Vapour Explosion» (BLEVE) [19] in the surroundings of the gas storage in commercial and industrial buildings, due to the lack of foresight and security measures. BLEVE is an explosion of vapors that expand as the liquid boils [20], with devastating consequences [21, 22], especially because of the energy release with separation of fragments of the involved containers [23] (Figure 4).
- Manipulation of the LPG systems by nonqualified personnel who ignores the current legal framework [24], and does not apply engineering criteria in the calculation and dimensioning

of such systems, thus making them insecure [25] (Figure 4).

The present work shows the losses of users of LPG systems with cylinders, caused by the return of non-consumed fuel, i.e. remaining, to the marketer. In addition, an analysis is carried out of the following security aspects of these facilities regarding the use of cylinders, which are considered in the current regulation for gas systems in Ecuador [26]:

Figura 4. LPG cylinder that has suffered BLEVE [27].

- Security distances to third parties.
- Ventilation of the storage area.
- Number of cylinders in storage.
- Availability of extinguishers in the storage area.
- Validity of extinguishers.
- Availability of leak detectors.
- General condition of accessories (valves, regulators and hoses).
- Availability of emergency plans in the facility.

At last, some advantageous aspects of the facilities that have stationary tanks are presented, compared to those that have returnable cylinders.

2. Materials and methods

In order to determine the gas remaining in the cylinders returned by the users of LPG systems, such cylinders have been weighted before connecting them for use, and after they have been emptied. For this purpose, a GTC scale with a capacity of 150 kg and a measuring sensitivity of 50 g was utilized. The remaining weight in kg is calculated as

$$kg = W_{comb} - (W_{lleno} - W_{serf}) \quad (1)$$

where kg are the returned (remaining) kilograms, W_{fuel} is the weight of the fuel, W_{full} is the weight of the full cylinder and W_{empty} is the weight of the empty cylinder.

A GTC 100 detector with a range 0-30000 ppm of propane, was used to measure if the presence of gas in the storage environment is greater than the lower limit of flammability of the fuel.

3. Presentation and analysis of results

3.1. Remaining gas

Tables 1 and 2 show the remaining gas returned in 15 kg and 45 kg cylinders, respectively, which were utilized for four weeks, by commercial and industrial users.

Tabla 1. Remaining gas returned in used 15 kg cylinders

User	Week 1		Week 2		Week 3		Week 4		Total				
N.	Cil	Kg. ret	Cil	Kg. ret	Cil	Kg. ret	Cil	Kg. ret	Cil	Kg. ret	$ US ret real*	Kg ret cil	% filling
1	4	8,5	3	7,1	4	8,7	4	8,4	15	32,7	$25,09	2,18	15
2	4	13,4	5	17,8	5	18,2	4	13	18	62,4	$47,88	3,47	23
3	5	15,1	5	15,7	6	21	6	20,8	22	72,6	$55,70	3,30	22
4	6	27,8	7	31,1	8	35,6	7	30,9	28	125,4	$96,21	4,48	30
5	10	41	9	35,9	8	33,2	8	32,7	35	142,8	$109,56	4,08	27
6	11	35,4	11	36,1	12	39,8	12	40,2	46	151,5	$116,24	3,29	22
7	12	55,6	11	50,1	10	47,1	11	52,1	44	204,9	$157,21	4,66	31
8	12	61,1	12	60,9	11	57	13	67	48	246	$188,74	5,13	34
								Average:	**32,00**	**129,79**	**99,58**	**3,82**	**25,48**

Tabla 2. Remaining gas returned in used 45 kg cylinders

User	Week 1		Week 2		Week 3		Week 4		Total				
N.	Cil	Kg. ret	Cil	Kg. ret	Cil	Kg. ret	Cil	Kg. ret	Cil	Kg. ret	$ US ret real*	Kg ret cil	% filling
9	4	35	4	34,2	4	32,9	4	33,5	16	135,6	$104,04	8,48	19
10	5	36,7	5	35,8	4	28,4	4	27,9	18	128,8	$98,82	7,16	16
11	5	53,1	4	47,6	6	62,9	6	61,4	21	225	$172,63	10,71	24
12	5	61,4	5	63	5	62,1	4	55,2	19	241,7	$185,44	12,72	28
13	6	58,8	5	49,2	6	61,5	6	62,4	23	231,9	$177,92	10,08	22
14	6	70	6	74,2	8	91,1	6	72,1	26	307,4	$235,85	11,82	26
15	7	43,7	6	37	8	51,7	8	54,6	29	187	$143,47	6,45	14
16	9	77,9	9	82,1	8	78,4	8	73,7	34	312,1	$239,45	9,18	20
17	9	88,4	8	78,9	10	101,1	8	82,4	35	350,8	$269,14	10,02	22
18	10	75,7	10	78	11	87,6	10	79,8	41	321,1	$246,36	7,83	17
19	10	114,6	10	117,5	9	105,4	9	106,3	38	443,8	$340,50	11,68	26
20	11	110,2	10	100,2	11	114,3	12	123,7	44	448,4	$344,03	10,19	23
								Average:	**28,67**	**277,80**	**213,14**	**9,69**	**21,54**

Simbology:

User: Número de usuario
Cap: Cylinder capacity of the facility
Cyl: Number of returned cylinders
kg ret: kg returned weekly
$ US ret:

- For 15 kg cylinders = kg ret x 0,10666 USD/kg (residential fare)

- For 45 kg cylinders = kg ret x 0,767229 USD/kg [17]

kg ret cyl: kg. promedio devuelto por cilindro
% filling: average filling percentage per returned cylinder

Based on the results presented in Table 1, the following can be stated:

- The difference between the values for users of 15 kg cylinders in the columns $ US ret vs. $ US ret real*, is because the $ US ret represents the value of the remaining gas returned by the user, but this is not a real value because this user should pay the industrial fare, result shown in the column $ US ret real*.

- There is remaining gas returned in all cylinders, which is money that the user has paid in advance.

- Among the users of 15 kg cylinders, N° 1 returns the least fuel (2.18 kg/cylinder), and N° 8 returns the most fuel (5.13 kg/cylinder).

- The average amount of fuel returned in 15 kg cylinders was 3.82 kg per cylinder, which represents 25.49 % of its capacity.

- Among the users of 45 kg cylinders, N° 15 returns the least fuel (6.45 kg/cylinder), and N° 12 returns the most fuel (12.72 kg/cylinder).

- The average amount of fuel returned in 45 kg cylinders was 9.69 kg per cylinder, which represents 21.54 % of its capacity.

3.2. Security

Figure 5 shows the quantitative results of the security inspection performed to the 20 users, according to the criteria established in the current legal framework in Ecuador [26]. The letter in the abscissa represents the violated criterion, and the number on the bar represents the number of users that violate that criterion.

It is important to remark that in the numerical criteria regarding installed capacity, the individual capacity, given in kilograms, of all cylinders in the storage area is added.

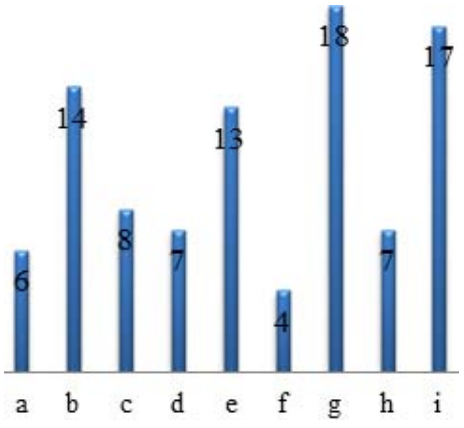

Figura 5. Users of LPG systems that violate security criteria.

a. Security distances to third parties: 6 users had the containers very close to open flame sources or spark generators. The Technical Regulation establishes a minimum security distance with respect to third parties that may be potential risks of fire generation or incentive [28].

b. Ventilation of the storage area: 14 users had the containers in areas without ventilation (Figura 6a).

c. Number of cylinders in storage: The regulation establishes a maximum number of 15 kg and 45 kg cylinders, which may be located for supply as well as for reserve. 8 users exceeded the maximum number of allowed cylinders.

d. Presence of gas leaks: 7 users exceeded the maximum allowed by the measuring device (1.93 % of LPG in the air). A probable cause of this situation is the wear in the connecting couplings, which are constantly connected and disconnected during the replacement of the cylinders.

e. Availability of fire extinguishers in storage area: 13 users did not have fire extinguishers.

f. Validity of extinguishers: Of the 7 users who did have extinguishers, 4 of them had them expired.

g. Availability of gas leaks detectors: The installation of detectors is recommended as an alternative measure to detect possible gas leaks in the surroundings of the storage. These detectors emit a high-pitched sound when the amount of fuel in the environment is close to the lower explosion limit. 18 users did not have this device.

h. General condition of accessories (valves, regulators, hoses) in the storage area: The accessories have a service life recommended by the manufacturer, according to treatment received [29]. 7 users had accessories that exhibited signs of excessive wear (Figure 6b).

i. Availability of emergency plans in the facility: In case of emergency with fuel leaks and fire, it is recommended to count with an emergency handling plan that considers the actions to be taken during such emergency. This plan should specify the people responsible of leading these actions, and should be always readily available. 17 users did not have emergency plans nor people responsible for handling such emergencies.

3.3. Users that have replaced cylinders by stationary tanks

Users that have opted to replace the system with cylinders by stationary tanks have seen the benefits immediately. Some of these benefits include:

- Zero gas remaining, because there is no return or replacement of the container; therefore, there is no return of fuel to the marketer.

- Since there is no LPG remaining, there is a saving of money that can be invested in other activities related to the commercial or industrial business.

- The storage is concentrated in a single space, which enables focusing the security and prevention efforts in a single point [30] (Figure 7a).

- More secure systems, since they are inspected by the competent authority and they should comply the current technical regulation for their approval and operation [26].

- Easy monitoring and control of the amount of fuel in reserve, since stationary tanks have measuring and control devices. If the system is connected to several users, the billing is done individually placing meters or counters for each user (Figure 7b).

- Comply the current legislation for commercial and industrial use (without subsidy) of LPG, and elimination of the use of the residential LPG for users that usufruct it.

- Minimum maintenance of the facilities, since there is no manipulation during the discharge because it is not necessary to disconnect couplings during the replacement [31].

- Comfort, since no personnel is required to take away and transport empty cylinders.

- The transportation of cylinders produces bumps and dents on structural parts of the building; these are eliminated with stationary systems.

- Flexibility for the installation of containers in hard-to-access areas, such as terraces [32].

a) b)

Figura 6. a) Tanks in an area without natural ventilation. b) LPG cylinder with the connecting valve in bad condition.

a) b)

Figura 7. a) Stationary LPG tanks. b) Meters of LPG consumption.

Equation 2 gives an expression to determine the time in which a facility with stationary tanks may be paid, considering the money that is not paid to the marketer as remaining fuel.

$$Recov = \frac{Facility\ cost}{\$US\ ret\ real} \tag{2}$$

Where:

Recov: is the time for recovering the investment on a new facility with stationary tanks.

Facility cost: Approximate cost of the facility.

$ US ret real: Monthly average of returned USD.

On the other hand, Table 3 shows the times for recovering the investment for the monthly averages of remaining gas, estimating an initial installation value of 1500 USD for a system with 15 kg cylinders and 2500 USD for a system with 45 kg cylinders.

Tabla 3. Recovery of the investment for a facility with stationary tanks

Cyl	$ US ret real*	Recov
15	99,58	15,06
45	213,14	11,73

Obviously, this will depend on the size of the facility and the number of accessories, pipes and stationary tanks that are placed, for the initial cost of such facility. However, considering reference values according to the reality of the market, the recovery time of the investment in 15 kg cylinders facilities is 15 months, and 12 months for the case of 45 kg cylinders facilities.

4. Conclusions

The replacement of a conventional system with cylinders by stationary tanks, generates saving to the user because there is no payment for remaining fuel. This can be seen immediately after the new system is put into operation, since no fuel is returned to the marketer.

As the consumption is greater, so will be the need to have a stationary gas system with tanks, since the payment for not utilized remaining fuel could be avoided.

There will always be return of remaining gas in a cylinder. For the cases considered, the averages were 3.82 kg/cyl. (25.49 %) for users of 15 kg cylinders and 9.60 kg/cyl. (21.59 %) for users of 45 kg cylinders.

The initial investment that could be made for replacing a system with cylinders by one with stationary tanks, is recovered in short time (15 months in 15 kg cylinders and 12 months in 45 kg cylinders) because there is no payment for the remaining gas; this time may vary depending on the size of the facility and on the fuel consumption.

In a system in which LPG is stored, there will always be physical and human risks. A system with stationary tanks does not eliminate this risk, but minimizes it compared to the system with returnable cylinders.

A gas storage system minimizes the risk in a commercial or industrial facility; however, the user is responsible for maintaining the level of security in the system, and may start with small routines such as:

- Revise the general condition of the accessories.
- Verify leaks with soapy water in the joints of the accessories.
- Request talks about prevention, and periodic inspection to the system by qualified personnel.
- Count with protection systems such as: extinguishers, leak detectors, fire alarms.
- It is necessary to have an evacuation and emergency plan.
- Request inspection and permission for operating the system to the competent authority.

Referencias

[1] D. Kimemia and H. Annegarn, "Domestic lpg interventions in south africa: Challenges and lessons," *Energy Policy*, vol. 93, pp. 150 – 156, 2016. [Online]. Available: https://doi.org/10.1016/j.enpol.2016.03.005

[2] L. Raslavičius, A. Keršys, S. Mockus, N. Keršienė, and M. Starevičius, "Liquefied petroleum gas (lpg) as a medium-term option in the transition to sustainable fuels and transport," *Renewable and Sustainable Energy Reviews*, vol. 32, pp. 513–525, 2014. [Online]. Available: https://doi.org/10.1016/j.rser.2014.01.052

[3] K. J. Morganti, T. M. Foong, M. J. Brear, G. da Silva, Y. Yang, and F. L. Dryer, "The research and motor octane numbers of liquefied petroleum gas (lpg)," *Fuel*, vol. 108, pp. 797–811, 2013. [Online]. Available: https://doi.org/10.1016/j.fuel.2013.01.072

[4] P. Boggavarapu, B. Ray, and R. Ravikrishna, "Thermal efficiency of lpg and png-fired burners: Experimental and numerical studies," *Fuel*, vol. 116, pp. 709–715, 2014. [Online]. Available: https://doi.org/10.1016/j.fuel.2013.08.054

[5] R. K. Andadari, P. Mulder, and P. Rietveld, "Energy poverty reduction by fuel switching. impact evaluation of the lpg conversion program in indonesia," *Energy Policy*, vol. 66, pp. 436–449, 2014. [Online]. Available: https://doi.org/10.1016/j.enpol.2013.11.021

[6] D. Venegas V and C. Ayabaca S, *Instalaciones de gas licuado de petróleo.* Editorial Académica Española, 2017. [Online]. Available: http://bit.ly/2JaTgfv

[7] F. Chica Segovia, F. Espinoza Molina, and N. Rivera Campoverde, "Gas licuado de petróleo como combustible alternativo para motores diesel con la finalidad de reducir la contaminación del aire," *Revista Ingenius*, no. 4, pp. 73–81, 2010. [Online]. Available: https://doi.org/10.17163/ings.n4.2010.08

[8] G. Paliwal, K. Agrawal, R. Srivastava, and S. Sharma, "Domestic liquefied petroleum gas: Are we using a kitchen bomb?" *Burns*, vol. 40, no. 6, pp. 1219–1224, 2014. [Online]. Available: https://doi.org/10.1016/j.burns.2013.12.023

[9] G. Astbury, "A review of the properties and hazards of some alternative fuels," *Process Safety and Environmental Protection*, vol. 86, no. 6, pp. 397–414, 2008. [Online]. Available: https://doi.org/10.1016/j.psep.2008.05.001

[10] J. Stawczyk, "Experimental evaluation of lpg tank explosion hazards," *Journal of Hazardous Materials*, vol. 96, no. 2, pp. 189–200, 2003. [Online]. Available: https://doi.org/10.1016/S0304-3894(02)00198-X

[11] NFPA. (2014) Nfpa 58 código del gas licuado de petróleo edición 2014. National Fire Protection Association. [Online]. Available: http://bit.ly/2KCNA0K

[12] D. Venegas V and C. Ayabaca S, *Gas Licuado de Petróleo (GLP): Un combustible eficiente, económico y seguro*. First Edition, 2018. [Online]. Available: http://bit.ly/2XxZXkL

[13] S. P. Kumar, B. Prasad, G. Venkatarathnam, K. Ramamurthi, and S. S. Murthy, "Influence of surface evaporation on stratification in liquid hydrogen tanks of different aspect ratios," *International Journal of Hydrogen Energy*, vol. 32, no. 12, pp. 1954–1960, 2007. [Online]. Available: https://doi.org/10.1016/j.ijhydene.2006.08.052

[14] K. Troncoso and A. S. da Silva, "Lpg fuel subsidies in latin america and the use of solid fuels to cook," *Energy Policy*, vol. 107, pp. 188–196, 2017. [Online]. Available: https://doi.org/10.1016/j.enpol.2017.04.046

[15] B. Creamer Guillén and R. Becerra Robalino, "Cuantificación de los subsidios de derivados del petróleo a los hidrocarburos en el ecuador," *Petróleo al día. Boletín Estadístico del Sector de Hidrocarburos*, vol. 2, pp. 9–26, 2016. [Online]. Available: http://bit.ly/2YgTMPo

[16] Presidencia de la República del Ecuador. (2015) Suplemento n 613, decreto ejecutivo n 799. Registro Oficial. [Online]. Available: http://bit.ly/2FzBrpr

[17] PETROECUADOR, *Precios de venta a nivel de terminal para las comercializadoras calificadas y autorizadas a nivel nacional*. EP PETROECUADOR Gerencia de Comericalización Nacional, 2019. [Online]. Available: http://bit.ly/2XeM8Zq

[18] M. A. Johnsen and G. Nardini, *Manual de seguridad: Aspectos de inflamabilidad de los gases hidrocarburos*. PNUMA, Programa de las Naciones Unidas para el Medio Ambiente, 2005. [Online]. Available: http://bit.ly/2X26fET

[19] T. Abbasi and S. Abbasi, "The boiling liquid expanding vapour explosion (bleve) is fifty ... and lives on!" *Journal of Loss Prevention in the Process Industries*, vol. 21, no. 4, pp. 485–487, 2008. [Online]. Available: https://doi.org/10.1016/j.jlp.2008.02.002

[20] B. Hemmatian, E. Planas, and J. Casal, "On BLEVE definition, the significance of superheat limit temperature (Tsl) and LNG BLEVE's„" *Journal of Loss Prevention in the Process Industries*, vol. 40, p. 81, 2015. [Online]. Available: https://doi.org/10.1016/j.jlp.2015.12.001

[21] T. Abbasi and S. Abbasi, "The boiling liquid expanding vapour explosion (bleve): Mechanism, consequence assessment, management," *Journal of Hazardous Materials*, vol. 141, no. 3, pp. 489 – 519, 2007. [Online]. Available: http://www.sciencedirect.com/science/article/pii/S0304389406011290

[22] G. Pinhasi, A. Ullmann, and A. Dayan, "1d plane numerical model for boiling liquid expanding vapor explosion (bleve)," *International Journal of Heat and Mass Transfer*, vol. 50, no. 23, pp. 4780–4795, 2007. [Online]. Available: https://doi.org/10.1016/j.ijheatmasstransfer.2007.03.016

[23] R. K. Eckhoff, "Boiling liquid expanding vapour explosions (bleves): A brief review," *Journal of Loss Prevention in the Process Industries*, vol. 32, pp. 30–43, 2014. [Online]. Available: https://doi.org/10.1016/j.jlp.2014.06.008

[24] D. F. Venegas Vásconez, C. Ayabaca Sarria, S. F. Celi Ortega, and J. C. Rocha Hoyos, "El riesgo en el almacenamiento de glp en el ecuador," *INNOVA Research Journal*, vol. 3, no. 1, pp. 19–29, 2018. [Online]. Available: http://bit.ly/2X6uP7E

[25] H. Albán. Comercialización de gas licuado de petróleo (GLP) en el Ecuador. Agencia de Regulación y Control Hidrocarburífero (ARCH). [Online]. Available: http://bit.ly/2J7uqNv

[26] INEN, *NTE INEN 2 260:2010 Instalaciones de gases combustibles para uso residencial, comercial e industrial. Requisitos*, Instituto Ecuatoriano de Normalización (INEN) Std. [Online]. Available: http://bit.ly/2ZPvnRk

[27] Bomberos Latacunga, *Archivo fotográfico del Benemérito Cuerpo de Bomberos de Latacunga*. Latacunga, Ecuador, 2017.

[28] D. Venegas V and F. O., "La bleve, un motivo para la seguridad en las instalaciones de glp," in *13° Congreso Iberoamericano de Ingeniería Mecánica*, 2017. [Online]. Available: http://bit.ly/2RHbwRu

[29] D. Venegas V, C. Ayabaca S, S. F. Celi Ortega, and J. Yánez, "Mantenimiento necesario en instalaciones de glp," in *XXI Congreso Nacional de Ingeniía Mecánica*, 2016. [Online]. Available: http://bit.ly/2LeqSf0

[30] J. E. López Sopeña, *Manual de Instalaciones de GLP*. CEPSA ELF GAS, S. A., 2001. [Online]. Available: http://bit.ly/31Sac2I

[31] D. F. Venegas Vásconez, *Gases combustibles*. Editorial Académica Española, 2019. [Online]. Available: http://bit.ly/2X9Yvpw

[32] ——, "Ubicación de recipientes para glp en terrazas," *Construcción & Servicios*, pp. 16–19, 2018. [Online]. Available: http://bit.ly/2Yc9pY1

UNIVERSIDAD POLITÉCNICA SALESIANA ECUADOR
INGENIUS
Revista de Ciencia y Tecnología
pISSN: 1390-650X / eISSN: 1390-860X

Guidelines for publication in Ingenius Journal

1. General Information

Ingenius is a scientific publication of the *Universidad Politécnica Salesiana* of Ecuador, published since January 2007, with a fixed biannual periodicity, specialized in Mechanical Engineering, Electrical Engineering, Electronics, Computer Science and its integration in what is now known as Mechatronics; these lines of action strengthen areas such as automation, control, robotics, among others..

It is a scientific journal, which uses the peer-review system, under double-blind review methodology, according to the publication standards of the Institute of Electrical and Electronics Engineers (IEEE). Compliance with this system allows authors to guarantee an objective, impartial and transparent review process, which facilitates the publication of their inclusion in reference databases, repositories and international indexing.

Ingenius is indexed in the directory and selective catalog of the Regional Online Information System for Scientific Journals of Latin America, the Caribbean, Spain and Portugal (Latindex), in the Directory of Journals of Open Access DOAJ, In the Information Matrix for the Analysis of Journals, MIAR, In the Ibero-American Network of Innovation and Scientific Knowledge, REDIB and in repositories, libraries and specialized catalogs of Latin America.

The journal is published in a double version: printed (ISSN: 1390-650X) and digital (e-ISSN: 1390-860X), in Spanish, each work being identified with a DOI (Digital Object Identifier System. The articles sent to Ingenius magazine must comply with the following criteria:

2. Scope and policy

2.1. Theme

Original contributions in Mechanical Engineering, Electrical and Electronic Engineering, Computer Science and its integration in what is now known as Mechatronics, as well as related areas: Automation, Control, Domotics, Robotics in their different fields of action and all those related disciplines with the same central theme.

All the work carried out by national or foreign researchers may be published once they meet the required scientific quality criteria.

2.2. Contributions

Ingenius Journal preferably publishes articles related to empirical research, and also reports of technological development, proposals for models and innovations, products for the elaboration of graduate and postgraduate thesis that contribute to the field of science and technology, as well as select revisions of literature. (state-of-the-art).

- **Research:** 5,000 to 6,500 words of text, including title, abstracts, descriptors, charts and references.
- **Reports:** 5,000 to 6,500 words of text, including title, abstracts, charts and references.
- **Reviews:** 6,000 to 7,000 words of text, including charts and references. Current, selective and justified references, would be specially valued from among 40 works

The Ingenius Journal publishes original and unpublished works written in Spanish and English, they may not have been published

through any printed or electronic media, nor be in the process of arbitration or publication.

Every article will be subjected to a rigorous arbitration process; the evaluation of the article will be made according to criteria of originality, relevance, relevance, contributions, scientific rigor and compliance with established editorial guidelines.

Being an arbitrated publication, the Editorial Board approves its publication based on the concept of specialized pairs. The reception of a document does not imply commitment of publication.

It is essential to present a letter of presentation and grant of rights which can be downloaded from: <
urlhttps://goo.gl/ZNkMRD>.

Contributions must be exclusively sent and through the OJS (Open Journal System) <`https://goo.gl/JF7dWT`>. In which all authors must previously register as a user. For any consultation of the procedure you should contact:

<revistaingenius@ups.edu.ec>,
<jcalle@ups.edu.ec> ó
<mquinde@ups.edu.ec>.

3. Presentation and structure of the manuscripts

For those works that are empirical investigations, the manuscripts will follow the IMRDC structure (Introduction, Materials and Methods, Results and Discussion and Conclusions), being optional the Notes and Supports. Those papers that, on the contrary, deal with reports, studies, proposals and reviews may be more flexible in their epigraphs, particularly in material and methods, analysis, results, discussion and conclusions. In all typologies of works, references are mandatory.

Articles may be written on Microsoft Word (.doc or .docx) or LaTeX(.tex). The template to be used can be downloaded from the journal's website, a, <`https://goo.gl/gtCg6m`>, while for LaTeX in <`https://goo.gl/hrHzzQ`>, it is necessary that the file be anonymised in Properties of File, so that the author(s) ID is not displayed.

Figures, Graphs and/or Illustrations, as well as Charts shall be numbered sequentially including an explanatory description for each. The equations included in the article must also be numbered; the figures, charts and equations must be cited in the text.

Use space after point, commas and question marks.

Use "enter" at the end of each paragraph and title heading. Do not use .enter.anywhere else, let the word processor program automatically break the lines.

Do not center headings or subheadings as they should be aligned to the left.

Charts must be created in the same program used for the document body, but must be stored in a separate file. Use tabs, not spaces, to create columns. Remember that the final size of printed pages will be 21 x 28 cm, so the tables must be designed to fit the final print space.

3.1. Structure of the manuscripts

3.1.1. Presentation and cover letter

1. **Título (español) / Title (inglés):** Concise but informative, in Spanish on the front line and in English on the second, when the article is written in Spanish and vice versa if it is written in English.
2. **Authors and affiliations:** Full name and surname of each author, organized by order of priority and their institutional affiliation with reference to the end of the first sheet, where it must include: Dependency to which belongs within the

institution, Institution to which he/she belongs, country, ORCID. A maximum of 5 authors will be accepted, although there may be exceptions justified by the complexity and extent of the topic.

3. **Abstract (Spanish) / Abstract (English):** It will have a maximum extension of 230 words, first in Spanish and then in English. : 1) Justification of the topic; 2) Objectives; 3) Methodology and sample; 4) Main results; 5) Main conclusions.
4. **Keywords (Spanish) / Keywords (English):** 6 descriptors must be presented for each language version directly related to the subject of the work. The use of the key words set out in UNESCO's Thesaurus will be positively valued.
5. **Presentation (Cover Letter):** A statement that the manuscript is an original contribution, not submission or evaluation process in another journal, with the confirmation of the signatory authors, acceptance (if applicable) of formal changes in the manuscript according to the guidelines and partial assignment of rights to the publisher, according to the format established in: <https://goo.gl/ZNkMRD>

3.1.2. Manuscript

1. **Título (español) / Title (inglés):** Concise but informative, in Spanish on the front line and in English on the second, when the article is written in Spanish and vice versa if it is written in English.
2. **Authors and affiliations:** Full name and surname of each author, organized by order of priority and their institutional affiliation with reference to the end of the first sheet, where it must include: Dependency to which belongs within the institution, Institution to which he/she belongs, country, ORCID. A maximum of 5 authors will be accepted, although there may be exceptions justified by the complexity and extent of the topic.
3. **Abstract (Spanish) / Abstract (English):** It will have a maximum extension of 230 words, first in Spanish and then in English. : 1) Justification of the topic; 2) Objectives; 3) Methodology and sample; 4) Main results; 5) Main conclusions.
4. **Keywords (Spanish) / Keywords (English):** 6 descriptors must be presented for each language version directly related to the subject of the work. The use of the key words set out in UNESCO's Thesaurus will be positively valued.
5. **Introduction:** It should include the problem statement, context of the problem, justification, rationale and purpose of the study, using bibliographical citations, as well as the most significant and current literature on the topic at national and international level.
6. **Material and methods:** It must be written so that the reader can easily understand the development of the research. If applicable, it will describe the methodology, the sample and the form of sampling, as well as the type of statistical analysis used. If it is an original methodology, it is necessary to explain the reasons that led to its use and to describe its possible limitations.
7. **Analysis and results:** It will try to highlight the most important observations, describing, without making value judgments, the material and methods used. They will appear in a logical sequence in the text and the essential charts and figures avoiding the duplication of data.
8. **Discussion and Conclusions:** It will summarize the most important findings, relating the observations themselves to relevant studies, indicating contributions

and limitations, without adding data already mentioned in other sections. It should also include deductions and lines for future research.

9. **Supports and acknowledgments (optional):** The Council Science Editors recommends the author (s) to specify the source of funding for the research. Priority will be given to projects supported by national and international competitive projects.
10. **The notes (optional):** will go, only if necessary, at the end of the article (before the references). They must be manually annotated, since the system of footnotes or the end of Word is not recognized by the layout systems. The numbers of notes are placed in superscript, both in the text and in the final note. The numbers of notes are placed in superscript, both in the text and in the final note. No notes are allowed that collect simple bibliographic citations (without comments), as these should go in the references.
11. **References:** Bibliographical citations should be reviewed in the form of references to the text. Under no circumstances should references mentioned in the text not be included. Their number should be sufficient to contextualize the theoretical framework with current and important criteria. They will be presented sequentially in order of appearance, as appropriate following the format of the IEEE.

3.2. Guidelines for Bibliographical references

Journal articles:

[1] J. Riess, J. J. Abbas, "Adaptive control of cyclic movements as muscles fatigue using functional neuromuscular stimulation". IEEE Trans. Neural Syst. Rehabil. Eng vol. 9, pp.326–330, 2001. [Onine]. Available: https://doi.org/10.1109/7333.948462

Books:

[1] G. O. Young, "Synthetic structure of industrial plastics" in Plastics, 2nd ed., vol. 3, J. Peters, Ed. New York: McGraw–Hill, 1964, pp. 15–64.

Technical reports:

[1] M. A. Brusberg and E. N. Clark, "Installation, operation, and data evaluation of an oblique–incidence ionosphere sounder system," in "Radio Propagation Characteristics of the Washington–Honolulu Path," Stanford Res. Inst., Stanford, CA, Contract NOBSR–87615, Final Rep., Feb. 1995, vol. 1

Articles presented in confeences (unpubished):

[1] Vázquez, Rolando, Presentación curso "Realidad Virtual". National Instruments. Colombia, 2009.

Articles of memories of Conferences (Published):

[1] L. I. Ruiz, A. García, J. García, G. Taboada. "Criterios para la optimización de sistemas eléctricos en refinerías de la industria petrolera: influencia y análisis en el equipo eléctrico," IEEE CONCAPAN XXVIII, Guatemala 2008.

Thesis:

[1] L.M. Moreno, "Computación paralela y entornos heterogéneos," Tesis doctoral, Dep. Estadística, Investigación Operativa y Computación, Universidad de La Laguna, La Laguna, 2005.

Guidelines:

[1] IEEE Guide for Application of Power Apparatus Bushings, IEEE Standard C57.19.100–1995, Aug. 1995.

Patents:

[1] J. P. Wilkinson, "Nonlinear resonant circuit devices," U.S. Patent 3 624 125, July 16, 1990.

Manuals:

[1] Motorola Semiconductor Data Manual, Motorola Semiconductor Products Inc., Phoenix, AZ, 1989.

Internet resources:

[1] E. H. Miller, "A note on reflector arrays" [Online]. Available. https://goo.gl/4cJkCF

3.3. Epigraphs, Figures and Charts

The epigraphs of the body of the article will be numbered in Arabic. They should go without a full box of capital letters, neither underlined nor bold. The numbering must be a maximum of three levels: 1. / 1.1. / 1.1.1. At the end of each numbered epigraph will be given an enter to continue with the corresponding paragraph.

The charts must be included in the text according to order of appearance, numbered in Arabic and subtitled with the description of the content, the subtitle should go at the top of the table justified to the left.

Figures can be linear drawings, maps or black and white halftone or color photographs in 300 dpi resolution. Do not combine photographs and line drawings in the same figure.

Design the figures so that they fit eventually to the final size of the journal 21 x 28 cm. Make sure inscriptions or details, as well as lines, are of appropriate size and thickness so that they are not illegible when they are reduced to their final size (numbers, letters and symbols must be reduced to at least 2.5 mm in height After the illustrations have been reduced to fit the printed page). Ideally, the linear illustrations should be prepared at about a quarter of their final publication size.

Different elements in the same figure should be spelled a, b, c, etc.

Photographs should be recorded with high contrast and high resolution. Remember that photographs frequently lose contrast in the printing process. Line drawings and maps should be prepared in black.

The text of the figures and maps must be written in easily legible letters.

If the figures have been previously used, it is the responsibility of the author to obtain the corresponding permission to avoid subsequent problems related to copyright.

Each figure must be submitted in a separate file, either as bitmap (.jpg, .bmp, .gif, or .png) or as vector graphics (.ps, .eps, .pdf).

4. Submission process

The manuscript must be sent through the OJS system of the journal, <`https://goo.gl/JF7dWT`>,the manuscript should be uploaded as an original file in .pdf without author data and anonymized according to the above; In complementary files the complete manuscript must be loaded in .doc or .docx (Word file), that is to say with the data of the author (s) and its institutional ascription; Also the numbered figures should be uploaded in independent files according to the corresponding in the manuscript (as bitmap .jpg, .bmp, .gif, or .png or as vector graphics .ps, .eps, .pdf). It is also obligatory to upload the cover letter and grant of rights as an additional file.

All authors must enter the required information on the OJS platform and only one of the authors will be responsible for correspondence.

Once the contribution has been sent the system will automatically send the author for correspondence a confirmation email of receipt of the contribution.

5. Editorial process

Once the manuscript has been received in OJS, a first check by the editorial team of the following points:

- The topic is in accordance with the criteria of the journal.
- Must have the IMRDC structure.
- Must be in the Ingenius format.
- Must use the IEEE citation format.
- All references should be cited in the text of the manuscript as well as charts, figures and equations.
- The manuscript is original; for this, software is used to determine plagiarism.

The assessment described above can take up to 4 weeks.

If any of the above is not complete or there is inconsistency, an email will be sent to the author to make the requested corrections.

The author will make the corrections and resend the contribution through an email in response to the notification and will also upload the corrected manuscript into OJS supplementary files.

The editorial team will verify that the requested corrections have been incorporated, if it complies, the manuscript will start the second part of the process that may be followed by the author through OJS, otherwise the author will be notified and the manuscript will be archived.

The second phase of the process consists of the evaluation under the methodology of double-blind review, which includes national and foreign experts considering the following steps:

- The editor assigns two or more reviewers for the article.
- After reviewing the article, the reviewers will submit the evaluation report with one of the following results.
  - Publishable
  - Publishable with suggested changes
  - Publishable with mandatory changes
  - Non publishable
- The editor once received the evaluation by the reviewers will analyze the results and determine if the article is accepted or denied.
- If the article is accepted, the author will be notified to make corrections if required and the corresponding editorial process will be continued.
- If the article is denied, the author will be notified and the manuscript will be archived.
- In the two previous cases the result of the evaluation of the reviewers and their respective recommendations will be sent.

The second phase of the process lasts at least 4 weeks, after which they will be notified to the author giving instructions to continue with the process.

6. Publication

The Ingenius Journal publishes two issues per year, on January 1st and July 1st, so it is important to consider the dates for sending the articles and their corresponding publication. Articles received until October will be considered for the January publication and those received until April for the July publication.

UNIVERSIDAD POLITÉCNICA SALESIANA DEL ECUADOR
Javier Herrán Gómez, sdb
Rector

Turuhuayco 3-69 y Calle Vieja
Postal code 2074
Cuenca, Ecuador
Teléfono: (+593 7) 205 00 00
Fax: (+593 7) 408 89 58
Email: srector@ups.edu.ec

Exchange

Exchange with other periodicals is accepted.

Address:
Secretaría Técnica de Comunicación
Universidad Politécnica Salesiana
Turuhuayco 3-69 y Calle Vieja
Postal code 2074
Cuenca, Ecuador
Phone: (+593 7) 205 00 00 Ext. 1182
Fax: (+593 7) 408 89 58
Email: rpublicas@ups.edu.ec
www.ups.edu.ec
Cuenca – Ecuador

INGENIUS, Journal Science of Technology,
Semester publication, N.° 21, january/june 2019
John Calle Sigüencia, Editor in chief
revistaingenius@ups.edu.ec

Printed
Centro Gráfico Salesiano: Antonio Vega Muñoz 10-68 y General Torres.
Phone: (+593 7) 283 17 45
Cuenca – Ecuador
Email: centrograficosalesiano@lns.com.ec